UNIVERSIDAD DE CANTABRIA

ESCUELA DE DOCTORADO DE LA UNIVERSIDAD DE CANTABRIA
DOCTORADO EN BIOLOGÍA MOLECULAR Y BIOMEDICINA

PhD Thesis

Inhibition of the conjugative traffic ATPase TrwD by fatty acid derivatives

- - - - - -

TESIS DOCTORAL

Inhibición de la ATPasa conjugativa TrwD por derivados de ácidos grasos

---

Presentada por: **Yolanda García Cazorla**

Dirigida por:

Prof. Elena Cabezón Navarro

Prof. Ignacio Arechaga Iturregui

Santander, 2018

Elena Cabezón Navarro e Ignacio Arechaga Iturregui, Profesores Titulares de la Fatultad de Medicina de la Universidad de Cantabria, certifican que:

Yolanda García Cazorla ha realizado bajo nuestra dirección el presente trabajo de Tesis Doctoral que lleva por título:

Inhibition of the conjugative traffic ATPase TrwD by fatty acid derivatives.

Inhibición de la ATPasa conjugativa TrwD por derivados de ácidos grasos.

Consideramos que este trabajo se encuentra terminado y reúne los requisitos de originalidad y calidad científica necesarios para su presentación como Memoria de Doctorado por la interesada, al objeto de poder optar al grado de Doctora en Biología Molecular y Biomedicina por la Universidad de Cantabria.

Y para que conste y surta los efectos oportunos, firmamos el presente certificado.

Santander, Junio 2018

Fdo. Elena Cabezón

Fdo. Ignacio Arechaga

El presente trabajo ha sido realizado en el grupo *"Molecular Motors in Nanobiotechnology"* del Departamento de Microbiología y Genómica del Instituto de Biomedicina y Biotecnología de Cantabria (IBBTEC) bajo la dirección de los profesores Elena Cabezón e Ignacio Arechaga.

Parte de los experimentos presentados en esta Memoria de Doctorado fueron realizados por Yolanda García Cazorla durante una estancia de tres meses en el laboratorio de la Prof. Cynthia Whitchurch (*University of Technology Sydney*, Australia) financiada por la Universidad de Cantabria a través de una ayuda para estancias en el extranjero. La autora de este trabajo ha disfrutado de un contrato predoctoral de la Universidad de Cantabria.

“There is nothing more wonderful than being a scientist.

Nowhere I would rather be than in my lab,

staining up my clothes and getting paid to play”

-Marie Curie-

Agradecimientos

Alguien me dijo una vez que es de bien nacidos ser agradecidos. Un proyecto científico nunca es llevado a cabo por una sola persona aislada en su laboratorio-búnker luchando contra el mundo, son muchas las personas que con su gran esfuerzo y dedicación han hecho posible que este trabajo vea la luz. Gracias por dejarme aportar mi granito de arena a este fascinante mundo.

En primer lugar, y como no podría ser de otro modo, debo mencionar a los verdaderos responsables de todo esto, quienes me dieron la gran oportunidad de venirme a Santander y emprender esta aventura científica. Gracias Elena e Iñaki por confiar en mí desde el principio, cuando sólo habíamos intercambiado unas cuantas palabras por email y Skype. La libertad y apoyo que dais a vuestros predoctorales es increíble. GRACIAS.

Gracias también a mis evaluadores, Matxalen y Gabi, por haber seguido con interés mi trabajo durante todo este tiempo. Tampoco podría olvidar mencionar en estas líneas a Fernando de la Cruz. Vuestros consejos e ideas han ayudado sin duda a dar forma a este proyecto.

Thanks to Cynthia, for the great opportunity to join your lab in Sydney. It was an incredible experience. I learnt even beyond what I thought possible (I even get some microscope imagines for my dissertation!). It was wonderful to share my time with such a fantastic group: Lynne, Lori, Joyce, David... it was a pleasure to meet you all. I am particularly grateful to Rosy and James, for your help and your patience. And Giulia for share our free time, the weekend trips… we have a journey yet to do in Europe!

Mención especial merecen dos personas sin las cuales habría tirado la toalla hace mucho, o seguiría dándome de cabezazos contra la pared. A Jorge, por enseñarme todo sobre TrwD y por tus siempre acertados consejos, gracias por tu infinita paciencia y por haber estado ahí a pesar de la distancia, fue una pena no haber podido compartir más horas de poyata. A Gerardo, por traer al labo la alegría y buen rollo que tanta falta nos hacía, por ser mi guía espiritual durante esta segunda etapa de mi tesis, echaré de menos todas esas tardes de politiqueo arreglando el mundo pipeta en mano.

A los *motores moleculares* del IBBTEC. A Mati, por ser la mejor, no sabríamos que hacer sin ti. A Sandra, gracias por tu ayuda en mis inicios, me hubiese encantado poder compartir más horas contigo. A Fernando, Bea, Sara… y en general a todo bicho viviente que haya pasado durante todos estos años por el labo 02.02. Gracias por las risas y por contribuir a los buenos momentos de grupo. Gracias también a todo el grupo de intergenómica, por haber sido tantas veces mi refugio y mi segunda casa en el IBBTEC. Y a todos esos predecesores que sentaron las bases, ideas y fundamentos para este trabajo.

A mis queridos precarios del IBBTEC. A la antigua generación por acogerme como una más de vuestra pequeña gran familia desde el minuto uno, esas cosas no se olvidan. A la "nueva" generación por tantos *cafeses*, birras, comilonas, festis, casas rurales, escapadas… e infinidad de noches que se nos hicieron días. En especial a Omar, por ser mi relaciones públicas a mi llegada a Santander. Y a Jorge, por empezar esta aventura norteña juntos y llevar caminos paralelos. Vuestra maldita locura contagiosa ha conseguido que no pierda del todo la cabeza durante estos años. Sois geniales, no cambieis nunca.

Tampoco podría olvidar a todas esas personas no científicas que me ha aportado Cantabria, por ayudarme a desconectar del mundo científico, enseñarme lugares ocultos, las lecciones musicales, vuestros ánimos constantes y esas escapadas en furgo. También a los que me han acompañado recorriendo medio mundo. Thanks to all those wonderful people that the science has allowed me to know around the world. Y por supuesto a los de siempre, que a pesar de todos los cambios y la distancia siguen estando ahí. Gracias por enseñarme y hacer nuestro el dicho de que la verdadera amistad no se trata de ser inseparables, sino de estar separados y que nada cambie.

Por último, y no por ello menos importante, a esas personas sin las que no podría haber llegado a ser quien soy hoy, a mi familia. Gracias por preguntar siempre cómo me va por estas tierras norteñas. A mis abuelos por tantas velas encendidas para iluminar nuestro camino. A mi padre, por haber estado ahí cuando más lo he necesitado, por apoyarme y sentir como tuyos mis logros. A mi madre, simplemente por ser como eres. Por darnos siempre todo lo que has podido y más, por ser el apoyo incondicional que todo el mundo querría tener a su lado. Por la infinidad de consejos y por los ánimos. Por sufrir mis penas y alegrías como tuyas. Por haber confiado siempre en mí. Y por su puesto a mi manito, gracias por ser más que mi hermano, mi amigo. Por haberme enseñado tanto y por saber que siempre puedo acudir a ti en busca de ayuda y buenos consejos. Gracias a todos, por tanto, os quiero.

A mi madre

INDEX

Chapter 1
INTRODUCTION

Rosalind Franklin

1.1. Horizontal gene transfer.

In bacteria, genes are transferred either vertically from one generation to another by clonal expansion or laterally, in the same generation, through horizontal gene transfer (HGT). HGT involves non-sexual exchange of genetic material between organisms. This transference of genes across cells is more versatile than sexual reproduction and leads to the introduction of new evolved genes into existing genomes. As a result, HGT plays an essential role in the genetic composition, variability and diversity of the bacteria populations. Bacterial conjugation can occur between species without a close evolutionary relationship and even between different kingdoms. But it is in bacteria where it accounts for the main mechanism of genome evolution [1]. This exchange of DNA compensates for the lack of sexuality in prokaryotes and affects the adaptation, speciation and bacterial evolution [2].

In most cases, this transfer of genetic information is mediated by mobile genetic elements (MGE), that is, DNA devices for the intra- or intercellular movement of DNA. Intracellular mobility is produced mainly by transposons, DNA fragments with the ability of moving through specific mechanisms of recombination from one genome location to another, including different replicons of the same cell [3]. Intercellular mobility occurs by one of the three main processes [4]: transformation, conjugation or transduction (Figure 1.1).

Transformation requires uptake, integration and functional expression of extracellular free DNA, usually released from dead cells. To acquire exogenous DNA, bacteria must be in a physiological state of competence, which could be natural or artificially induced. Most naturally transformable bacteria develop competence in response to specific environmental conditions, such as altered growth conditions, nutrient access, cell density or starvation. Homologous recombination between transformed DNA and the resident genome can lead to the acquisition of a new phenotype [5].

Transduction is mediated by bacteriophage infection. Bacterial viruses accidentally pack DNA segments from the host and inject them into a new host, in which they can be established by a process of homologous recombination and be inserted in the chromosome or replicate autonomously within a plasmid. Transduction may be generalized or specialized, depending on whether any gene may be transferred or only those located near the site of prophage integration [6].

Conjugation involves the transfer of genetic elements (usually plasmid DNA) from a donor to a recipient bacterium through direct contact, via the formation of a protein structure called conjugative *pilus* [3].

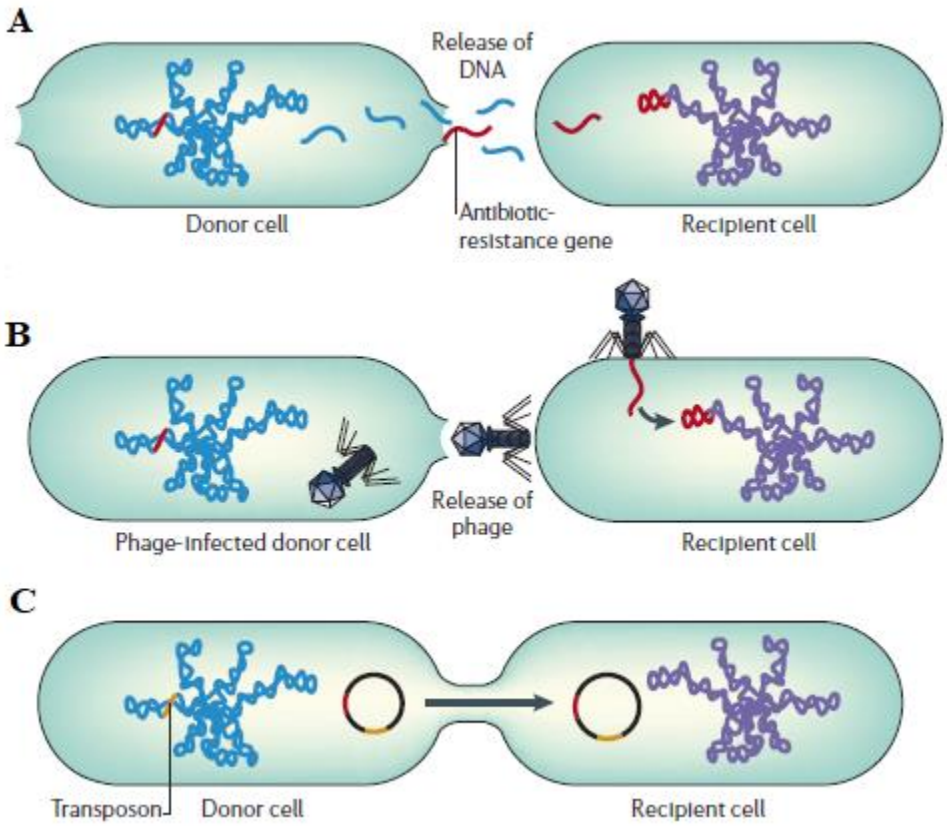

Figure 1.1. Mechanisms for horizontal DNA transfer in bacteria. Schematic representation of the three main mechanisms involved in horizontal DNA exchange in the prokaryotic kingdom. (A) Transformation: information is taken from a dead bacterium, which releases it to the environment. (B) Transduction: it requires bacteriophages that accidentally pack DNA from a bacteria host and inject it into a new host. (C) Conjugation: plasmid DNA transfer between two cells through direct contact. Taken from [7].

1.1.1. Bacterial conjugation.

Unlike transformation or transduction, which are a side effect of nutrient uptake or phage propagation respectively, bacterial conjugation is a specialized process of HGT. It is a widespread mechanism in the nature [8], the most common mechanism of HGT [9,10] and the one with the broadest host range [11]. Therefore, bacterial conjugation has intrinsic interest as a mechanism which transfers diverse adaptive traits and generates genetic variability [12]. It contributes to the spread of virulence factors [13], metal ion resistance determinants [14] and antibiotic resistances [15,16], being the major vehicle for the spread of Antibiotic Resistance (AbR) genes [17,18].

Lederberg and Tatum discovered bacterial conjugation in 1946, when they mixed two *E. coli* populations with different nutritional mutations and found prototrophic recovery [19–21]. In 1950, Davis demonstrated that direct contact between bacteria was required for prototrophic recovery [22]. In 1953, Watson and Hayes defined the process as a unidirectional transfer mediated by the fertility factor F from a F^+ donor to a F^- recipient [23]. It was not until two decades later that plasmids were classified by incompatibility groups (Inc), depending on the ability of two plasmids to coexist stably in the same bacteria [24], and F conjugation was analysed by electron microscopy [25].

Typically, DNA is transferred from a donor bacterium to a receptor by a self-transmissible plasmid (they can be transferred by themselves as they encode for the required machinery) or by a mobilizable one (with the help of the conjugative plasmid) [26]. Conjugation may also involve the transfer of chromosomic sequences via plasmids that are integrated into the chromosome forming a *Hfr* (high frequency of recombination) strain [27], or by integrative and conjugative elements (ICE, conjugative transposons) [28].

Under laboratory conditions, conjugation has been described between different kingdoms: from *E. coli* to the budding yeast *S. cerevisiae* [29]; from bacteria to plants [30,31], and even from bacteria to mammalian cells [32]. Natural DNA transfer between bacteria and plants occurs in certain species of *Agrobacterium* that have the ability to mobilize a DNA segment, T-DNA, in a very similar way to bacterial conjugation [33].

Although the study of conjugation covered plasmids from gram-positive bacteria, as it is the case for *Streptomyces* [34], the majority of the transfer systems studied belong to gram-negative bacteria. Of particular importance are those of *Enterobacteriaceae,* which are extensively used as a model for general conjugation. This family of plasmids has been classified in 19 incompatibility groups according to the specificity of their replication apparatus, since plasmids sharing the same replicon are incompatible in the same cell line [35]. From these, six groups of self-transmissible plasmids have been used to establish a general model for conjugation, with five different variants corresponding to groups: IncW (R388) & IncN (pKM101), IncP (RP4, RK2) and IncX (R6K), which are broad host range plasmids, and IncF (F, R1, R100) and IncI (R64), which are stable in a limited number of bacteria. Mobilizable plasmids have also been described in detail. Some examples include the broad host range RSF1010 and R1162 IncQ plasmids and plasmids ColE1 and CloDF13 [36]. Half of the natural plasmids studied are auto-transmissible or mobilizable [12].

1.1.1.1. Conjugative Secretion System.

Bacterial conjugation requires direct contact between donor and recipient cells through a specific conjugative secretion system (conjugative pilus). In general, bacterial secretion systems are multi-protein complexes that span the inner and outer membranes, allowing the molecular exchange between cells and with the extracellular milieu. They are crucial components of bacteria implicated in multiple processes such as adhesion, nutrient acquisition, spread of antibiotic

resistance, genomic plasticity, acquisition of new bacterial metabolic pathways, bacterial virulence and pathogenesis [37].

Bacterial secretion systems have been classified in different groups according to the nature of the secreted substrates and the biosynthesis, structure, evolutionary and functional relatedness. In Gram-negative bacteria, nine protein secretion systems have been unravelled so far. These systems have been designated by Roman or Arabic numerals from the type I (T1SS) to type IX secretion systems (T9SS) (Figure 1.2) [38].

In general, proteins are transported by a one- or two-stage process. The first uses a complex transporter machinery to deliver effector molecules directly from the bacterial cytoplasm to the extracellular medium (T1SS) or to the cytosol of a wide range of eukaryotic and/or prokaryotic cells (T3SS, T4SS, T6SS) [39]. In a two-stage transport, proteins are first delivered to the periplasm through the bacterial inner membrane, and then they are transported across the outer membrane using various mechanisms (T2SS, T5SS, T7SS, T8SS, T9SS) [40–42].

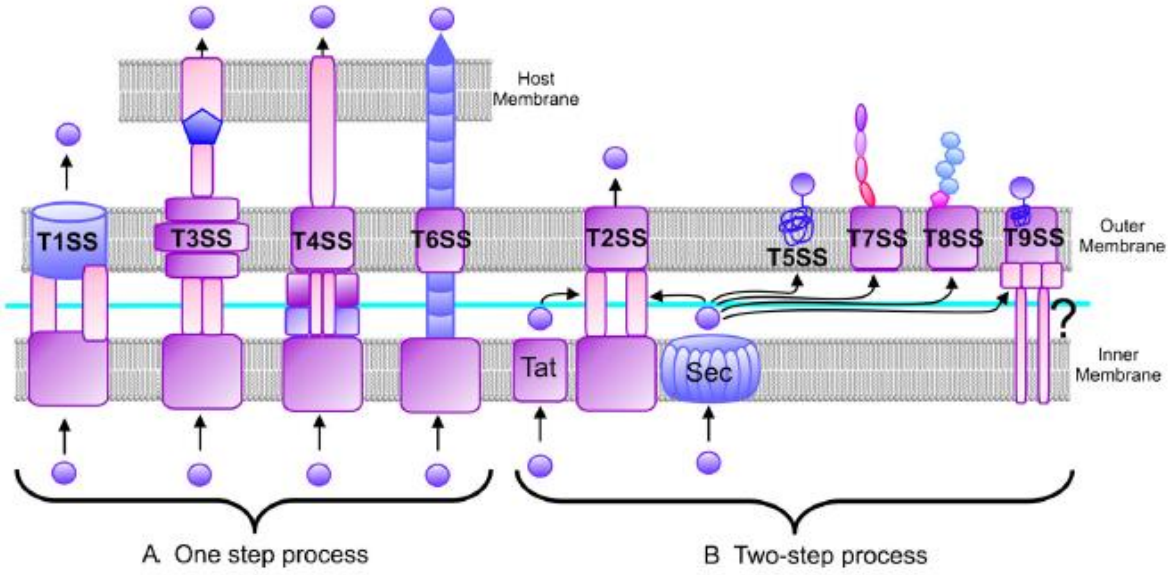

Figure 1.2. Secretion systems of Gram-negative bacteria. In this simplified view only the basic building blocks of each secretion system are sketched. **(A)** One-step systems. In these systems effector molecules are delivered directly to the extracellular medium (T1SS) or to the cytosol of the host cell (T3SS, T4SS, T6SS) through secretion channels that span three membranes: the inner and outer bacterial cell membranes and the membrane of a receptor cell. The architecture of the secretion apparatus of each type of system is unique. **(B)** Two-step systems. T2SS, general secretion pathway, involved also in the formation of Type 4 pili; T5SS pathway used by autotransporters which do not need any auxiliary proteins to traverse the outer membrane; T7SS-chaperone-usher pathway involved in pili formation; T8SS-extracellular-nucleation-precipitation pathway involved in curli formation; and T9SS-Porphirin secretion system. In these systems proteins cross the inner membrane with the help of either the Sec (secretion) or Tat (twin arginine transportation) pathway and next they are transported across the outer membrane using various mechanisms. Taken from [43].

In comparison to other secretion systems, the type IV secretion system (T4SS) is unique in its ability to transport nucleic acids in addition to proteins into plant and animal cells, as well as into yeast and other bacteria [44]. Therefore, T4SS is the only secretion system that performs the conjugative process and the subject of the present PhD work.

1.1.1.2. A model for bacterial conjugation.

Despite the clear difference shown in the conjugative strategy from different class of plasmids, they all share some characteristic mechanical components: the need for the synthesis of a conjugative pilus to promote cell surface contact; a set of molecular motors (ATPases) that provide the energy for every single step of the process, the presence of DNA processing enzymes for the initiation of DNA transfer; a mechanism for guaranteeing the establishment of the incoming plasmid in the recipient cell, a regulatory system for transfer control and induction, and the origin of transfer (*oriT*), the unique element required *in cis* for being mobilizable [45].

The conjugative machinery in Gram-negative bacteria is composed by three different functional units that are assembled to conform a complete system [46]:

- Type IV secretion system (T4SS) forms the multi-protein transmembrane channel for the DNA transfer [47,48].

-Relaxosome is responsible for the process of the DNA and formation of the substrate to be transferred. It involves the relaxase protein that specifically binds and cleaves the plasmid DNA, and leads it to the recipient cell [49].

-Coupling protein (CP) connects the relaxosome (ralaxase covalently bind to DNA) with the channel.

Following the “Shoot and Pump” model [50], bacterial conjugation can be considered as the association of two separate mechanisms: a rolling-circle replication (RCR) and a T4SS. This assumption is based on the fact that conjugative DNA processing proteins show high sequence similarities with proteins implicated in RCR. Moreover, their target *oriT* and the origins of replication by rolling-circle, *oriV*, share sequene similarities [51]. In the shooting step the relaxase is actively transferred by the T4SS with the plasmid DNA covalently attached; the pumping step involves the movement of the DNA across the channel, mediated by the ATPase activity of the CP [50].

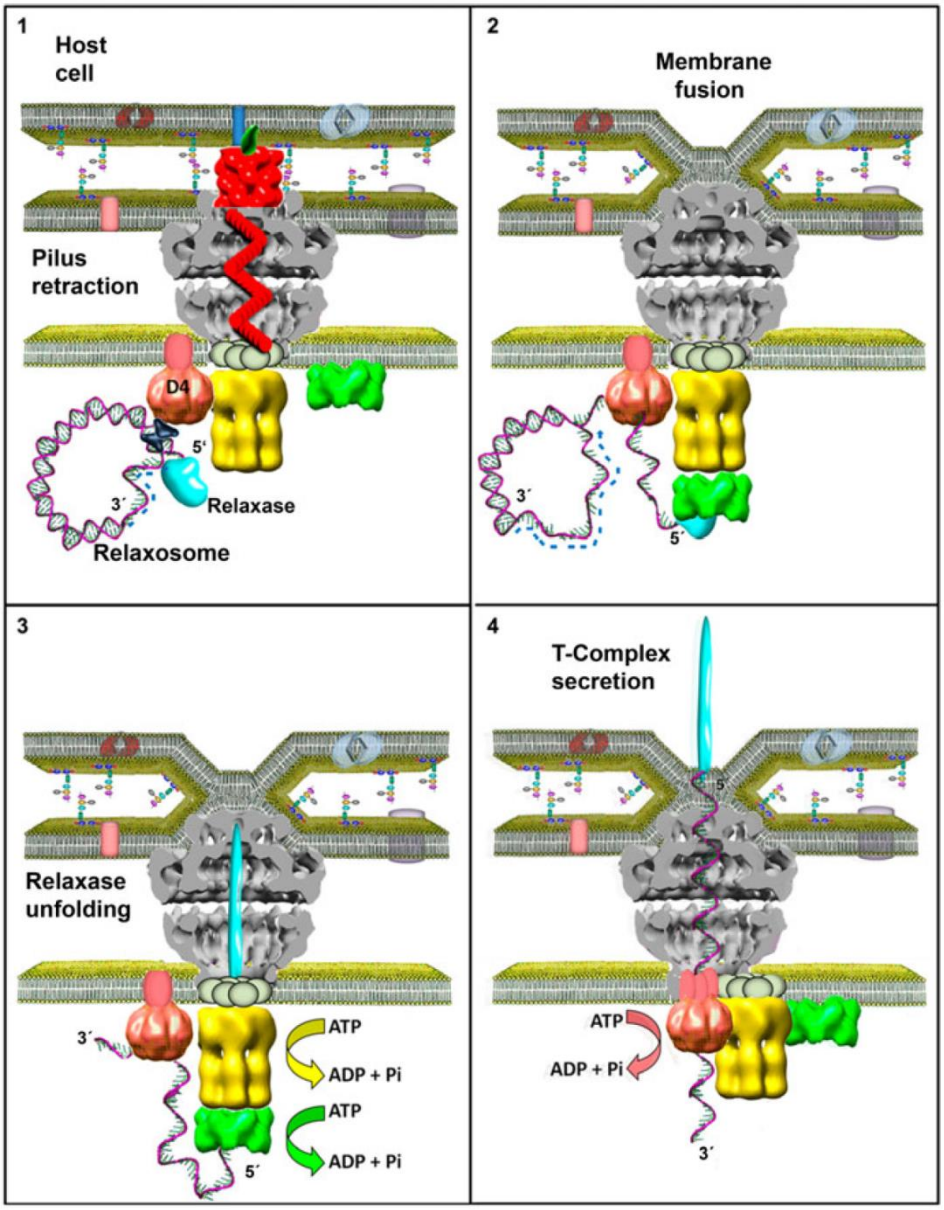

Figure 1.3. Model for DNA processing in bacterial conjugation. (1) A donor and a host cell get in contact through a protein structure synthesized by the donor denominated pilus (red). Most conjugative systems contain four ATPases involved in the transfer of the conjugative plasmid to the recipient cell. Two of these ATPases (TrwK and TrwD in the case of the conjugative plasmid R388, yellow and green respectively), are involved in the biogenesis of the T4SS apparatus. Auxiliary factors TrwA and IHF bind to the origin of transfer region (*oriT*) of plasmidic DNA and the relaxase (blue) cleaves it at the *nic* site and remains covalently bound to the 5' end of *oriT*. **(2)** Upon cell contact, the retraction of the extracellular pilus facilitates the interaction between membranes of donor and recipient cells, resulting in a membrane fusion process. Simultaneously, or prior to this membrane fusion, the coupling protein (salmon) drives the relaxosome towards the secretion channel. **(3)** The nucleoprotein substrate is transferred to TrwD/VirB11 (green). The relaxase is unfolded and translocated through the channel covalently bound to the DNA. **(4)** TrwK/VirB4 (yellow) is displaced at the base of the secretion channel by the coupling protein, which assists DNA translocation in a 5´- 3´ direction. Taken from [52].

1.2. Conjugative system for the plasmid R388.

R388 was originally isolated from *E.coli* strains in 1972 [53]. R388 is a broad host range conjugative plasmid that belongs to the IncW group [54]. It can be transferred to different species of proteobacteria, like *Salmonella typhimuriun*, *Shigella flexneri*, *Pseudomonas aeruginosa* [55] and *Agrobacterium tumefaciens* [56]. It encodes resistance to trimethoprim and sulphonamides [53]. Its constitutive pilus is stiff and thin, so R388 is better transferred in solid media than in liquid [57]. Bacteria carrying this plasmid are sensitive to phage PRD1, which attaches to the R388 conjugative pilus [58].

Conjugative plasmids of the IncW group are among the smallest (30-40 Kb) self-transmissible plasmids. R388 has 33,926 pb, and includes 43 detected ORFs. It is organised in a set of five functional blocks, corresponding to all the basic functions implicated in survival and spreading of a plasmid: replication, stable inheritance, establishment and conjugative transfer, which include two further regions: Mpf (mating pair formation) and Dtr (DNA transfer region) [59].

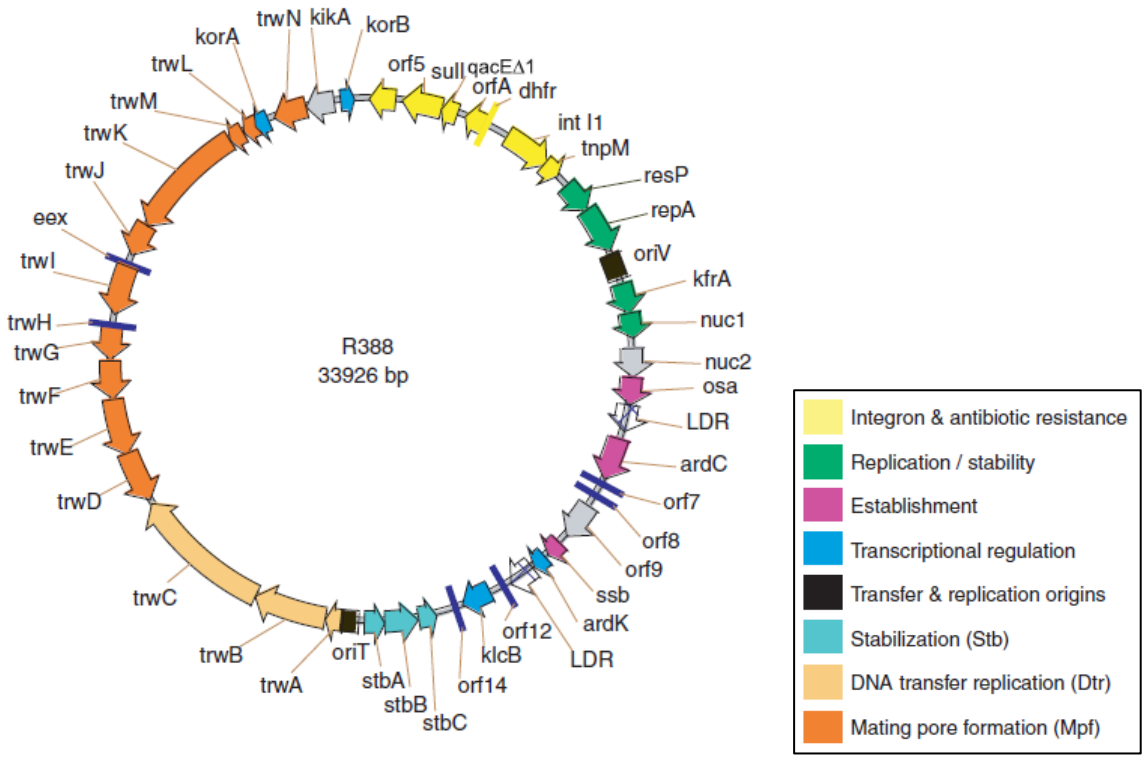

Figure 1.4. Genetic map of plasmid R388. The plasmid was divided into functional regions and each one is identified with one colour, which is detailed in the legend. Adapted from [59].

Almost half of the plasmid is devoted to code for the genes involved in conjugative transfer. This region, called TRA_W, is mapped within a 14.9 kb region of the plasmid and it can be dissected into two units [60]: a sequence containing the genes responsible for pilus synthesis and assembly, PIL_W or Mpf, and a sequence containing those responsible for DNA processing and mobilization, MOB_W or Dtr [59]. These two blocks can be separately cloned *in trans* and complemented for efficient conjugation; *oriT* is the only element necessary in *cis*. This discrete arrangement of the conjugative transfer modules and its peculiarities are very similar to those of the IncN plasmid pKM101. Indeed, IncN and IncW transfer modules show functional complementation [60].

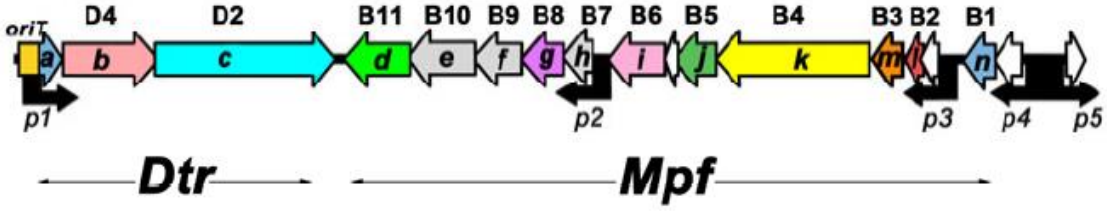

Figure 1.5. Genetic organization of the R388 transfer region. Genes encoding proteins involved in mating pair formation (Mpf) are organized in operons which are separated from those involved in DNA processing and transfer (Dtr). Dtr/MOB_W region is composed by three genes (trwA, trwB and trwC) coded in a single transcription unit and a non-coding sequence corresponding to the *oriT* (origin of transference). The Mpf/PIL_W transcriptome consists of four transcripts and encodes the genes responsible for T4SS and pilus formation (TrwD-N), regulators of transcription and entry exclusion determinants. This molecular gene organization is shared by most conjugative systems, showing a high degree of gene synteny conservation. *Agrobacterium tumefaciens* nomenclature for VirB/D proteins is indicated on top of each trw gene. Taken from [52].

1.2.1. Dtr Region of R388.

The R388 Dtr region is a 5.2 kb segment lying next to the Mpf region and includes three genes transcribed from a single operon, *trwABC*, and a *oriT* [61]. The *trwABC* operon codes for three proteins: TrwA, a relaxosome accessory protein; TrwC, the relaxase-helicase protein, and TrwB that is the CP that connects the relaxosome with the secretion channel [62].

TrwB and TrwC genes are indispensable for R388 conjugation [61], while the absence of TrwA produces a 100-fold decrease in conjugation [63]. Neither TrwA or TrwC can be replaced by their homologs in IncN plasmids (R46 and pKM101), which indicates a high specificity in the interaction of these proteins with the *oriT* [61].

Except for TrwB, the components of the Dtr region are involved in the formation of the relaxosome, which is a nucleoprotein complex assembled for DNA mobilization. The relaxosome of R388 has several components: a fragment of DNA that contains the *oriT* (transfer origin), the conjugative pilot protein or relaxase (TrwC), the helper protein TrwA and the Integration Host Factor (IHF). IHF, a small heterodimeric protein encoded by the host cell chromosome, binds DNA specifically [64]. This binding stabilizes distinct DNA conformations that are required during several processes, like transcription or recombination. IHF binds specifically to two sites in the *oriT* of R388, *ihfA* and *ihfB*, and its binding inhibits, both *in vivo* and *in vitro*, the nicking reaction mediated by the relaxase TrwC, but not TrwC binding. The initiation of the conjugative process in R388 could start when IHF is released from the *oriT* [65].

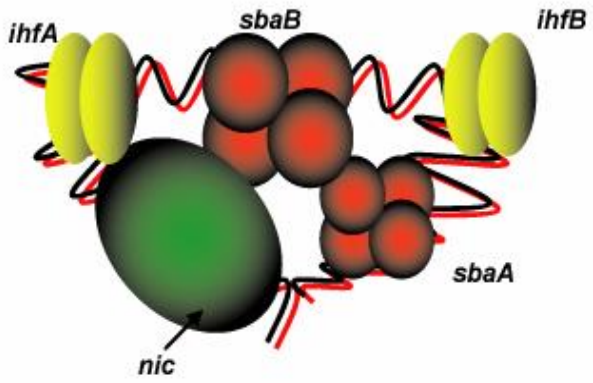

Figure 1.6. Architecture of the R388 relaxosome. TrwA (represented in red) is shown as tetramers bound to their specific *sbaA* and *sbaB* binding sites. IHF (in yellow) and its binding sites, *ihfA* and *ihfB*. TrwC is represented in green. The *oriT nic* site is also indicated. Modified from [65].

The components of the Dtr of R388 are detailed below:

R388 *oriT.* It is a sequence of 330bp [66], defined as the minimal sequence required for mobilisation [67]. It is a A+T riched region, with a set of direct and inverted repeats (DRs and IRs), which include binding sites for TrwA [63], relaxase [68,69], and IHF [70] [65] . It also includes a *nic* site where TrwC introduces a nick [71]. Since the transferred strand is the nicked strand and the 5' end is transferred first, *trw* genes enter the recipient cell in the last place [69].

TrwA. It is a protein of 121 aa and 13 kDa, which oligomerizes as tetramers of 53 kDa in solution. TrwA has two structural domains: an N-terminal domain, involved in DNA binding, and a C-terminal domain, responsible for its oligomerization [72]. Based on the conservation of a series of polar residues in the N-terminal region of the protein, TrwA was assigned as a member of ribbon-helix-helix (RHH) protein family. This family of transcriptional regulators RHH is represented by the Arc repressor [73].

TrwA has a repressive effect, since its overexpression decreases the conjugation frequency. This protein binds specifically to two regions within the R388 *oriT*, *sbaA* and *sbaB,* that

results in transcriptional repression of the *trwABC* operon [63]. Moreover, TrwA enhances TrwC relaxation activity *in vitro* [63], increases TrwC mediated site-specific recombination [66] and TrwB ATPase activity [74]. These features of TrwA are shared by protein TraY from F plasmid, which is also a member of the RHH family [75]. TraY enhances the nicking activity of relaxase TraI [76] and up-regulates *tra* expression by interacting with the *tray* promoter [77].

TrwC. This protein is included in the MOB_F family of relaxases. It is composed by two functional domains, the N-terminal and the C-terminal, with relaxase and DNA helicase activity respectively [78]. TrwC is a 966 aa enzyme, with a molecular weight of 108 kDa that forms dimers in solution [79]. The dimerization region is located at the C-terminal half of the protein (472-966) [80]. The catalytic residues of the TrwC relaxase domain have been elucidated [81], as well as its 3D structure [68].

TrwC is the responsible for the initiation and ending of the conjugation process. It presents sequence-specific endonuclease activity and is able to nick an *oriT*-containing scDNA in the absence of other accessory proteins [69]. The DNA helicase activity of TrwC is dependent on ATP, Mg^{2+} and ssDNA. Unwinding is unidirectional in the 5' to 3' direction. TrwC also produces site-specific recombination between two *oriT* sequences *in vivo* [66,82]. TrwC enters the receptor cell, presumably guiding the DNA chain, and once there must play an essential role in the termination of the conjugation [49]. In fact, the expression of anti-TrwC antibodies in the host bacterium inhibits the conjugative process [83]. Moreover, TrwC can integrate the covalently attached incoming DNA strand into DNA sequences resembling its target sequence which are present in the human genome [84], and the integrase domain of TrwC targets the nucleus [85].

TrwB. The last component of R388 MOB_w is the coupling protein TrwB. This protein will be extensively reviewed later.

1.2.2. Mpf Region of R388.

The Mpf region expands from genes *trwN* to *trwD*, and is involved in the formation of the T4SS and the conjugative pilus. All these genes are essential for conjugation of R388. Bacteria are resistant to phage PRD1 when those *trw* genes are mutated [60]. This region also contains the *eex* gene, which encodes for the entry exclusion determinant and *kil-kor* genes for regulation and stability functions [59].

Most Trw proteins of the Mpf region form a T4SS. T4SS are a versatile family of secretion systems, mediating transport of proteins and nucleoprotein complexes, and have been found in both Gram-positive and Gram-negative bacteria, and even in some *archaea* [86]. Apart from conjugative plasmids, T4SS also appear in chromosomes of pathogens playing a role in infection of eukaryotic cells. The prototypical T4SS is VirB of Ti plasmid from *A. tumefaciens* [87]. Trw proteins of R388 Mpf have 42 to 58% of similarity with proteins of VirB, and the genetic organization is similar [88,89]. All the T4SS studied so far show a similar architecture [90].

Conjugative T4SS can be functionally exchanged between different plasmids. T4SS from R388 can be substituted by the Mpf region from IncN (plasmid pCU1) and IncI plasmids, but not IncP [60,91] to mobilize plasmids with the Dtr region from R388. However, the individual genes of the Mpf region are not interchangeable between both plasmids. These data suggest that there is a high specificity of recognition between Mpf proteins, whereas the relaxosome recognition by the full T4SS is less specific. Coupling proteins and relaxosomes from different systems are not exchangeable, suggesting a highly specific interaction between them [91]. The efficiency of the heterologous mobilisation correlates with the strength of the interaction between the CP and VirB10. CP also interacts with VirB10 homologues from T4SSs involved in virulence [88].

The fact that many T4SS are able to mediate the horizontal gene transfer suggests that there is a very important impact on its evolution and distribution among bacteria [92,93]. A consequence of the genetic mobility is that some T4SS with independent evolutionary origin could be in the same bacteria acquiring different functions [94–96]. In general, horizontal transference and T4SS evolution illustrate that these systems can have different proposes and their basic mechanism can be adapted to new and versatile functions [97].

T4SS elements will be studied in more detail later in the next section.

1.3. Type IV Secretion System (T4SS).

T4SS are a family of macromolecular complexes able to transport different molecules [98]. This family have great versatility according the nature of the subtract transported, which could be DNA, proteins, o nucleoprotein complexes; and the destination of the transported substrate [99]. DNA can be mobilized between bacteria through conjugation, transported form/to the medium, or sent to eukaryotic cells. The proteins can be secreted to the extracellular medium (such as T4SS Ptl from *Bordetella pertussis*), to other bacteria (conjugation), or to a eukaryotic cell (Such as the Cag system from *Helicobacter pylori*), or after the bacteria has been infected (intracellular pathogens as *Bartonella* spp., *Brucella* spp., or *Legionella pneumophila*) [100–102].

As result of this great biological versatility, we can classify T4SS in three big groups according to their main function [103]:

-Conjugative T4SS (T4SSc): constitute the conjugative machinery of plasmids that participate in the DNA horizontal transfer between bacteria. They have implications in the genomic plasticity, so important for the incorporation of new antibiotic resistant genes in many species. [104,105]

-Pathogenic T4SS (T4SSp): required for a great number of pathogens to be able to infect eukaryotic cells. In many cases, they are the essential channels for the transport of virulence factors, necessary for the bacterial establishment inside the host cell. This family includes T4SS of several human pathogens such as *H. pylori*, *Bartonella* spp and *Brucella* species.

-DNA transport to/from the medium through T4SS (T4SSd). It includes the ComB T4SS from *H. pylori* which takes DNA from the extracellular medium and the Tra system from *Neisseria gonorrhoeae* that secretes DNA to the milieu. As with the conjugative systems, this subfamily also promotes a way for the genetic exchange between bacteria.

T4SS from *A. tumefaciens* is the most studied and known, and it is used as reference for the T4SS study. There is another group of T4SS that is less related to this model and is considered as a different T4SS subfamily, T4SSB, while those more similar to the *A. tumefaciens* model are named T4SSA [106]. Some examples are T4SS conjugative plasmid R64 or Dot-Icm T4SS implicated in the pathogenicity of *L. pneumophila* [107,108]. There are huge differences with *A. tumefaciens* model in terms of protein composition, with the exception of VirB10 and VirB11 homologues [109].

The aim of this thesis work is focus on T4SSA.

1.3.1. General architecture for T4SS.

Despite the differences between T4SSs regarding the nature of the secreted substrates, their biological role, and the destination of the substrates, there are important homologies between different T4SS. Most of them are composed by 11 proteins, named form VirB1 to VirB11, components of the prototypic T4SS of *A. tumefaciens*. Homology between T4SS family are present in their genetic organization (sintenia), topology of the different membrane proteins and their conservation [110].

A near complete structure of T4SS from R388 plasmid recently published revealed the general architecture of the secretion system [111]. T4SS proteins can be distributed in four different groups. The first group would be formed by proteins with ATPase activity that energize the system. Two of them are cytoplasmic proteins, but associated to the inner membrane (VirB4, VirB11). A third ATPase is a membrane protein, named coupling protein (CP), which connects the T4SS with the subtract to be transported and it is present in all T4SS that are involved in DNA transfer. A second group would be constituted by the proteins that form the Core Complex, which can be divided in two sub-complexes; the outer membrane cap, formed by VirB7, VirB9 and the C-terminus of VirB10 proteins, and the periplasmic domain formed by most of VirB8, VirB10 and the N-terminus of VirB6 proteins. The last group would be form by the proteins that are on the outer face of the bacteria, constituting the structure known as pilus (VirB2 and VirB5). Pili have different sizes and present different number and distribution. The objective of this appendix is put in contact some cells with others, although their role in substrate transport is still a matter of debate. Finally, many T4SS also present a protein with a lytic transglycosylase (VirB1) [62] (Figure 1.7).

Some T4SS present variations, such as the T4SS VirB from *Brucella*, that lacks a protein similar to virD4, but it presents an extra component named VirB12. Another example is the T4SS ComB from *H. pylori*, which takes DNA from the medium and only presents homology with 8 proteins (VirB2-VirB4 and VirB6-VirB10) [112].

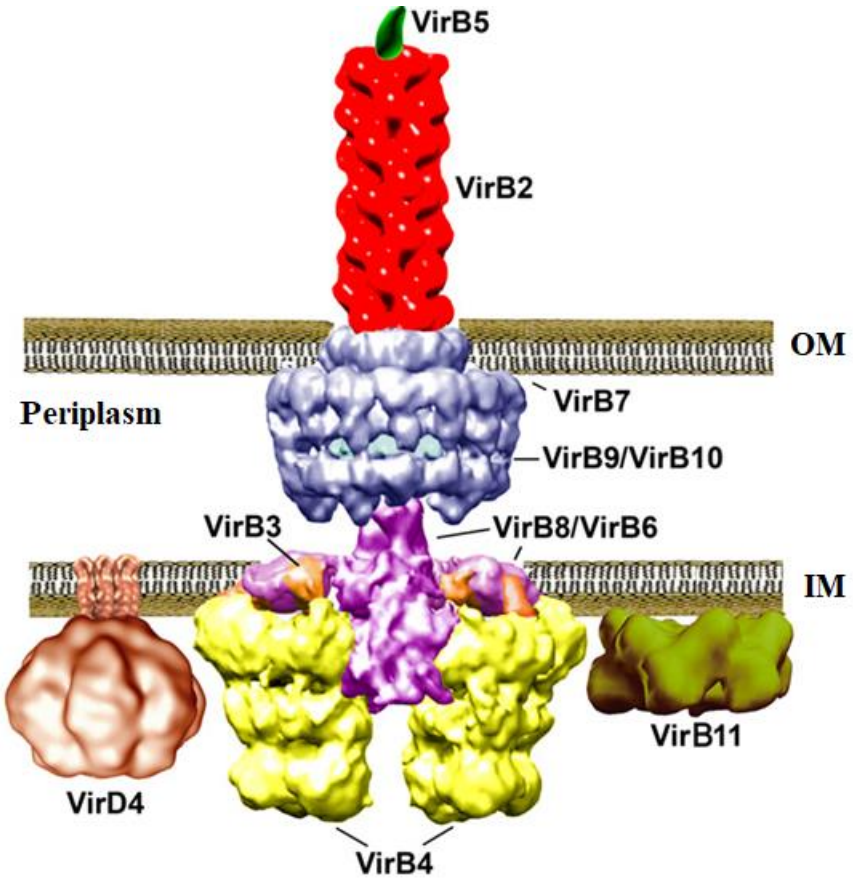

Figure 1.7. Architecture of a conjugative T4SS. Schematic representation of the typical conjugative T4SS structure. Proteins are named according to the prototypical T4SS of *Agrobacterium tumefaciens*. Four distinct domains can be distinguished: the pilus, the core complex, the inner membrane platform and the cytoplasmic ATPases. The pilus is formed by a helical assembly of pilin (VirB2) molecules (red) with adhesin molecules (VirB5) at the distal end (dark green). The core complex can be divided in two sub-complexes: the outer membrane cap, formed by VirB7, VirB9 and the C-terminus of VirB10, with a 14-fold symmetry (depicted in deep blue color); and the periplasmic domain (magenta), formed by most of VirB8, VirB10, and the N-terminus of VirB6. The inner membrane platform (magenta), consisting of the transmembrane domains of VirB3, VirB6, VirB8 and VirB10. Finally, attached to the inner membrane are three hexameric ATPases: VirB4, VirB11 and the coupling protein VirD4. In the EM structure [111], two hexameric barrels of VirB4 (yellow), anchored to the inner membrane through VirB3 (orange), were present, whereas VirB11 (green) and VirD4 (salmon) were absent. Taken from [52]

1.3.2. Structural and functional analysis of the different components of T4SS.

1.3.2.1. Core complex.

VirB3/TrwM has highly conserved transmembrane motifs [106] and is located in the inner membrane for *A. tumefaciens*, RP4 and plasmid F homologues [113–115]. pVIR T4SS from *Campylobacter jejuni* presents a protein composed of two fused domains similar to VirB3 and VirB4 [116]. Considering that VirB4 is found on the cytoplasmic side of the inner membrane, VirB3 could form a complex with VirB4 allowing its anchorage to the inner membrane [106].

VirB6/TrwI. This protein family present low sequence homology with the exception of a conserved region situated approximately between the residues 170 and 205 from *A. tumefaciens* [115,117,118]. It is an integral, polytrophic inner membrane protein, with a medium size of 369 residues and at least five transmembrane regions [119]. VirB6 presents a periplasmic NTD and a cytoplasmic CTD linked by a central loop whose secondary structure is important for DNA translocation [119,120].

VirB6 proteins play an important role in the formation of the complex between VirB7 and VirB9. Its absence reduces the levels of VirB5, VirB3 and VirB7 homodimers, while VirB6 overproduction creates the formation of VirB7-VirB9 aberrant heterodimers [121–123]. VirB6 is located in the cellular poles of *A. tumefaciens*, its polar location depends on virB8 which suggests an interaction between both proteins [118,124].

VirB8/TrwG. VirB8, with a medium size of 246 residues, is a central T4SS component. It is a membrane protein with a cytoplasmic NTD, a transmembrane region and a long conserved periplasmic region [125]. One of its main characteristics is its sequential interaction with many other proteins from the channel [125–128]. All T4SS components have been detected in the *A. tumefaciens* poles during the first phases in T4SS assembly [118]. Nevertheless, many of them, with the exception of VirB3, VirB4 and VirB11 are widely distributed along all bacteria when they are VirB8 deficient. The mayor number of VirB8 interactions take place in the periplasmic region, but cytoplasmic NTD region and transmembrane region could also be implicated on specific interactions with others proteins and/or the substrate translocated [129].

VirB4 is essential during the first stages of the pilus biogenesis for VirB8 stabilization [128]. Also during the first stages VirB8 plays a main role for VirB9 and VirB10 interaction [126,127,130]. Moreover, VirB8 has a fundamental role in the posterior steps for the pilus formation via VirB4-VirB8-VirB5-VirB2 [128] and binds to translocated substrates in *A. tumefaciens* [131]. Therefore, this protein plays different roles. VirB8 forms dimers [132] and the crystallographic structure for VirB8 periplasmic region allowed the identification of the key domains for protein dimerization [133].

VirB7-VirB9-VirB10/TrwH-TrwF-TrwE complex. Cryo-microscopy structure of the central core complex (Figure 1.8) defines a heteromultimer of 14 subunits of VirB7-VirB9-VirB10 with an internal channel connecting the inner membrane with the external membrane [134]. It consists of two layers, which are either entirely (outer, O layer) or in part (inner, I layer) composed of two walls. The O layer has the cap region, which is 110 Å in diameter and 40 Å high, and the main body which is 185 Å in diameter and 60 Å in high. In the cap, the internal wall forms a 20 Å hole that tapers off to a 10 Å diameter constriction at the main body. In the main body, the internal wall forms a chamber that is 110 Å wide and 30 Å high. Internal protuberances are clearly visible at the bottom of the chamber; these leave a large opening of 55 Å (Figure 1.8). In the I layer, the two walls merge into a single wall near the base. The internal wall defines a chamber that is 110 Å wide and 60 Å high. This chamber tapper off at the bottom to a diameter of 55 Å, where it reaches the 30 Å high base (Figure 1.8).

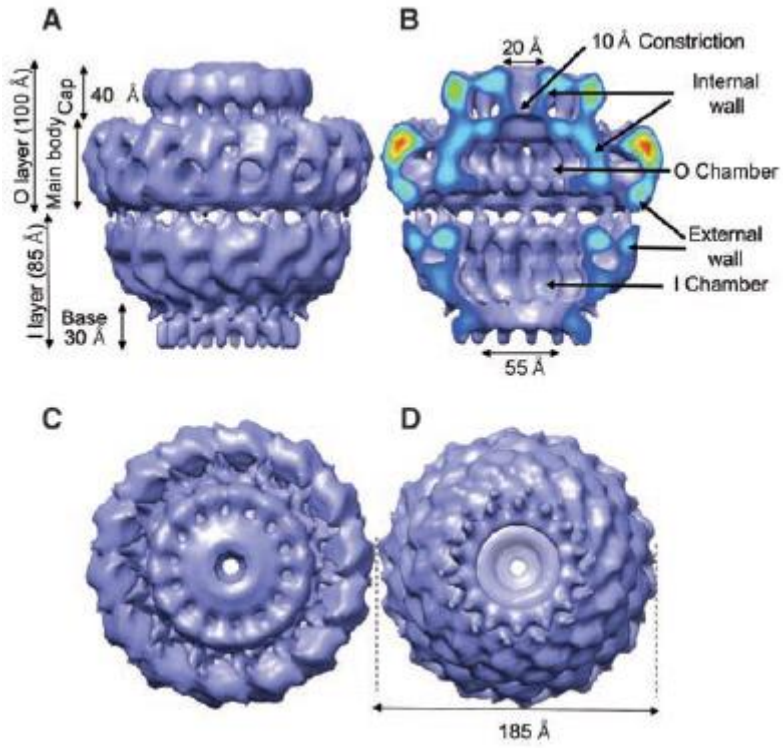

Figure 1.8. Cryo-electron microscopy structure of TraN/VirB7, TraO/VirB9, and TraF/VirB10 core complex from pKM101. (A) Side view. (B) Cutaway side view. Electron density is color-coded from red to blue to indicate regions of strong to weaker density, respectively. (C) Top view from outside the cell. (D) Bottom view from the cytoplasm. Taken from [134].

VirB9 protein family contains a peptide signal to be exported to the periplasm, where it is anchored to the outer membrane in complex with the small lipoprotein VirB7 (58 aa), which carries a typical lipoprotein signal sequences [135,136]. In *A. tumefaciens*, VirB9 and VirB7 are covalently linked by di-sulphure bridges between cysteine residues, being VirB7 the nexus of union with the pilus. However, such residues are not conserved in all T4SSs and they are not

essential for interaction, suggesting that perhaps this covalent union can be replaced by strong non-covalent protein interactions [137]. VirB9 not only plays an important role in pilus assembly, but also works as a modulator of translocation through the pore [138,139].

VirB10 is located mainly in the periplasm. It has a small cytoplasmic NTD tail, a transmembrane region and most homologs have a Proline-rich region that extends into the periplasm [140]. In addition to the interactions with VirB9 and VirB7, there is also evidence of interactions with VirB4 and VirB11 [141]. TrwE forms oligomers that interact with the coupling protein TrwB. When TrwB or TrwE transmembrane domains are removed, this interaction is lost, suggesting that the interaction takes place between the membrane or the periplasmic segments of both proteins [91]. VirB10 has also been described as a sensor of the ATPase activity of the coupling protein [140]. Furthermore, VirB10 seems to be an important and independent modulator between substrate secretion and pilus biogenesis [142].

The crystal structure of the outer membrane complex containing the entire O layer showed VirB10 as the only known protein crossing both membranes. Viewed from the top, the crystal structure contains a central hydrophobic ring of 76 Å in diameter with a 32Å pore in the middle (Figure 1.9). The differences between cryo-EM and X-ray structures (outer opening of 20 and 32 Å, respectively), could suggest different energetic states, where VirB10 would modulate the conformation of the channel, allowing or not the passage of substrates [131,143], since VirB10 presents energy-dependent conformational changes [140].

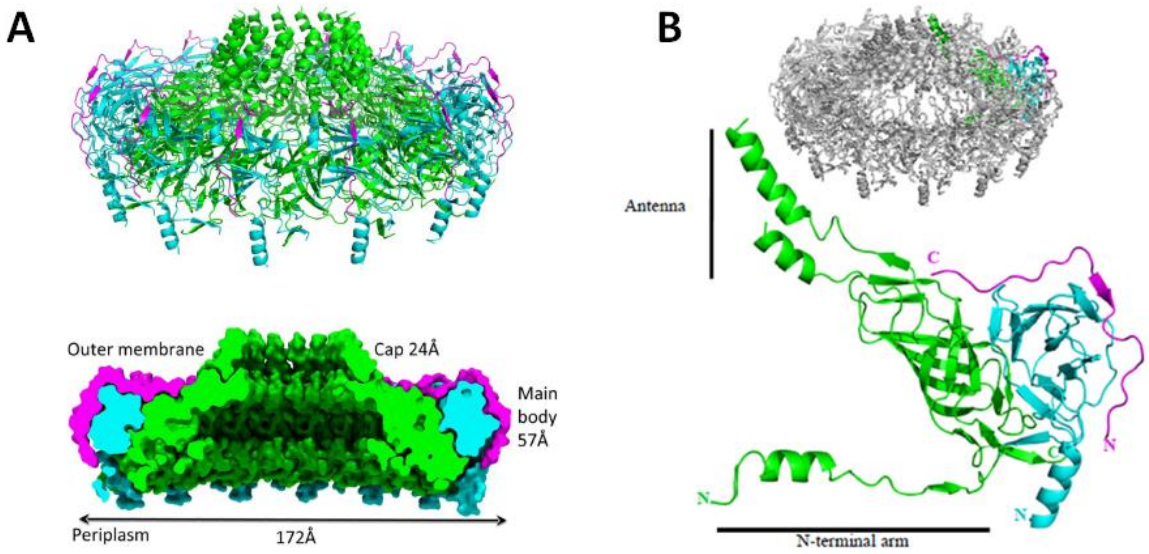

Figure 1.9. Crystal structure of the outer membrane core complex from pKM101. The core complex consists of 14 copies of each of the three proteins assembled. TraN/VirB7, TraO/VirB9 and TraF/VirB10 subunits are colour-coded magenta, cyan and green, respectively. **(A)** Ribbon diagram (upper panel) and space-filling cut-away (down panel) of the tetradecameric complex. **(B)** Ribbon diagram of the heterotrimer unit formed by TraN/VirB7, C-terminal domain from TraO/VirB9 and C-terminal domain from TraF/VirB10 is shown. The insert locates the shown heterotrimer within the tetradecameric structure. Taken from [143].

1.3.2.2. VirB1/TrwN.

VirB1 has great structural similarities with proteins of the lytic transglycosylases family [144,145]. In fact, proteins from this family have muramidase activity, which possibly favours a better assembly of the T4SS multi-protein complex [146]. These proteins have a mean size of 238 residues [117] and contain peptide signals to be exported to the periplasm. In the case of *A. tumefaciens*, VirB1 experiences a processing on its Ct, generating a product (VirB1*) that is secreted [147].

Although VirB1 is a member of a widely distributed family that is presented in T2SS, T3SS and T4SS, as well as in bacteriophage entry systems and DNA incorporation systems, it is not essential for T4SS formation. However, the assembly of the complex is affected in its absence [121,146,148]. In some cases, the lack of VirB1 can be compensated by proteins that present a similar activity [149,150].

1.3.2.3. Pilus.

VirB2/TrwL. VirB2, a small hydrophobic protein known as pilin, is the major component of the pilus [121,138,151]. The VirB2 protein family presents a low degree of homology, although there are different Gly residues conserved. In some cases, pilins are processed into cyclic polypeptides [152], which serve as bricks for pili construction [151,153]. In some others, propylene molecules are located in the inner membrane where they suffer a cutting process by peptidases at the N-terminal region and a subsequent acetylation. Thus, the mature pilin could form a reservoir [115,154] in the base of the pilus during pilus biogenesis [155]. Recently, high-resolution structures have revealed an integral association between the pilin subunit and a phospholipid molecule, which may facilitate DNA transport [156,157]. VirB2 plays an important role in the binding of the pilus to the surface of host cell [158,159].

VirB5/TrwJ. VirB5 is considered the minor component of the pilus. It is exported to the periplasm, where interacts with VirB2 but finally it will be located extracellularly as part of the pilus [128,160,161]. This protein consists of three rigid α-helices and a flexible, globular appendix that could be a site of interaction with other proteins. The C-terminal region is exposed. Changes in that region have an important impact on the ability to select the recipient cell [162]. The exact position of this protein in the pilus is not completely clear. VirB5 could be at the *apix* of the pilus or it could reside inside the structure, being only observed at the end of the broken pili [162,163]. Its most likely function is adhesion, allowing contact of the pilus with specific receptors in the host cells [97,164–167].

1.3.2.4. Molecular motors of the system.

1.3.2.4.1. VirD4/TrwB.

The coupling proteins (CP) can be considered as an element of the T4SS. The term coupling protein was coined after obtaining genetic evidence that they serve as a link between relaxosome and T4SS [168]. However, they are not involved in DNA processing reactions [69,169,170] or in the production of the pilus [60,171]. They are present in all the conjugative systems and are essential for the translocation of substrate (even in the absence of DNA [49]) but dispensable for the biogenesis of the pilus [172].

TrwB from conjugative plasmid R388 is the best characterized coupling protein. It has 507 residues and a molecular weight of 56 kDa. It is a DNA-dependent ATPase [173] that interacts not only with DNA, but also with the relaxosome through TrwA protein [74] and with the channel of secretion through TrwE protein (VirB10 homologue in R388) [91]. In some cases, CP can be exchanged from one system to another, being very specific with the relaxosome that they recognize, but not so much with the T4SS [174,91].

The crystallographic structure of the TrwB soluble domain showed an almost spherical hexameric structure with a central channel of a diameter of 20 Å and an external pore of 8 Å [175,176]. TrwB is anchored to the cytoplasmic side of the IM by the N-terminal transmembrane domain. However, the function of the transmembrane domain (TMD) is not only anchoring the protein to the membrane. TrwB presents a greater stability against different denaturing agents that its cytoplasmic derivative [177,178]. TrwBΔN70, the soluble domain of TrwB that lacks the first 70 residues from the N-terminal domain, behaves like a monomer in solution, while TrwB forms hexamers [179]. The TMD also affects the specificity of nucleotide binding [180,181]. The cytosolic motif includes conserved Walker A and a Walker B motifs for nucleotide binding [61]. These motifs are essential for conjugation, since a TrwB mutant with a single amino acid alteration in the ATP-binding Walker A motif (K136T) was totally deficient for transference [182]. Proteins and DNA molecules have the same molecular requirements for translocation, with residues at both ends of the TrwB channel controlling the opening-closing mechanism [183]. In general, N-terminal of the TMD is important for the interaction with T4SS, protein oligomerization and cellular location, whereas the cytoplasmic C-terminal region is necessary for the interaction with the components of the relaxosome and for ATPase activity [184–191].

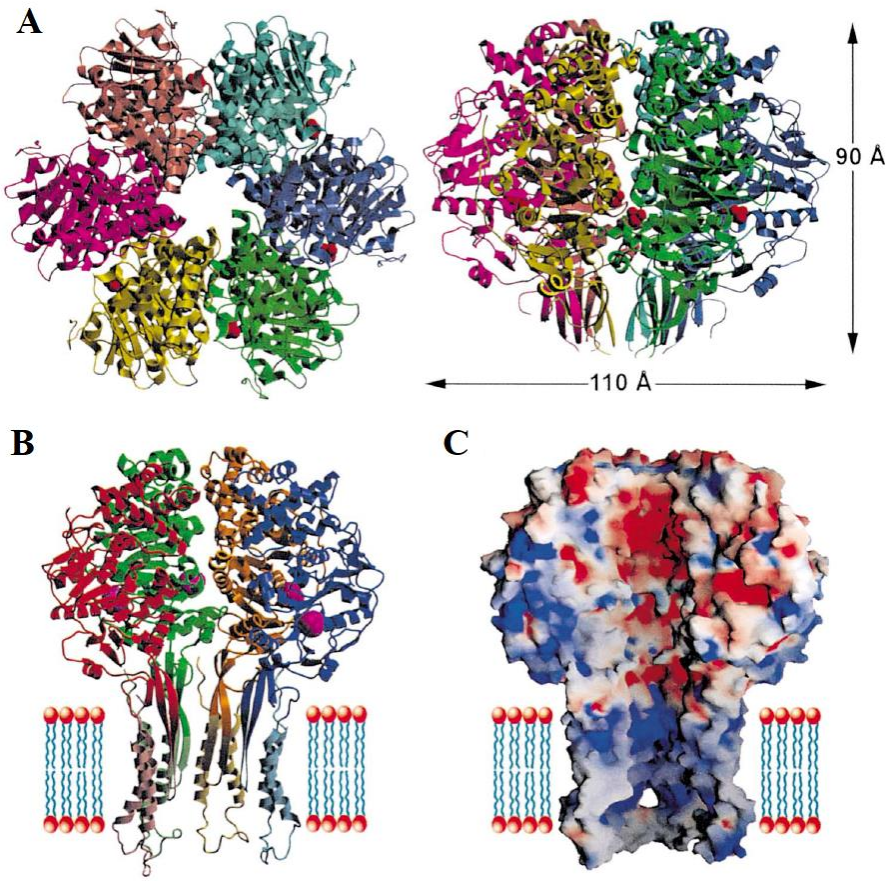

Figure 1.10. **Structural characteristics of TrwB**. **(A)** Ribbon representation of TrwBΔN70 homohexamer particle, as viewed from the cytosol in an axial view (left) and from a side view (right). The dimensions of the particle are indicated. **(B**) Ribbon plot of four TrwBΔN70 monomers within a particle with the modelled transmembrane segments (residues 1-70). **(C)** Same as B, but showing the corresponding Connolly surface to highlight the central channel that connects the cytosol (up) with the periplasm (down) across the bacterial inner membrane. Taken from [192].

TrwB shows a striking similarity with other hexameric ATPases of the RecA family, like F1-ATPase, T7 helicase, Ftsk or SpoIIIE [173,193–199], suggesting that TrwB works like a molecular motor that uses the energy released from the hydrolysis of ATP to pump single-stranded DNA through its central channel [198].

Recently, our research group have shown that TrwB binds DNA substrates with specific structure, being G-quadruplex DNA its preferred substrate [200]. TrwB could act by solving this type of secondary structures after DNA processing during conjugation or, alternatively, these structures could act as loading site for this motor. More studies are needed to try to clarify the *in vivo* function that these G-quadruplex structures have on TrwB activity.

It is also interesting to note the sequence identity and structural similarity between the C-terminal domain (the motor domain) of TrwK (VirB4) and TrwB [201].

1.3.2.4.2. VirB4/TrwK.

Proteins from the VirB4 family are very conserved and, unlike other components of the system, are present in all T4SSs [59]. These proteins play an essential role in the biogenesis of pilus, virulence and substrate transport [202]. VirB4 is the largest protein that constitutes the T4SS (between 600 and 900 amino acids) and it is formed by two structural domains, N and C-terminal, well differentiated.

The N-terminal motif is the least conserved and could play an important role in the oligomerization of the protein and/or in the binding to the IM. There was some controversy about its location in the membrane. Bioinformatic models predicted several transmembrane segments, data consistent with studies of susceptibility to proteases [202,203]. Nevertheless, there was also evidence of homologues like TraCF and TrhCR27 that are associated with the membrane through protein interactions with other subunits [204,205]. The most decisive test in favour of the hypothesis that TrwK is not a protein anchored to the inner membrane by transmembrane segments, could probably be the fact that it was possible to purify TrwK without using detergents [206]. TrwK membrane binding could be mediated by the interaction with the integral membrane protein VirB3 [116,206].

The C-terminal domain, of about 400 amino acids, constitutes the motor domain of the protein. It is the most conserved and contains the catalytic motifs Walker A and Walker B, characteristic of the RecA family. For a few years, there was also controversy about the ability of this protein to hydrolyse ATP, but the presence of Walker motifs that were essential for its functionality [128,202,207] suggested the ATP hydrolytic function. *In* vitro, TrwK hydrolyses ATP in the absence of its potential substrates and any other T4SS components [206]. Mutations in these motifs in TrbE protein from plasmid RP4 showed that are essential for the production of the pilus and DNA transfer [202]. A mutation in the Walker B motif of TrwK from the plasmid R388 totally inhibited the ATPase activity, as well as the conjugation process [206]. The last 51 residues in this C-terminal domain form 3 α-helices that give an important regulatory role in the ATPase activity of this protein family [208].

The homology between the C-terminal domain of VirB4 proteins and the coupling protein TrwB, suggests that this motor domain of VirB4 can also form a heterohexamer with TrwB [201]. In fact, heterohexamer formation between the two proteins was proved when the ATPase activity of TrwB was affected by the presence of a TrwK mutant that lacked the ability to hydrolize ATP [209]. There was also some controversy regarding the oligomeric state of this protein family. The membrane fraction of TraB from pKM101 was found to form stable dimers, while the soluble fraction could form hexamers [210]. However, TrwK is a soluble hexameric protein in presence of acetate salts [206]. Its hexameric nature was evident also by bioinformatics predictions [201], gel filtration analysis [128] and by sedimentation velocity [206].

TrwK structure has been obtained by electron microscopy (EM) (Figure 1.11), being this the first structure of the protein in its hexameric state [209]. The crystallographic structure of the motor domain of the VirB4 homologue of *Thermoanaerobacter pseudethanolicus* has confirmed a structural homology with TrwB/VirD4 proteins [211]. In addition, an evolutionary relationship has been suggested between the motor domains of these two proteins and various translocases of DNA [209,212].

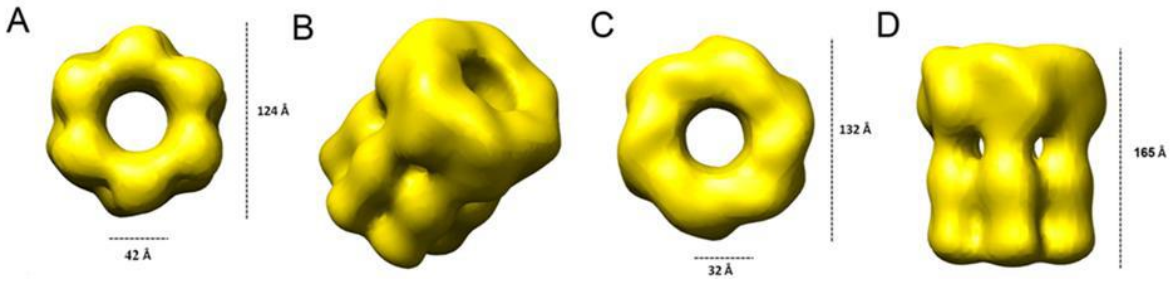

Figure 1.11. 3D reconstruction of TrwK. Final volume obtained by projection matching and angle refinement and low-passed filtered to 22Å. Bottom (A), oblique (B), top (C) and side (D) views of the volume. The bottom (A) and top (C) views, corresponding to the C-terminal and N-terminal ends of the protein, respectively, differ in size (124 Å and 132 Å, respectively), and the longitudinal dimension is 165 Å. Modified from [209].

The presence of VirB4 is important for the stabilization of the rest of the components of the T4SS [128]. VirB4 is responsible for dislocating pilin subunits (VirB2) from the IM to the periplasm [213]. VirB4 also interacts with the other two ATPases of the system, VirD4 and VirB11 [201,209,214–216]. In *A. tumefaciens*, the secretion pathway for the DNA substrate has been defined. The intermediaries and the order of transfer of the substrate would be the following: VirD4-VirB11-VirB6-VirB8-VirB9 and VirB2 [131]. Mutating the Walker A motif of VirB4 blocks the passage of substrate at the point mediated by VirB11 [214]. Recently, T4SS encoded by R388 has been reconstructed by electron microscopy (EM). The structure showed a 3 MDa nanomachine that spans the entire cell envelope. The inner membrane complex is dominated by a battery of twelve VirB4 ATPase subunits organised as side by side hexameric barrels [111].

1.3.2.4.3. VirB11/TrwD.

The VirB11 protein family is widely distributed in conjugative systems and pathogenic systems of Gram-negative bacteria [98]. VirB11 is required for both, translocation of substrate [131] and T4SS assembly [217]. However, unlike the VirB4 family that is present in all T4SS, there are systems that do not have a VirB11 homolog. Some examples are the ComB capture systems of *H. pylori*, the conjugative system of plasmid F, or the majority of Gram-positive bacteria systems [110,218].

HP0525, the ViB11 homolog from *H. pylori,* was the first T4SS component whose structure was resolved by X-ray [219], revealing the hexameric nature of the protein, with a central chamber that is open on one end and closed on the other one. The charge distribution indicated that one of the protein faces could be associated with the inner membrane.

Among the members of this family, we find four motifs with a high degree of conservation: the Walker A and B motifs for nucleotide binding and hydrolysis, the His box and the Asp box [220,221]. Mutations in the Walker A motif suppress both, the substrate transfer and the pilus formation [221–223]. The His and Asp boxes are also important for pilus formation, as demonstrated in PilQ mutants (VirB11 homologue in R64) [224]. VirB11 mutants from *A. tumefaciens* can affect the production of T-pilus without interfering with substrate transfer [217].

Members of the VirB11 family are proteins that have no obvious transmembrane regions, but they are closely associated with the IM. They are in a dynamic equilibrium between the cytoplasmic form and the form associated with the IM. This dynamic behavior could regulate its activity [220,225]. Although VirB11 proteins have ATPase activity by themselves, this activity can be stimulated by interacting with membrane lipids, suggesting that their association with the membrane is biologically relevant [220,221]. Results obtained from reconstruction experiments in liposomes and HP0525 structure from *H. pylori* suggest that TrwD could interact with the lipid bilayer through hydrophobic regions in its N-terminal domain, which would lead to a certain degree of destabilization of the membrane [223,226].

With respect to the oligomeric state, VirB11 from *A. tumefaciens* is able to associate with itself [227] and electronic microscopy revealed that TrbB from RP4, HP0525 from *H. pylori* and TrwD from R388 form hexameric rings [220,223]. In addition, structural studies in homologs, such as HP0525 from *H. pylori* and VirB11 from *B. suis,* provided evidence that these ATPases are assembled as homohexamers formed by two stacked rings [219,228].

The proteins of this family share a common structural organization that consists of two domains, an N-terminal domain (NTD) and a catalytic C-terminal domain (CTD) with ATPase activity, connected by a flexible linker. The crystallographic structures of HP0525 and VirB11 revealed a pivoting movement of the NTD domain over the CTD domain through the linker, without affecting the structure [228]. Although the global structure is not affected, there are differences in the interaction between contiguous subunits that affect the nucleotide binding site. Thus, in HP0525, this site is coordinated between the NTD and the CTD of the same subunit, while in VirB11 from *B. suis* it is located between the NTD of a subunit and the CTD of the next subunit. The direct consequence of this difference is that the ATPase activity of VirB11 of *B. suis* would be dependent on the oligomerization, while HP0525 might be able to hydrolyze ATP independently of the hexamer formation [229].

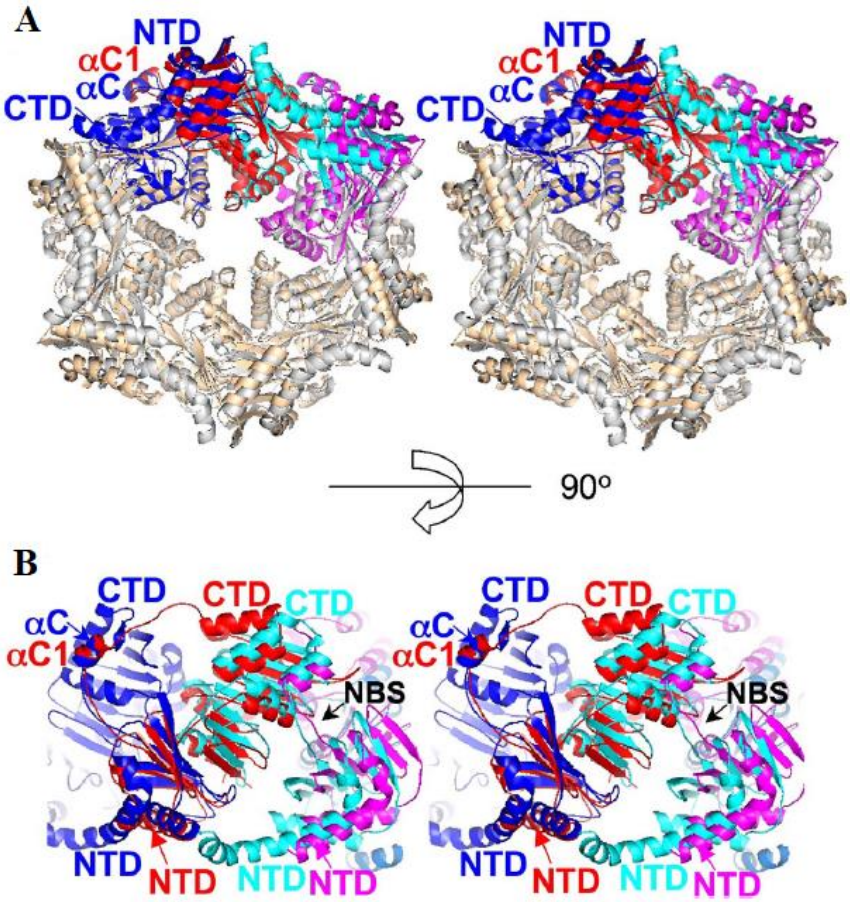

Figure 1.12. Comparison of VirB11 from *B. suis* and HP0525 from *H. pylori* hexameric structures. (A) Two contiguous subunits from VirB11 (red and magenta) and HP0525 (blue and cyan) are shown as well as the remaining subunits in wheat for VirB11 and grey for HP0525. **(B)** Closer view of the subunit-subunit interface zooming in on the subunits highlighted in blue and cyan (HP0525) and red and magenta (VirB11). The orientation is rotated 90˚ along the horizontal axis of the hexamer shown in A. The nucleotide binding site of one monomer of HP0525 is indicated (NBS). Taken from [228].

VirB11 homologs belong to the traffic ATPase superfamily, which includes ATPases from the T2SS (GspE), ATPases involved in the synthesis of type IV pilus and ATPases involved in the flagellum assembly in archea [230]. All members of the secretion traffic ATPase superfamily are characterized by forming hexameric toroidal rings, where the subunits interact with each other in a very narrow way and consist of an NTD domain and another CTD separated by a linker. Both, the NTD and the CTD domains, are in general structurally conserved, despite the poor sequence identity among homologs belonging to this family [231].

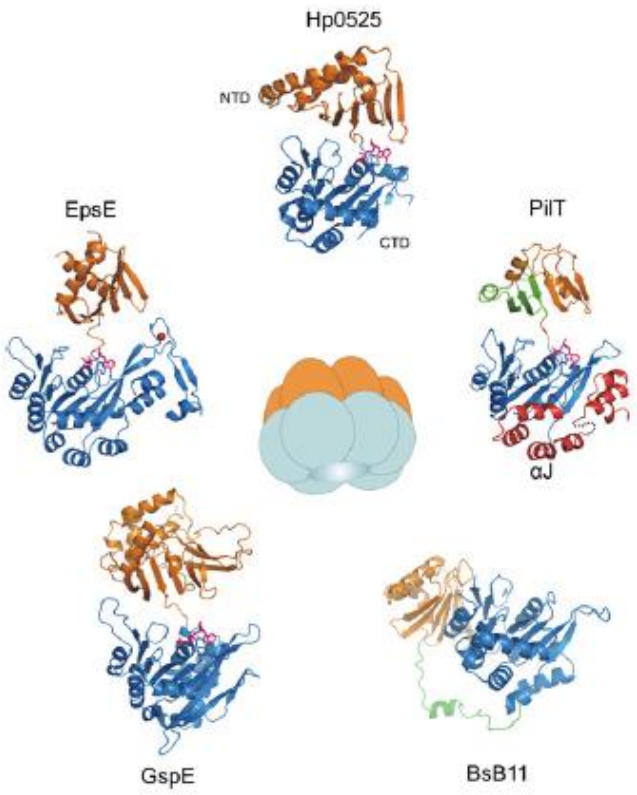

Figure 1.13. **Crystallographic structures of five traffic superfamily ATPases**. HP0525 from *H. pylori* (PDB ID: 1g6o), PilT from *A. aeolicus* (PDB ID: 2ewv), VirB11 from *B. suis* (PDB ID: 2gza), GspE from *Archaeglobulus fulgidus* (PDB ID: 2oap), and EpsE from *V. cholerae* (PDB ID: 1p9w). NTDs and CTDs are colored in orange and blue, respectively. The schematic in the center illustrates the toroidal hexameric structures typically adopted by these ATPases. For PilT additional secondary structure elements in the NTD and CTD are shown colored in green and red, respectively. Taken from [232].

The study of both the ATPase HP0525 from T4SS of the human pathogen *H. pylori* [229] and GspE from T2SS of *A. fulgidus* [233], combined with crystallographic, analytical ultracentrifugation and small-angle x-ray scattering (SAXS) studies, have shown that members of this traffic ATPase superfamily are dynamic hexameric rings that suffer large readjustments in the disposal of their domains due to ATP binding and hydrolysis. Based on these studies, a model of action has been proposed for GspE that can be extrapolated to all members of this protein family. On the other hand, PilT could suffer great conformational changes derived from ATP binding and hydrolysis, as well as GspE and HP0525, which would make possible the displacement of pilus subunits dozens of amstrongs towards their final location. This hypothesis was corroborated by resolving the PilT structures of *P. aeruginosa* in its absence and presence of nucleotides AMP-PNP [234].

Biochemical and structural studies of HP0525 from *H. pylori* have provided details about the dynamism in the proteins belonging to the VirB11 family. HP0525 has conformational changes that depend on the nucleotide binding. While in the structure resolved with ADP the six

monomers have this nucleotide, in the structure with ATP-γS only one of the two monomers in the asymmetric unit is occupied [229]. In the absence of nucleotides, the ring formed by the CTD domains remains immobile, maintaining contacts between subunits in the hexameric structure, whereas the NTD domains are flexible and show several conformations that cause asymmetries in the ring. These results lead the authors to propose a catalytic mechanism for this family of proteins. The union of three molecules of ATP would induce a conformational change of three NTDs towards a rigid conformation. Later, the hydrolysis of these molecules together with the binding of three other molecules of ATP to the remaining free subunits, would block the hexamer in a rigid and symmetric structure. When all nucleotides are hydrolyzed and released, the structure relaxes and the hexamer returns to its apo nucleotide-free state [229]. Additional insights into the catalytic mechanism of the secretion ATPase superfamily have found that the ATP turnover of TrwD is down-regulated by physiological concentrations of magnesium. This regulation is exerted by increasing the affinity for ADP. Therefore, this inhibitory role is independent of ATP concentration. Circular dichroism and limited proteolysis analysis indicate that magnesium induces conformational changes in the protein that promote a more rigid, but less active, form of the enzyme [235].

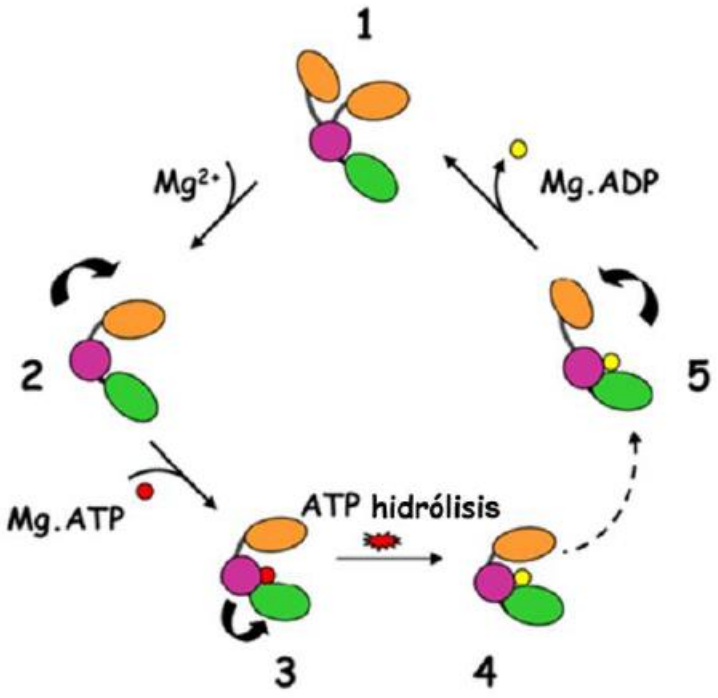

Figure 1.14. Catalytic mechanism proposed for VirB11 ATPases. *Step 1*, the nucleotide-free apo form would be flexible with the NTD (orange) and CTD (magenta/green) in equilibrium between an open and closed conformation. *Step 2*, high Mg^{2+} concentrations (similar to the free Mg^{2+} found in bacteria) would induce a conformational change that would be followed by MgATP binding (*Step 3*), which, in turn, would promote a conformational change in the CTD. After ATP hydrolysis, an inhibited MgADP state (*Step 4*) would be stabilized, resulting in an ATP turnover decrease. Upon specific signal (for instance, substrate binding or release), the MgADP-inhibited state would be unlocked (*Step 5*), and hence, the cycle could resume with ADP release, returning to the initial apo form. Taken from [235].

Interactions between VirB11, VirB4, and VirD4 were mainly inferred from two-hybrid and co-immunoprecipitation assays [141,214,215]. More recently, our group reported direct evidence for interactions of TrwD with TrwK and TrwB proteins [236]. Furthermore, replacement of TrwD by its homolog in plasmid pKM101 (TraG) or *Bartonella tribocorum* (TrwD) does not affect the interactions with TrwK, whereas replacement by its homolog in RP4 (TrbB) disrupts it. In contrast to TrwD and TraG, which have a large linker domain similar to that of *B. suis* VirB11, the linker domain of TrbB is short, like that of *H. pylori* HP0525. These results suggest that this linker domain is crucial in establishing VirB11-VirB4 interactions. Interestingly, TrwK-TraG binding is not sufficient to promote R388 conjugation, which indicates that more specific interactions are required for DNA transfer. Moreover, TrwD is able to interact with TrwB, which further supports the idea that VirB11 proteins act as a molecular switch by regulating pilus morphogenesis and substrate transport steps in T4SSs [236].

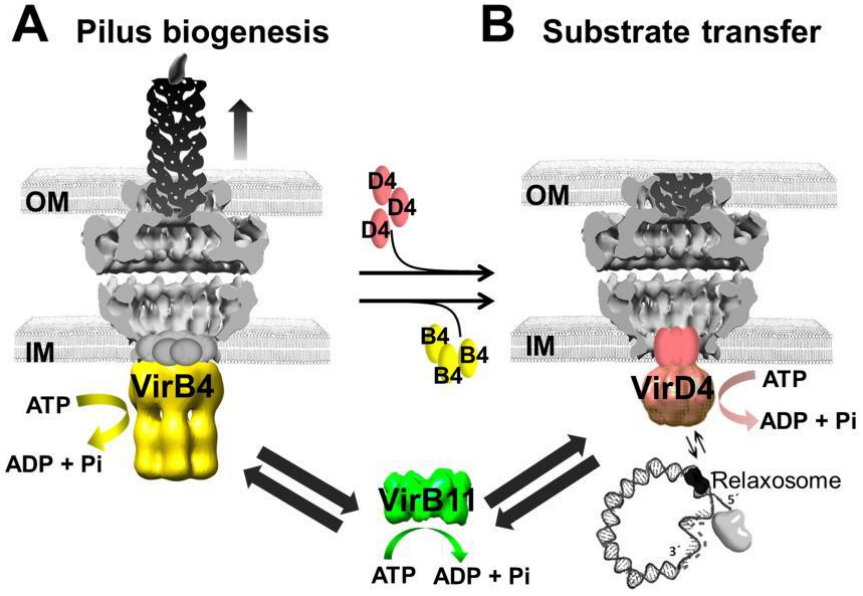

Figure 1.15. Model of VirB11 acting as a switch between pilus biogenesis and DNA transport. (A) During pilus biogenesis, VirB4/TrwK (yellow) is associated with the inner membrane (IM), at the base of the core complex (gray). VirB11/TrwD (green) interacts with VirB4/TrwK, modulating its pilin dislocase activity. Successive polymerization reactions of pilin monomers would promote pilus growth. **(B)** In substrate transfer, VirB11/TrwB (salmon) displaces VirB4 from the base of the cannel. OM, outer membrane. Taken from [236].

The role of VirB11 proteins in substrate transport is not clear yet. A possible role as chaperone in the traffic of effectors through T4SS has been postulated for this family of proteins. It could use the energy release from ATP hydrolysis to facilitate the movement of proteins deployed through T4SS [223,237]. This hypothesis is supported by the fact that translocation through T4SS requires the unfolding of the protein substrate, due to the inner diameter of the secretion channel [238] and similitudes with other secretion systems [239]. However, further biochemistry and structural studies of this family of proteins are needed to determine the biological function and the mechanism by which they transfer the energy released from their activity to the performance of a certain work.

1.4. Clinical relevance of the bacterial conjugative process.

1.4.1. Antibiotic resistance dissemination.

The clinical relevance of the conjugative process resides in their main role for the rapid adaptation of bacterial populations to a strong selective pressure, as in the case with antibiotics [240]. This swift adaptation usually does not occur by mutation of the menaced populations, but mainly by acquisition and dissemination of antibiotic resistance genes (AbR) by horizontal mobile genetics elements (MGE) among many different genera and species of bacteria [241,242].

Since Alexander Fleming discovered penicillin in 1928, antibiotics have saved thousands of lives [243]. Human intensive application of antibiotics conduced to the emerge of AbR, which are rapidly disseminated through the biosphere, as a result of a large selection pressure [244]. It is thought that AbR arose originally as a self-protection mechanism of the producer organisms [245]. Nowadays, more than 20,000 potential resistance genes of nearly 400 different types have been predicted from available bacterial genome sequences [246].

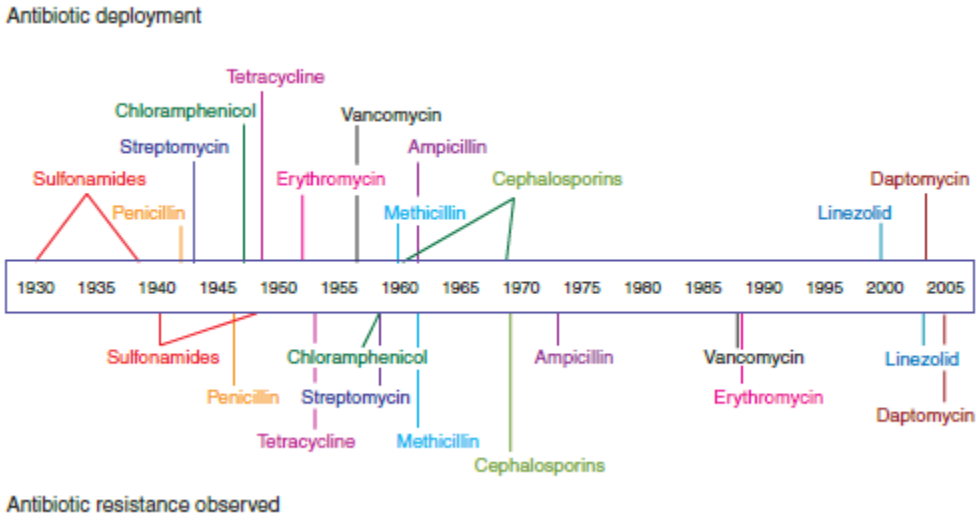

Figure 1.16. Schematic timeline of antibiotic deployment and the evolution of antibiotic resistance. Few years after a new antibiotic is commercially adopted (Above the timeline), clinically significant resistance to that treatment is detected (below the timeline). Taken from [247].

Resistance mechanisms emerge rapidly and render new antimicrobial therapies ineffective [247]. Bacteria resist antimicrobial action by five main mechanisms [248]:

Bypass pathways: bacteria can avoid inhibited steps using a different way to produce the target compound.

Overproduction of target: bacteria can also produce higher amounts of the target, allowing antibiotic-free targets to act normally.

Intracellular target modification: the site where an antibiotic acts, such as the ribosome, can be altered to avoid antibiotic action. For example, the acquisition of a plasmid or transposon that codes for a resistant dihydrofolate reductase confers trimethoprim resistance to bacteria [249].

Decreased penetration/increased efflux: intracellular concentration of a drug can be diminished either by reducing membrane permeability to avoid its entry, as shown in *Pseudomonas aeruginosa* [250] or by actively pumping the antibiotic outside the cell to eliminate, for instance, tetracyclines, chloramphenicol and fluoroquinolones [251].

Enzymatic inactivation or modification: antibiotics can also be altered by specific enzymes to prevent their action. For example, an specific β-lactamase, an enzyme able to hydrolyse the penicillin β-lactam ring, prevents penicillin action against bacterial cell-wall synthesis [252]. This was the first reported mechanism of AbR, which was identified in *Escherichia coli* even before penicillin was introduced as therapeutic agent [253].

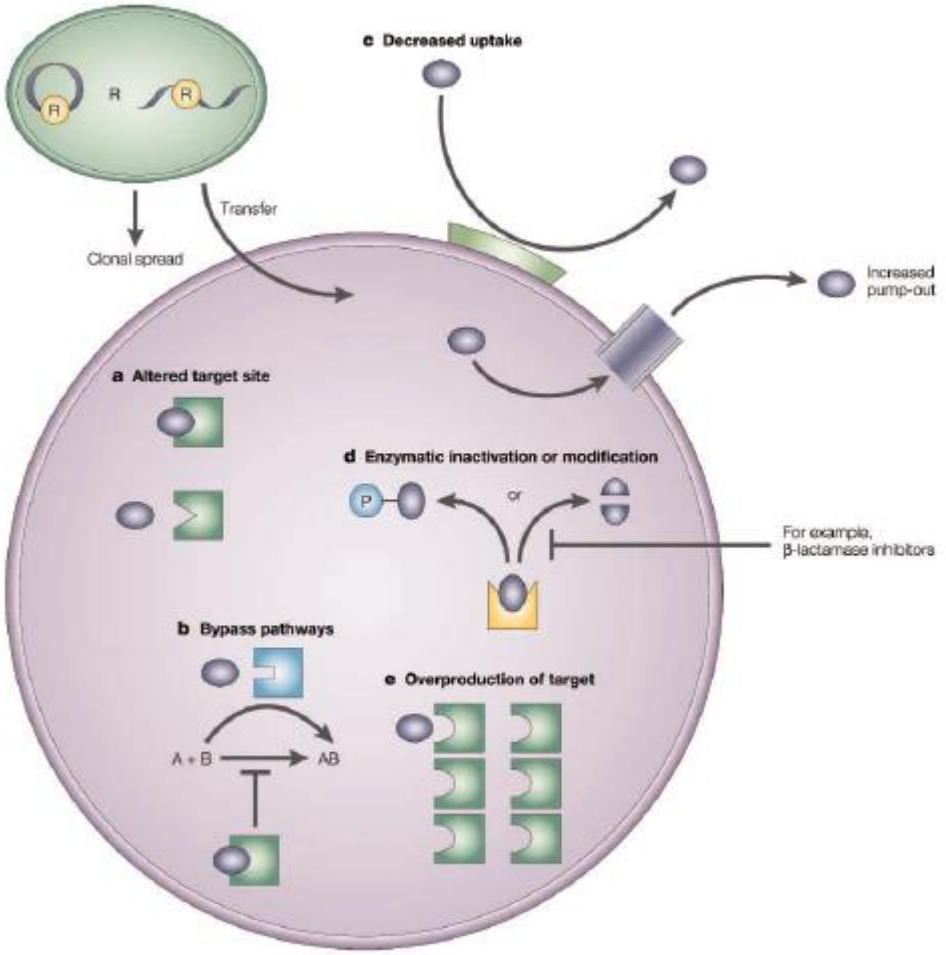

Figure 1.17. Mechanisms of genetic resistance to antibiotics. A summary of the main mechanisms that bacteria use to resist antibacterial drugs is shown. a) The site of action (enzyme, ribosome or cell-wall precursor) can be altered. b) The inhibited steps can be by-passed. c) Bacteria can reduce the intracellular concentration of the antimicrobial agent, either by reducing membrane permeability or by active efflux of the agent. d) The drug can be inactivated. e) The target enzyme can be overproduced by the bacteria. Taken from [248].

The global crisis with AbR is even worse because of the high cost for developing new antimicrobial compounds. These drugs will be sold for short treatments and resistance will rapidly emerge. Therefore, pharmaceutical companies prefer to focus on developing drugs for chronic conditions, such as diabetes, obesity, or high blood pressure, which provide higher economic benefits [254].

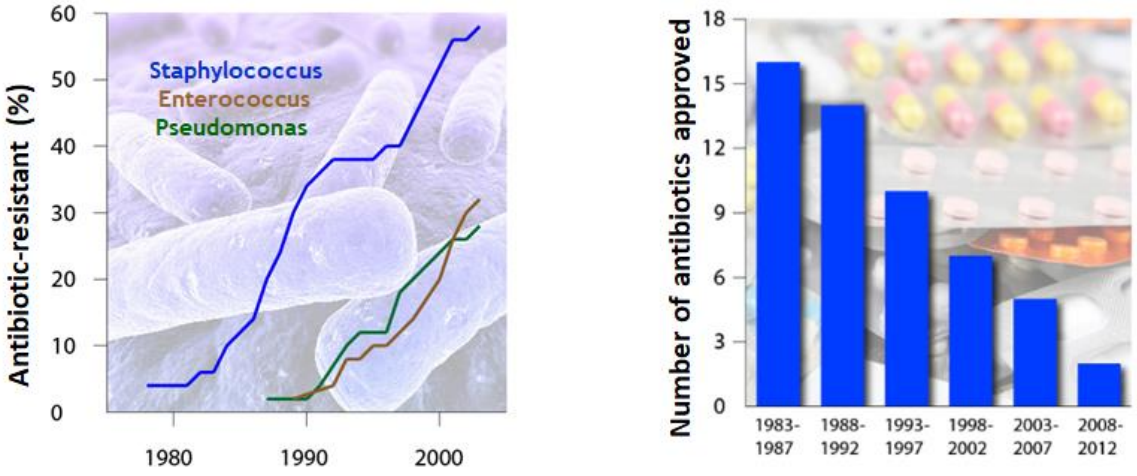

Figure 1.18. Antibiotic resistance vs new antibiotics. **(Left)** Proportion of clinical isolates that are resistant to antibiotics are increasing significantly. *Staphylococcus aureus* methicillin-resistant (blue), *Enterococcus* cancomycin-resistant (brown) and *Pseudomonas aeruginosa* fluoroquinolone-resistant (green). **(Right)** Number of new antibiotics approved has fallen sharply in the past few years. As bacterial infections grow more resistant to antibiotics, companies are pulling out of antibiotics research and fewer new antibiotics are being approved. Modified form [255].

Currently, antimicrobial resistance causes nearly 700,000 annual deaths worldwide [254,255]. This alarming situation demands solutions. Therefore, alternatives to conventional antibiotics are emerging. For example, inhibitors of resistance mechanisms, such as efflux pumps [256], or β-lactamase inhibitors [257], in combination with antibiotics. However, bacteria evolve rapidly to counteract them and β-lactamases resistant to clavulanic acid have also appeared [258]. Inhibitors of bacterial virulence are promising alternatives with an advantage over antibiotics in that selection for resistance might not occur because the growth of the pathogen would not be impaired [259]. Thus, anti-toxin compounds [260], adhesion inhibitors [261,262], or transcriptional regulators of virulence genes [263], including quorum quenchers [264], are some of the strategies proposed to block virulence.

Additional developing lines of attack are the search of inhibitors of plasmid replication and stability [5,265,266], antimicrobial peptides [267], bacterionics [268], inhibitors of iron metabolism [269], antimicrobial polymers [270], enzybiotics [271], antisense antibiotics [272], antimicrobial nanoparticles [273], light based anti-infectives [274], vaccines [275], probiotics [276], or phage therapy [277], among others.

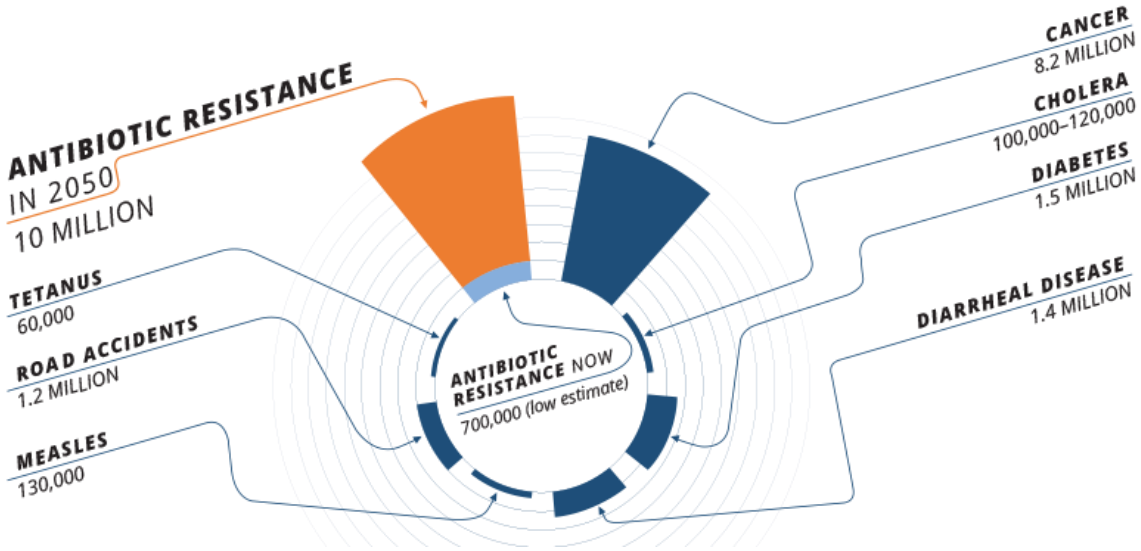

Figure 1.19. Estimation of deaths caused by antibiotic resistant infections. Worldwide number of deaths attributable to antibiotic resistance every year compared to other causes of death nowadays (blue) and estimated for year 2050 (orange). Taken from [255].

1.4.2. Inhibitors of bacterial conjugation (COINs).

Bacteria have diverse mechanisms to regulate DNA horizontal transfer through conjugation. While narrow host range (NHR) plasmids, such as F plasmid, rely on many host-encoded natural barriers that act at DNA, RNA, or protein level [278], broad host range (BHR) plasmids, such as R388 plasmid, regulate their transfer mostly through plasmid-encoded repressors [279].

Among host barriers, there are two main mechanisms. The innate immune system known as restriction-modification (RM), where a restriction endonuclease (REase) recognizes and cleaves foreign DNA and a methyltransferase (MTase) confers protection to host genome by methylation [280–284]. The adaptive immunity known as CRISPR-Cas (clustered regularly interspaced short palindromic repeats); sequences from the invading genome are integrated into the CRISPR array, transcribed and processed to generate small CRISPR RNAs (crRNAs) that serve as a guide to cleavage the invading DNA by Cas nucleases. [285–289].

Plasmid-encoded barriers are very diverse [290,291]. The most conserved are entry exclusion, which prevents competition among identical plasmids, uneconomical excess of DNA transfer and death by zygosis (membrane damage caused by excessive cell contact) [292–294]. Surface exclusion reduces the ability to form stable mating aggregates, whereas entry exclusion inhibits DNA transfer [295,296]. Fertility inhibition systems are also very common to reduce the conjugative transfer [297–300].

In recent years, interest in barriers that prevents plasmid dissemination has grown enormously, since they are a potential tool to fight against the antibiotic resistance dissemination. Efforts have not only been focused on natural barriers, but artificial barriers have also been studied. Conjugation inhibitors (COINs) have been employed to target specific components of the conjugation machinery [301]. Nevertheless, a variety of compounds such as heterocyclic compounds, intercalators, acridine dyes or quinolones considered to be COINs were later revealed as inhibitors of different cellular processes [15,302–305]. For instance, bisphosphonates were first described as relaxase-specific inhibitors [306], but then reappraised to act as chelating agents [302]. The increased sensitivity of *E. coli* containing F plasmid to bile salts and sodium dodecyl sulfate could be other examples of this effect [307]. A similar behavior was found by overexpressing RP4 genes, which caused an enhancement of cell permeability [308]. Similarly, several antimicrobial drugs have been described as inhibitors of plasmid conjugation, but their lethal effects in donors and recipients or the absence of COIN activity in non-growing bacteria suggested that these compounds interfere with essential bacterial functions rather than recognizing a specific plasmid target [309,310].

Due to its key role in plasmid conjugation, relaxases have been considered as potential targets for inhibitors. Relaxase activity of F plasmid TraI was targeted *in vitro* by bisphosphonates, such as etidronate (Didronel) and clodronate (Bonefos). They are a set of small molecules that could apparently interfere with relaxase active site by mimicking a covalent phosphotyrosine intermediate [306]. A bottom-up approach, based on crystallographic data and *in vitro* nicking activity of wild type and mutants of TraI relaxase, was used to find compounds that could selectively block its activity. Two of the most potent compounds acting at nanomolar levels were promising hits because they had already been approved to clinically treat bone loss, a fact that would facilitate their inclusion into the market. However, besides the inhibition of F transfer *in vivo*, they also caused unexpected selective death of bacteria containing both a catalytically active TraI and F plasmid. This result was investigated concluding that bisphosphonates may act as mere chelating agents which could affect several other metal-dependent cellular processes [302]. An alternative method to inhibit specifically the conjugative relaxase consisted of the expression of specific single chain intrabodies against the relaxase TrwC of conjugative plasmid R388 [83]. Expression of these intrabodies in the recipient cell prevented the accretion of the conjugative plasmid. However, the usefulness of intrabodies in practical clinical care is hampered by the need of a transgenic recipient population expressing them. Besides, each intrabody would be specific only against its cognate plasmid. Although intrabodies are not the most suitable therapeutic candidates for conjugation control due to the pharmacokinetic problems of any macromolecule as a drug, the recognized epitopes of the relaxase could be targeted by other means in order to generate better applicable COINs.

VirB8 is an essential assembly protein of bacterial T4SS that also acts as molecular target of small-molecule inhibitors [311]. A high throughput assay based on the restoration of interactions between two split domains of the *Brucella* VirB8 protein allowed the identification of several compounds that inhibited protein-protein interactions [312]. One of the most efficient molecules, B8I-2, is a salicylidene acyl-hydrazide derivative, also known to inhibit T3SS [313]. Posterior analysis by X-ray crystallography and *in silico* docking of several of these compounds

allowed the determination of VirB8 binding site [311]. Recently, it has been reported that these small molecules also bind TraE, the VirB8 homolog of the conjugative plasmid pKM101, and some of them inhibit plasmid transfer [314]. Although some of these molecules displayed a low Kd value *in vitro*, no significant impact was observed on plasmid transfer frequencies, with a 10-fold reduction as the strongest effect. Moreover, none of these molecules had an effect on the conjugation of the unrelated plasmid RP4, diminishing the effectiveness of these compounds to overcome antibiotic resistance.

Considering that conjugative pili are needed for bacterial cell contact [315], the use of specific compounds that inhibit pilus formation could result in a powerful strategy to fight against this problem. Conjugative pilus is targeted by a variety of bacteriophages that, upon binding to them, enter inside the bacteria cytoplasm. For instance, filamentous bacteriophages, such as M13, display high affinity for F-type pilus [316]. Moreover, a kinetic competition study between conjugation and M13 infection suggested that phages must be in significant abundance to be effective antagonists to conjugation. At lower phage concentrations, conjugation persists despite phage inhibition, even in the absence of selective pressure [317]. Besides conjugation and phage infection, conjugative pili are involved in the elaboration of biofilms, important targets in the battle against resistance [318]. Therefore, bacteriophages affecting F conjugation could also prevent biofilm formation[319]. Antibodies directed against conjugative pilus are also an interesting strategy, since they are able to inhibit conjugation of specific plasmids even more specifically than bacteriophages [320]. Otherwise, peptidomimetic small molecules, such as C10 and KSK85, have been found to disrupt T4SS-dependent transport of pathogenic factors, as well as DNA transfer in conjugative *Escherichia coli*. KSK85 acts impeding biogenesis of the pilus appendage, whereas C10 disrupts T4SS activity without affecting pilus assembly [321]. However, conjugation efficiency was only decreased to 25%. Therefore, although these compounds are promising scaffolds, new derivatives need to be found to inhibit more effectively the conjugative process [301].

The first systematic high-throughput search for COINs employed plasmid R388 and *E. coli* as a model system [322]. A luminescence-based assay was used to measure R388 conjugation in the presence of more than 12,000 microbial extracts known to contain a wide variety of bioactive compounds (the NatChem library) [302,309,323–325]. The most effective COIN found in this screening was dehydrocrepnynic acid (DHCA) [322]. Considering that this compound was extracted from tropical plant seeds [326] the viability of using it without vast downstream process improvement is limited. Nevertheless, two additional potential COINs were found as promising hits; oleic and linoleic acids, C_{18} fatty acids containing one or two double bonds, respectively. They were analysed by conventional conjugation assays using IncW, IncF, and IncP plasmids. R388 and pOX38 plasmids were affected, whereas RP4 or R6K were not. The fact that some plasmids were not affected could discard general metabolic disturbances as cause. These natural COINs present reduced toxicity, some of them being normal constituents of the human diet [327]. Therefore, they could be suitable compounds for preventing plasmids conjugation in natural environments [328]. However, one of the down sides of uFAs is that they are prone to auto-oxidation because of the presence of double bonds in their structure.

To overcome the chemical instability typical from uFAs, a new set of chemically synthetized triple bounded fatty acids were developed using DHCA structure as a chemical template. In particular, synthetic 2-hexadecynoic acid (2-HDA) and other 2-alkynoic fatty acids (2-aFAs) were found to be specific inhibitors of a wide range of conjugative plasmids in different bacteria, including the highly infective and prevalent IncF plasmids [329]. Furthermore, due to the effect of plasmid burden on host fitness, 2-aFAs could in fact eliminate transmissible plasmids, such as IncF, from bacterial populations. However, other plasmid groups, such as IncN and IncP, were not affected [322,329]. Moreover, 2-aFAs present toxicity against fungi [330,331], protozoa [332,333], Gram-positive bacteria, such as *Staphylococcus saprophyloticus* and *Bacillus cereus*, some Gram-negative bacteria like *Klebsiella pneumoniae* and *Pseudomonas aeruginosa*, and eukaryotic cells [334–336]. These toxicity problems exclude their application from environmental settings, where biodiversity must be maintained, and confine its use to academic setups.

Recently, a new collection of bioactive compounds isolated from aquatic microorganisms (AQUAc) was screened in search for better COINs; that is, compounds with different target specificity, better potency and stability, or less toxic to different cell types. As result, tanzawaic acids (TZAs) A and B were discovered as natural COINS with reduced toxicity compared to synthetic ones, able to inhibit bacterial conjugation of an important fraction of relevant plasmid groups [337]. TZAs are fungal polyketides more complex than previous COINs but they are carboxylic acids too, with two aromatic rings at the end of an unsaturated aliphatic chain, so they are also prone to auto-oxidation, which makes them poor candidates as effective, deliverable COINs.

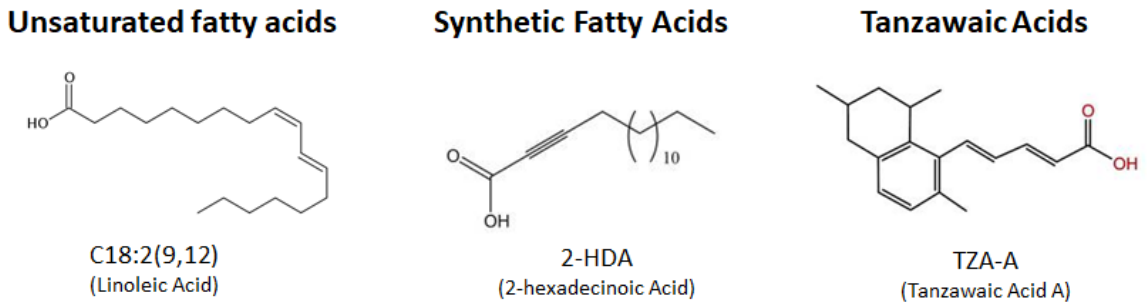

Figure 1.20. Conjugation inhibitors (COINs). Comparing prototype structures from the three groups of COINs described so far. Linoleic acid (C18:2$_{(9,12)}$), 2-hexadecinoic acid (2-HDA) and tanzawaic acid A (TZA-A) as the archetype representatives of unsaturated fatty acids (uFAs), 2-alkynoic chemically synthetic fatty acids (2-aFAs) and tanzawaic acids (TZAs), respectively. Modified from [322,329,337].

uFAs, 2-aFAs and TZAs share similar chemical characteristics: a carboxylic group, a long unsaturated aliphatic chain and the presence of double or triple bonds (Figure 1.20). Additional conjugation analysis using saturated fatty acids and related compounds suggested that carboxylic group, long carbon chain and double bond position are important features for the inhibitory ability [322].

COINs discovered to date have some limitations, such as obtainability, stability or toxicity. Their potential application in clinical and environmental settings demands non-toxic, easy to obtain, chemically and biologically stable molecules. Therefore, novel approaches are necessary in the near future to discover more COINs. Even though these compounds present a 100-fold reduction in plasmid transfer frequencies, higher inhibition rates must be achieved to maximize their effectiveness. In any case, they constitute key scaffold structures on which to develop more potent and specific COINs. In that respect, knowing the molecular target and mechanism of inhibition of these compounds is extremely important, since the use of structure-based drug design (SBDD) methods will allow the design of modified synthetic compounds with higher binding affinities. That might open a promising new avenue for the battle against the dissemination of antibiotic resistance genes [338].

Chapter 2
AIMS AND SCOPE

Nettie Stevens

Bacterial conjugation constitutes the main mechanism for the dissemination of antibiotic resistance genes among human pathogens. Therefore, the search for specific conjugation inhibitors is paramount in the fight against the spread of these genes.

For this reason, our main objectives are:

1. To identify the specific target and characterize the molecular mechanism of inhibition by conjugation inhibitors (COINs) in our model system, the conjugative plasmid R388.

2. To acquire a deeper knowledge about the biological role and mechanism of action of the conjugative traffic ATPase TrwD.

3. To localize TrwD and other components of the T4SS and analyze the conjugative process *in vivo* by fluorescence microscopy techniques.

This thesis work aims to gain knowledge on the biology of T4SS and the molecular basis of the conjugative process. Our goal is the characterization of the mechanism of inhibition by COINs in the conjugative plasmid R388. Such a knowledge may open a new avenue for the rational design of new and potent drugs in the battle against the dissemination of antibiotic resistance genes.

Chapter 3
EXPERIMENTAL PROCEDURES

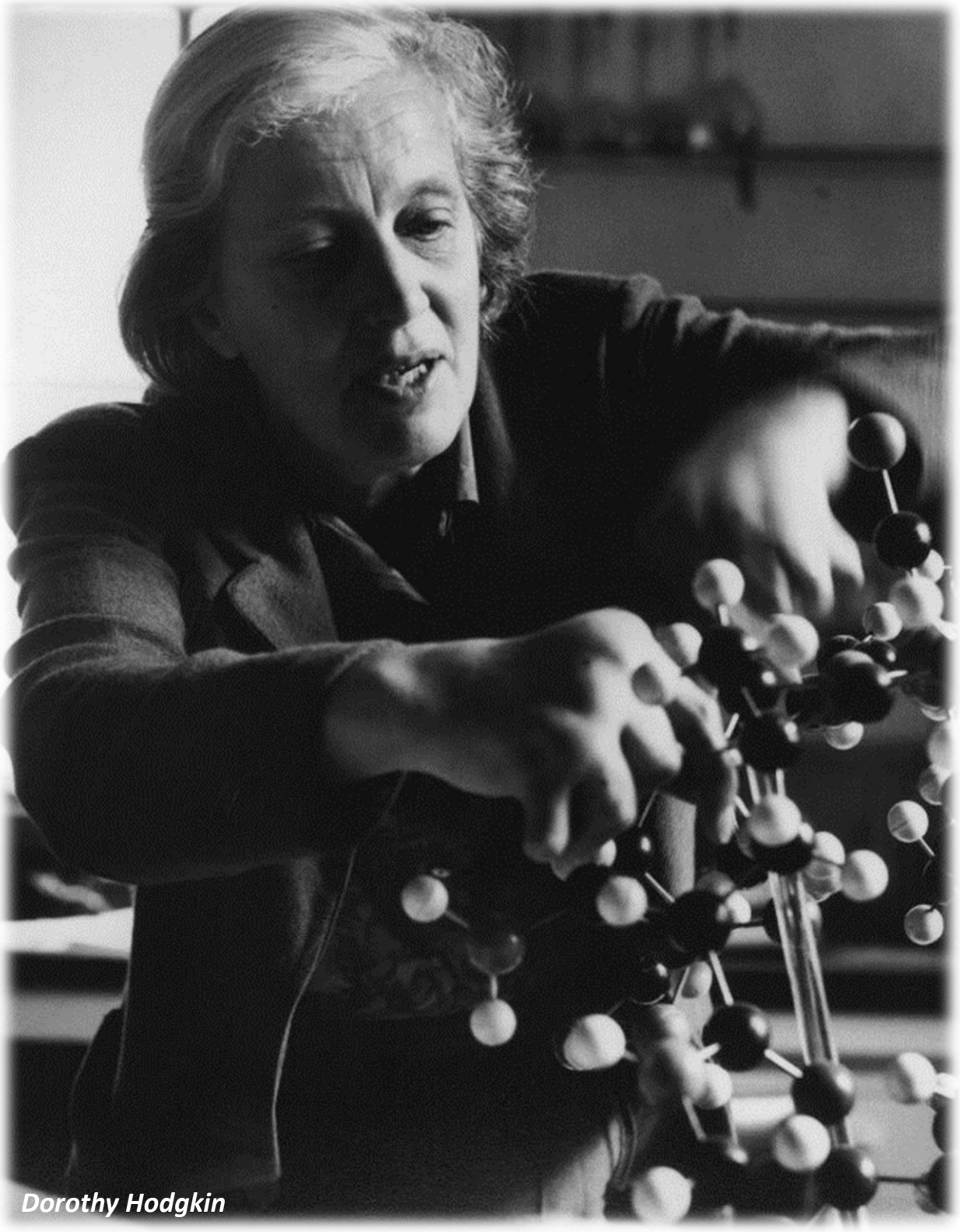

Dorothy Hodgkin

MATERIALS

3.1. Bacterial strains.

Strains	Genotype	Reference
DH5α	*F⁻ supE44 DlacU169 (f80lacZDM15) hsdR17 recA1 endA1 gyrA96 thi-1 relA1*	[339]
D1210	*F⁻ recA hspR hsdM repsl LaqI^q*	[340]
C41	*F⁻ dcm ompT hsdS (r_B^- m_B^-) gal λ (DE3)*	[341]
C43	*F⁻ dcm ompT hsdS (r_B^- m_B^-) gal λ (DE3)*	[341]
BL21	*F⁻ ompT hsdS gal (DE3)*	[342]
MG1655	*Dam$^+$, F⁻, lambda⁻, rph-1*	[343]
TB10	*AsqhCΔsodF::tet, tet*	[344]
UB1637	*F⁻ recA56 his lys trp rpsL*	[345]
MG1655::*seqA-gfp*	*Dam ⁻, seqA-gfp, F⁻, lambda⁻, rph-1*	Donated by de la Cruz F.

Table 3.1. *E. coli* derivative strains used in this work.

3.2. Bacterial plasmids.

Plasmids	Description	Phenotype	Reference
pET3a	Expression vector	Ap^R, Cm^R, Rep (pMB8)	[346]
pJR01	pET3a::*trwD*	Ap^R, Rep (pMB8)	[347]
pJR03	pET3a::*trwC*	Ap^R, Rep (pMB8)	Ripoll-Rozada, Doctoral Thesis
pMEC05	pET28a::*TrwBΔN70*	Km^R, Rep (pMB8)	[236]
pSU1547	pET22b::*trwA*	Ap^R, Rep (pMB8)	[72]
pSAN2	pET28a::*trwK*	Km^R, Rep (pMB8)	[209]
R388	IncW conjugative plasmid wild type	Tp^R	[348]
pSU4039	R388-ΔtrwD::*omega deltaE*	Cm^R	[221]
pJC01	R388::*gfpmut2*	Cm^R	[349]
pIM17	pWX295::*P1-TrwBmCherry-Km*	Km^R, Rep (pMB1)	Matilla, Doctoral Thesis
pRSETa::*mEos4b*	Expression vector	Ap^R	Addgene (nonprofit plasmid repository)
pHis17::*ATPf/mCherry fusion*	Expression vector	Ap^R	Donated by Miroux B.
pANT::*gfp*	Expression vector	Ap^R	Donated by de la Cruz F.

Table 3.2. Plasmids used in this work.

3.3. Plasmid DNA constructs.

Plasmid	Description	Resistance	Template	Oligonucleotides 5 '3'
pYGC01	pET3a::*trwD (C44N)*	Ap^R	pJR01	Quickchange CTGTCCATTAACCGCCCTGGAGAGGTTTGG TTCCGTAACCTCCGGCGCATC
pYGC02	pET3a::*trwD (H119D-V123D)*	Ap^R	pJR01	Quickchange CTTGTCGACAAGACACTGGAAGAACTCGATGCG GGAGTCTTTGCGGATGAGGAAAGACAG
pYGC03	pET3a::*trwD (Δ15link)*	Ap^R	pJR01	Quickchange TTGGAGCCGTTCGAGGTTGAG CGAGGGCTTGTTAAAGCTCAC

Table 3.3. Plasmids constructed for the mutational analysis of the traffic ATPase TrwD.

Plasmid	Resistance	Template	Enzymes / Oligonucleotides 5 '3'
pHis17:: *TrwDmCherry*	Ap^R	R388	AAAATCATATGTCTACAGTCTCGAAAGC AAAATAAGCTTAGCCATCTTGGA
pHis17:: *TrwBmCherry*	Ap^R	R388	AAAATCATATGCATCCAGACGATCAA AAAATAAGCTTGATAGTCCCCTCAAC
R388:: *TrwBmCherry*	Tp^R, Km^R	pIM17	GAGCGCGTGCGCGAGCGCGTCGTGATGCCGGCG TGTCGGGTCAATACCATGTGACTGAGCATTAGATA GTCCCCTCAACGACATGGGAATTAGCCATGGTCC
			PCR control CGCAAGCTTACTACGGGAGAGGACATGCATCCAG ACGATCAAAGAAAG GGGTCAATACCATGTGACTG

Table 3.4. Plasmids constructed for fluorescence microscopy assays.

3.4. Fatty acids and derivatives.

Compound	Description	Reference
Linoleic acid	C18:2*(9,12)*	Purchased from Sigma-Aldrich
Oleic acid	C18:1*(9)*	Purchased from Sigma-Aldrich
Lauric acid	C12:0	Purchased from Sigma-Aldrich
Palmitic acid	C16:0	Purchased from Sigma-Aldrich
2-HDA	2-hexadecynoic acid	Synthesized as described [331]
2,6-HDA	2,6- hexadecadiynoic acid	Synthesized as described [331]
2,9-HDA	2,9-hexadecadiynoic acid	Synthesized as described [331]
2-ODA	2-octadecynoic acid	Synthesized as described [331]
2-HDOH	2-hexadecyn-1-ol	Synthesized as described [336]
2-HDOTHP	2-(2-hexadecynyloxy)-tetrahydro-2H-pyran	Synthesized as described [336]
2-ODOH	2-octadecyn-1-ol	Synthesized as described [336]
2-ODOTHP	2-(2-octadecynyloxy)-tetrahydro-2H-pyran	Synthesized as described [336]
2-BP	2-Bromopalmitic acid	Purchased from Sigma-Aldrich
[^{14}C(U)]-Palmitic acid	Radiolabeled ^{14}C palmitic acid	Purchased from PerkinElmer
[Palmitoyl-1-^{14}C]-Palmitoyl Coenzyme A	Radiolabeled ^{14}C palmitoyl Coenzyme A	Purchased from PerkinElmer

Table 3.5. Fatty acids and derivatives used in this work.
*****Fatty acids were diluted in DMSO. The final concentration of the fatty acids solvent (DMSO) in the ATP hydrolysis assays (2%) did not affect the enzymatic activity.

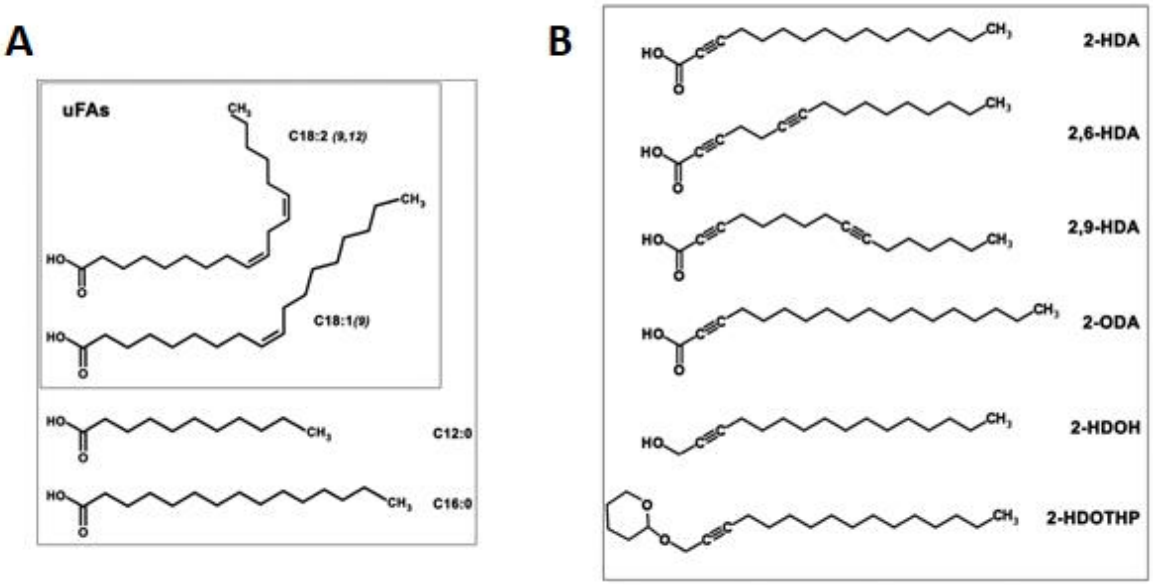

Figure 2.1. Schematic representation of fatty acids and derivatives from Table 3.5. (A) Saturated and unsaturated fatty acids. Lauric (C12:0), palmitic (C16:0), oleic (C18:1*(9)*) or linoleic (C18:2*(9,12)* acids, as representatives of saturated and unsaturated fatty acids (uFAs), respectively. **(B) 2-alkynoic fatty acids and derivatives**. 2-hexadecynoic acid (2-HDA), 2-octadecynoic acid (2-ODA), 2,6- hexadecadiynoic acid (2,6-HDA), 2,9-hexadecadiynoic acid (2,9-HDA) and their corresponding alcohol (OH) or tetrahydropyranyl-ether (THP) derivatives. For simplicity, only 2-HDA, 2-HDOH and 2-HDOTHP derivatives are shown. Taken from [350].

3.5. Growth and selection media.

Luria-Bertani broth (LB) (10 g/l tryptone, 5 g/l yeast extract, 5 g/l NaCl) [351] was used for bacterial growth, supplemented with agar 1,5% (w/v) for solid culture. In the case of growth in selective media, antibiotics were added at the following concentrations: Chloramphenicol (Cm, Sigma-Aldrich) 25 μg/ml, Nadilixic acid (Nx, Sigma-Aldrich) 25 μg/ml, Streptomicin (Sm, Apollo) 300 μg/ml, Ampicillin (Ap, Apollo) 100 μg/ml, Kanamycin (Km, Sigma-Aldrich) 25 μg/ml and Trimethoprim (Tp, Sigma-Aldrich) 10 mg/ml.

To preserve *E. coli* cells, cultures were harvested at stationary phase and suspended in 50% glycerol and 50% peptone 1.5% (p/v). Strains were kept at -80˚C.

METHODS

3.6. Molecular biology experimental techniques.

3.6.1. Standard cloning procedures.

DNA extraction. Comercial kits were used for the extraction of plasmidic DNA. QIAprep Spin Miniprep Kit (QIAGEN) was used for general plasmid isolations. QIAGEN Plasmid Maxi Kit (QIAGEN) was used for the isolation of large amounts of DNA, required for ATPase activity assays. In the latter case, DNA samples (40 µl) were dialyzed for 30 minutes to eliminate the salts by using a Millipore GS nitrocellulose filter (0.05 µm pore size), on a Petri plate with sterile distilled water (DWE). The concentration of the DNA samples was determined with a Nano-Drop Spectrophotometer ND-1000.

PCR amplification. In order to amplify samples used for cloning, 50 µl sample reactions were prepared, containing 10 pmol/µl of each primer, 50-100 ng of template, 200 µM of dNTPs, 1U of Phusion polymerase, 1x polymerase buffer and DWE. Vent DNA polymerase (Bioline) and Phusion High-Fidelity DNA polymerase (Biolabs Inc. New England) were used for amplification. A iCycler (BioRad) was used with the following program: 1 minute of denaturation at 98˚C, 30 cycles fo amplification (including 10 seconds at 98 ˚C, 15 seconds at a temperature according to TM of primers used, 1.5 minutes at 72 ˚C (30 seconds per kb) and 10 minutes of elongation at 72 ˚C. GenElute PCR Clean-Up Kit (Sigma-Aldrich) was used for purification of dsDNA PCR products. GenElute Agarose Spin Columns (Sigma-Aldrich) were used for DNA purification from agarose gels.

Enzymatic digestions. The amplified DNA was digested on reactions containing 500 ng of the PCR product, 1 mg/ml of BSA, 1-5U the restriction enzyme (Fermentas), 1x restriction enzyme buffer and DWE. Reactions were performed in 30 µl for a minimum of two hours, following the manufacturer's indications. Samples were purified from an electrophoresis gel by using a PCR purification kit (QIAGEN) and eluted in 40 µl of TE. In some exceptional cases, *DpnI* enzyme was used to remove selectively the methylated DNA template. The treatment consisted of Adding 10U of DpnI enzyme and the enzyme buffer to the PCR Products, in 50 µl of final volume. Samples were digested at 37 ˚C for 2 hours. After the treatment, the DNA was purified using a PCR Purification Kit (QIAGEN).

DNA dephosphorylation. Cloning vectors were dephosphorylated to increase the efficiency of DNA cloning by decreasing the amount of religated vector (false positives). DNA samples were supplemented with 1 U of Shrimp Alkaline Phosphatase (Fermentas) after enzymatic digestion, in the same reaction buffer, and incubated for 1 hour at 37˚C following the manufacturer's instructions. Heat inactivation of the enzymes for 20 minutes at 65˚C was performed prior to ligation.

Ligation. Inserting fragments were obtained by either restriction endonucleases and subsequent gel extraction or by PCR with primers incorporating the adequate restriction sites at both ends of the amplified fragment. Cloning vector and fragments were added to a reaction in a 5:1 molar ratio (insert/vector), used as a general rule for the ligation reactions. *T4* DNA ligase was used to ligate vector and insertion fragments used for cloning. 10 µl sample reactions were prepared, containing 10 – 15 ng of vector, 5-fold molar excess of insert, 5U of *T4* DNa ligase (Fermentas) 1x ligase buffer and DWE. Samples were incubated at 16 ˚C overnight. As a negative control, the same reaction without insert was used, adding water to reach the final volume.

3.6.2. DNA sequencing.

DNA sequences of all cloned PCR segments were determined. Samples were sent to MACROGEN Inc. DNA Sequencing Service (Amsterdam, Holland). Samples for sequencing contained 500 ng of template DNA and 25 pmol of the oligonucleotide required in a final volume of 10 µl.

3.6.3. DNA electrophoresis in agarose gels.

Plasmid DNA was analysed/visualized by agarose gel electrophoresis. Agarose was dissolved in 0.5x TBE (45 mM Tris-HCl pH 8.2, 45 mM Boric Acid, 0.5 mM EDTA) to a concentration of 0.7 – 1% w/v, as needed according to the size of the DNA fragments to be resolved. SYBR® Safe (Invitrogene) was used for DNA staining, added to a final concentration of 0.25 µg/ml or 0.05 µg/ml, respectively.

Loading buffer (0.25% Bromophenol Blue (w/v), 30% glycerol (v/v) in 0.5x TBE) was added to the DNA samples in a 5:1 relation of DNA sample volume/blue dye. HyperLadder I (Biolabs) was used as a molecular weight market. A horizontal BioRad electrophoretic system was used (80 – 120 V). Agarose DNA gels were visualized with a Gel Doc 2000 UV system and images were analyzsed with Quantity One software (BioRad).

3.6.4. Site directed mutagenesis.

Point mutations in specific residues of the protein were performed using the QuickChange® site-specific mutagenesis kit (Stratagene). The amplification reaction was performed in a reaction mixture containing 2 µl 10X buffer, 25 ng template plasmid, 0.5 µM each mutagenic oligonucleotide, 1 µM dNTPs and 0.25 µl KDO Hot-Star DNA polymerase enzyme (2.5 U/ml) in a total volume of 20 µl. The products were analyzed by electrophoresis in 1% (w/v) agarose gel. The amplified product was treated for 2 hours at 37°C with 10 U/µl of DpnI endonuclease and electroporated into competent *E. coli* DH5α cells (1 µl DNA / 50 µl *E. coli*).

Finally, transformation reaction (100 µl) was seeded onto LB-Agar plates containing the appropriate antibiotic for the vector and incubated overnight at 37°C.

3.6.5. Cloning of fusion-fluorescent protein with an antibiotic resistance gene on R388 plasmid.

Fluorescent fusion-proteins constructs were built by PCR (template and primers described in Table 3.4). These PCR cassettes had flanking ends homolog to the insertion region in R388, in order to increase the possibility to recombine with this region on the plasmid. This event happens in a very low frequency so, for this reason, a resistance gene is inserted to select only colonies in which recombination has occurred. *E.coli* recombination system (via RecA) only recombines when the size of the homologous region is more than 250-500 bp. However, TB10 strain presents a different recombination system (phage lambda -RED recombination system-). This system is very efficient, since only 30 bp are required for the recombination reaction. In order to avoid toxicity, this is a recombination system inducible by temperature. Therefore, the system is not expressed at 30˚C, but at 42˚C.

To carry out these experiments, R388 plasmid was firstly conjugated from DH5α to TB10 strain. TB10 (R388) competent cells were prepared and shifted to 42˚C for 15 minutes, since the recombination system of TB10 cells needs to be induced at 42˚C. Then, competent cells were transformed with the constructs. Cells were plated on the appropriate antibiotic to select colonies with a R388 plasmid (Tp^R) that also carries the protein fused to the fluorescent proteins and to an antibiotic resistance cassette (Km^R). Constructs on TB10 cells were conjugated to UB1637 cells in order to avoid recombination.

We performed an additional PCR to confirm the presence of the cassette and discard the mixed bacterial populations, that is, bacteria containing wild type R388 and fusion-fluorescent protein in the same cell (Table 3.4, PCR control).

3.7. Microbiological techniques.

3.7.1. Preparation of *E. coli* competent cells.

The following procedure can yield competent cultures of *E. coli* strains DH5α, D1210 and C41 that can be transformed at frequencies ≥ 5 x 10^8 colonies/μg [352]. Using a sterile wire, *E. coli* strain was streaked directly from a frozen stock on an agar plate and incubated at 37˚C overnight.

Isolated colonies were transferred into 10 ml of LB and grown with shaking at 37˚C overnight. Cells were diluted in 1:20 dilution of LB (200 ml) and incubated with shaking at 37˚C to an OD_{600} ≈ 0.5. Then, cells were incubated on ice for 30 minutes, transferred to Falcon tubes and recovered by centrifugation at 5,000 g for 10 minutes at 4˚C. The obtained supernatant was decanted and pellets were washed, by gently vortexing, in approximately 20 ml of autoclaved and cold distilled water (DWE). Cells were again recovered by centrifugation at 5,000 g for 10 minutes.

The supernatant was decanted from the cell pellets and the pellets were resuspended by vortexing in another 20 ml of DWE. After a new centrifugation step, cells were resuspended in 20 ml of ice-cold autoclaved sterile 10% glycerol (w/v). Finally, cells were recovered by centrifugation and the supernatant was removed, leaving a minimum volume of approximately 1 ml of the remaining glycerol to resuspend the cells. 60 µl aliquots were dispensed into sterile Eppendorf tubes. Competent cells were stored at -80˚C until needed.

TB10 cells were prepared as described above, with the exception that competent cells had to be freshly prepared, just before being transformed.

3.7.2. Transformation by electroporation.

This method provides transformation frequencies really high; up to 10^{10} transformants can be obtained by µg of DNA [353]. Competent cells to electroporate were prepared as described in the previous section.

DNA samples were dialyzed for 30 minutes on nitrocellulose filters with 0.05 µm pore size (Millipore) on a Petri dish containing MilliQ water, in order to minimize the salt content of the sample. Dialyzed DNA was collected from the filters and (1-100 pg) was added to an aliquot (60 µl) of competent cells. The mixture was placed in a 0.2 cm electroporation cuvette Gene Pulser® (BioRac Laboratories) at 4˚C, previously cooled on ice. The electroporation process was carried out in a Micropulser ™ electroporator (BioRad) under the following conditions: 2.5 kV, 25 µF and 200 Ω. Electroporated cells were resuspended in 1 ml of sterile LB and incubated at 37˚C with shaking, in order to allow antibiotic resistance expression (different times, from 60 to 90 minutes, according to the type of antibiotic used). Finally, transformed cells were plated on LB-Agar with the corresponding antibiotic.

3.7.3. Bacterial conjugation experiments.

3.7.3.1. Plate conjugation assay.

Cultures were grown overnight with shaking at 37 ˚C in 10 ml of LB with the corresponding antibiotic. At the following day, donor cells cultures were diluted 1:20 in fresh LB and grown up to exponential phase ($OD_{600} \approx 0.6$). Then, 200 µl of diluted donor cells and 500 µl of recipient cells at stationary phase were mixed in an Eppendorf tube and the sample was spun down at 15,000 g for 5 minutes. The supernatant was poured off and cells were resuspended in 1 ml of fresh LB and centrifuged again to eliminate antibiotics. Resulting precipitate was resuspended in an approximate volume of 100 µl of fresh medium.

Samples were placed on cellulose acetate filters of 0.2 µm pore size (Sartorius Stedim Biotech) on a plate of LB-Agar medium for 1 hour at 37˚C. Then, the filter was washed in 2 ml of LB medium without antibiotics and resuspended by vortexing. Serial dilutions were made from 1:10 to 1:10,000 and 100 µl samples were plated, selecting for transconjugants and donor cells with the appropriate antibiotic. Counting the number of cells, the conjugation frequencies could be calculated and expressed as the number of transconjugants per donor cell, according to the following equation:

$$Conjugation\ frequency = \frac{Transconjugants\ number\ x\ dilution}{Donors\ number\ x\ dilution}$$

3.7.3.2. Fluorescence-based conjugation assay.

A whole-cell automated assay for conjugation, based on fluorescence emission in transconjugants cells, was used [329]. DH5α with the conjugative plasmid pJC01, which contains GFP under the control of T7 promoter, was used as donor cell and Streptomycin-resistant derivative *E. coli* BL21 (DE3) was used as recipient strain expressing T7 RNA polymerase. Using recipient cells encoding T7 RNA polymerase we guarantee GFP production only in transconjugant cells. Both strains were grown to stationary phase in LB broth with appropriate antibiotics. Then, donor and recipient cells were concentrated 4-fold and mixed at a 1:1 ratio. Mixture samples (10µl) were spotted onto 96-well microtiter plates (Bioster a.s.) with the help of a Biomek 3000 liquid-handling robot (Beckman Coulter). Cells were grown in 150 µl LB, 1% agar, 1 mM IPTG and different concentrations of fatty acids diluted in DMSO by well. The transfer of pJC01 into the BL21(DE3) recipient strain during conjugation was allowed by incubation at 37˚C for 6 h. Then, cells were resuspended in 200 µl of Phosphate-Buffered Saline (PBS) buffer and 150 µl of the suspension was transferred to a new plate. The optical density at 600 nm (OD_{600}) and GFP emission were measured in a Victor3 multi-label counter (PerkinElmer). Conjugation frequencies (CF) were calculated as the ratio of absolute fluorescence emitted by transconjugant cells and the total number of cells (OD_{600}). Relative CF in the presence of a compound was determined as a fraction of the CF observed in controls performed in the absence of the inhibitor. To reproduce the same conditions, an equivalent volume of solvent (DMSO) was added to control samples.

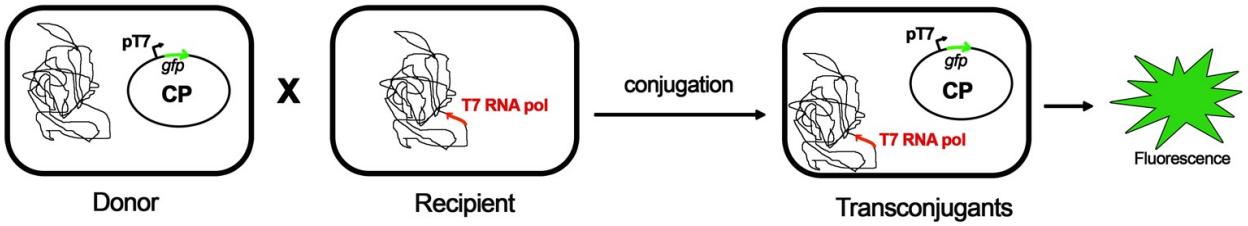

Figure 2.2. Schematic diagram of fluorescence-based conjugation assay. GFP is not expressed in donor cells due to the lack of an active promoter. GFP expression is induced in recipient cells by the presence of T7 RNA polymerase, expressed from the recipient chromosome. Modified from [338].

3.8. Biochemical techniques.

3.8.1. Production of recombinant proteins in *E. coli*.

For the production of recombinant proteins, plasmids containing the gene to be overexpressed under the promoter of the T7 RNA polymerase were used. Over-expressions were carried out in C41 (DE3) strain, except in cases where the protein had low levels of overexpression or overexpression was toxic to the cell. In these cases, C43 (DE3) strain was used. The over-expressions were carried out in 1 liter flasks of LB medium with the corresponding antibiotic at a temperature of 37°C, inoculating from a single colony. Induction of over-expression of the corresponding gene was carried out in late exponential phase (OD_{600}≈0.5) by the addition of 1mM IPTG (isopropyl 1-thio-β-D-thiogalactopyranoside) (Apollo Scientific, Bredbury, UK). After the addition of IPTG (6 hours in the case of TrwD and TrwK, 8 hours for TrwA and 3 hours for TrwBΔN70 and TrwC) the cultures were centrifuged at 5,000 g for 15 min at 4˚C. Supernatants were removed, leaving a minimum volume of approximately 5 ml per liter of culture to resuspend the cells.

3.8.2. Protein purification.

3.8.2.1. TrwD purification.

We followed the procedure previously described [347]. Briefly, as a first step in the purification, the cells used for the over-expression of TrwD were lysed. The volume equivalent to 2 liters of culture was thawed and resuspended in 24 ml of buffer (50 mM Tris-HCl pH 7.6, 10% sucrose, 2 mM EDTA, 5 mM benzamidine, 1 mg/ml lysozyme, 2 µg/ml aprotinin, 2.5 µg/ml leupeptin, 1 mM PMSF and one tablet of a cocktail of inhibitors from the commercial house Roche). After 15 min of incubation on ice, another 24 ml of buffer (50 mM Tris-HCl pH 7.6, 1 M NaCl, 1 mM EDTA and 0.6% (w/v) Triton X-100) were added. The lysis mixture was kept for 20 min on ice and then the lysed cells were ultra-centrifuged at 100,000 g for one hour at 4 ° C with a 50.2 Ti rotor. The supernatant was precipitated by the addition of a saturated solution of 60% (w/v) $(NH_4)_2SO_4$ for 1 hour. Subsequently, it was centrifuged at 100,000 g for 30 min. The pellet was resuspended in 40 ml of buffer A (20 mM Hepes pH 6.8, 0.1 M NaCl, 1 mM DTT, 10% glycerol, 1 mM PMSF) and dialyzed o/n in 4 liters of the same buffer. It was filtered and loaded onto a HiTrap Q-Sepharose ion exchange column (5 ml) (Amersham, GE). The volume not retained in the column was dialysed for 3 hours with 4 liters of buffer A pH 7.6. After that time, the sample was loaded onto a Resource Q column (6 ml) and the protein was eluted using a linear gradient of 0.1 M to 1 M NaCl. Finally, it was concentrated and loaded onto a HiLoad 16/60 Superdex200 column (Amersham, GE). The fractions were eluted in 20 mM Hepes / NaOH pH 7.6, 0.2 M NaCl, 1 mM PMSF and 5% glycerol (w/v) and stored at -80°C.

3.8.2.2. TrwK purification.

We followed the procedure previously described [206]. Briefly, lysates from 3 liters of culture were collected by centrifugation, diluted four times in buffer A 50 mM Tris-HCl pH 7.6, 2 mM $MgCl_2$, 0.1 mM EDTA, 0.5 mM phenylmethylsulfonyl fluoride and applied to a HiTrap SP-Sepharose (5-ml) column (Amersham, GE). TrwK-containing fractions were collected in the flow-through and applied to a HiTrap Q-Sepharose (5-ml) column. TrwK was eluted from this column in a linear gradient of NaCl at a 250 mM salt concentration. The enriched fractions were pooled and diluted to a final concentration of 50 mM NaCl and applied to a second HiTrap Q-Sepharose (5-ml) column. TrwK-containing fractions were pooled, concentrated, and loaded onto a Superdex200 GL10_30 column. After isocratic elution in a buffer consisting of 50 mM HEPES-NaOH pH 7.2, 150 mM NaCl, 10% (w/v) glycerol, 2 mM $MgCl_2$, 0.1 mM EDTA, and 0.5 mM phenylmethylsulfonyl fluoride, the fractions with the richest content in TrwK were pooled and stored at −80°C.

3.8.2.3. TrwC purification.

We followed the procedure previously described [79]. Briefly, cell lysis followed the same steps as in the previous two cases. Here we started with 1 liter of culture. The lysate was diluted to a final concentration of 200 mM NaCl. A first ion exchange chromatography was performed on a phosphocellulose-P11 column (Whatman). The resin was activated according to the instructions of the commercial house and 15 ml were packed with a 2.5 cm internal diameter adapter (BioRad). The lysate was loaded onto the column previously equilibrated with buffer A (50 mM Tris HCl, 0.1 mM EDTA, 200 mM NaCl, 1 mM PMSF and 10% (w/v) glycerol) and washed with 5 column volumes of buffer A. The protein was eluted with buffer B (50 mM Tris-HCl, 0.1 mM EDTA, 600 mM NaCl, 1 mM PMSF and 10% (w/v) glycerol). The fractions enriched in TrwC were pooled, diluted in a buffer (50 mM Tris-HCl pH 7.6, 0.1 mM EDTA, 200 mM NaCl, 1 mM PMSF and 10% (w/v) glycerol) and loaded on a HiTrap SP column (5 ml) (Amersham, GE). The protein was eluted by a linear gradient of 200 mM NaCl to 600 mM NaCl. As a final purification step, a Mono S HR 5/5 column (1 ml) (Amersham, GE) was used. The protein was diluted to 200 mM NaCl, loaded onto this column and eluted in the same linear NaCl gradient. Fractions containing TrwC were eluted at 400 mM NaCl and stored at -80°C.

3.8.2.4. TrwBΔN70 purification.

We followed the procedure previously described [173]. Briefly, bacteria were grown in 4 liters of LB medium. Cell lysis was performed as described previously and the final supernatant was diluted with buffer B (50 mM Tris-HCl pH 7.6, 0.1 mM EDTA, 2 mM $MgCl_2$ and 0.001% PMSF) to a final concentration of 0.15 M NaCl and absorbed to a phosphocellulose-P11 column (Whatman) equilibrated with buffer B and 150 mM NaCl. Bound proteins were eluted with buffer B plus 1 M NaCl. TrwBΔN70 containing fractions were pooled and diluted to 0.15 M NaCl with buffer B. Then, they were loaded onto a 5-ml HiTrap-SP (Amersham Pharmacia Biotech) column equilibrated with buffer B plus 0.15 M NaCl. Proteins eluted in a 120-ml salt gradient (0.15-1 M

NaCl) were pooled and concentrated in a Centricon YM30 (Amicon) concentrator to 4 ml. Finally, TrwBΔN70 was loaded on a superdex-200 HiLoad 16/60 column (Amersham Pharmacia Biotech) equilibrated with buffer 50 mM Piped-NaOH pH 6.2, 100 mM NaCl, 2 mM $MgCl_2$, 0.1 mM EDTA, 10% glycerol and 0.001% PMSF. Glycerol was added to TrwBΔN70 containing fractions up to 10% final concentration and the protein was stored at -80 ˚C.

3.8.2.5. TrwA purification.

We followed the procedure previously described [63]. Briefly, for TrwA protein purification, cells were grown in 2 liters of LB medium. After cell lysis, the final supernatant was diluted with buffer A to 0.15 M NaCl final concentration and adsorbed to a 5-ml HiTrap Q chromatographic column (Amersham Biosciences), equilibrated with buffer A supplemented with 0.15 M NaCl. Bound proteins were eluted in a 0 – 0.5 M NaCl gradient. Pooled fractions were diluted in buffer A to 0.15 M NaCl final concentration and adsorbed to a second 5-ml HiTrap Q column, equilibrated with buffer A supplemented with 0.15 M NaCl. In this case, bound proteins were eluted in a 0 – 0.35 M NaCl gradient. Pooled fractions were diluted with buffer A to 0.15 M NaCl final concentration and loaded to a 5-ml Heparine column (Amersham Biosciences), equilibrated with buffer A supplemented with 0.15 M NaCl. Bound proteins were eluted in a NaCl gradient (0 – 1 M). TrwA containing fractions were pooled and concentrated in a Centricon YM10 (Amicon) concentrator up to 4 ml. Then, protein was loaded on a Superdex-200 HiLoad 16/60 column (Amersham Biosciences) equilibrated with buffer 50 mM Pipes-NaOH pH 6.2, 100 mM NaCl, 2 mM $MgCl_2$, 0.1 mM EDTA, 10% glycerol and 0.001% PMSF. Protein was stored at -80˚C

3.8.3. Protein analysis.

3.8.3.1. Protein quantification.

Protein concentration measurement in solution was carried out by two different spectroscopic methods:

Bradford assay: the Bradford dye assay [354] is based on the equilibrium between three forms of Coomassie Blue G-250 dye (Protein Assay, Biorad). Under strongly acid conditions, the dye is most stable as a doubly-protonated red form. Upon binding to protein it is most stable as an unprotonated, blue form. This effect can be detected by changes in the absorbance at 595nm. The response to the Bradford reagent is dependent on protein concentration, so a convenient standard curve was made by using Bovine Serum Albumin (BSA, sigma-Aldrich) as a reference (range 0 – 15 µg). Protein samples were mixed with the protein buffer up to a volume of 50 µl and DWE was added to 100 µl of final volume. 900 µl of a 1:5 dilution of Bradford reactive with distilled water was mixed with 100 µl of protein sample. The reaction was then allowed to proceed. After 10 minutes, the absorbance at 595 nm was measured on a Shimadzu UV-1800 spectrophotometer, and its value plotted against the standard curve.

BCA Protein Assay: Protein samples can also be quantified by BCA™ Protein Assay Kit (Pierce). The BCA Protein Assay combines the reduction of Cu^{2+} to Cu^{1+} by the protein in an alkaline medium with the highly sensitive colorimetric detection of the cuprous cation (Cu^{1+}) by Bicinchoninic acid (BCA). The response is also dependent on protein concentration and, therefore, a standard curve was prepared with BSA (range 0 – 40 µg), as explained in the Bradford assay. Protein samples were mixed with the protein buffer as in the Bradford system to a final volume of 100 µl, completed with DWE. 900 µl of a mixture sample of reagents A (BCA) and B (Cupric Sulfate) was prepared in a 50:1 stoichiometry and added to 100 µl of protein sample. The reactions were incubated at 37˚C for 30 minutes and then, absorbance at 562 nm was measured on a Shimadzu UV-1630 spectrophotometer and plotted against the standard curve.

3.8.3.2. Protein electrophoresis in SDS-PAGE gels.

Denaturing protein electrophoresis was carried out according to the method previously described [355] on 10% SDS-polyacrylamide gels (acrylamide:bisacrylamide 29:1) to the visualization of protein samples. Electrophoresis was carried on a Mini-PROTEAN II system (BioRad) in 6.1 cm x 0.75 mm gels. Loading buffer (50 mM Tris-HCl pH 6.8, 4% (w/v) SDS, 4% (w/v) glycerol and 0.02% (w/v) bromophenol blue and 50 mM DTT) was added to the samples at a 5:1 ratio. Samples were heated at 100˚C for 5 minutes, before being loaded on the polyacrylamide gel. As a control for standard molecular weights, the Low Range or High Range standards weight markers (BioRad) were used. The electrophoretic run was performed at 200V for 1 hour, on buffer 25 mM Tris-HCl pH 8.3, 200 mM glycine and 1% (w/v) SDS. Then, gels were stained with a solution containing 0.1% (w/v) Coomassie Brilliant Blue R-250 (Merck), 50% (w/v) methanol and 10% (v/v) acetic glacial acid for 30 minutes at room temperature [356]. Gels were destained using 10% (v/v) methanol and 10% (v/v) acetic glacial acid buffer.

3.8.3.3. Protein electrophoresis in Tricine-SDS-PAGE gels.

Tricine-SDS-PAGE was carried out according to the method previously described [357] on uniform acrylamide Tricine-SDS 16% gels, which cover a narrow protein mass ranger (1-70KDa) and offer high resolution, especially for the small proteins. Polymerized separating Tricine-SDS 16% gels (acrylamide:bisacrylamide 48:1) were overlayed with stacking Tricine-SDS 4% gels, both of them performed with buffer 1 M Tris-HCl pH 8.45, 0.1% (w/v) SDS and polymerized by adding APS (10%) and TEMED. Electrophoresis was carried on a Mini-PROTEAN II system (BioRad) in 6.1 cm x 1 mm gels. Loading buffer (50 mM Tris-HCl pH 6.8, 4% (w/v) SDS, 4% (w/v) glycerol, 0.02% (w/v) bromophenol blue and 50 mM DTT) was added to the samples at a 5:1 ratio. Samples were incubated at 37˚C for 20 minutes, before being loaded on the polyacrylamide gel. As a control for standard molecular weights, the Low Range standard weight markers (BioRad) was used. The electrophoretic run was performed at 30V as initial voltage for 1 hour following by 100V for 4 hours. The anode buffer was 100 mM Tris-HCl pH 8.9, while the cathode buffer was 100 mM Tris-HCl pH 8.25, 100 mM Tricine, 0.1% (w/v) SDS. Protein was visualized directly in the gel by Coomassie staining. Gels were stained with a solution containing 0.1% (w/v) Coomassie Brilliant Blue R-250 (Merck), 50% (w/v) methanol and 10% (v/v) acetic glacial acid for 30 minutes at room

temperature [356]. Gels were destained using 10% (v/v) methanol and 10% (v/v) acetic glacial acid buffer.

3.8.3.4. Protein electrophoresis in Native-PAGE gels.

Native polyacrylamide gel electrophoresis (Native-PAGE) uses the same discontinuous chloride and glycine ion fronts as SDS-PAGE to form moving boundaries that stack and then separate polypeptides by charge to mass ratio. Proteins are prepared in a non-reducing non-denaturing sample buffer, which maintains the proteins' secondary structure and native charge density.

Electrophoresis was carried on a Mini-PROTEAN II system (BioRad) in 6.1 cm x 1.5 mm gels. Polymerized separating 4.5% gels (acrylamide:bisacrylamide 30:0.8) 375 mM Tris-HCl pH 8.8 and polymerized by adding APS (10%) and TEMED. Loading buffer (250 mM Tris-HCl pH 6.8, 50% (w/v) glycerol and 0.02% (w/v) bromophenol blue) was added to the samples at a 5:1 ratio. Samples were not heated before being loaded on the polyacrylamide gel. The electrophoretic run was performed on ice and at low voltage to avoid protein denaturalization. Gels were powered up at a constant current (30 mA) for 140 min. The electrophoretic run was performed on buffer 25 mM Tris-HCl and 192 mM glycine, this running buffer is already ≈ pH 8.3, so we do not need to adjust the pH. Gels were stained with a standard Coomassie-blue protocol as was described in the previous sections.

3.8.3.5. Protein electrophoresis in Blue Native (BN)-PAGE gels.

Blue native polyacrylamide gel electrophoresis (BN-PAGE) is performed essentially as described previously [358,359]. First, samples are stained with a charged (Coomassie Blue G-250) dye. The intact protein complexes are then separated by electrophoresis based upon how much dye was bound, which is proportional to their size. After this first dimension gel, the protein components of the resolved complexes can be further separated in a second denaturing dimension after soaking the gel in denaturing SDS buffer.

As previously, electrophoresis was carried on a Mini-PROTEAN II system (BioRad) in 6.1 cm x 1.5 mm gels. Separating native gels were performed with a linear acrylamide concentration 4-13%, for that, 4% acrylamide and 13% acrylamide stocks were prepared separately and mixed before polymerization taken place. Polymerized separating 4-13% gels (acrylamide:bisacrylamide 30:0.8) were overlayed with stacking 3.5% gels, both of them 500 mM aminocaproic acid, 50 mM Tris-HCl pH 7.0 and polymerized by adding APS (10%) and TEMED. Loading buffer (250 mM Tris-HCl pH 6.8, 50% (w/v) glycerol and 0.02% (w/v) bromophenol blue) was added to the samples at a 5:1 ratio. Samples were not heated before being loaded on the polyacrylamide gel. The electrophoretic run was performed on ice and at low voltage to avoid protein denaturalization. Gels were powered up at a constant current (150V) for 120 min. For the electrophoresis running, the anode buffer was 25 mM imidazole, 100 mM Tris-HCl pH 7.0, while the cathode buffer was

75 mM imidazole, 50 mM tricine, 100 mM Tris-HCl pH 7.0 and 0,02% (w/v) Coomassie blue G-250 (Coomassie blue G-250 stock previously prepared in 500 mM aminocaproic acid pH 7.0). Finally, to improve the visualization of the protein bands, gels were stained with a standard Coomassie-blue protocol as was described in the previous sections.

3.8.4. Radio-labeling assays.

Purified proteins were incubated with ^{14}C-labeled fatty acids for 10 min at room temperature. Then, samples were analyzed by native polyacrylamide gel electrophoresis (Native-PAGE), following the protocol previously described [360]. 4.5 % polyacrylamide gels were run at pH 8.5 for 140 min in an ice bath, with a constant amperage (30 mA). Then, gels were dried, exposed overnight and reveled using a Fluoro Image Analyzer FLA-5100 (FujiFilm) to detect radiolabeled protein on electrophoretic bands.

3.8.5. Analysis of activity.

A specific buffer was used for each ATPase to register ATP hydrolysis at optimal conditions at steady-state. TrwD and TrwC ATP hydrolysis rates were determined in buffer DC: 50 mM Tris-HCl pH 8.5, 75 mM potassium acetate, 10 µM magnesium acetate and 10% (w/v) glycerol. ATP hydrolysis by TrwBΔN70 was measured in buffer 50mM Pipes-NaOH pH 6.2, 35 mM sodium chloride, 5 mM magnesium acetate and 5% (w/v) glycerol. ATP hydrolysis by TrwK was measured in buffer 50 mM Pipes-NaOH pH 6.45, 75 mM potassium acetate, 10 mM magnesium acetate, 5% (w/v) glycerol, 1 mM sodium acetate, 1 mM DTT and 0.1 mM EDTA. Before starting the reaction by adding the corresponding ATPase, ATP and fatty acids diluted in DMSO were added to the concentrations indicated in the text.

3.8.5.1. ATPase activity assays.

EnzCheck™ assay: due to the magnesium dependence of the pyruvate kinase enzyme, this assay replaced the coupled assay when the magnesium concentrations were not saturating. The ATPase activity was measured using the commercial kit EnzCheck™ "phosphate assay kit" (Invitrogen). The reactions were carried out in the presence of 0.15 units PNP (purine nucleoside phosphorylase) and 0.2 mM MESG (2-amino-6-mercapto-7-methylpurine riboside). ATP and magnesium were added according to the requirements of each specific experiment and the reactions were started by adding the protein assayed. The activity was characterized by measuring the absorbance at 360 nm for 5 minutes at 30°C in a UV-1800 spectrophotometer (Shimadzu). Previously, a standard curve was made using KH_2PO_4 as P_i source.

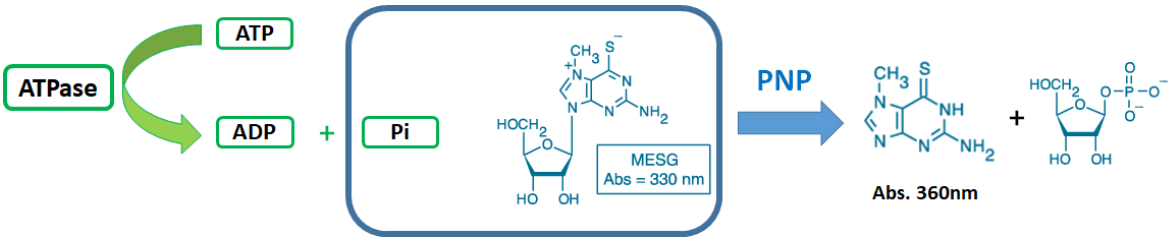

Figure 2.3. Representative diagram of the EnzCheck™ assay. Enzymatic conversion of MESG in ribose 1-phosphate and 2-amino-6-mercapto-7-methylpurine by PNP. The change in absorption at 360 nm allows the quantification of the inorganic phosphate (P_i) consumed in the reaction.

Coupled assay: Proteins were pre-incubated with the different substrates for 5 minutes at 37˚C. Reactions were started by the addition of ATP. Activity was measured by the decrease in NADH absorbance at 340 nm for 10 minutes at 37˚C in a UV-1800 spectrophotometer (Shimadzu).

Figure 2.4. Representative diagram of the coupled-enzyme assay. The assay is based on a reaction in which the regeneration of hydrolyzed ATP is coupled to the oxidation of NADH (0.25mM). Following each cycle of ATP hydrolysis, the regeneration system consisting of 0.5 mM Phosphoenolpyruvate (PEP) and 60 µg/ml Pyruvate kinase (PK) converts one molecule of PEP to Pyruvate when the ADP is converted back to the ATP. The Pyruvate is subsequently converted to Lactate by 60 µg/ml Lactate dehydrogenase (LDH) resulting in the oxidation of one NADH molecule. The assay measures the rate of NADH absorbance at 340 nm, which is proportional to the rate of steady-state ATP hydrolysis. The constant regeneration of ATP allows monitoring the ATP hydrolysis rate over the entire course of the assay [361].

3.8.5.2. Kinetic parameters determinations.

Analysis of ATP turnover: the kinetics parameters of ATP hydrolysis were obtained after fitting data to the Hill equation.

$$v = \frac{V_{max} \cdot [S]^{nH}}{K_{0.5}{}^{nH} + [S]^{nH}}$$

where v is the measured velocity, v_{max} is the speed limit of the reaction when all the enzyme is saturated by the substrate, $K_{0.5}$ is the substrate concentration which reaches half of the v_{max}, [S] is the substrate concentration and nH is the Hill number.

Inhibition of the ATPase activity by COINs: inhibitors displayed cooperativity in binding and data did not followed a Michaelis-Menten, but to a Hill-type inhibition kinetic, defined as:

$$v = \frac{v_{max}^{*}}{1 + \left[\frac{[I]}{K_{iapp}}\right]^{nH}}$$

where v is the enzyme velocity, v_{max}* is the speed limit of the reaction when all the enzyme is saturated by the substrate maximum amplitude of inhibition, [I] is the concentration of inhibitor, K_{iapp} is the apparent inhibition constant for the inhibitor and nH the Hill number.

Kinetics of inhibition by ADP: kinetics of inhibition by ADP for the calculation of $K_{iapp}^{[ADP]}$ and $K_d^{[ADP]}$ were adjusted using a version of the competitive inhibition function:

$$v = \frac{X}{K_{iapp} + [ADP]}$$

Where:

$$K_{iapp} = K_i \cdot \left[1 + \frac{[S]}{K_{0.5}}\right] \quad ; \quad X = V_{max}^{*} \cdot K_i \cdot \frac{[S]}{K_{0.5}}$$

The dissociation constant for ADP, $K_d^{[ADP]}$, was calculated by fitting the data to the following equation:

$$v = \frac{[ATP] \cdot K_c}{K_{0.5}^{[ATP]} \cdot \left[1 + \frac{[ADP]}{K_d^{[ADP]}}\right] + [ATP]}$$

where v is the enzymatic velocity, K_c is the catalytic constant (ATP turnover), [ATP] is the concentration of ATP, $K_{0.5}^{[ATP]}$ is the concentration of ATP at which 50% of the rate is reached, [ADP] is the ADP inhibitor concentration and $K_d^{[ADP]}$ is the dissociation constant for ADP.

3.8.6. Limited proteolysis of TrwD.

To check possible conformational changes in TrwD by the effect of fatty acid and inhibitors, papain (Sigma-Aldrich) was used. Papain is a nonspecific protease useful to delimit structural domains in proteins, since it has low activity in stable tertiary and secondary structures [362]. Digestion was carried out at 25°C in 20 mM Tris-HCl pH 8.5, 75 mM potassium acetate and 10% (w/v) glycerol. Papain was dissolved in the same buffer and activated by addition of 50 mM β-mercaptoethanol at 37°C for 30 min just before use. TrwD (18 µM) was pre-incubated for 15 minutes at 25°C in the presence of different concentrations of fatty acids. Proteolysis was initiated by addition of papain from the activated stocks at 1:80 papain:TrwD molar ratios. After 90 minutes at 25˚C, the reaction was stopped by adding 100 µM E-64 inhibitor (Sigma Aldrich). Proteolysis products were analyzed by Tricine-SDS-PAGE electrophoresis (16.5% (w/v) acrylamide gels) followed by staining with Coomassie Brilliant Blue.

3.8.7. Mass spectrometry analysis of TrwD.

Mass spectrometry studies proteins by causing the formation of gaseous ions, with or without fragmentation, which are then characterized by their mass to charge (m/z) ratios and relative abundances and can provide both qualitative (structure) and quantitative (concentration) information on the analyzed molecules [363]. The molecules of interest are first introduced into the ionization source, where they are ionized. Two main ionization techniques are used with biological samples: MALDI (Matrix Assisted Laser Desorption/Ionization), where the ionization of the molecules is triggered by a laser beam and ESI (electrospray ionization), where high electrical voltage is applied. Charged molecules (positive or negative) are then separated according to their quotient mass to charge (m/z) and their signal is measured electrically. This technique allows calculate the mass of the molecules with high accuracy and sensitivity and is the most widely used technique to identify proteins and peptides [364].

The experiments were carried out in the Proteomics Core Facility-SGIKER (member of ProteoRed-ISCIII) at the University of the Basque Country (UPV/EHU). The equipment used was a MALDI-SYNAPT HDMS mass spectrometer (Waters, Milford, MA, USA). Samples were acidified to a final concentration of 2.5% formic acid. The samples were cleaned with a spin column (Harvard apparatus) C4 and C18, eluted with a buffer of 90% acetonitrile, 2.5% formic acid. Then, the sample was dried in a speed-vac, resuspended in 25 µl of 50% acetonitrile, 2.5% formic acid and injected by direct infusion into the mass spectrometer. Raw mass spectra were processed with ProteinLynx Global Server software (Waters, Milford, MA, USA) and internal mass calibration was performed using a Trypsin auto digestion peptide as reference (m/z = 2211.1046).

3.8.8. Gas Chromatography-Mass Spectrometry (GC-MS) of fatty acids.

The experiments were performed at the Inter American University of Puerto Rico. *E. coli* ATCC 25922 (American Type Culture Collection, Manassas, VA) was grown in Luria-Bertani Broth (LB, Lennox, Fisher Scientific, Fair Lawn, NJ) medium in the presence and absence of 2-HDA (50 µg/mL) at 37˚C for 18 h. Then, cells were collected, extracted by using 15 mL of chloroform:methanol (2:1, v/v), shaken (Labnet, Edison, NJ) for 30 min at 200 rpm, and sonicated into Ultrasonic Cleaner (Fisher Brand FB11201, Germany) at 37 kHz (100% power, 390 W) for 15 min at room temperature. Phospholipids and free fatty acids were separated from total lipids by using silica gel column chromatography. Free fatty acids were eluted by adding 15 mL of acetone, while phospholipids were eluted by adding 15 mL of hexane. Solvents from both acetone and hexane fractions were removed by rotoevaporation (Büchi, Rotavapor R-114, Switzerland) and the resulting lipid content was treated with 3 mL of methanol and catalytic amounts of 12 M HCl and subsequently refluxed for 3 h. Once the transesterification reaction was completed, methanol was removed by rotoevaporation and fatty acid methyl esters (FAMEs) were analyzed by using GC-MS (Hewlett Packard Series II MS ChemsStation coupled to a Hewlett Packard 5972 Series Mass Selective Detector equipped with a 30 m x 0.25 mm special performance capillary column HP-5MS of polymethyl siloxane crosslinked with 5% phenyl methylpolysiloxane). The selected temperature method was: 120˚C initial temperature, 5˚C/min temperature rate, and 260˚C final temperature. The split ratio was set at 10:1 for all analyses. All fatty acids were identified based on their molecular ion, base peak, fragmentation pattern and retention time and then expressed as a percentage of relative abundance (%) of total FAs.

3.9. Bioinformatics techniques.

3.9.1. Alignment of sequences and prediction of secondary structure.

The sequences corresponding to the different representative homologs of the VirB11 protein family were aligned using the T-coffee program [365] and were plotted using the Jalview program [366]. For the prediction of secondary structures, the Psi-Pred program was used [367].

3.9.2. Molecular modeling and prediction of three-dimensional structure.

The atomic models of TrwD (R388), TraG (pKM101) and TrbB (RP4) were generated by molecular threading using the Phyre 2 tertiary structure prediction server [368]. The atomic coordinates of VirB11 from *B. suis* (PDB ID: 2gza) [228] were used as a template for TrwD and TraG, and the coordinates of HP0525 from *H. pylori* (PDB ID: 1nlz) [219] for TrbB. The hexameric

models, both TrwD and TraG, were generated by UCSF Chimera [369] based on the hexamer structure of VirB11 from *B. suis*. The hexameric model of TrbB, on the other hand, was based on the structure of HP0525.

3.9.3. Ligand blind docking.

The structural coordinates of COINs and fatty acids derivatives were retrieved from PubChem database (https://pubchem.ncbi.nlm.nih.gov/). Molecules were prepared for docking using the DockPrep tool of UCSF Chimera software package [369]. This involved the addition of hydrogens, the replacement of incomplete side chains with Dunbrack rotamer library [370], the removal of solvent water molecules, and the inclusion of partial charges using AMBERff12SB force field. Files containing the atomic coordinates of the target protein and the fatty acids were submitted to the SwissDock server (http://www.swissdock.ch/), which uses an EADock dihedral spacing sampling (DSS) engine for docking drug-like ligands into macromolecules [371]. Docking runs were blind performed over the entire molecule, without defining any specific region of the protein in order to prevent bias. Results were examined with UCSF chimera and outer clusters were ranked according to Full-Fitness (FF) score of Swissdock. Binding poses with the best FF score and minimal energy were finally selected. Structural molecular representations were rendered with PyMOL [372]. Electrostatic potential maps were calculated with the PDB2PQR application [373], using PROPKA for pKa calculations, and the resulting APBS files [374] were rendered with Pymol.

3.10. Cellular biology techniques.

3.10.1. Fluorescence microscopy techniques.

Fluorescence microscopy was performed using a DeltaVision personal IDV high resolution imaging system (inverted epifluorescent deconvolution microscope) with a × 100 1.4 numerical aperture objective, CCD camera and lasers as light source fitted with a WeatherStation environmental chamber (Applied Precision, GE Healthcare, Issaquah, WA, USA) during my research stay at the University of Technology Sydney (UTS). Alternatively, images were adquired with a widefield epifluorescence microscope Nikon Eclipse Ti2 equipped with an APO TIRF x100/1.49 objective, with LED as light source and a sCMOS camera (Hamamatsu Orca-Flash4.0) at the Institute of Biomedicine and Biotechnology of Cantabria (IBBTEC).

Microscope slides were performed following the procedure previously described by [375]. 1.5% agarose pads were performed with M9 minimal medium supplemented with 100µM $CaCl_2$, 20 mM $MgSO_4$, 0.2 % casaminoacids and 0.5 % glucose to improve cell growth rates. For microscopy, M9 is preferred to LB due to its lower auto-fluorescence. However, even though minimal medium is supplemented, the growth rates are lower than with rich medium. To overcome this inconvenient, GellaGum (GG) pads with rich-medium were performed as described previously by [376]. Gellan gum is optically clearer than agar and agarose as a setting agent and

does not auto-fluoresce. This reduces background for fluorescence microscopy and enables the addition of fluorescent dyes to the GG or to use bacteria expressing fluorescent proteins for the assay. Gellan gum media (GG) contains 8 g/L gellan gum, 10 g/L tryptone, 5 g/L yeast extract and 5 g/L NaCl, the full strength of NaCl used is sufficient to cross link the gellan gum. This rich-medium allowed optimal growth rates.

Cells preparation for visualization under the fluorescence microscope was performed from a well-isolated colony picked form a fresh restriking of cells and grown in LB media with the corresponding antibiotic. Otherwise, a sterile inoculating loop was used to gently scrape two or three large bacteria colonies from a petri plate and transferred them directly to the microscope slide previously prepared.

Chapter 4
RESULTS

Esther Lederberg

4.1. Identification of the molecular target to inhibit bacterial conjugation.

Unsaturated fatty acids (uFAs) have been defined as effective inhibitors of bacterial conjugation by high-throughput screening (HTS) assays [322]. However, at the beginning of this thesis project, it was not known the exact mechanism by which these compounds were exerting their effect on the conjugative bacteria. Therefore, this was one of the main objectives of this work.

The bibliography led us to think that uFAs might target the conjugation machinery by affecting any of the ATPases associated with the type IV secretion system (T4SS), since it was previously reported that uFAs, such as linoleic acid or oleic acid, are inhibitors of ATPases like DNA polymerase β [377], Na+, k(+)-ATPase [378] or G-proteins [379]. Accordingly, in a previous work to this thesis, the effect of these compounds on two of the four ATPases encoded by the conjugative plasmid R388 was tested (Cristina Machón, Doctoral Thesis, 2004, *results not published*). Whereas no effect on TrwC ATPase activity was detected, TrwD ATPase activity was reduced more than ten times, suggesting that TrwD might be a target for these compounds on the conjugative plasmid R388. Nevertheless, at that time, none of the other ATPases were analyzed and these results were not further pursued.

The effect of uFAs was not only analyzed on R388, but also on other conjugative systems from different incompatibility groups (Inc) and mobilizable plasmids [322,329]. In addition to IncW, it was found that uFAs also inhibited IncF plasmids and, less efficiently, IncH plasmids. While IncI, IncX, and IncL/M plasmids were moderately inhibited, IncN and IncP plasmids were completely resistant to COIN action. During her thesis, Dr. Cristina Machón reported that uFAs could be affecting the DNA transfer region (Dtr) of the conjugative plasmid R388, since the conjugative frequency (CF) of R388 was reduced, but the frequency of mobilization of plasmid CloDF13 was not altered in the presence of uFAs. This plasmid uses the mating pair formation system (Mpf) region of R388 to be mobilized, but it encodes its own coupling (MobB) and relaxase (MobC) proteins [380]. Therefore, her results pointed out that TrwB and TrwC from R388 could also been possible targets for COINs. Nevertheless, more recent assays have concluded just the opposite. Only when the helper plasmid is affected by COINs, conjugation of the mobilizable plasmid is inhibited [329]. Therefore, contrary to previous studies, these new results suggested a shared target of COINs in mobilization and conjugation, pointing to a component of the Mpf system, probably the ATPases TrwD or TrwK [329]. Additional assays support the last hypothesis: *oriT*-MOB region of R388 (pHP161) [381] was mobilized using the Mpf system of plasmid pKM101 [49]. When COINs were added to conjugation media, no inhibition effect was observed, as occurred for plasmid pKM101 transfer itself. In addition, the effect on donor and recipients cells was also assayed, showing that the inhibitory effect is exerted only on donor cells [329].

4.1.1. Effect of linoleic acid on the ATP hydrolysis activity of conjugative ATPases.

In order to determine the specific target of uFAs in our model system, the conjugative plasmid R388, the activity of the four ATPases involved in the conjugative process (TrwB, TrwC, TrwD and TrwK) was analyzed. We followed the purification protocols described in *Experimental Procedures* for TrwD, TrwC, TrwB and TrwK, [235,79,173,206] respectively.

We decided to start by assaying the effect of the linoleic acid, since this uFA had been described as one of the most powerful inhibitors of R388 conjugation [322]. We assayed the effect *in vitro* (50 µM linoleic acid) over the four ATPases (2 µM) that participate in the processing and transport of the nucleiprotein complex. At this concentration, 95% reduction of the ATPase activity of TrwD was observed, whereas no statically significant effect on the activity of any of the other three ATPases was detected (Figure 4.1). These results suggest that TrwD is a specific target of uFAs.

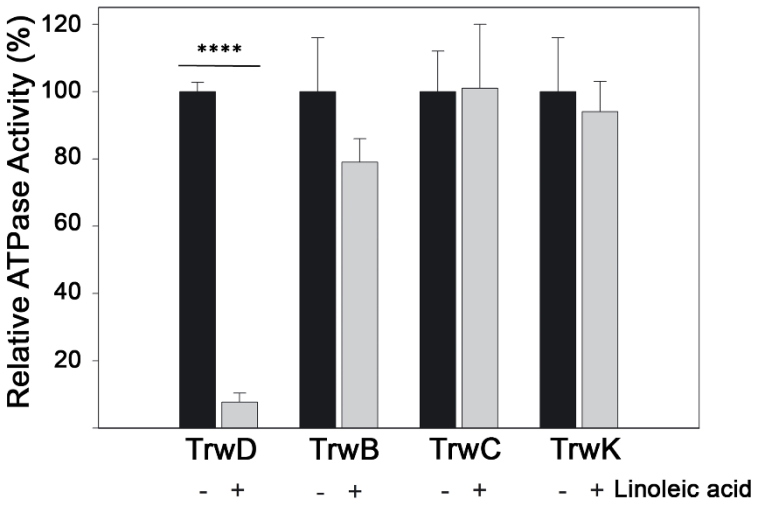

Figure 4.1. Effect of linoleic acid on the ATPase activity of conjugative ATPases. Bacterial conjugation is powered by four ATPases: the relaxase TrwC, the coupling protein TrwB, TrwK and TrwD. TrwC and TrwB are involved in the processing and transport of conjugative DNA (Dtr region of the conjugative plasmid R388), whereas TrwK and TrwD are involved in pilus biogenesis and substrate transport across the Type IV secretion system (Mpf region of the conjugative plasmid R388). ATPase activity by each of the four ATPases (2 µM) was measured in the absence or presence of linoleic acid (50µM). As ATPase rates are different for each ATPase, hydrolysis activity is expressed as relative ATPase activity. (Error bars: SD). Statistical significance analyzed by Student's t-test (****p<0,0001).

4.1.2. Effect of saturated and unsaturated fatty acids on TrwD ATPase activity.

In contrast to uFAs, saturated fatty acids are not able to inhibit bacterial conjugation [322]. In order to determine whether there was a correlation between the *in vivo* experiments and the *in vitro* analysis, we tested the effect of different type of fatty acids on TrwD ATPase activity, the specific molecular target of COINs. Oleic ($C_{18:1\ (9)}$) and linoleic ($C_{18:2\ (9,12)}$) acids (cis-unsaturated C_{18} fatty acids, with one and two double bonds, respectively), previously identified as effective inhibitors of bacterial conjugation *in vivo* [322], were selected as uFAs. Lauric ($C_{12:0}$) and palmitic ($C_{16:0}$) acids, which are unable to inhibit R388-mediated conjugation [322], were chosen as representative examples of saturated fatty acids. TrwD (2 µM) ATPase activity was measured in the presence of each fatty acid (50 µM). At this concentration, oleic and linoleic acids were able to inhibit more than 90 % of TrwD ATPase activity whereas in the presence of saturated fatty acids no inhibition was observed (Figure 4.2). These results strongly support that the presence of unsaturation in the fatty acids is essential to inhibit TrwD ATPase activity, and show a perfect correlation with the results observed *in vivo*.

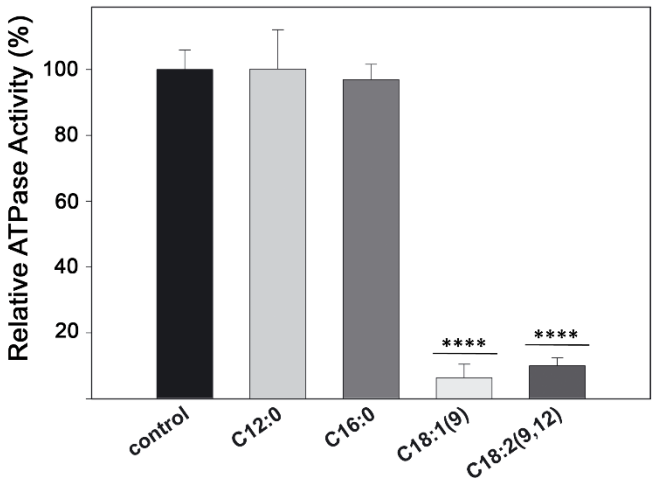

Figure 4.2. Effect of saturated and unsaturated fatty acids on TrwD ATPase activity. The ATPase activity of TrwD (2 µM) was measured in the presence of 50 µM lauric (C12:0), palmitic (C16:0), oleic (C18:1(9)), and linoleic (C18:2(9,12)) acids. (Error bars: SD). Statistical significance analyzed by Student's t-test (****p<0,0001).

4.1.3. Effect of 2-alkynoic fatty acids and derivatives on TrwD ATPase activity.

Synthetic fatty acids, such as 2-alkynoic fatty acids (2-aFAs), a class of acetylenic fatty acids with a triple bond between the C-2 and C-3 carbons of the alkyl chain, have also been found to be effective in inhibiting bacterial conjugation [329]. Therefore, we decided to test whether TrwD was also the molecular target of 2-aFAs, as in the case of the linoleic acid. For this analysis, we proceeded to analyze the ATPase activity of TrwD in the presence of these compounds, as in the previous section.

The three compounds found to be able to inhibit TrwD *in vitro* in a significant way were 2-hexadecynoic acid (2-HDA), 2-octadecynoic acid (2-ODA), and 2,6 hexadecadiynoic acid (2,6-HDA). Interestingly, alcohol (OH) or tetrahydropyranyl-ether (THP) derivatives of these compounds were unable to inhibit the ATPase activity of TrwD (Figure 4.3).

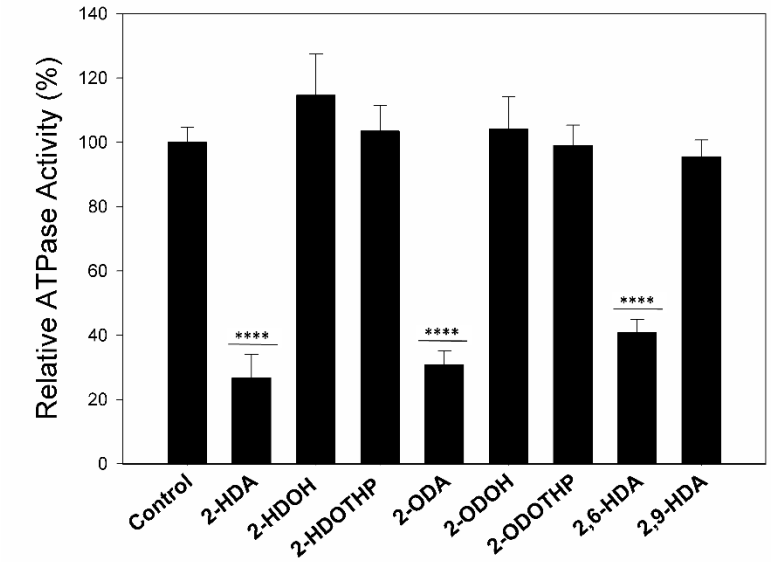

Figure 4.3. Effect of 2-alkynoic fatty acids and derivatives on TrwD ATPase activity. ATPase activity by TrwD (2 µM) was tested in the presence of 50 µM of 2-octa (2-ODA) and 2-hexa-decynoic acids (2-HDA, 2,6-HDA and 2,9-HDA), and alcohol (OH) or tetrahydropyranyl-ether (THP) derivatives. (Error bars: SD). Statistical significance analyzed by Student's t-test (****p<0,0001).

In order to analyze if there was a direct correlation between the results obtained *in vivo* and TrwD ATPase activity *in vitro*, we decided to increase the concentration of fatty acids in our analysis (from 50 to 500 µM), to mimic the conjugation inhibition assays.

Even at such a high concentration, the results obtained *in vitro* where equivalent to those obtained with the low concentration of inhibitors (50 µM), discarding an unspecific mechanism of inhibition. Again, 2-HDA, 2-ODA and 2,6-HDA were able to inhibit TrwD while alcohol (OH) or tetrahydropyranyl-ether (THP) derivatives of these compounds did not have any effect on TrwD ATPase activity (Figure 4.4). Exactly the same compounds that inhibited TrwD *in vitro* were also able to inhibit bacterial conjugation *in vivo*, whereas those with no effect *in vivo* did not have any effect on the *in vitro* TrwD activity (Figure 4.4). These results strongly reinforce the hypothesis that TrwD is the specific target for both alkenoic and alkynoic fatty acids.

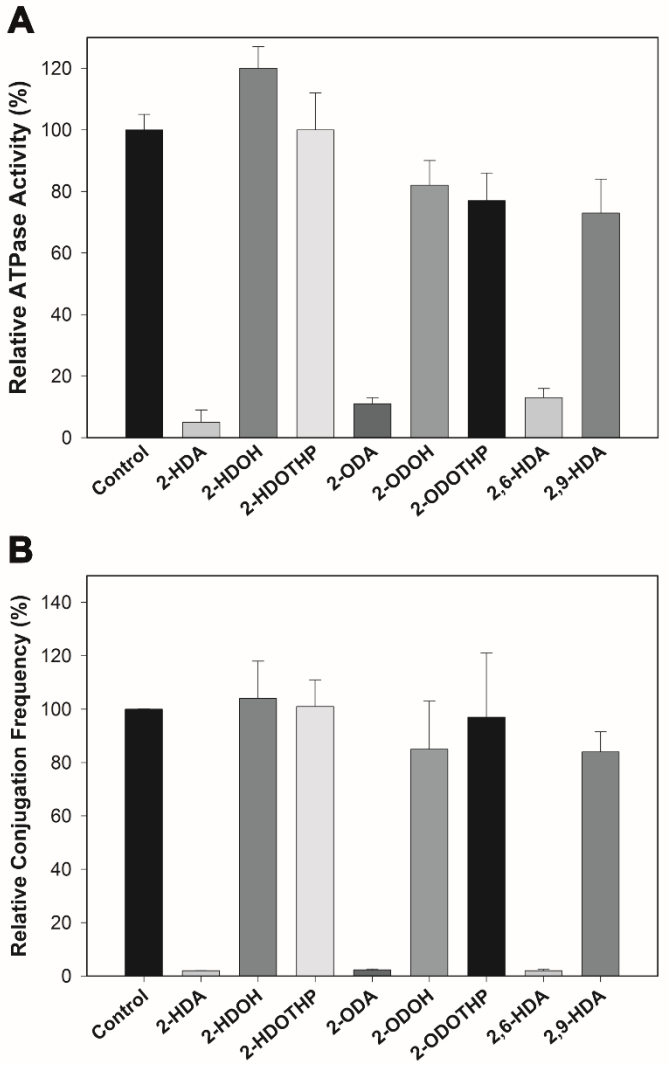

Figure 4.4. Effect of 2-alkynoic fatty acids and derivatives on TrwD ATPase activity and bacterial conjugation. (A) Bacterial conjugation was monitored in the presence of 2-alkynoic fatty acids derivatives (500 µM). **(B)** ATPase activity by TrwD (2 µM) was tested in the presence of 500 µM of 2-octa (2-ODA) and 2-hexa-decynoic acids (2-HDA, 2,6-HDA and 2,9-HDA), and alcohol (OH) or tetrahydropyranyl-ether (THP) derivatives. (Error bars: SD).

4.2. Identification of a conjugation inhibitor (COIN) with new structural characteristics.

As outlined in the previous section, the carboxylic acid group of COINs is essential to exert their inhibitory effect, since alcohol or tetrahydropyranyl-ether derivatives of these fatty acids were unable to inhibit TrwD ATPase activity *in vitro* and R388 conjugation *in vivo* (Figure 4.4). Moreover, this inhibitory effect was observed only in the presence of unsaturated fatty acids, such as oleic and linoleic acids, but not in the presence of saturated fatty acids like lauric or palmitic acids (Figure 4.2). Therefore, we decided to determine if fatty acids exert their inhibition effect because of the presence of double or triple bonds in their aliphatic chains or, indirectly, by the conformation that these fatty acids acquire due to the geometrical constraints in the alkane chain provided by unsaturations, disrupting the regular periodic structure.

We tested the effect of a saturated fatty acid derivative, 2-Bromopalmitic acid (2-BP). 2-BP is an analogue of palmitic acid described as inhibitor of many enzymes associated with membranes [382–384]. This simple and inexpensive reagent has been widely used for more than 50 years for the evaluation of free fatty acids metabolism [385,386].

4.2.1. 2-Bromopalmitic acid inhibits TrwD ATPase activity.

We analyzed *in vitro* the ATPase activity of TrwD (2 μM) in the presence of 2-BP (50 μM). The results showed that 2-BP was able to inhibit TrwD in the same range as 2-HDA or uFAs. TrwD ATPase activity was reduced to 23.4 ± 4.3% in the presence of 2-BP (50 μM), whereas in the presence of 2-HDA and linoleic acid the relative activities were 26.7 ± 7.3% and 10.0 ± 2.4%, respectively. In the presence of the saturated palmitic acid, TrwD ATPase activity was not affected (Figure 4.5).

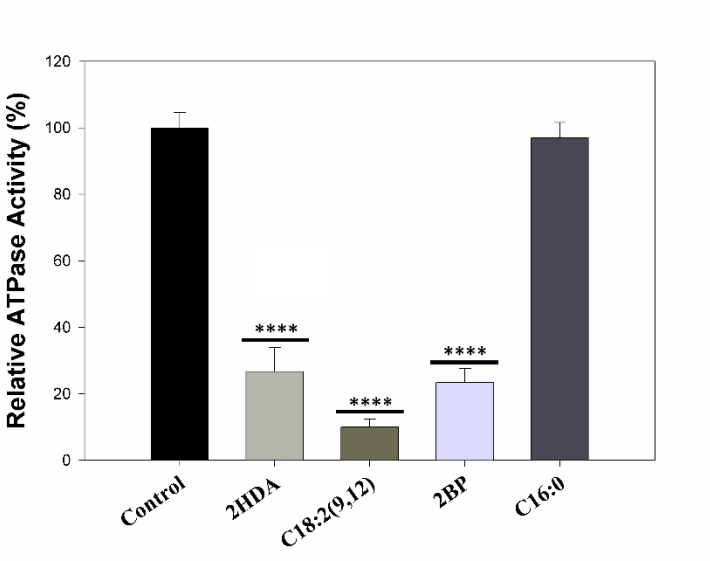

Figure 4.5. Effect of 2-Bromopalmitic acid (2BP) on TrwD ATPase activity. ATP hydrolysis of TrwD (2 µM) was monitored in the presence of 2-Bromopalmitic acid (2-BP) (50 µM) and compared with 2-hexadecynoic (2-HDA), linoleic (C18:2(9,12)) and palmitic (C16:0) acids (50 µM). (Error bars: SD). Statistical significance analyzed by Student's t-test (****p<0,0001).

4.2.2. 2-Bromopalmitic acid inhibits R388 bacterial conjugation.

As we identified TrwD as the specific molecular target of COINs and we found that 2-BP inhibits TrwD ATPase activity, we decided to check if this compound could also inhibit R388 bacterial conjugation. Therefore, R388 conjugation frequency was monitored *in vivo* following an assay previously described [329], based on GFP fluorescence emission by transconjugant cells. Conjugation frequency (CF) of the conjugative plasmid R388 in the presence of 2-BP (500 µM) was reduced to values similar to those obtained with 2-HDA and linoleic acid (500 µM) without affecting bacterial growth. 2-HDA (500 µM) inhibits R388 conjugation to 2%, whereas in the presence of 2-BP or linoleic acid (500 µM) conjugation frequency is even lower (CF = 1%).

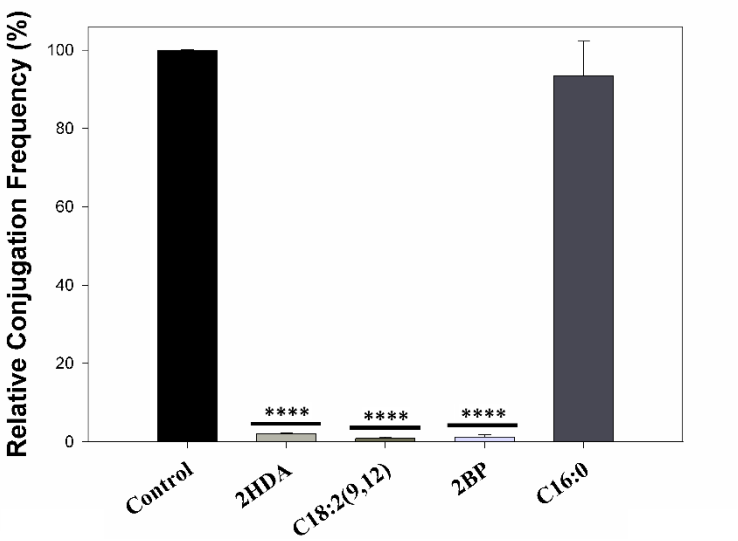

Figure 4.6. Effect of 2-Bromopalmitic acid (2BP) on bacterial conjugation. R388 Conjugation Frequency (CF) was monitored in the presence of 2-Bromopalmitic acid (2-BP) and compared with 2-hexa-decynoic (2-HDA), linoleic (C18:2(9,12)) and palmitic (C16:0) acids (500 μM). (Error bars: SD). Statistical significance analyzed by Student's t-test (****p<0,0001).

The finding of 2-BP as an effective conjugation inhibitor (COIN) allows us to conclude that unsaturation itself cannot explain the inhibitory effect exerted by these fatty acid derivatives that act as COINs.

4.3. TrwD binding to COINs: characterization of the mechanism of inhibition.

4.3.1. TrwD inhibition kinetics.

With the aim of a better understanding of the mechanism of inhibition of TrwD ATP hydrolysis activity by fatty acids, the characterization of the inhibition kinetics was carried out. First, the ATPase activity rates of TrwD (2 μM) at increasing concentrations of different fatty acids were determined. Analysis of the kinetics of inhibition of TrwD ATPase activity by all the unsaturated fatty acids showed a similar inhibition pattern. In all cases, data did not fit to a Michaelis-Menten inhibition kinetic curve, but to a sigmoidal Hill equation for inhibition, which suggested a cooperative effect in the inhibition kinetics (Figure 4.7).

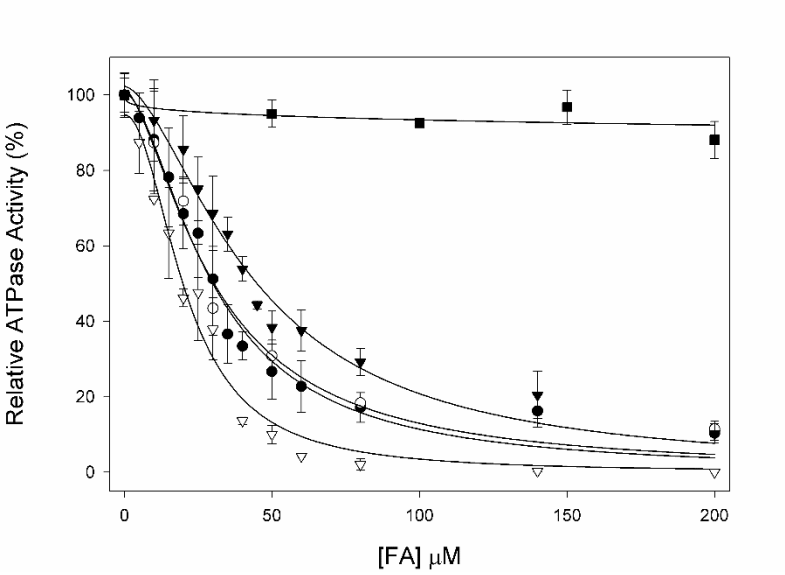

	Fatty Acid	$K_{i[app]}$ (μM)
■	Palmitic Acid	> 1mM
▼	2,6-HDA	43,8 ± 2,9
○	2-ODA	29,8 ± 4,1
●	2-HDA	29,7 ± 2,1
▽	Linoleic Acid	20,9 ± 1,7

Figure 4.7. Determination of the kinetic parameters of inhibition by fatty acids. ATP hydrolysis by TrwD (2 μM) was measured at increasing concentrations of linoleic acid (*white triangles*), 2-HDA (*black circles*), 2-ODA (*white circles*), 2,6-HDA (*black triangles*) and palmitic acid (*black squares*). Data were fitted to a Hill inhibition equation. (Error bars: SD).

As we have already described in the previous section, 2-BP is also able to inhibit both the conjugation of the conjugative plasmid R388 *in vivo* and the ATP hydrolysis activity of ATPase TrwD *in vitro*. Therefore, 2-BP emerges as a potential new conjugation inhibitor (COIN).

To define if we can really catalog 2-BP in the same group of inhibitors as these fatty acids with unsaturated bonds in its structure, we performed an analysis of the kinetic parameters of 2-BP, which were compared with those compounds previously described as COINs. ATPase activity rates of TrwD (2 μM) were measured at increasing concentrations of 2-BP. Analysis of the kinetics of inhibition of TrwD showed an inhibition pattern similar to that obtained for previously described COINs. Data fit to a sigmoidal Hill equation for inhibition. The apparent inhibition constant ($K_{i[app]}$) of 2-BP was 21.5 ± 2.5 μM, very similar to that obtained for 2-HDA (29.7 ± 2.1 μM) or linoleic acid (20.9 ± 1.7 μM) (Figure 4.8). With these results, we can confirm 2-BP as a new COIN.

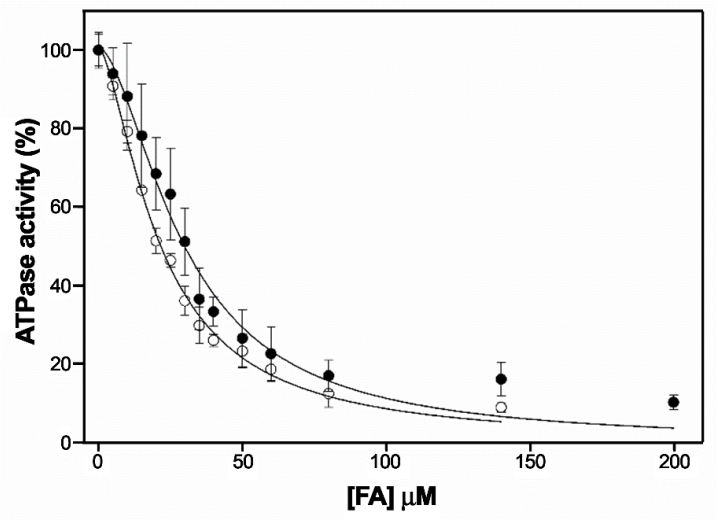

	Fatty Acid	$K_{i[app]}$ (μM)
●	2-HDA	29,7 ± 2,1
○	2BP	21,5 ± 2,5

Figure 4.8. Determination of the kinetic parameters of inhibition by 2-bromopalmitate. ATP hydrolysis by TrwD (2 μM) was measured at increasing concentrations of 2-bromoplamitate (white circles) and compared with the values obtained at increasing concentrations of 2-HDA (black circles). Data were fitted to a Hill inhibition equation. (Error bars: SD).

4.3.2. Effect of COINs on the nucleotide binding site of TrwD.

4.3.2.1. Effect on substrate binding (ATP).

Further characterization of the mechanism of inhibition at steady-state was conducted. For this assay, we selected linoleic acid and 2-HDA as representatives of the rest of COINs. ATP turnover was measured at increasing concentrations of ATP in the presence or absence of fatty acids. The concentration of linoleic acid and 2-HDA was 21 μM and 30 μM, respectively, which correspond to their respective $K_{i[app]}$. In both cases the mechanism of inhibition was non-competitive, as V_{max} was reduced without affecting the $K_{0,5}^{[ATP]}$. This result indicated that ATP binding was not affected by fatty acids (Figure).

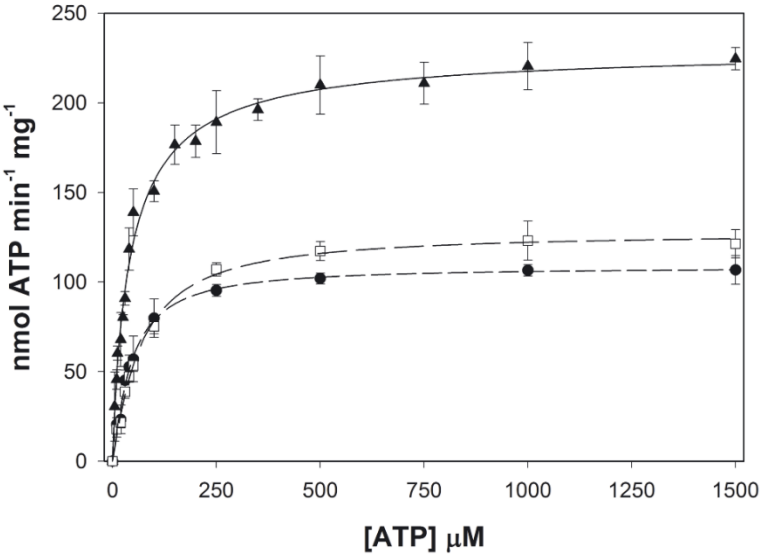

Figure 4.9. Effect of fatty acids on ATP binding. ATP hydrolysis by TrwD (2 μM) was measured in the presence of 21 μM of linoleic acid (black circles), 30 μM of 2-HDA (white squares), and in the absence of fatty acids (black triangles). Data were fitted to a Hill equation. The $K_{0,5}^{ATP}$ was 44 μM in the absence of fatty acids, 66 μM in the presence of 2-HDA and 44 μM in the presence of linoleic acid. (Error bards: SD)

4.3.2.2. Effect on product release (ADP).

In order to conduct a complete characterization of the effect of COINs over the nucleotide binding region, we analyzed the effect of ADP on TrwD ATPase activity in the presence and absence of 2-HDA. Interestingly, 2-HDA did not affect significantly the affinity of the enzyme for the ADP. In the presence of 2-HDA, the calculated K_d^{ADP} was 51 μM, and in its absence K_d^{ADP} was 44 μM (Figure 4.10). This result indicated that the inhibition was not caused by the stabilization of the enzyme TrwD in a product inhibited state.

Altogether, these results show that the inhibitory effect of COINs was not exerted by modifying the affinities of the enzyme for ATP or for the product, ADP.

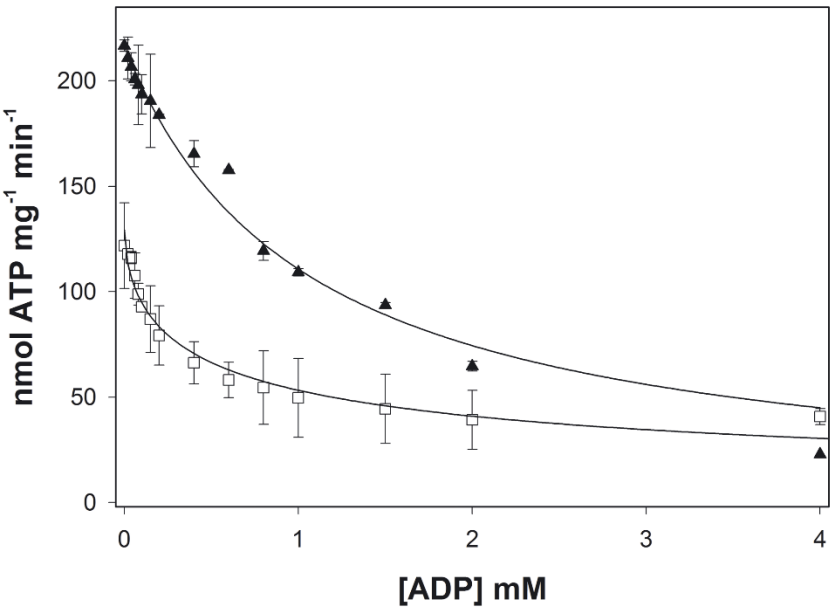

Figure 4.10. Effect of fatty acids on ADP binding. ADP titration in the presence of 2-HDA. ATP hydrolysis by TrwD (2 µM) was measured at increasing concentrations of ADP in the presence of 30 µM 2-HDA (white circles) and in its absence (black circles). Data were fitted as previously described [235]. The K_D^{ADP} in the presence of 2-HDA and in the control were 51 µM and 44 µM, respectively. (Error bars: SD)

4.3.3. Analysis of putative structural changes in TrwD produced by COINs.

As COINs do not affect significantly ATP or ADP affinities, they must bind to another region of the protein different from the nucleotide binding site. It is likely that binding of COINs to that other region results in protein conformational changes that lead to ATPase inhibition.

To test this hypothesis, we analyzed the susceptibility of TrwD to partial digestion by papain in the presence of different fatty acids. The unspecific protease papain is useful for delimiting structural domains in proteins, since it presents a low activity on stable secondary and tertiary structures [362]. Incubation of TrwD with increasing concentrations of 2-HDA (1:10 to 1:100 TrwD:2-HDA molar ratios) resulted in high susceptibility to papain degradation. In contrast, similar experiments performed in the presence of palmitic acid (1:100 TrwD : palmitic acid molar ratio) did not affect the susceptibility of TrwD to papain digestion (Figure 4.11).

These results suggest that COIN binding induces an open conformation of TrwD, resulting in the exposition of protein domains to papain. Such a conformational change was not induced by palmitic acid, which is in accordance with the fact that saturated fatty acids do not exert any inhibitory effect.

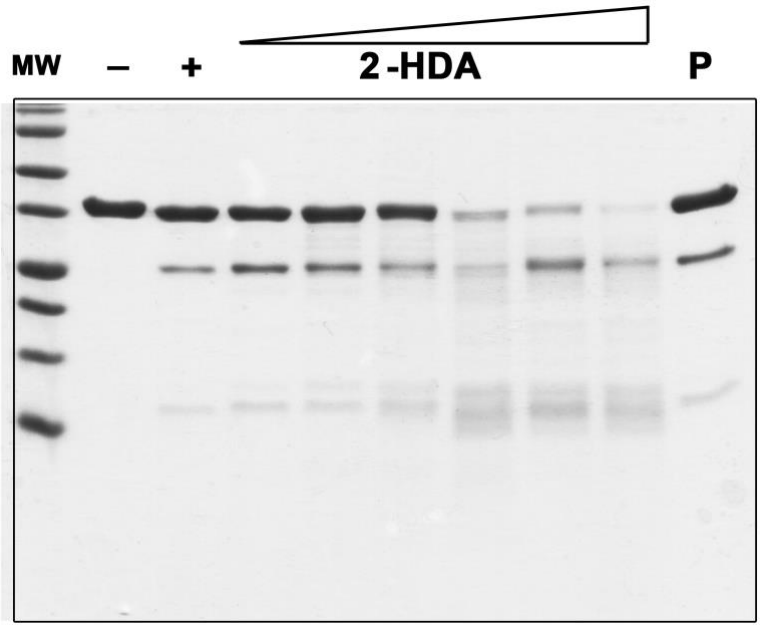

Figure 4.11. Partial proteolysis of TrwD by papain. TrwD (lane -) was incubated with papain at a molar ratio of 1:80 (TrwD : papain) (lane +). Digestion performed in the presence of increasing concentrations of 2-HDA (1:10 to 1:100, TrwD : 2-HDA molar ratios) or palmitic acid (1:100, TrwD : palmitic acid molar ratio, lane P) revealed a different proteolysis pattern. Digestion was performed for 90 min at 25˚C and proteolytic products were analyzed by Tricine-SDS-PAGE (16.5 % polyacrylamide gels).

4.3.4. *In silico* prediction of TrwD-Inhibitor interactions.

In order to explore putative binding sites for COINs in TrwD, a computer assisted analysis was performed. TrwD structural model was built by molecular threading using *Brucella suis* VirB11 [228] as a template, as previously described [235]. Fatty acid ligands were retrieved from Pubchem repository (http://pubchem.ncbi.nlm.nih.gov/) and prepared for docking as described in *Experimental Procedures*. Blind docking predictions using the EADock dihedral spacing sampling engine [371] of the Swiss-dock server (http://www.swissdock.ch/) showed a region located between the NTD (residues 37-54) and the linker region (residues 118-125) of TrwD as the site with the highest probability for COINs binding. All binding poses clustered at this same pocket formed by the NTD and the linker region when the structure of the hexameric form of TrwD was used as a target. The binding mode with the best energy and Full-Fitness is shown in the figures.

Interestingly, docking predictions with palmitic acid suggests that the binding site for this saturated fatty acid is in the same region that the one found for COINs: linoleic acid, 2-HDA and 2-Bromopalmitic acid. However, COINs fill much better the binding pocket. uFAs, aFAs and 2-BP, due to their unsaturated nature or the bromo residue respectively, acquire a different conformation, making more contacts with the protein.

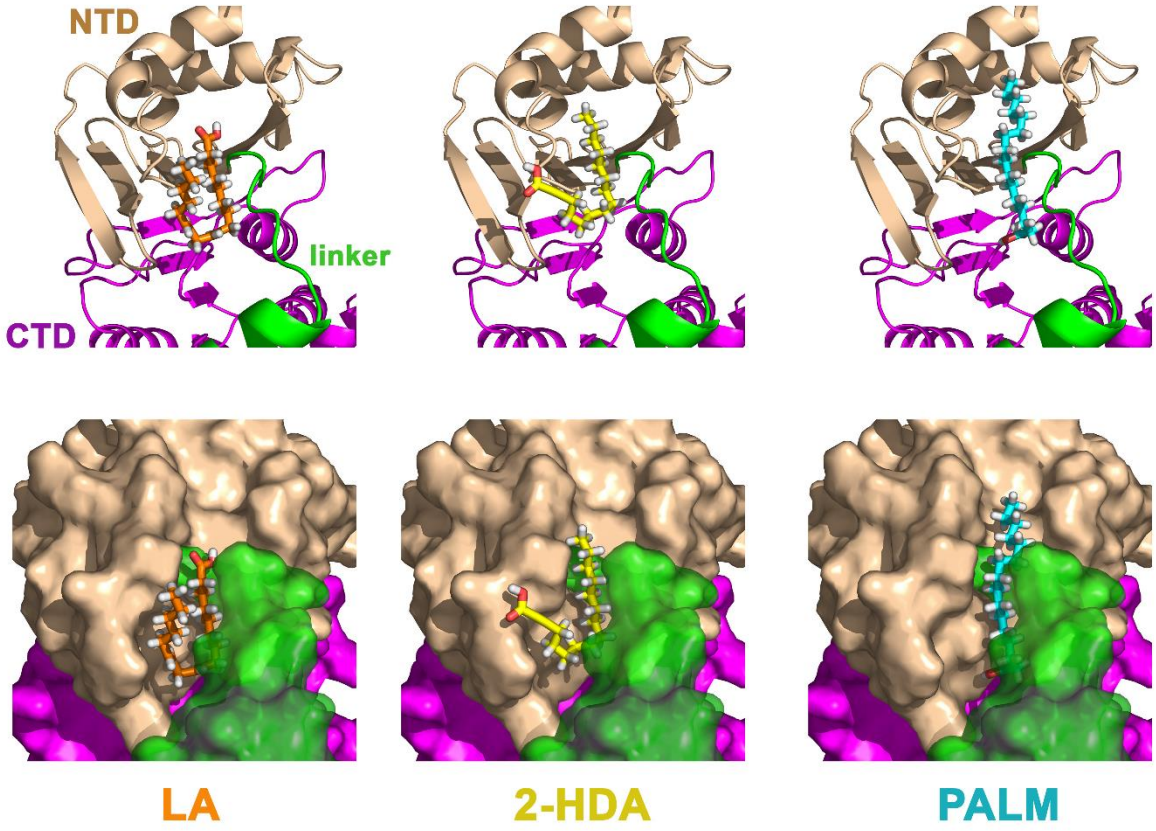

Figure 4.12. Blind docking of uFAs into the molecular model of TrwD. Blind docking predictions between a molecular model of TrwD [235] and fatty acids ligands (linoleic acid (LA), 2-hexadecanoic acid (2-HDA), and palmitic acid (PALM)). Most of the binding poses clustered at a pocket localized at the interface between the N-terminal domain (NTD, wheat) and the linker region (green), which connects the NTD with the catalytic C-terminal domain (CTD, purple). The binding modes with the best energy and Full-Fitness are shown. Upper and bottom panels correspond to the same views in cartoon and surface representations, respectively. For clarity, transparency was applied to the linker region (green) in the surface presentations (bottom panel).

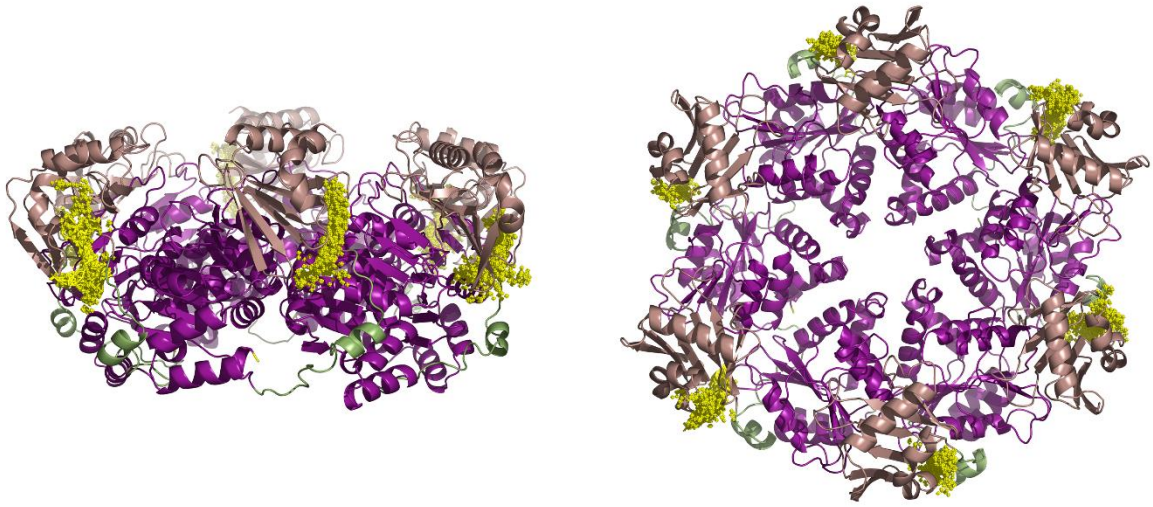

Figure 4.13. Side and top views of TrwD hexamer and 2-HDA docking. TrwD consists of an N-terminal domain, NTD (dark salmon), with is the domain that interacts with the inner membrane and the catalytic-terminal domain. CTD (magenta), bound by a long, flexible linker (smudge green). Blind docking with Swiss-Dock of 2-HDA (yellow) using hexameric TrwD coordinates as a target identified as the putative binding site of 2-HDA the region at the interface between the NTD and the linker region, exactly the same pocket shown in the previous figure. All the hits retrieved from Swissdock (256 compounds) were grouped in 6 clusters. Each of these clusters was mapping the same region within each monomer, the pocked complised by the NTD and the linker region.

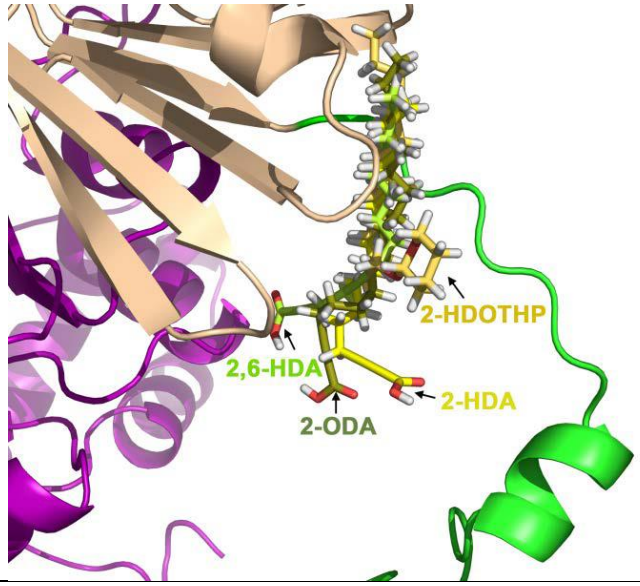

Figure 4.14. Docking of 2-alkynoic fatty acids and derivatives into TrwD. Blind docking of 2-HDA, 2,6-HDA, 2-ODA and 2-HDOTHP into TrwD. Although all compounds bind to the same site, the pocket complissed by the NTD and the linker region, the conformation of the carboxylate group is not exactly the same. In the case of 2,6-HDA the carboxylate group is at a larger distance from the linker region, which could explain its lower inhibitory effect. The tetrahydropyrane ester derivative (2-HDOTHP) cannot make electrostatic interactions with basic residues from the linker region as it lacks the carboxylate group, which might explain why it is not able to inhibit TrwD.

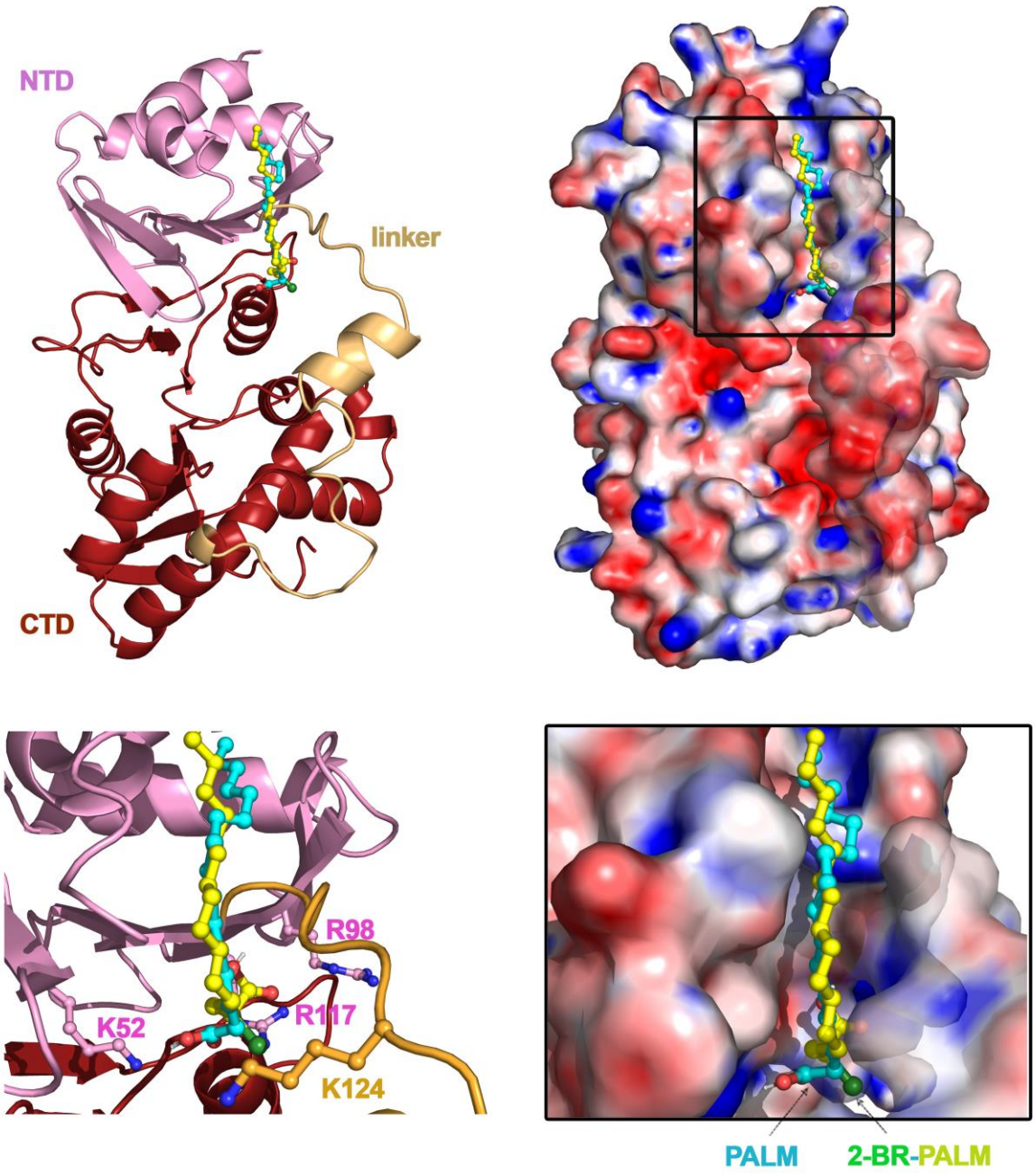

Figure 4.15. Blind docking of 2-BP and palmitic acid into the molecular model of TrwD. Blind docking between a molecular model of monomeric TrwD and fatty acid ligands (palmitic and 2-bromopalmitic acids) was performed using Swiss-dock server. Both fatty acids fit into a pocket located at the interface between the N-terminal domain (NTD, *pink*) and the linker region (*light orange*), which connects the NTD with the catalytic C-terminal domain (CTD, *brown*), as in the case of the other COINs showed in previous figures. The carbon chain of both fatty acids has a similar orientation. However, the carboxylic group of the 2-bromo derivative is buried inside a pocket formed by the NTD and the linker domain of the protein, being the bromide atom (*dark green*) stabilized by electrostatic groups located in the region (residues 115-118 of the flexible linker). On the contrary, the carboxylic group of the palmitic acid (red) is 120 degrees apart, making closer contacts with lysine 52, out of the linker region.

4.4. COINs are incorporated to membranes.

As shown in the previous section, the pocket identified by blind docking as the binding site for COINs in TrwD is in the interphase between the NTD and the linker region. Since TrwD associates to the membrane through the NTD [219], the protein might interact with the membrane via this fatty acid binding pocket.

Previous experiments had shown that TrwD ATPase activity is stimulated by phospholipids [221]. *In vitro,* TrwD interacts with phospholipids in lipid vesicles, causing lipid vesicle aggregation, leakage and intervesicular lipid mixing [226]. However, even though it is widely recognized that the traffic ATPase TrwD interact and localize to the cytoplasmic side of the bacterial inner membrane, the molecular bases underlying this interaction and binding to membrane phospholipids are not known with precision [387]. In the literature, there are several examples of proteins that associate to the membrane via a non-covalent binding to saturated fatty acids, such as palmitic acid [388]. An example are the Toll-like receptors (TLRs) [389,390], in which the fatty acid binds to lipid binding pockets. Intriguingly, TLRs are also inhibited by polyunsaturated fatty acids [391], as in the case of TrwD. Otherwise, a wide variety of proteins associate to the membrane covalently attached to palmitic acid [392,393]. In these S-palmitoylated proteins, the fatty acid is bonded to a cysteine residue through a thioester linkage. It is a reversible process that allows a transient binding to the membrane; playing a crucial role in many biological processes [392–394].

Independently of the membrane binding mode, it is tempting to speculate that uFAs and aFAs are occupying a binding site in TrwD that is otherwise occupied by bacterial membrane phospholipids involved in the association of the protein to the membrane. Therefore, if this hypothesis is correct, COINs should be incorporated to the bacterial membrane in order to exert its inhibitory effect. In an attempt to find out if fatty acid derivatives defined as COINs are incorporated to membranes, *E. coli* cells were grown in the presence and absence of the 2-alkynoic fatty acid inhibitor 2-HDA. After 18 h of incubation, the composition of the free fatty acids and the esterified fatty acids from phospholipids was checked by chromatography-mass spectrometry (GC-MS) (Figure 4.16).

The results revealed that the esterified fatty acids from the phospholipid fraction of the untreated bacteria were primarily saturated, with a chain length from 14 to 20 carbon atoms, being palmitic acid (16:0) the most abundant (≈ 44%) (Figure 4.16). Results are very similar in the free fatty acid fraction, with the exception of a decrease in palmitic acid composition and an increase in heptadecenoic acid.

In treated bacteria, 2-HDA was the major component of the total phospholipid fraction (44 %). This fact illustrates a significant alteration on the utilization of endogenous fatty acids in the biosynthesis of phospholipids and indicates that 2-HDA was activated to acyl coenzyme A thioester, which acts as substrate for the acyl coenzyme A phospholipid acyl transferase in *E. coli*.

The incorporation of 2-HDA to the bacterial membrane was accompanied by a 2-fold decrease of the most abundant fatty acid in the phospholipid fraction of untreated bacteria: palmitic acid. 2-HDA was also present in the free fatty acid fraction, but the relative proportion of free fatty acids was not significantly altered in this fraction with the treatment (Figure 3.16).

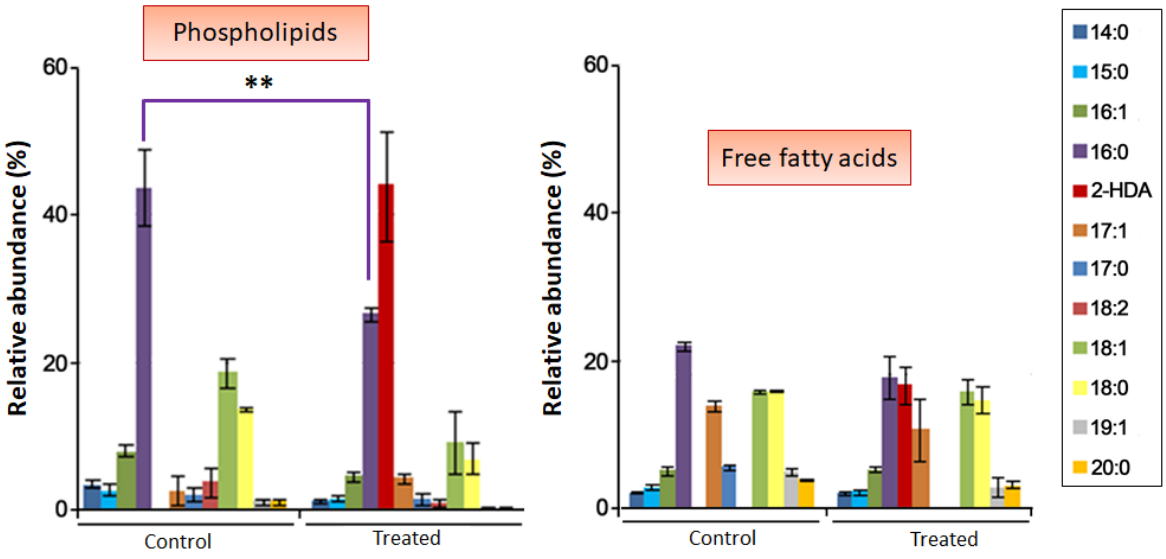

Figure 4.16. Composition of free fatty acids and phospholipid fatty acids of *E. coli* after the exposure to 2-HDA. *E. coli* cells were grown in Luria Broth (LB) containing 50 µg/ml 2-HDA at 37˚C for 18 h. Fatty acids were converted to methyl-esters and analyzed by Gas Chromatography – Mass Spectrometry (GC-MS). Values were obtained from three separated experiments. Fatty acid nomenclature indicates the number of carbons followed by the number of double bonds. (Error bars: SD). Statistical significance analyzed by Student's t-test (**p<0.005).

The results showed a replacement of saturated palmitic acid by the unsaturated 2-HDA in the phospholipids of the bacterial membrane. The molecular bases that underlie TrwD binding to the bacterial membrane are unknown but, taking into account all the results recapitulated so far, it is reasonable to think that TrwD could bind to the cytoplasmic side of the inner cell membrane through the interaction with esterified fatty acids, as palmitic acid. Such a significant replacement of palmitic acid by 2-HDA in phospholipids might be perturbing TrwD association to the bacterial membrane and its activity, resulting in an inhibitory effect.

4.5. TrwD binding to saturated fatty acids: characterization of a putative membrane binding mechanism.

4.5.1. TrwD binds palmitic acid.

Even though COINs inhibit TrwD ATPase activity while saturated fatty acids, such as palmitic acid, do not have any effect on ATP turnover, docking predictions suggest that all of them bind to the same region on TrwD (Figure 4.12). In an attempt to probe this predicted interaction between TrwD and palmitic acid, a metabolic labeling with radiolabeled palmitate assay was carried out *in vivo*, adapting protocols already used for eukaryotic cultures to bacteria [395]. *E. coli* C41 cells were cultured in the presence of different concentrations of [^{3}H]palmitate, collected and analyzed by SDS-PAGE electrophoresis. Gels were stained with Coomasie blue to detect the presence of TrwD, dried and exposed to photographic films to detect the presence of radioactivity. No radioactive signal was obtained, neither in the presence of native R388 nor overexpressing pET3a::*trwD* plasmid with IPTG.

As bacteria lysis and denaturing electrophoresis could be breaking the possible interaction between TrwD and [^{3}H]palmitate, a new protocol was developed where the traditional chemical method for cell lysis was substituted by a mechanical method based on cell homogenization with a matrix of ceramic spheres (Fast protein blue matrix, *MP Biomedicals*). After cell lysis, TrwD proteins were immunoprecipitated with magnetic balls attached to protein G. The result of that precipitation was analysed after washing the sample with PBS to eliminate free [^{3}H]palmitate. As we recover the protein by immuno precipitation, it was not necessary to perform any electrophoresis, avoiding the possible dissociation of the protein-fatty acid during the process. However, despite the fact that inmunoprecipitation was optimized, with this milder treatment, no radioactive signal was detected in the samples over background noise. Different incubation times and concentrations were tested, obtaining the same negative results.

Since it was not possible to obtain any positive result with the different procedures tested *in vivo*, we decided to carry out radiolabel binding assays *in vitro*. Purified TrwD protein was incubated with ^{14}C-labeled palmitic acid at different molecular ratios and the possible protein-ligand interaction was analyzed by native non-denaturating electrophoresis. Radioactive signal of TrwD was directly correlated to increasing palmitic acid: protein molar ratios. As negative control, the enhancer protein TrwA was assayed. No radiolabel signal was observed for this protein, not even at the highest fatty acid: protein ratio. This result confirms a specific binding of TrwD to palmitic acid (Figure 4.17).

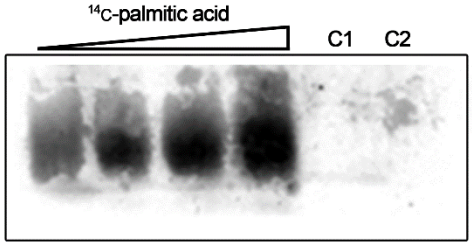

Figure 4.17. Binding of TrwD to ^{14}C-labeled palmitic acid. TrwD (80 µM) was incubated at increasing ^{14}C-labeled palmitic acid ratios (1:0.25, 1:0.5, 1:0.75 and 1:1 protein:palmitic acid molar ratios, respectively) and the protein-fatty acid complexes were analyzed by Native-PAGE. Radiolabeled images were obtained after overnight exposure, as described in *Experimental Procedures*. Lane C1 corresponds to a control experiment of TrwD (80 µM) in the absence of fatty acids. No radioactivity endogenous signal was detected. Lane C2 is another negative control experiment in which protein TrwA (80 µM) was incubated with ^{14}C-palmitic at a 1:1 protein: palmitic acid molar ratio.

The same experiment was carried out with an intermediate in phospholipid synthesis, the activated fatty acid palmitoyl-CoA. The results were similar to those obtained with free palmitic acid. A specific interaction at increasing palmitoyl-CoA:TrwD molar ratios was observed, as an increasing TrwD radiolabel signal (Figure 4.18). In this experiment it was also possible to observe the migration of the free labeled palmitoyl-CoA at the front of the gel.

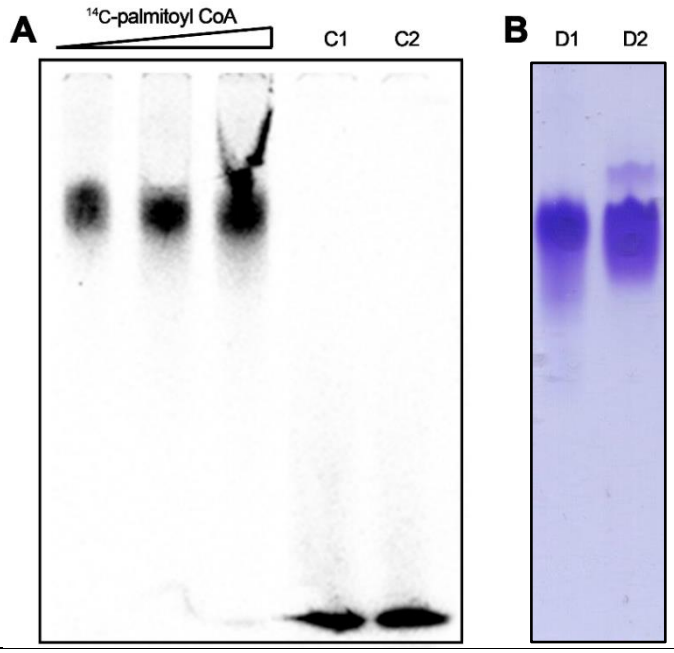

Figure 4.18. Binding of TrwD to ^{14}C-palmitoil Co-A. (A) TrwD (80 µM) was incubated at increasing ^{14}C-labeled palmitoil Co-A ratios (1:0.5, 1:0.75 and 1:1 protein:palmitoil Co-A molar ratios, respectively) and the protein-fatty acid complexes were analyzed by Native-PAGE. Radiolabeled images were obtained after overnight exposure, as described in *Chapter3*. Lane C1 corresponds to a control experiment of ^{14}C-palmitoil Co-A (80 µM) in the absence of any protein. Lane C2 is another negative control experiment in which protein TrwA (80 µM) was incubated with ^{14}C-palmitoil Co-A (80 µM). **(B)** Coomassie Brilliant Blue-stained Native-PAGE. TrwD (80 µM) (Lane D1) and purified TrwA (80 µM) (Lane D2) in the absence of fatty acids run at the same high at 4.5% native polyacrylamide gel for 140 min with a constant amperage (30 mA).

4.5.2. Palmitic acid and 2-Bromopalmitic acid compete for the same binding site in TrwD.

In an attempt to determine if COINs and palmitic acid compete for the same binding site, as was predicted by blind docking modeling, we conducted a further characterization of the mechanism of inhibition. ATP turnover was measured *in vitro* at increasing concentrations of 2-BP in the presence of palmitic acid (500 µM). Under these experimental conditions, the apparent inhibition constant [$K_{i(app)}$] of 2-BP was increased from 21.5 ± 1.5 µM to 65.4 ± 1.4 µM. This increase in the value of the apparent inhibition constant in the presence of the saturated fatty acid indicates that both fatty acids (palmitic acid and 2-BP) compete for the same binding site in TrwD.

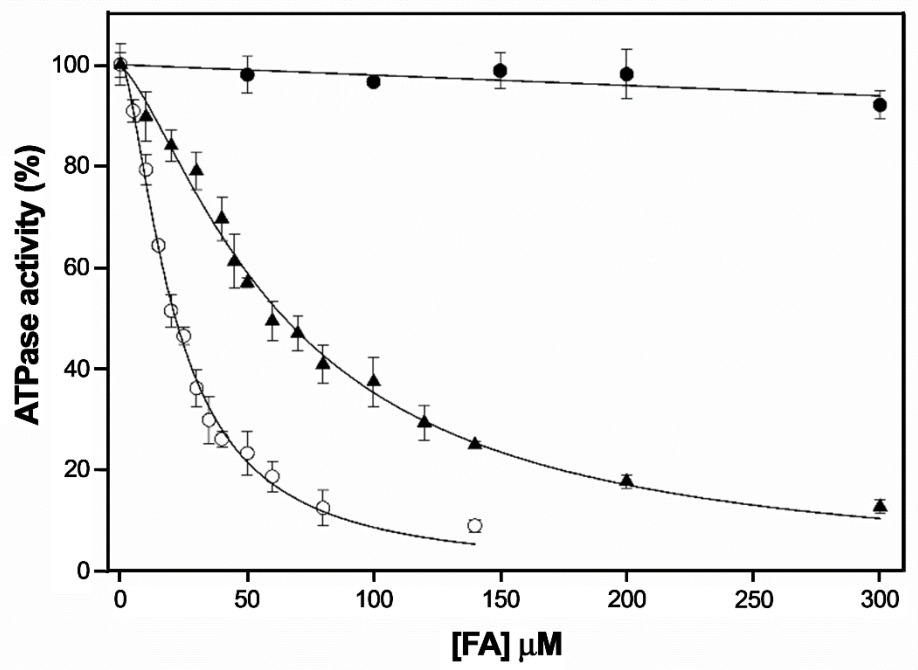

Figure 4.19. 2-bromoplamitate and palmitic acid compete for the same binding site in TrwD. TrwD ATPase rates (2 µM) were measured at increasing concentrations of palmitic acid (*dark circles*), 2-bromoplamitate (*white circles*) and mixtures of both fatty acids consisting of a fixed concentration of palmitic acid (500 µM) and increasing concentrations of 2-bromopalmitate (*dark triangles*). In the latter case, protein sample was first incubated with palmitic acid for 5 min, and then 2-bromopalmitate was added at the indicated concentrations. Data were fitted to a sigmoidal Hill equation for inhibition. (Error bars: SD).

In parallel, R388 conjugation frequency was monitored *in vivo* in the presence of palmitic acid (500 µM). Under these conditions a statistically significant higher concentration of 2-BP was required to reach a similar inhibitory effect. This correlation between the results obtained *in vivo* and *in vitro*, strongly support that both fatty acids (palmitic and 2-bromopalmitic acids) compete for the same binding site in TrwD.

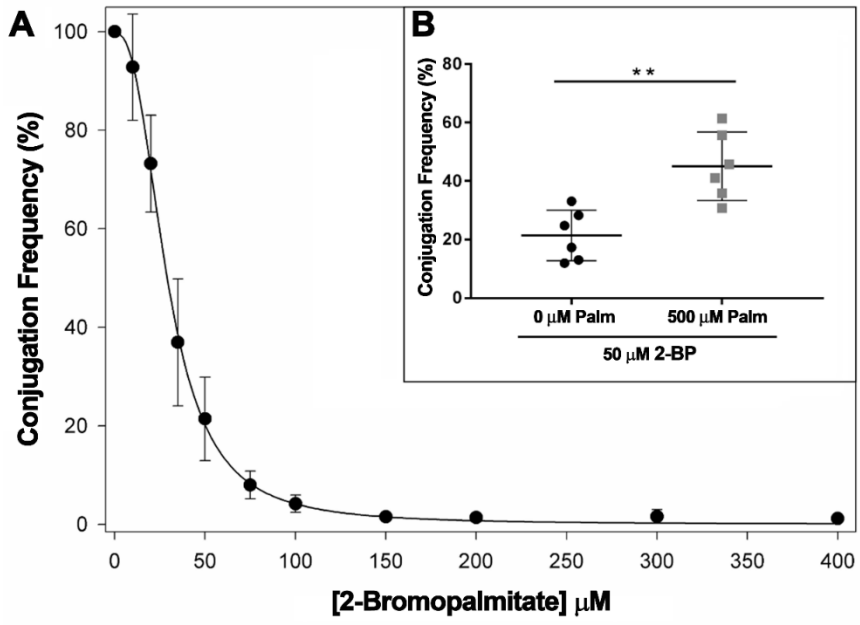

Figure 4.20. R388 Conjugation Frequency (CF) in the presence of increasing concentrations of 2-bromopalmitate. (A) Bacterial conjugation experiments were performed as described in *Chapter 3*. Values represent the mean CF ± SD of at least four independent experiments, measured by fluorescence-based HTC assay and relative to positive control in the absence of any inhibitor (100%). **(B)** Panel B (insert figure) shows the R388 conjugation frequency in vivo measured in the presence of 2-bromoplamitic acid (50 μM) (*black circles*) and a mixture of both palmitic (500 μM) and 2-bromopalmitic acid (50 μM) (*grey squares*). Horizontal and vertical bars represent the mean ± SD of each group of data. Statistical significance analyzed by Student's t-test (**p<0.005).

4.5.3. Mutagenesis of potential TrwD binding sites for palmitic acid and 2-BP.

2-Bromopalmitic acid has been described as inhibitor of many membrane-associated enzymes that bind palmitic acid [382,393]. It is an irreversible inhibitor that blocks palmitic acid incorporation onto proteins, but the exact mechanism responsible for 2-BP mediated inhibition is not known [396–398,392,394]. During this work, we have characterized 2-BP as a new COIN which inhibits bacterial conjugation and also the ATPase activity of the traffic ATPase TrwD, and determined that 2-BP and palmitic acid compete for the same binding site in TrwD. Therefore, we decided to conduct a further characterization of the mechanism of interaction. In order to explore putative binding sites for palmitic acid and 2-BP in TrwD, a mutational analysis of the traffic ATPase TrwD was performed.

2-BP has been described as an irreversible inhibitor of protein palmitoylation, a post-translational process by which a saturated fatty acid covalently binds to a cysteine residue [392,394]. *In silico* screening with the protein palmitoylation sites predictor CSS-Palm 4.0 server

[399] identified Cys44 as a potential palmitoylation site in TrwD, while no results were obtained with a negative control, the conjugative cytoplasmic protein TrwC. We performed a site directed mutagenesis and changed cysteine 44 (C44) by asparagine (TrwD C44N) (pYGC01 plasmid, Table 3.3). With this mutation, we tested the possibility that this cysteine residue was involved in the binding to palmitic acid.

On the other hand, by comparing TrwD sequence with its homologs [236], there is a region in the linker A with basic residues that conversely are acidic in the VirB11 homologs resistant to COINs (HP0525 from *H. pylori* and TraG from pKM101). We also decided to modify this region, so histidine 119 (H119) and valine 123 (V123) were both replaced by aspartic acid in a single mutant (TrwD H119D-V123D) (pYGC02 plasmid, Table 3.3). In relation to the linker, when TrwD sequence is compared with that of other VirB11 homologs [236], it is clear that TrwD shows the longest linker. Therefore, we also decided to eliminate a fragment of the linker in TrwD that is not present in TraG, the closer homolog in pKM101 plasmid (residues between alanine 148 and arginine 162 (TrwDΔ15link) (pYGC03 plasmid, Table 3.3) (see also Figure 4.21. for more clarity).

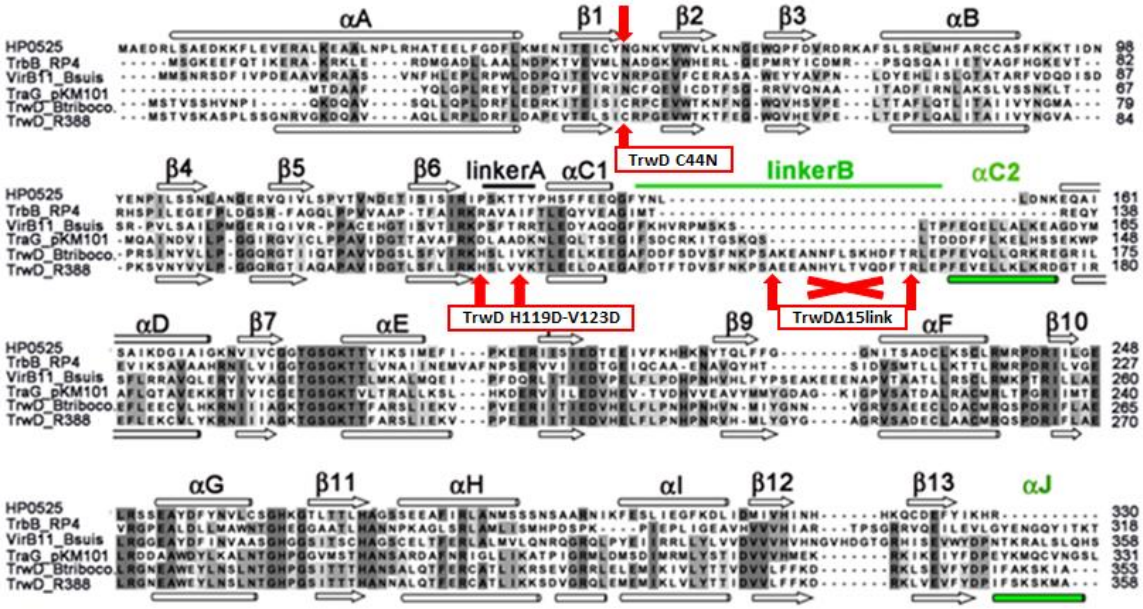

Figure 4.21. Sequence alignment of VirB11/TrwD homologs. TrwD mutants selected for this analysis are indicated in the sequence (red color). Modified from [236].

We performed an analysis in order to determine if TrwD folding and stability was affected by these modifications. Protein misfolding and inclusion bodies formation in *E. coli* cells overexpressing proteins can be identified in cell lysates by protein aggregation at low speed centrifugation. TrwD C44N and H119D-V123D mutants did not show any effect on overexpression and solubility. However, deletion of a small fragment in TrwD linker (TrwDΔ15link) resulted in an insoluble protein that formed inclusion bodies, that is, aggregated proteins that precipitate by low speed centrifugation (5,000 g) (Figure 4.22).

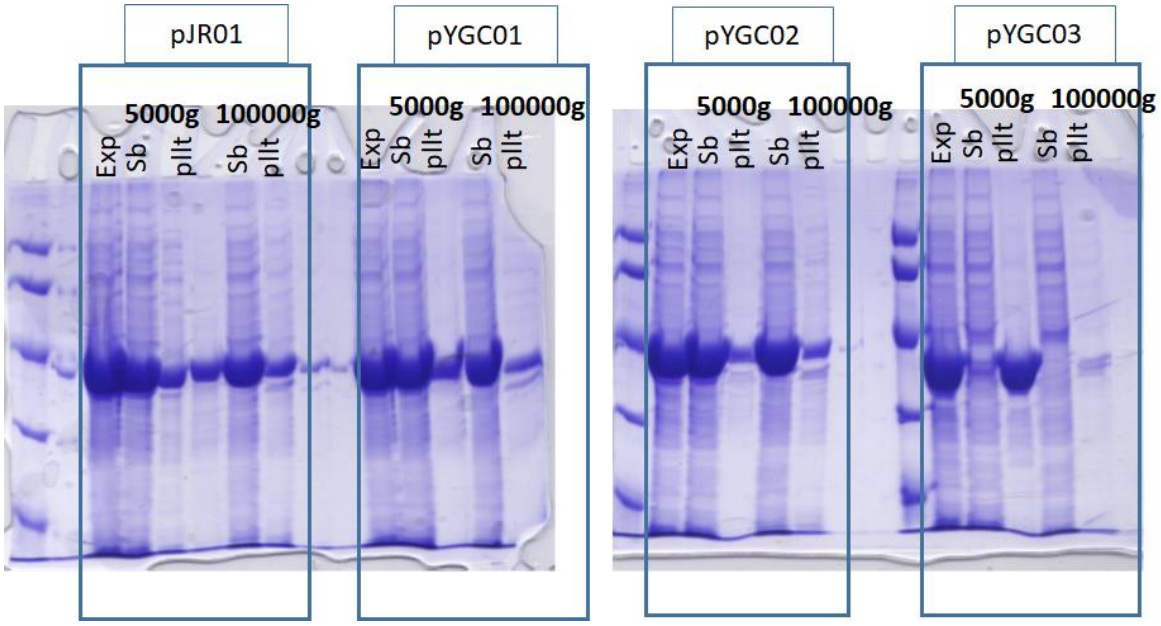

Figure 4.22. Analysis of protein aggregation. *E. coli* cells overexpressing pJR01, pYGC01, pYGC02 and pYGC03 plasmids, corresponding to TrwD wilde type, TrwD C44N, TrwD H119D-V123D and TrwDΔ15link proteins, respectively, were lysed and analyzed by centrifugation to detect protein aggregation. Lanes in each gel correspond to total protein expressed in the whole cell lysate (Exp), soluble fraction (Sb) and aggregated in the pellet fraction (pllt) after sequential centrifugation at low speed (5,000 g) and ultracentrifugation (100,000 g). TrwD wild type, C44N and H119D-V123D mutants are soluble proteins after ultracentrifugation (Sb; 100,000 g). In contrast, TrwDΔ15link protein precipitates at low speed centrifugation (pllt, 5,000 g), forming inclusion bodies. Centrifugation products were analysed by SDS-PAGE (10% polyacrylamide gels).

Finally, the ability of TrwD mutants to replace TrwD wild type was tested *in vivo* by complementation assays in R388-mediated bacterial conjugation. Without a functional *trwD* gene, there was no conjugation of plasmid pSU4039 (a R388 mutant with a transposon insertion within the *trwD gene*). Conjugation was restored when pSU4039 was complemented with a plasmid containing a functional *trwD* gene. Conjugation of pSU4039 was restored to wild-type frequencies by trans-complementation with plasmid pJR01 (*trwD* wild type) and pYGC01 plasmid (TrwD C44N mutant), but pYGC02 and pYGC03 plasmids (TrwD H119D-V123D and TrwDΔ15link proteins) were not able to complement the mutation (Table 4.1). Since TrwD H119D-V123D double mutant is a soluble protein, this result indicates that H119 and V123 are essential residues in TrwD for the conjugative process. Another interesting result is the lack of complementation by TrwDΔ15link mutant. This fragment of 15 residues is not present in protein TraG (VirB11 homolog in pKM101 plasmid), but there is a strong conservation in the residues flanking this region (TrwD and TraG present a 37% of sequence identity). Therefore, we can conclude that this small fragment in TrwD linker is essential and specific for R388 conjugation.

The results also showed that 2-BP (500 µM) was able to inhibit TrwD C44N mutant at the same range as TrwD wild type. Therefore, 2-BP is binding TrwD in a site different from cysteine residue 44. The low levels of R388-mediated bacterial conjugation by pSU4039 transcomplementation with pYGC02 and pYGC03 plasmids defined the regions modified in both clones as fundamental for protein functionality, but the results did not allow us to determine if the 2-BP binding site in TrwD is affected in these mutants.

	Conjugation Frequency NO 2-BP	**Conjugation Frequency 2-BP (500 µM)**
R388	$1{,}1 \times 10^{-2}$	$3{,}1 \times 10^{-3}$
pSU4039	---	---
pSU4039 + pJR01	$2{,}5 \times 10^{-3}$	$3{,}4 \times 10^{-4}$
pSU4039 + pYGC01	$2{,}2 \times 10^{-3}$	$3{,}4 \times 10^{-4}$
pSU4039 + pYGC02	$2{,}2 \times 10^{-6}$	$5{,}3 \times 10^{-6}$
pSU4039 + pYGC03	$5{,}1 \times 10^{-5}$	$6{,}6 \times 10^{-5}$

Table 4.1. *In vivo c*omplementation assays in the presence and absence of 2-BP (500 µM). Conjugative plasmid R388 (wild type) was used as positive control. pSU4039 plasmid is a R388 derivative plasmid without a functional *trwD gene*, so it is defective in conjugation. pSU4039 plasmid was transcomplemented with pJR01, pYGC01, pYGC02 and pYGC03 plasmids, respectively, and the conjugation frequency was analyzed in the absence and presence of 2-BP (500 µM). Donor strains *E. coli* D1210 were mated with recipient strain *E. coli* DH5α for 1h at 37˚C. Results are the means of at least three independent experiments.

4.5.4. Non-covalently binding of palmitic acid and 2-BP to TrwD.

Although the results presented in the previous section, showing that TrwD C44N mutant was a functional protein, pointed out to a non-covalently binding of the fatty acids, we decided to carry out specific experiments to determine the nature of the interaction of palmitic acid and 2-Bromopalmitic acid with TrwD.

Following the same radio-labelling assays to identify palmitic acid binding to TrwD described in section 4.5.1., we checked if the association between TrwD and the ^{14}C-labeled palmitic acid was resistant to denaturation induced by SDS gel electrophoresis. No signal of radiolabeled protein was observed, neither in the case of free palmitic acid nor in that of the thioester palmitoyl-CoA. Therefore, although radiolabel binding assays confirmed a specific interaction between TrwD and palmitic acid (Figures 4.17 and 4.18), the interaction is not resistant to protein denaturation, which suggests that the binding is non-covalent and there is not a thioester bond involved in the association between TrwD and saturated fatty acids.

Additionally, TrwD was mass-analyzed in the absence or presence of 2-BP (500µM) by mass spectrometry. This analysis technique is based on obtaining ions from organic molecules that are separated according to their mass and charge. Incubation of TrwD with 2-BP at a molar ratio of 1:10 (TrwD : 2-BP) did not result in a protein with higher molecular mass. The molecular masses determined were 39,980.5 ± 6.5 and 39,997.5 ± 3.5 Da in the absence and presence of 2-BP, respectively (Figure 4.23). The results allowed us to conclude that 2-BP binds non-covalently to TrwD.

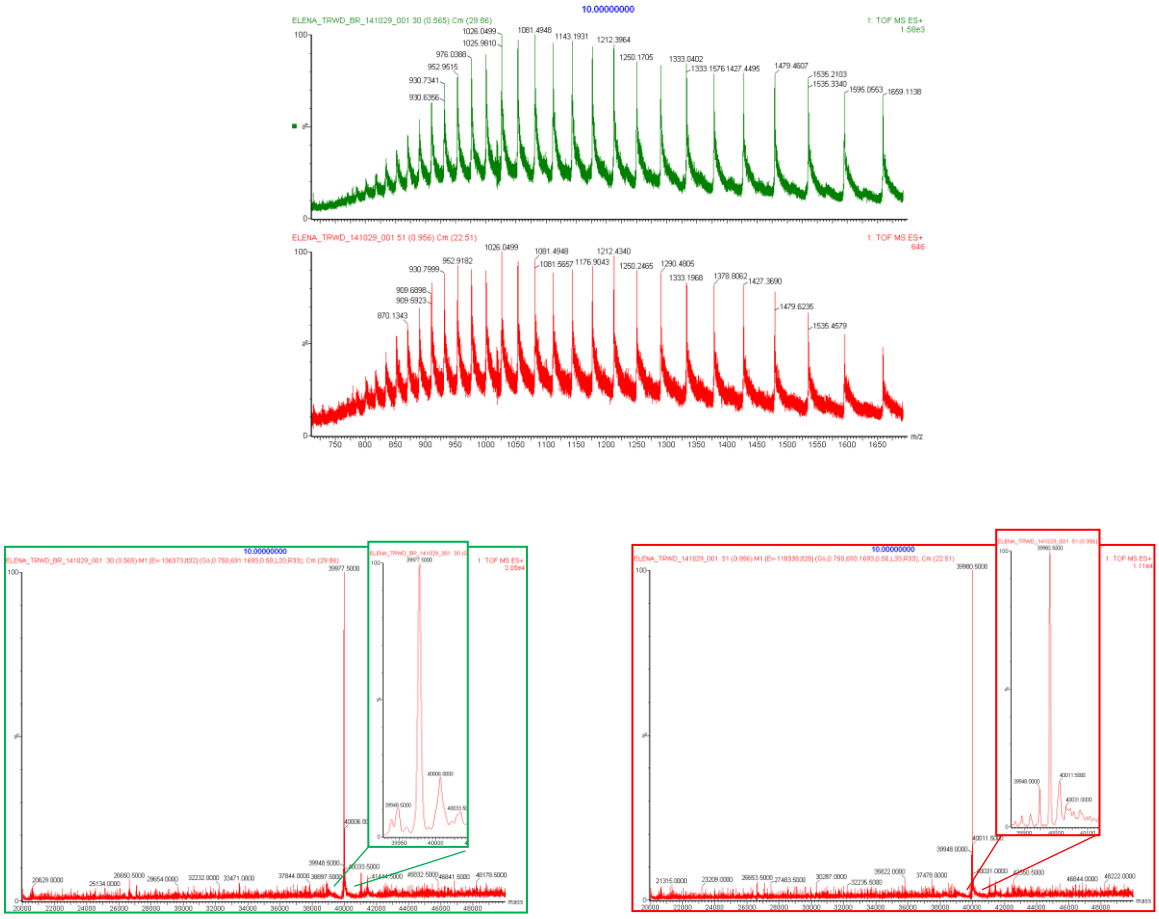

Figure 4.23. Mass spectroscopic analysis of TrwD. Upper panel. The crude, unprocessed mass spectrum of TrwD in the absence (red) or presence (green) of 2-BP (1:10, TrwD : 2-BP molar ratio). There are no differences between both samples in the peak pattern that represents the ionic abundances obtained as a function of the mass/charge ratio. **Bottom panels.** Data processing in the range of 20,000-50,000 Da revealed 39,980.5 ± 6.5 and 39,997.5 ± 3.5 Da as TrwD molecular mass in the absence (red) and presence (green) of 2-BP, respectively. The rest of peaks are below 10% signal (background). TrwD:2-BP incubation was performed for 15 min at 25˚C.

4.6. Analysis of the molecular interaction between TrwD and TrwC.

As discussed in the introduction, the substrate to be transported during the conjugative process is a nucleo-protein complex formed by the pilot protein TrwC, which is secreted into the recipient cell covalently linked to the DNA [338,400]. Taking into account the large size of TrwC (108 kDa) and the internal dimensions that presents the central channel in the core complex (10-32 Å) [134,143] is evident that an unfolding step of the protein to be transported must take place [238]. TrwD presents important structural similarities with chaperones from different secretion systems [401,402]. Therefore, one of the working hypotheses in our group is that TrwD is responsible for deploying and/or maintain unfolded TrwC, previously to its translocation through the secretion channel.

In order to test this hypothesis, Dr. Jorge Ripoll performed a series of assays focused mainly on analysing TrwD and TrwC activities. These assays did not allow us to identify any TrwC-TrwD interaction (Jorge Ripoll, Doctoral Thesis, 2014, *results not published*). Here, following these previous studies, we decided to delve deeper into the analysis of this possible interaction between TrwD and TrwC by detecting a possible direct binding between the two proteins.

We aimed to obtain a complex between TrwD and TrwC by means of molecular size chromatography. As a control, TrwD and TrwC samples were injected separately on a Superdex200 PC 3.2 / 30 column, previously equilibrated in buffer 50mM Tris-HCl pH 7.2, 200mM NaCl and 5% (w/v) glycerol. Then, TrwD:TrwC proteins were incubated for 15 minutes at room temperature in the presence and absence of ATP and/or magnesium, to be subsequently loaded into the Superdex200 PC 3.2 / 30 column. After incubating both proteins at different molar ratios, it was not possible to observe the formation of a complex with a higher molecular weight that might correspond to a complex between the two proteins.

A weak interaction between two proteins is very difficult to observe by gel filtration chromatography, since the complex might not be very stable. Therefore, we decided to perform a new approach, based on the study of possible TrwD:TrwC complexes by electrophoresis in native non-denaturing conditions. Proteins run on PAGE in the absence of SDS are separated on the basis of their charge/mass ratio. While native (nondenaturing) PAGE does not provide direct measurement of molecular weight, the technique can provide useful information, such as protein charge or subunit composition. The interpretation of native gels is more complex than the interpretation of SDS-PAGE gels. Changes in relative mobility can reflect differences in charge, mass or both, but proteins may also have an isoelectric point (pI) above the pH of the buffer, and in this case they will not migrate or migrate backward into the upper buffer chamber. The pI values of TrwD and TrwC are 5.97 and 9.36, respectively. Such a difference did not allow us to find a Native-PAGE condition to observe both proteins in the same gel. The best results were obtained with 4.5 % polyacrylamide gels in electrophoretic buffer Tris-Glycine, pH 8.3 (Figure 4.24). Higher pH values did not improve these results. Since TrwC is not charged, the protein cannot be mobilized during electrophoresis.

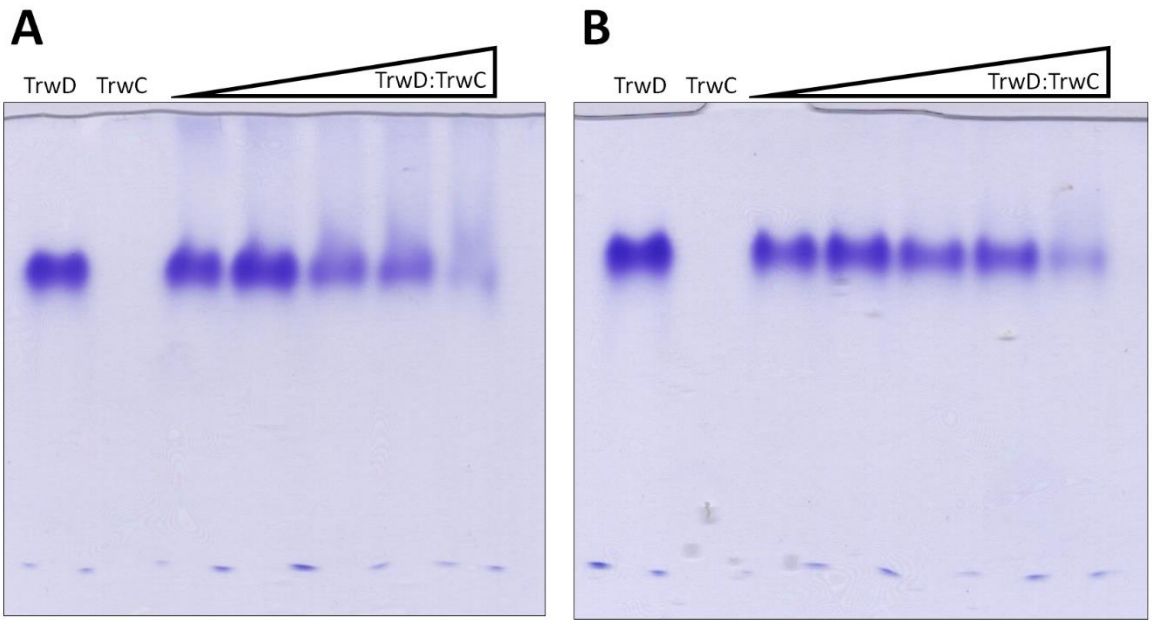

Figure 4.24. Analysis of TrwD:TrwC interaction by Native-PAGE. Lanes TrwD (25 µM TrwD) and TrwC (25 µM TrwC) are the controls. Only TrwD protein is able to enter in native polyacrylamide gels under our experimental conditions. TrwD (25 µM) was incubated in the presence of increasing concentrations of TrwC (1:0.5 to 1:4, TrwD:TrwC molar ratios), using TrwC native **(A)** or TrwC previously denatured by thermal shock for 10 min at 98°C **(B)**. Results revealed a disappearance of the intensity of the TrwD band following the same pattern for both conditions (native and denatured TrwC protein). TrwD:TrwC incubation was performed for 15 min at 25˚C and the samples were analyzed by Native-PAGE (4.5 % native polyacrylamide gels) at pH 8.3 for 90 min with a constant amperage (25 mA) and another additional 90 min with a constant voltage (80 V). Finally, gels were stained with Coomassie Brilliant Blue to detect the different protein bands.

As expected, in the native gel at pH 8.3 we can only observe TrwD protein. Nevertheless, when TrwD has been pre-incubated with TrwC, the intensity of the TrwD band disappeared at increasing concentrations of TrwC. This result is observed both with native TrwC and with denatured TrwC. Although we cannot rule out the possibility that TrwD is aggregated, a negative control consisting of TrwD incubated in the presence of TrwC buffer alone (without TrwC protein), does not show any variation in the intensity of the TrwD band. This result seems to indicate that a TrwD:TrwC complex has been formed, but this complex is not able to enter the gel under the tested conditions. Lower pH values (inverting electrodes for the electrophoresis) did not improve the results. The latter condition let us observe TrwC but, on the contrary, TrwD was not able to migrate into the gel. Under those conditions, at a lower pH value (pH 5.7), TrwD is probably forming a precipitate.

In a third attempt to observe the complex, we performed a blue native polyacrylamide gel electrophoresis (BN-PAGE), as described in *Experimental Procedures*. This technique allows the separation of multiprotein complexes in a native conformation with a higher resolution than that offered by gel filtration or sucrose density ultracentrifugation. Samples are stained with a charged dye (Coomassie Blue G-250), the intact protein complexes are then separated by electrophoresis based upon how much dye was bound, which is proportional to their size.

Samples were incubated with 2 mM ATP and 10 µM Mg^{2+} for 15 min at 25˚C previously to be loaded in a native acrylamide gradient gel (4-13%). This new protocol gives a different mobility to the samples. Now, at pH 7.0, it is possible to observe the migration of TrwD, whereas TrwC can be detected in the gel wells. The great advantage of this new analysis is that after TrwD:TrwC incubation we can detect a new band that might correspond to a complex formed by both proteins (Figure 4.25).

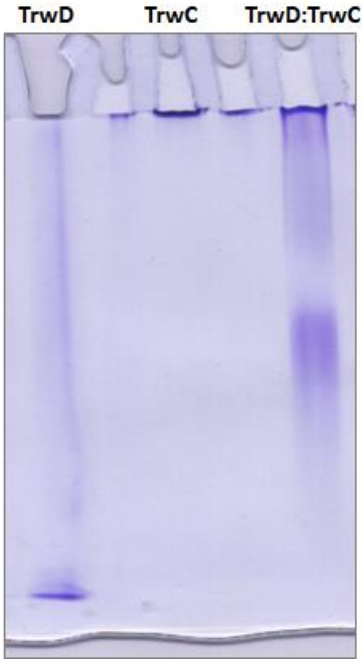

Figure 4.25. Analysis of TrwD:TrwC interaction by Blue-native polyacrelamide gel electrophoresis (BN-PAGE). Lanes TrwD and TrwC are the controls TrwD (25 µM) and TrwC (50 µM), respectively. TrwD (25 µM) was incubated in the presence of native TrwC (50 µM) 2 mM ATP and 10 µM Mg^{2+} for 15 min at 25˚C and then the sample was loaded into the gel (Lane TrwD:TrwC). Results revealed an additional protein band that might correspond to a TrwD:TrwC complex. The samples were analysed by BN-PAGE (4% - 13% native polyacrylamide gradient gel) at pH 7.0 for 30 min with a constant voltage (100 V) and another additional 60 min with a constant amperage (25 mA).

Finally, as an additional analysis, we used a combination of first dimension BN- and second dimension SDS-PAGE techniques, where the complex separated by BN-PAGE can be further subdivided into their individual constituents by SDS-PAGE. The bands detected by BN-PAGE were

excised, dried out and, after being soaked in denaturing SDS buffer, were analyzed by SDS-PAGE (Figure 4.26). Direct interaction of the proteins was apparent from the dissociation of the new band obtained in the first dimension after TrwD:TrwC incubation into TrwD and TrwC during the second dimension.

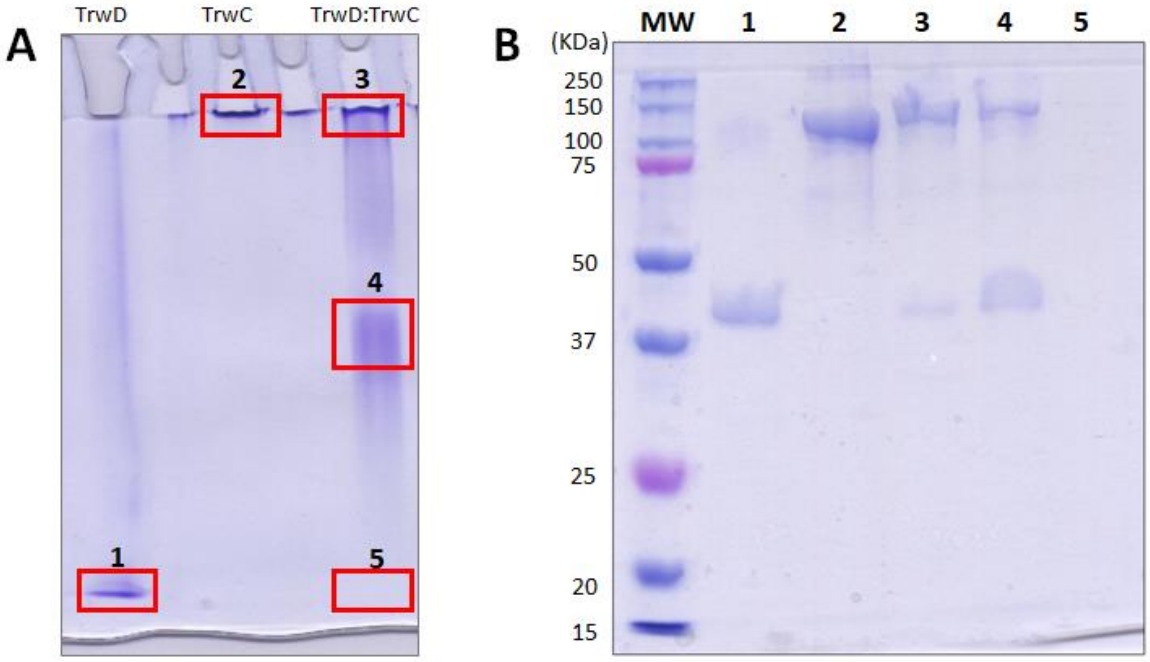

Figure 4.26. Analysis of TrwD:TrwC interaction by second dimension SDS-PAGE (2D-SDS-PAGE). A) BN-PAGE (same experimental conditions that previous Figure 4.25). Bands detected in first dimension BN-PAGE (red) were excised, dried out and soaking in denaturing SDS buffer. **B)** After soaking in denaturing SDS buffer, bands were analyzed by 2D SDS-PAGE (10% polyacrylamide gel). Lanes 1 and 2 are the controls, TrwD and TrwC respectively. When TrwD was incubated in presence of TrwC (1:2, TrwD:TrwC molar ratio), we can observe that, together with TrwC, part of TrwD has also been retained in the BN-PAGE well (Lane 3). Direct protein interaction was apparent from the dissociation into TrwD and TrwC in Lane 4. The absence of band in lane 5 indicates that there is not free TrwD protein and the total amount of TrwD protein assayed is forming a complex with TrwC.

4.7. *In vivo* localization and dynamics of TrwD and other T4SS components.

As part of this thesis work, we also decided to analyze the localization *in vivo* of TrwD and other molecular motors that might interact with this protein. Based on the wide palette of fluorescent proteins (FPs) with different spectral properties [403], fluorescence-based methods constitute an interesting option for the direct visualization of protein distribution and plasmid conjugation in single cells and in real time.

Therefore, our initial objective was to study protein localization and mobility of two molecular motors: the traffic ATPase TrwD and the coupling protein TrwB. In these experiments, we monitored TrwDmCherry and TrwBmCherry fluorescent proteins by fluorescence microscopy. In order to obtain TrwD and TrwB fused to FP we followed the steps described previously in *Experimental Procedures*. The design of the experiment allowed us to study any difference on protein localization in the absence or presence of the conjugative plasmid R388, since fusion proteins are in plasmids different from R388. Donor cells containing the fluorescent fusion proteins with FP were visualized on the fluorescence channel according to protein localization, while recipient cells did not contain any plasmid and, therefore, did no express fluorescence.

Observation of the distribution of the TrwDmCherry protein revealed a homogeneous fluorescence in the cells (Figure 4.27). TrwBmCherry is cloned in a high number copy plasmid, which could explain why we observed an excess of TrwDmCherry throughout the cytoplasm. However, when all the T4SS components were present in the donor cell (pHis17::TrwDmCherry + R388), we observed a change in the distribution pattern of this protein, being TrwDmCherry visualized in a membrane localization (Figure 4.27).

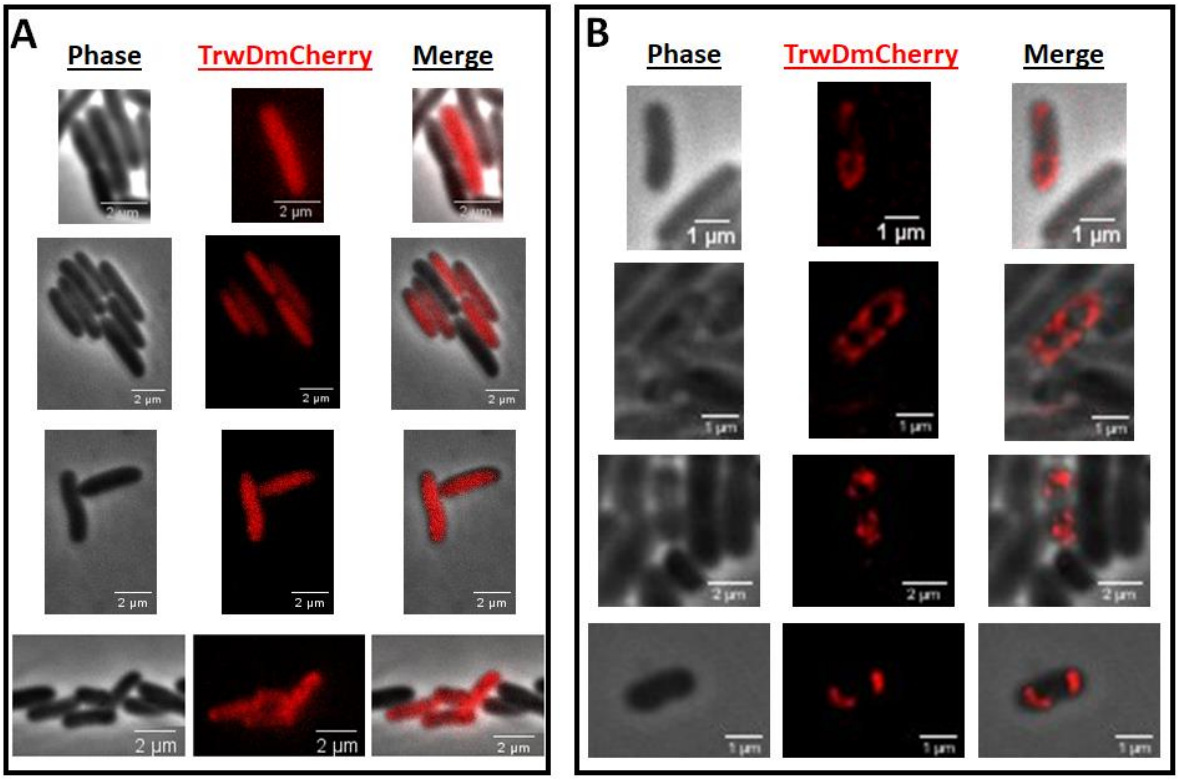

Figure 4.27. TrwDmCherry fusion protein location *in vivo* in the presence and absence of other components of the T4SS. (A) *E. coli* D1210 cells with plasmid pHis17::TrwDmCherry (red) and *E. coli* MG1655 cells without any plasmid (no fluorescence). **(B)** *E. coli* D1210 donor cells with the conjugative plasmid R388 wild type and pHis17::TrwDmCherry (red). *E. coli* MG1655 receptors cells without any plasmid (no fluorescence). The phase-contrast, mCherry fluorescence channel and the merge of phase-contrast and mCherry channels are shown.

As expected, TrwBmCherry was localized at the bacterial membrane, which is in full agreement with the presence of a transmembrane domain in the protein TrwB. However, we also observed a difference in the pattern of distribution of the fluorescence in the presence and absence of R388. TrwBmCherry location was brighter and formed discrete foci in the membrane when all the T4SS components were present in the donor cells (Figure 4.28). In both experimental conditions, TrwBmCherry showed a high mobility throughout the membrane.

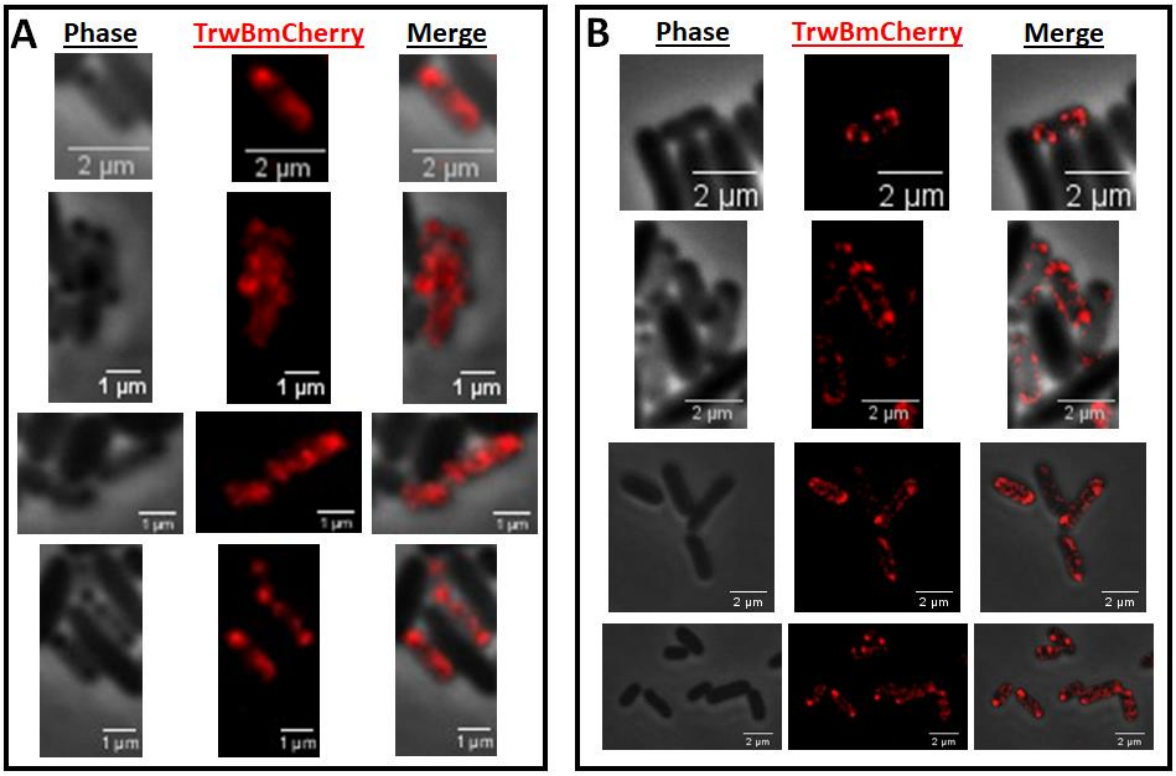

Figure 4.28. TrwBmCherry fusion protein location *in vivo* in presence and absence of other components of the T4SS. (A) *E. coli* D1210 donor cells with the plasmid pHis17::TrwBmCherry (red) and *E. coli* MG1655 receptor cells without any plasmid (no fluorescence). **(B)** *E. coli* D1210 donor cells with the conjugative plasmid R388 wild type and pHis17::TrwBmCherry (red). *E. coli* MG1655 receptors cells without any plasmid (no fluorescence). The phase-contrast, mCherry fluorescence channel and the merge of phase-contrast and mCherry channels are shown.

Altogether, the results showed differences in the protein localization pattern depending on the presence or absence of the rest of the T4SS components for the molecular motors assayed. In the presence of all the T4SS components both of them localized in discreet loci in the bacterial membrane. Our preliminary results could suggest that these discrete loci in the membrane with a prevalent location next to the bacterial poles might indicate the regions where the T4SS secretion channels are assembled. However, these results are very preliminary and further analyses are required to confirm this hypothesis. Moreover, it is important to point that these experiments have been carried out by expressing proteins in high copy number vectors and, therefore, there may be an excess of protein that distorts the interpretation of these results. To

overcome this potential problem, conjugative fusion-fluorescent proteins will be cloned on plasmid R388 under their native promoter.

We decided to perform a further characterization of the conjugative process with the aim of discriminate under the fluorescence microscope donor, host and transconjugant cells in a complex population mix. This requires tagging these subpopulations with different detectable markers, such as the expression of different FPs in each of the subpopulations. The cloning of one FP in the genome of the conjugative plasmid allows the detection of donor cells. The cloning of a second, distinguishable FP in a non-mobilizable plasmid in the recipients allows the detection of these cells in a second fluorescence channel. Transconjugants, which express both FPs, produce a signal in both fluorescence channels. The basic requisite for the performance of this protocol is that the FPs selected must be compatible, that is, fluorescence bleed through from one fluorescence channel to the other should not prevent the clear differentiation between both fluorophores.

Donor cells containing the conjugative plasmid R388::TrwBmCherry expressed TrwBmCherry fusion protein, which was visualized on mCherry channel according to protein localization. As expected, TrwBmCherry showed a membrane localization. Recipient cells containing the non-mobilizable plasmid pANT::mGFP expressed mGFP fluorescent protein, which had a cytoplasmatic localization and was visualized on GFP channel. Therefore, host cells are visualized in green while donor cells are visualized in red. Only when the conjugative process has taken place, we could observe cells with red membrane and green cytoplasm, transconjugant cells.

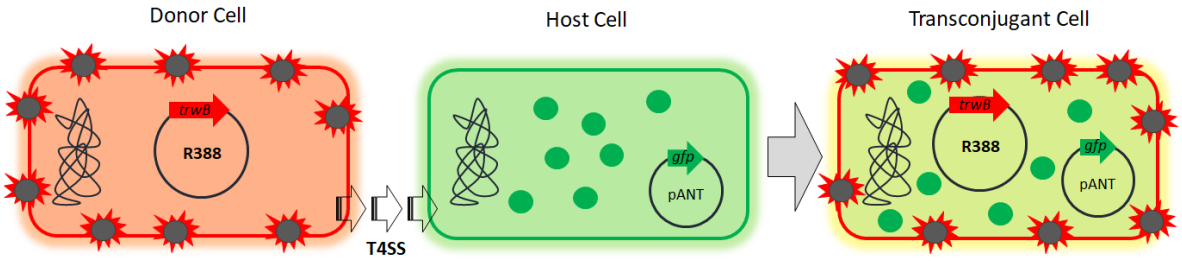

Figure 4.29. Analysis of transconjugant cells *in vivo*. Scheme of the FP-based assay for donor, host and transconjugant subpopulations discrimination using fluorescence microscopy. A gene for mCherry expression is inserted in the conjugative plasmid (*trwBmCherry* fusion protein, red arrow), while a gene for mGFP expression is inserted in a non-mobilizable plasmid in host cells (green arrow). Upon transfer of the plasmid, transconjugant cells express both FPs.

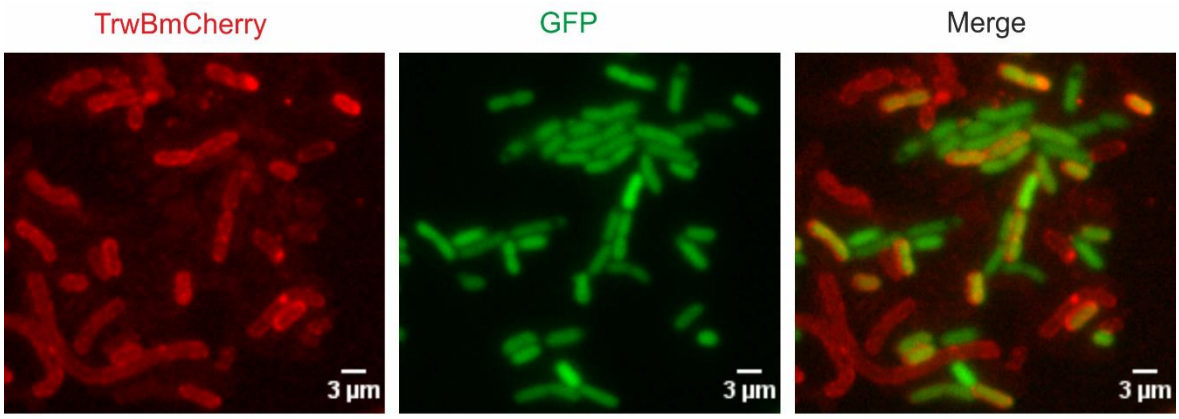

Figure 4.30. Analysis of transconjugant cells *in vivo*. Donor *E. coli* MG1655 cells contain the conjugative plasmid R388:TrwBmCherry (red). Host *E. coli* MG1655 cells contain the non-mobilizable plasmid pANT::mGFP (green). Only transconjugant cells contain TrwBmcherry and mGFP proteins (red and green). The mCherry fluorescence channel (left), GFP fluorescence channel (middle) and the merge of mCherry and GFP channel (right) are shown. Conjugation was conducted for 3 h at 37˚C.

Within this experimental approach, transconjugant cells are only detectable after the maturation time of the conjugative plasmid R388::TrwBmCherry, that is after the expression of TrwBmCherry protein in the recipient cell, which requires a long incubation period. Since we aimed for a direct visualization of plasmid transfer under the microscope, we decided to perform an additional characterization with a different FP approach. Plasmid visualization would depend on the ability of protein SeqA to bind hemimethylated DNA, since this method is based on an FP-tagged derivative of protein SeqA [404]. In wild type cells, Dam methylase incorporates a methyl group at the A residue of 5'GATC sequences. Being that sequence palindromic, both DNA strands are usually methylated. SeqA is a negative regulator of initiation of *E. coli* replication, and it binds only to newly replicated sequences hemimethylated, preventing premature DNA replication [405–407]. Therefore, in wild type cells, a SeqA-GFP fusion protein forms foci on active replication forks, while in a Dam^- mutant SeqA-GFP generates a uniform, diffuse cytoplasmatic fluorescence pattern.

To investigate the localization of SeqA-GFP protein during conjugation, we mated a mixture of Dam^+ donor cells with the conjugative plasmid R388:TrwBmCherry, and Dam^- SeqA-GFP host cells without any plasmid. The process was observed with time-lapse fluorescence microscopy. A few minutes after mixing the parental cells, distinct SeqA-GFP foci started to appear in recipient cells (Figure 4.30). A single recipient cell could receive DNA more than once, as shown by the presence of independent foci (Figure 4.30). As negative control, in the absence of donor cells no SeqA-GFP foci were observed in Dam^- SeqA-GFP host cells.

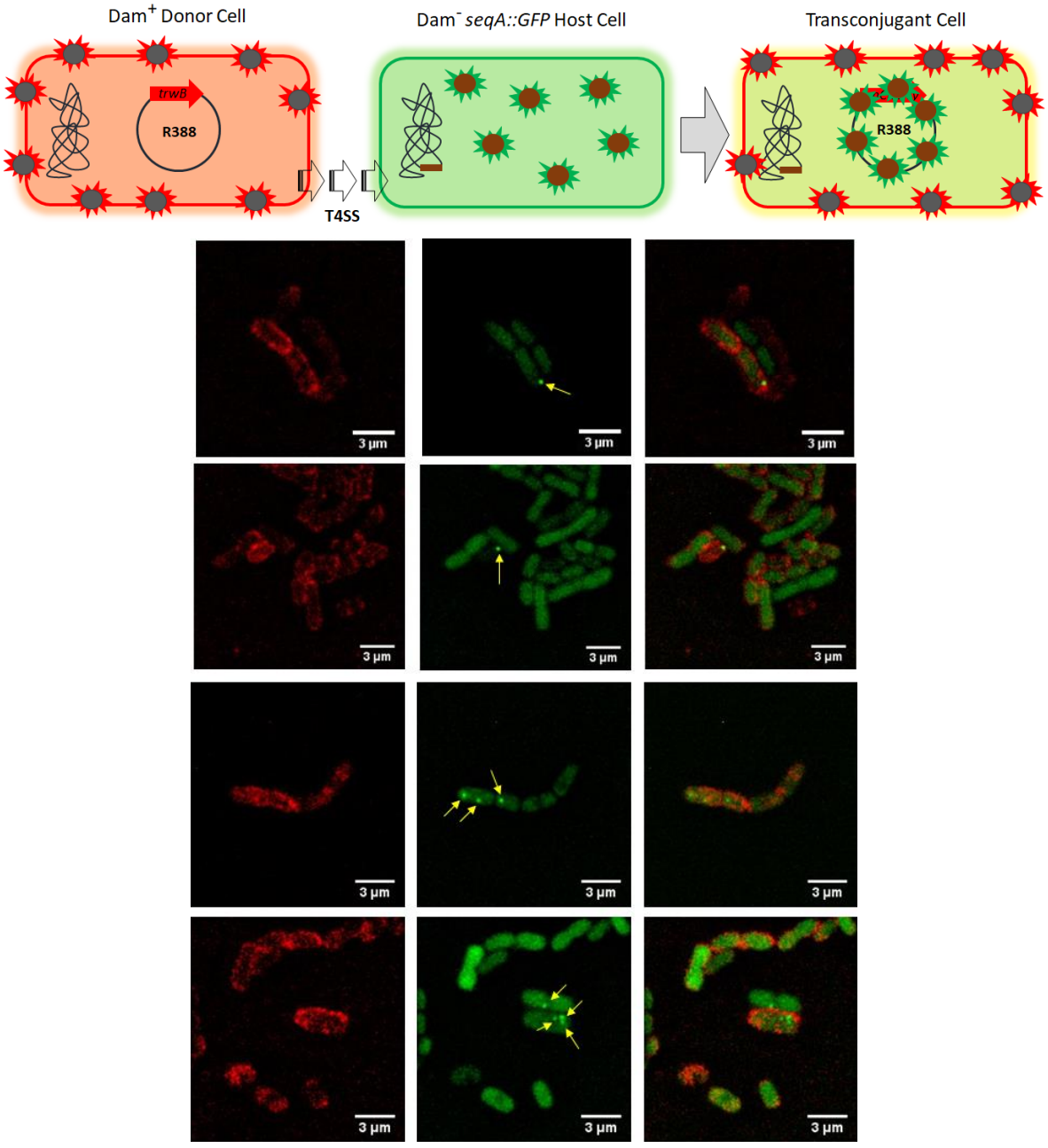

Figure 4.31. Direct visualization *in vivo* of plasmid DNA transferred into recipient cells. (Upper panel) Scheme of the SeqA-GFP assay for visualization of plasmid conjugation under the microscope. The assay is based on a Dam$^+$ methylation-proficient donor cells with methylation-deficient Dam$^-$ host cells producing the SeqA-GFP fusion protein, which enabled us to specifically label only the transferred DNA. Once methylated donor DNA is transferred to the Dam$^-$ recipient as a single strand and converted to a DNA duplex by the synthesis of the complementary no methylated strand, the acquired DNA is hemimethylated and therefore bound by SeqA-GFP (green focus). **(Bottom panels)** Donor *E.coli* MG1635 Dam$^+$ cells contains the conjugative plasmid R388::TrwBmCherry (red). Host *E. coli* MG1635 mutant Dam$^-$ SeqA-GFP cells (green). The mCherry fluorescence channel (left), GFP fluorescence channel (middle) and the merge of mCherry and GFP channel (right) are shown. Foci formation in transconjugant cells is indicated by yellow arrows. Conjugation was conducted for 90 min at 37˚C.

Even though the results obtained so far in this last section are preliminary, all of them are very promising. We are currently working on the design of different fluorescent fusion-proteins with the objective of generate a library of endogenously tagged fluorescent fusion proteins to track R388 conjugative proteins in living cells, measure the protein dynamics and test for interaction partners. This library could be used in a variety of different experimental live cell microscopy procedures to answer some of the questions raised in this work and better understand the bacterial conjugation process.

Chapter 5
DISCUSSION

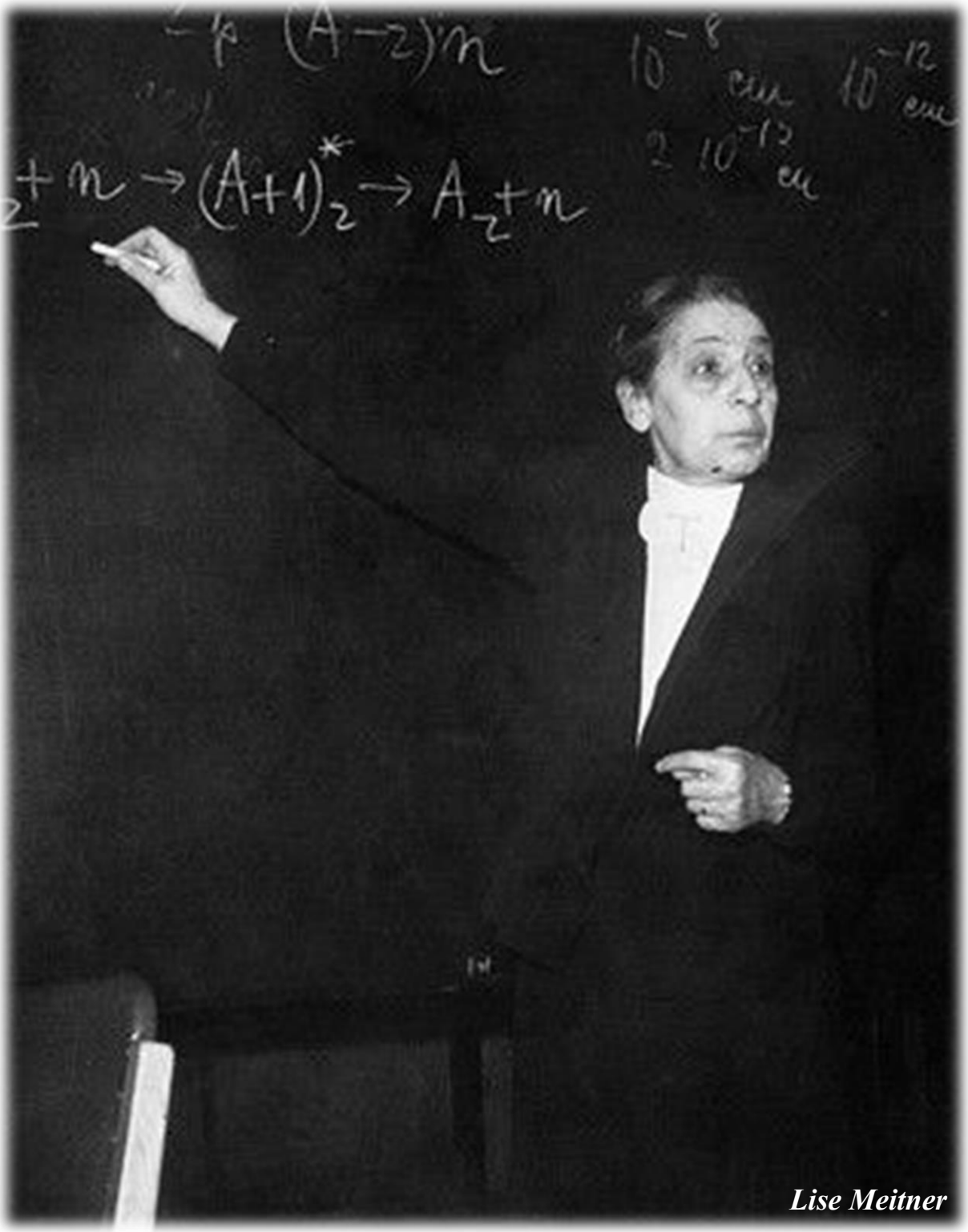

Lise Meitner

Antibiotic resistance (AbR) dissemination has become a worldwide crisis [408]. Since conjugative plasmids are the main carriers involved in this dissemination [9,15], strategies to control plasmid conjugation have been proposed as potential solutions [266]. In addition to barriers that bacteria naturally impose, such as the innate immune system known as restriction-modification (RM) and the adaptive immunity known as CRISPR-Cas systems, bacterial conjugation can be artificially controlled by molecules interfering with specific components of the process, such as the relaxase [83] or the conjugative pilus [316].

Conjugation inhibitors (COINs) can be found by screening a collection of compounds for their ability to reduce conjugation in whole cells. By definition, a compound can be considered a specific COIN when it is able to inhibit conjugation without affecting bacterial growth. After analyzing 12,000 natural compounds from the NatChem library, unsaturated fatty acids (uFAs) were described as COINs [322]. Additional high-throughput screening assays to measure plasmid transfer allowed the identification of two novel sets of COINs, synthetic 2-AFAs [329] and natural tanzawaic acids (TZAs), obtained from a collection of bioactive compounds isolated from marine microorganisms [337].

Toxicity properties of COINs discovered to date were tested against different human cell lines, bacteria, and fungi. 2-aFAs presented toxicity against fungi [330,331], protozoa [332,333], Gram positive bacteria, such as *Staphylococcus saprophyloticus* and *Bacillus cereus*, some Gram-negative bacteria like *Klebsiella pneumoniae* and *Pseudomonas aeruginosa*, and eukaryotic cells [334–336]. These toxicity problems exclude their application from environmental settings, where biodiversity must be maintained, and confine its use to academic setups. On the contrary, natural COINs (uFAs and TZAs) present reduced toxicity, some of them being normal constituents of the human diet [327]. Therefore, natural COINs could be suitable compounds for preventing plasmid conjugation in natural environments [328]. However, one of the down sides of uFAs is that they are prone to auto-oxidation. TZAs are fungal polyketides more complex than previous COINs but they are carboxylic acids too, with two aromatic rings at the end of an unsaturated aliphatic chain, so they are also prone to auto-oxidation, which makes them poor candidates as effective, deliverable COINs. On the other hand, synthetic triple-bonded fatty acids (2-aFAs) are not susceptible to oxidation. Studying its spectra of action, it has been proven that COINs inhibited IncF plasmids, the most common carriers of AbR genes in pathogenic *Enterobacteriaceae* [409]. In addition to IncF, they also inhibited IncW plasmids and, less efficiently, IncH plasmids. While IncI, IncX, and IncL/M plasmids were moderately inhibited, IncN and IncP plasmids were completely resistant to COIN action. Interestingly, mobilization helped by affected conjugative plasmids was also inhibited, suggesting a shared target in the mating pair formation (MPF) system. Also interesting is the fact that conjugation was inhibited irrespective of the bacterial host used as donor. Moreover, the presence of COINs in the mating medium not only blocked plasmid invasiveness, but also reduced the prevalence of plasmid-containing cells [329], which makes them very promising candidates to control antibiotic resistance dissemination.

Characterization of these compounds and their analogs confirmed the importance of a carboxylic group and an unsaturated hydrocarbon chain for COIN activity [322,329,337]. Other features, such as carbon chain length or triple bond position, influenced as well in the effectiveness. The inactivity of TZA-E, which contains an additional hydroxyl group distal to the carboxylic group, suggested that a substantial hydrophobic moiety was important for COIN activity as well [337]. These common structural characteristics and the spectra of plasmids affected by COINs suggest a common mechanism of action. However, the mechanism by which the fatty acids exerted the inhibition was unknown. Although HTS methods have been widely used by pharmaceutical companies in hit identification [410,411], the finding of a molecular target by structural-based design of new inhibitors could be a powerful tool in the development of new drugs, as it allows the investigation of the interactions between ligands and targets [412,413]. In that sense, the main goal of this work has been the identification and characterization of the molecular target for the inhibition by fatty acids.

uFAs are known to affect the function of some proteins that have a transient association with the bacterial membrane, such as the AAA+ ATPase DnaA [414]. The ATPase activity of this DNA replication initiator is regulated by acidic phospholipids. The presence of saturated or unsaturated fatty acids (uFAs) on these phospholipids regulates the ADP-ATP exchange in the protein [415]. Based on this, we decided to analyse the activity of conjugative ATPases in the presence of uFAs [350]. In our model system, the conjugative plasmid R388, four ATPases provide the energy for the conjugative process: the relaxase TrwC, the coupling protein TrwB, TrwK and the traffic ATPase TrwD [52]. Analysis of ATP hydrolysis rates by each of the four proteins in the presence of uFAs showed that only TrwD was significantly inhibited under the tested conditions (Figure 4.1). This inhibitory effect was observed only in the presence of unsaturated fatty acids, such as oleic and linoleic acids, but not in the presence of saturated fatty acids like lauric or palmitic acids (Figure 4.2). These results correlate with previous observations, in which uFAs but not saturated fatty acids were able to inhibit bacterial conjugation [322]. In addition to uFAs we also observed that 2-aFAs, like 2-hexadecynoic acid (2-HDA), 2-octadecynoic acid (2-ODA) and 2,6 hexadecynoic acid, were also efficient conjugation inhibitors. Fatty acid conformation is important, as unsaturation placed in C_9 instead of C_6, abolished the inhibitory effect of the hexadecynoic acid, both *in vivo* and *in vitro* experiments [329,416]. Therefore, *in vivo* and *in vitro* experiments (conjugation and analysis of TrwD ATPase activity, respectively) are perfectly correlated. Fatty acids that inhibit conjugation *in vivo* are also able to inhibit TrwD activity, while those with no effect *in vivo*, such as saturated fatty acids, or alcohol and tetrahydrophyranyl-ether derivatives, did not have any effect on the *in vitro* activity either, proving that the presence of the carboxylic acid group is essential to exert the inhibitory effect (Figure 4.4) [416].

During this work, we have characterized a new COIN. A saturated fatty acid derivative, 2-Bromopalmitic acid (2-BP), is able to inhibit bacterial conjugation and also the ATPase activity of the traffic ATPase TrwD (Figures 4.5 and 4.6). 2-BP inhibition kinetic is similar to that obtained with other COINs (Figure 4.8), without affecting bacterial growth or metabolism. The finding of 2-Bromopalmitic acid as a new specific inhibitor (COIN) allows us to conclude that COINs do not exert their inhibition effect because of the presence of instaurations, but indirectly by the

conformation that these fatty acids acquire after TrwD binding. Double or triple bonds provide geometrical constraints in the alkane chain, disrupting the regular periodic structure.

Kinetic analysis of TrwD ATPase inhibition by COINs showed similar $K_{i[app]}$ parameters for all the compounds, with values in the range of 20 - 30 μM (Figure 4.7 and 4.8). ATP titration in the presence of any of COINs (at their respective MIC_{50}) revealed not significant variation of the $K_{0.5}^{ATP}$ (44 μM and 66 μM for linoleic acid and 2-HDA, respectively) when it was compared with the control (44 μM), whereas the V_{max} value was reduced by half, suggesting a non-competitive inhibition (Figure 4.9). The affinity for ADP did not changed significantly either (44 μM for the control and 51 μM in the presence of 2-HDA) (Figure 4.10). These results point to a non-competitive inhibition, where the binding site for fatty acids in TrwD would differ from the nucleotide binding site.

TrwD has been proposed to play a central role during conjugation acting as a molecular switch between the other two molecular motors of the conjugative system [236]. Therefore, TrwD would coordinate pilus formation and DNA transport [229,233,236]. VirB11 proteins belong to a large family of hexameric AAA+ traffic ATPases, which includes proteins involved in Type II secretion and in Type IV pilus and flagellar biogenesis [230]. They are soluble, hexameric proteins located at the cytoplasmic side of the inner membrane. These proteins consist of two domains, an N-ter (NTD) and a C-ter (CTD), connected by a flexible linker of variable length [230,228,417]. A catalytic mechanism has been proposed not only for VirB11 proteins but it has been extended to all members of the secretion ATPase superfamily [233]. According to this mechanism, in the apo-state the enzyme could be in two conformational states, with the NTD alternating between an open and closed state, but only the open state would be able to bind ATP. Upon ATP binding, the NTD closes over the CTD and ATP is hydrolyzed. The release of the γ-phosphate after ATP hydrolysis induces a conformational change to an open state that favors ADP release, so the cycle can resume.

As fatty acids do not affect significantly the affinity for ATP or ADP, they may act over another region of the protein. In fact, blind docking search of a putative binding site on TrwD identified a pocket comprised by the N-terminal domain (NTD) and the linker region of TrwD with a high probability to bind COINs (Figure 4.12). It is likely, then, that binding of fatty acids on this region results in a restriction of movement of the NTD over CTD, with fatal consequences on TrwD ATPase activity [350]. Although all fatty acid derivatives tested so far bind to the same pocket, there are some differences in the mode of binding that might explain the different behavior of saturated fatty acids and other derivatives that act as inhibitors. While 2-HDA is an effective COIN, 2,6-HDA does not have the same effect. In the latter case, the carboxylic group is at a larger distance from the basic residues that are located inside the pocket formed by the NTD and the linker region (Figure 4.14), which could explain its lower inhibitory effect. On the other hand, derivatives in which the carboxylate group has been substituted for alcohol (-OH) or tetrahydropyrane ester (-OTHP) groups, cannot make electrostatic interactions with the linker region, because of the absence of this carboxylic group. This might explain why these compounds are not able to inhibit the ATPase activity of TrwD. Blind docking with saturated fatty acids, such as palmitic and 2-BP, also predict a binding to this same pocket. However, while the aliphatic

chains of 2-BP and palmitic acid have a similar orientation, the carboxylic group of the 2-bromo derivative is buried inside the pocket formed by the NTD and the linker domain of the protein, being the bromide atom stabilized by electrostatic groups located in the region (residues 115-118 of the flexible linker). On the contrary, the carboxylic group of the palmitic acid is 120 degrees apart, making closer contacts with lysine 52, out of the linker region (Figure 4.15). This difference modifies to mode of binding and again it might explain why only 2-BP is able to produce a restriction in the flexibility of the linker, even though both, palmitic acid and 2-BP, are binding to the same TrwD region.

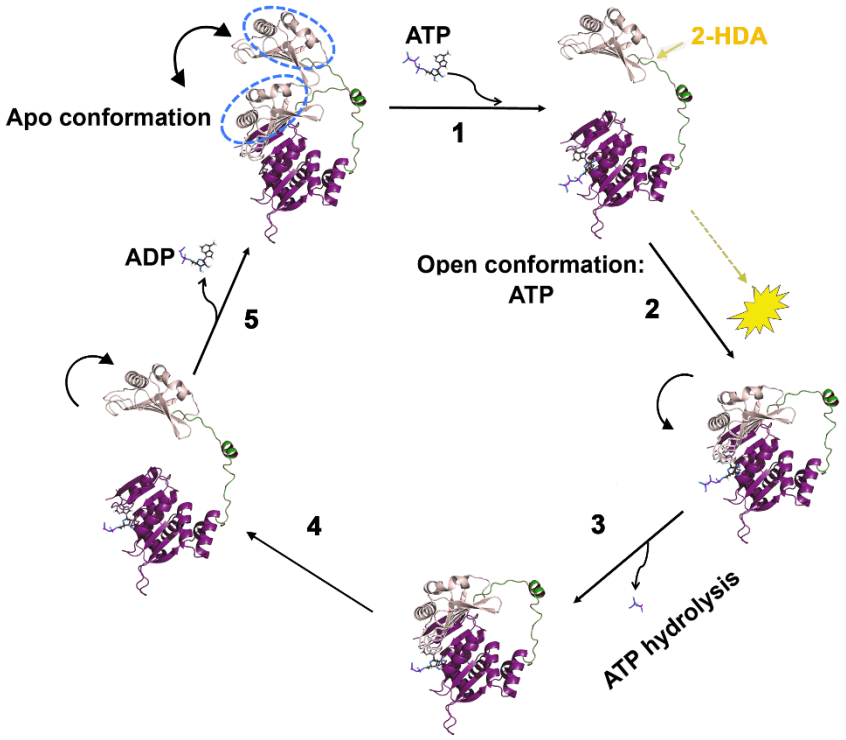

Figure 5.1. Mechanistic model of TrwD ATPase inhibition by fatty acids. Proposed mechanism of the catalytic cycle of ATP hydrolysis (adapted from [235]). According to this mechanism, which is shared by other members of the secretion ATPase superfamily [233], in an *apo*- conformation, the protein can alternate between an open and a closed state, with the NTD pivoting over the CTD about the linker (*step 1*), but only the open conformation is able to bind ATP. Upon ATP binding, the NTD closes over the CTD (*step 2*) so ATP hydrolysis can take place (*step 3*). After ATP hydrolysis, the NTD opens up (*step 4*) allowing ADP release, so the cycle can resume (*step 5*). Considering that the binding affinities for ATP and ADP are not significantly affected by COINs, it is likely that the inhibitory effect is exerted by preventing the movement of the NTD over the linker, which, in turn, results in inhibition of ATP hydrolysis [416].

Previous data suggested that VirB11 proteins interact with the cytoplasmic site of the membrane through the NTD [219]. Moreover, TrwD ATPase activity is stimulated by phospholipids [221] and TrwD interaction with phospholipids in lipid vesicles causes lipid vesicle aggregation, leakage and intervesicular lipid mixing [226]. However, even though it is widely recognized that TrwD interacts and localizes to the cytoplasmic side of the bacterial inner membrane, the molecular bases underlying this interaction with the membrane are not known [387]. The pocket identified in TrwD as the binding site for fatty acids is next to the NTD. Since it is known that the NTD is the domain involved in membrane binding, TrwD might interact with the membrane via this binding site. Thus, it is tempting to speculate that uFAs and aFAs are occupying a binding site in TrwD, which is otherwise occupied by bacterial membrane phospholipids involved in the association of the protein to the membrane. TrwD ATP hydrolysis is dependent on protein dynamic and membrane localization [229,233,221,235] so, if COINs were incorporated into the bacterial membrane, they could exert their inhibitory effect by interfering TrwD interaction with the phospholipids.

In this thesis work, we have proved that COINs are efficiently incorporated to bacterial membranes. Chromatography-mass spectrometry (GC-MS) revealed that the phospholipid fatty acids composition in bacteria grown in LB medium are primarily saturated, being palmitic acid the most abundant (44%) (Figure 4.16). However, when the 2-alkynoic fatty acid 2-HDA was added to that medium, the utilization of endogenous fatty acids in the biosynthesis of phospholipids was altered significantly. In treated bacteria, 2-HDA is not only able to incorporate to bacterial membrane, but else it is the major component of the total phospholipid fraction (44%) (Figure 4.16). To make this possible, 2-HDA must be incorporated from the medium and activated to acyl coenzyme A thioester. That activated form would act as a substrate for the acyl coenzyme A phospholipid acyl transferase in *E. coli*, allowing its incorporation to the bacterial membrane [418–420]. 2-HDA incorporation to the bacterial membrane was accompanied by a significant 2-fold decrease of palmitic acid, the most abundant fatty acid in the phospholipid of untreated bacteria. This result indicates that there is a replacement of saturated palmitic acid by COINs in the phospholipids of the bacterial membrane. Such a significant replacement of palmitic acid by COINs might be affecting TrwD association to the bacterial membrane. Therefore, we wondered whether TrwD interaction with the membrane occurs via esterified fatty acids. A radiolabel binding assay confirmed a specific interaction between TrwD and palmitic acid *in vitro* (Figure 4.17). We performed similar assays with an intermediate in phospholipid synthesis, the activated fatty acid palmitoyl-CoA, obtaining exactly the same results: a specific interaction protein:ligand (Figure 4.18). Therefore, our results support the idea of an interaction *in vivo* between TrwD and the palmitic acid of phospholipids.

A wide variety of proteins associate to the membrane covalently attached to palmitic acid [392,393]. In these S-palmitoylated proteins, the fatty acid is bonded to a cysteine residue through a thioester linkage. It is a reversible process that allows a transient binding to the membrane; playing a crucial role in many biological processes [392–394]. This lipid modification is common in eukaryotic cells but is poorly documented in prokaryotes. It is thought that bacteria use the host palmitoylation capacity to modify their own proteins. However, to our knowledge, there is at least one example of auto S-palmitoylation in bacteria, indicating that this modification

either occurred spontaneously or that bacteria produce unknown enzymes yet to be identified [421]. We checked if the association between TrwD and ^{14}C-labeled fatty acids was resistant to denaturation induced by SDS gel electrophoresis. No signal of radiolabeled protein was observed, neither free palmitic acid nor thioester palmitoyl-CoA. Therefore, the interaction is not resistant to denaturation, which suggests that the binding is non-covalent and there is not a thioester bond involved in the association between TrwD and fatty acids. Samples of purified protein incubated with 2-Bromopalmitic acid were also analyzed by mass spectrometry, but no difference in molecular mass was observed when the sample was compared to a control in the absence of the fatty acid (Figure 4.23). Moreover, a TrwD mutant where the potential site for S-palmitoylation was removed (mutant C44N in the NTD domain) shows exactly the same pattern of inhibition and the same conjugation frequency values that the wild type protein (Table 4.1). Altogether, our data strongly support that the binding to palmitic acid is non-covalent, excluding the possibility that the association of palmitate with TrwD is due to protein S-palmitoylation. In the literature, there are also several examples of proteins that associate to the membrane via a non-covalent binding to saturated fatty acids [388], such as Toll-like receptors (TLRs) [389,390], in which the fatty acid binds to a lipid binding pocket. Intriguingly, TLRs are also inhibited by polyunsaturated fatty acids [391], as in the case of TrwD.

2-Bromopalmitic acid (2-BP), the saturated fatty acid derivative defined as COIN during this thesis work, is an irreversible inhibitor that blocks palmitic acid incorporation onto proteins [422]. The exact mechanism responsible for 2-BP mediated inhibition generates controversy. It is generally accepted that 2-BP blocks S-palmitoylation by inhibiting protein acyl transferases [385,396], but some others reports have shown this palmitic acid analog as a nonselective probe, with many targets beyond palmitoyl transferases, leading the authors to suggest that this compound might act as an inhibitor by direct competition with palmitic acid, without protein acyl transferases mediation [382,397,398]. The results obtained *in vitro* with TrwD in this work support this idea, a 2-BP inhibition mechanism no mediated by protein acyl transferases, and might be extensive to other proteins that associate to the inner membrane via interaction with palmitic acid [135].

As mentioned above, a blind docking search of palmitic acid and 2-BP in TrwD structure revealed the same binding site for both compounds, albeit adopting a different conformation and mode of binding [416]. Therefore, in an attempt to determine if COINs and palmitic acid compete for the same binding site in TrwD, we conducted a further characterization of the mechanism of inhibition. ATP turnover was measured at increasing concentrations of 2-BP in the presence of palmitic acid (500 μM). The apparent inhibition constant [$K_{i(app)}$] of 2-BP was significantly increased from 21.5 ± 1.5 μM to 65.4 ± 1.4μM (Figure 4.19). This increase in the value of the apparent inhibition constant in the presence of the saturated fatty acid indicates that both fatty acids (palmitic acid and 2-BP) compete for the same binding site in TrwD. Moreover, when R388 conjugation frequency was monitored *in vivo* in the presence of palmitic acid (500 μM), a statically significant higher concentration of 2-BP was required to reach the same inhibitory effect (Figure 4.20). This result can be explained by the incorporation of 2-BP to the bacterial membrane and the consequent replacement of palmitic acid by 2-BP. This correlation between the results obtained *in vivo* and *in vitro*, strongly support the idea that COINs exert their inhibitory effect by

occupying a binding site on TrwD that is otherwise occupied by palmitic acid. This interaction with phospholipid fatty acids would mediate TrwD interaction with the cytoplasmic site of the inner bacterial membrane.

In summary, in this work we have identified the T4SS traffic ATPase TrwD as a potential target for the inhibition of bacterial conjugation by fatty acids, characterizing the molecular basis for the mechanism of action of COINs. In addition, we have identified for the first time a new COIN without unsaturation in its aliphatic chain, the palmitate analog 2-Bromopalmitic acid (2-BP). As previously described COINs, this compound has the traffic ATPase TrwD as molecular target. The results presented here demonstrate that these inhibitors can incorporate into the bacterial membrane and displace the more abundant saturated acid in phospholipids (palmitic acid), which could affect those proteins that interact with the membrane through this fatty acid. Although it was known that VirB11 proteins localize in the bacterial inner membrane, the molecular bases of this interaction had not been identified. We have proven that TrwD interacts with palmitic acid, and that COINs compete with this saturated fatty acid for the same binding side. Altogether, our results support a TrwD-membrane interaction mediated by saturated fatty acid phospholipids that is perturbed when COINs are added to the culture medium.

However, many questions remain unanswered. For instance, which is the target in IncF plasmids? Why IncN and IncP plasmids are resistant to COIN activity? ATPase activity studies of TrwD homologs or other potential targets in these conjugative systems might reveal useful information to answer these questions.

The crystallographic structures of HP0525 from *H. pylori* and VirB11 from *B. suis* revealed the length of the linker produces differences in the interaction between contiguous subunits that in turn affect to the nucleotide binding site [220,223]. Thus, in homologs with a short linker, like HP0525 from *H. pylori*, this site is coordinated between the NTD and the CTD of the same subunit, while in homologs with a much longer linker, like VirB11 from *B. suis*, it is located between the NTD of a subunit and the CTD of the next subunit [229]. TrwD shows the longest linker, as shown when the sequence of the different homologs is compared [236]. TrwD structural three-dimensional model was generated by molecular threading using the crystal structure of VirB11 from *B. suis* as a template [236]. Blind molecular docking assays showed that all the fatty acids studied interact with both proteins, TrwD and VirB11, through a pocket located in the interface between the linker and the NTD domain (Figure 5.2.). In both cases, the carboxylate group of 2-HDA seems to contact a basic residue in the linker region of both proteins (residue K124 and residue R127 in TrwD and VirB11, respectively).

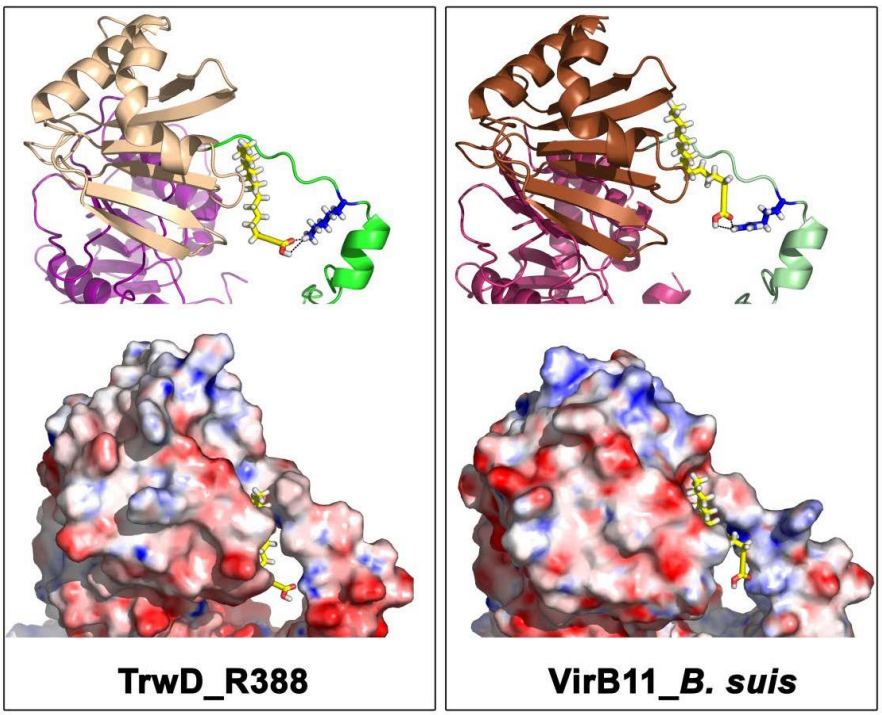

Figure 5.2. 2-HDA binding pocket. Best binding poses after blind docking of 2-HDA (*yellow*) into monomeric TrwD from plasmid R388 **(left panel)** and VirB11 from *Brucella suis* **(right panel)** [416]. Putative interactions between the carboxylate group of 2-HDA and a basic residue in the linker region of TrwD (K124) and VirB11 (R127) are shown. Cartoon and surface representations of the binding pockets are depicted at the top and the bottom sides of both panels, respectively. Electrostatic maps were calculated with the PDB2PQR application [373] and the resulting APBS files [374] were rendered with Pymol [423].

On the contrary, when the sequence of HP0525 from *H. pylori* is analyzed, the length of its linker is much smaller (19 residues vs 47 residues in TrwD and 29 residues in VirB11) [236]. TrwD and VirB11 long linkers are divided into linker-A and linker-B by a short helix (αC1). However, all these domains are not conserved in HP0525 or other homologues with a short linker. HP0525 does not have linker-B and does not conserve either helix αC2. As a consequence, the αC helix of HP0525 is an integral part of the CTD, while the equivalent helix in TrwD and VirB11 (αC1) is part of the long linker and does not interact with any other element of the monomer [228]. Interestingly, a blind docking search of COINs in HP0525 structure did not identify the pocket found in TrwD and VirB11 from *B. suis* as a potential binding site. The search did not show any other potential binding site for fatty acids. TrbB, the VirB11 homolog from plasmid RP4 (IncP) was also analyzed by molecular modelling. This protein also presents a short linker, comparable to that of protein HP0525. The structure of TrbB has not been solved so far and, therefore, the structural tridimensional-model for this protein was generated by molecular threading using as a template the crystal structure of HP0525 of *H. pylori* [236], the closer homolog (Figure 5.3). Blind docking assays showed the same results as in HP0525; an absence of the potential binding site for fatty acids in the interface between NTD and linker region.

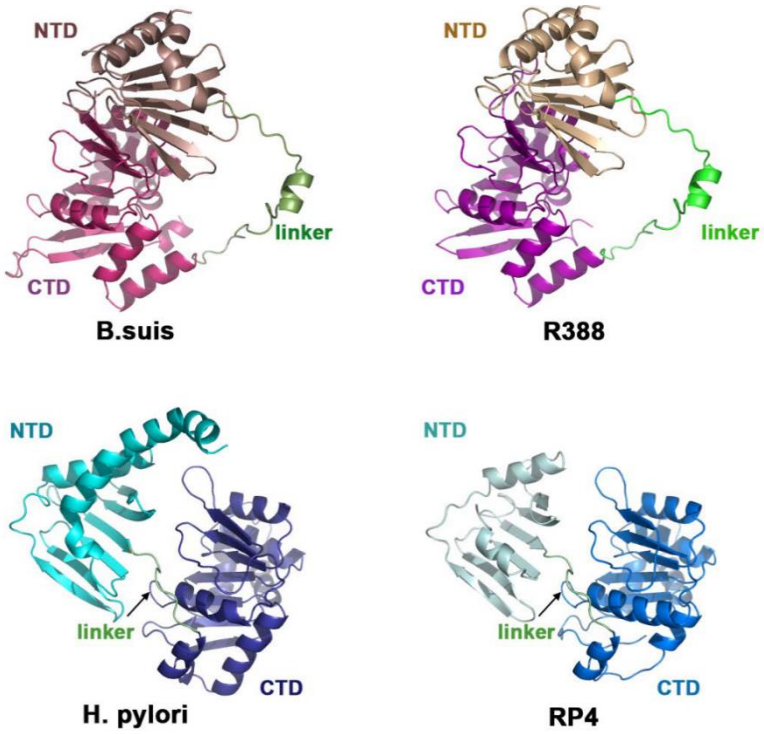

Figure 5.3. Structure of VirB11 homologs. VirB11 proteins are members of the superfamily of traffic AAA+ ATPases. The atomic structures of VirB11 from *Brucella suis* (2gza.pdb) and HP0525, its homolog in *Helicobacter pylori* (1g6O.pdb) are known. Models of TrwD of plasmid R388 and TrbB of plasmid RP4, obtained by molecular threading using *B. suis* and *H. pylori* structures as templates, respectively, have been previously described [235,236]. The size of the linker is very short in *H. pylori* and RP4 homologs, in comparison to the linker of *B. suis* and R388 counterparts. As a consequence, the NTD-CTD inter-domain interactions are different in both types of structures [416].

TraG is the VirB11 homolog from plasmid pKM101 (IncN). The analysis of its sequence shows a shorter linker in comparison with that of TrwD, but longer that VirB11 from *B. suis*. Therefore, its structural tridimensional-model was generated by molecular threading using as template the crystal structure of VirB11 from *B. suis* [236]. Surprisingly, blind molecular docking search did not show any potential binding site for fatty acids in TraG, even though we can find a pocket located in the interface between the linker and the NTD region. By analyzing the amino acids within this region, it is clear that the global charge in this area is very different. In TrwD and VirB11 from *B. suis* the carboxyl group of fatty acids interacts with a series of basic residues located at the base of the pocket. Those amino acids are different in the case of TraG, being especially noteworthy the substitution of lysine 52 of TrwD by an aspartic acid residue, which would prevent the electrostatic interaction with the carboxyl group of the fatty acids.

It is important to note that IncP and IncN plasmids are not inhibited by COINs. Therefore, the structural differences observed in these VirB11-homologs might explain why these systems are not affected by the inhibitors described in this work. However, this explanation leaves some others interrogates; additional molecular and structural studies are required to identify and characterize the binding mechanism of TraG and TrbB to the membrane.

Another open question is the fact that IncF plasmids are inhibited *in vivo* with values similar to those of the IncW plasmids and, yet, no homolog of the VirB11 family has been described in IncF. Which is then the molecular target for COINs in these plasmids? More studies focused on this incompatibility group are needed to answer this question but it is important to keep in mind that IncF plasmids are narrow host range (NHR) plasmids, while IncW are broad host range plasmids (BHR). Bacteria have different natural mechanisms to regulate DNA horizontal transfer by conjugation. While NHR plasmids rely on many host-encoded natural barriers that act at DNA, RNA, or protein level [278], such as restriction-modification (RM) or CRISPR-Cas systems, BHR plasmids regulate their transfer mostly through plasmid-encoded repressors. Therefore, it is likely that the molecular target for COINs in IncF is encoded by the bacterial chromosome, instead of being encoded by the conjugative plasmid, as occurs in R388 plasmid. In order to answer this question, additional assays focused on this line must be carried out.

In conclusion, although additional studies are necessary to characterize the molecular mechanism of action in more detail, our findings open a new avenue for the development of rational design drugs based on the interactions between VirB11 and potential inhibitors, which may help in the fight against the emergence of antibiotic multi-resistant bacteria. Moreover, COINs might be a tremendously useful tool to better understand the mechanism of action and biological function of the cytoplasmic traffic ATPase TrwD, with the aim of studying and understanding in more detail the conjugative process. An additional objective of this thesis was in fact to discern the biological role played by the traffic ATPase TrwD. VirB11 is an essential protein during the first steps of substrate transfer through the secretion channel [131] and also during the biogenesis of pilus [202]. Therefore, TrwD can be defined as a molecular switch between pilus biogenesis and substrate transport [236]. Additionally, given the structural similarity of TrwD with other members of the traffic ATPase superfamily that work as chaperones, it is reasonable to think that VirB11 proteins could also play a role as chaperones, using the energy released from ATP hydrolysis for the assembly/disassembly of the T4SS components during pilus biogenesis and/or for the translocation of substrates through the membrane [237].

During the conjugative process, the relaxases are secreted through the T4SS covalently bound to the processed DNA. Many relaxases, as in the case of TrwC, present an extra C-terminal domain with different activities (helicase, primase or recombinase) [78] which means they have a large molecular size. This fact, added to the dimensions of the secretion channel, means that these proteins have to be unfolded to be secreted through the T4SS channel [238]. This unfolding process might be carried out by TrwD. This hypothesis is based on the structural similarity between the homolog HP0525 from *H. pylori* [219] and the molecular chaperone family ClpB/Hsp104 [401], which deploy partially folded proteins that have been trapped in molecular aggregates [402]. During this work, we have identified the formation of a putative complex

between TrwD and TrwC. The complex was only detected under native non-denaturing conditions, by native polyacrylamide gel electrophoresis assays (Figure 4.26). However, other experiments performed in denaturing conditions or in gel filtration chromatography assays turned out negative. TrwD and TrwC seem to have a very weak interaction. This fact greatly hinders its study and would explain why no interaction between the two proteins has been described so far. The results in this line of work are still very preliminary and additional new approaches are required to study and characterize in detail this TrwD:TrwC molecular interaction. One of these approaches consists of analyzing the localization of these conjugative proteins *in vivo,* by fluorescence microscopy techniques. In this respect, I did a research stay of three months in the laboratory of Dr. Cynthia Whitchurch at the University of Technology Sydney (UTS) (September 2017 - December 2017). Our analysis was primary focused on the localization and mobility of two proteins: TrwD and the coupling protein TrwB. Contrary to most previous data that locate these proteins in the bacteria poles, independently of the rest of the T4SS components [190,424,425], we have observed differences in their localization depending on the presence or absence of the rest of the T4SS components. TrwD was homogeneously distributed through the cell, but in the presence of T4SS components it was localized in discreet loci in the bacterial membrane (Figure 4.27). The coupling protein TrwB has a transmembrane domain and, therefore, it was observed always in the membrane. However, when the rest of the T4SS components are present TrwB forms brighter and more discrete foci (Figure 4.28). Our preliminary results suggest that these discrete loci in the membrane in the presence of all the T4SS components could be the regions where the T4SS secretion channels are assembled. However, further analyses are required to confirm this hypothesis. It is important to note that these experiments have been carried out by expressing proteins in high copy number vectors and, therefore, there may be an excess of protein that distorts the interpretation of these results. We are currently working on the expression of different fluorescent fusion-proteins in the conjugative plasmid R388. By using live cell microscopy, we expect to answer some of the questions raised in this work and better understand the bacterial conjugation process.

Chapter 6
CONCLUSIONS

Barbara McClintock

1. TrwD, an essential Type IV secretion traffic ATPase, is the specific molecular target for fatty acid derivatives that act as conjugation inhibitors (COINs) in the conjugative plasmid R388.

2. The same compounds that inhibit bacterial conjugation are also able to inhibit TrwD ATPase activity whereas those with no effect *in vivo* also fail to inhibit TrwD activity. Therefore, there is a perfect correlation between the *in vivo* and *in vitro* data.

3. We have identified 2-Bromopalmitic acid (2-BP), a palmitate analog without any unsaturation in its aliphatic chain, as an inhibitor of TrwD ATPase activity and bacterial conjugation.

4. The carboxylic group of COINs is essential for its effectivity. However, inhibition is not due to the presence of double or triple bonds in these compounds but, indirectly, by the conformation these fatty acids can acquire upon TrwD binding.

5. COINs act as non-competitive inhibitors, with no effect on the affinity of TrwD for ATP or ADP substrates. Therefore, COINs are binding to TrwD in a site different from the nucleotide binding site.

6. COINs binding induce a conformational change and an open conformation on TrwD, resulting in the exposition of protein domains to unspecific proteases such as papain.

7. Blind docking search identified a pocket comprised by the N-terminal domain (NTD) and the linker region of TrwD with high probability to bind fatty acids. It is likely that binding of COINs to this region results in the restriction of a critical movement of the NTD over CTD, which, in turn, would result in a reduction of TrwD ATPase activity.

8. When bacteria cells are grown in the presence of 2-HDA, they incorporate this exogenous fatty acid to their membranes. This incorporation is accompanied by a 2-fold decrease of palmitic acid in the phospholipid fraction. Therefore, it is very likely that the inhibitory effect of COINs is by affecting the membrane binding mode of TrwD.

9. TrwD binds palmitic acid. Palmitic fatty acid compete with 2-BP for the same binding site in TrwD. Both of them (palmitic acid and 2-BP) bind non-covalently to TrwD.

10. We have identified the formation of a weak complex between TrwD and the relaxase TrwC. The formation of this complex can only be observed by non-denature electrophoresis.

Chapter 7
SPANISH REVIEW

7.1. Introducción.

La resistencia a antibióticos se ha convertido en uno de los principales problemas de salud pública [408], ya que las tasas de morbilidad y mortalidad debidas a la infección por patógenos multirresistentes se han incrementado drásticamente en las últimas décadas [426,427]. Uno de los principales mecanismos por el que las bacterias se convierten en resistentes a los antibióticos es mediante la adquisición de genes de resistencia a través de la conjugación bacteriana [15,17,241]. Por tanto, la búsqueda de inhibidores específicos de la conjugación (COINs) es crucial para el control de la diseminación de genes de resistencia a antibióticos. Diversos grupos han descrito diferentes compuestos como potenciales inhibidores de la conjugación pero la mayoría de estos compuestos han resultado ser inhibidores inespecíficos del crecimiento y metabolismo celular [303,306,428–430]. Los hallazgos más prometedores se han obtenido con ácidos grasos insaturados (uFAs, de sus siglas en inglés *unsaturated fatty acids*), con los compuestos sintéticos 2-alquinoicos y con los ácidos tanzawaicos [322,329,337]. Todos ellos han demostrado ser inhibidores específicos de la conjugación (COINs) y se caracterizan por la presencia en su estructura de un grupo carboxílico y una cadena alifática con dobles o triples enlaces [322,329,337].

Los sistemas de secreción tipo IV (T4SS) son los encargados de mediar la transferencia de ADN y proteínas a la célula receptora durante el proceso conjugativo. Se trata de complejos macromoleculares que se expanden desde la membrana interna a la externa y están compuestos por 12 proteínas (11 más la proteína acopladora), denominadas desde VirB1 a VirB11 tomando como referencia el sistema VirB de *Agrobacterium tumefaciens* [52]. La conjugación bacteriana tiene lugar gracias a un grupo de ATPasas situadas en la cara citoplasmática de la membrana interna y que aportan la energía necesaria para cada paso del proceso conjugativo: la relajación del plásmido y el desenrollamiento del ADN, la transferencia del ADN, la biogénesis del pilus y el transporte proteico [52]. Estos procesos están catalizados en el plásmido conjugativo R388 por TrwC, TrwB, TrwK y TrwD, homólogos de VirD2, VirD4, VirB4 y VirB11, respectivamente. TrwC es la proteína que se une al ADN en el origen de transferencia y presenta actividades relaxasa y helicasa [78,400]. TrwB es una ATPasa dependiente de ADN que media la transferencia del ADN a través del sistema de secreción [173]. TrwK es una ATPasa [206] que media la dislocación de moléculas de pilina desde la membrana interna durante la biogénesis del pilus [213]. La cuarta ATPasa, TrwD, participa en la biogénesis del pilus [213] y en la translocación del sustrato nucleo-proteico [214], actuando como un interruptor molecular entre ambos procesos [236].

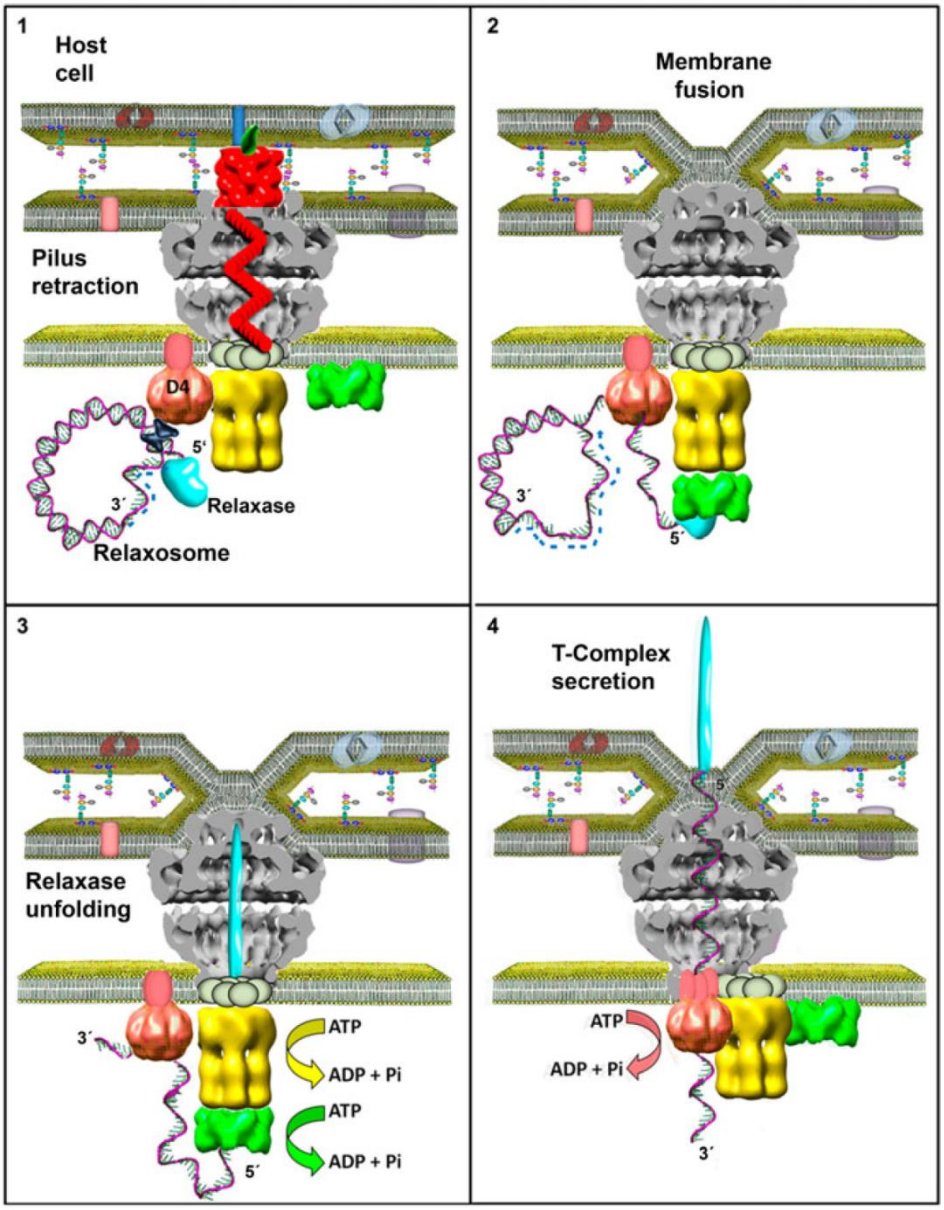

Figura 7.1. Modelo del procesamiento del ADN durante la conjugación bacteriana a través del T4SS. (1) Una célula donadora y una receptora entran en contacto a través del pilus conjugativo (rojo) sintetizado por la donadora. La mayoría de los sistemas conjugativos presentan cuatro ATPasas implicadas en la transferencia del plásmido a la célula receptora. Dos de esas ATPasas (TrwK y TrwD en el caso del plásmido R388, amarilla y verde respectivamente), están implicadas en la biogénesis del T4SS. Los factores auxiliares TrwA y IHF se unen al origen de transferencia (*oriT*) del ADN plasmídico y la relaxasa (azul) corta en el sitio *nic* permaneciendo covalentemente unida al extremo 5' del *oriT*. **(2)** Tras el contacto celular, la retracción del pilus extracelular facilita la interacción entre las membranas de la célula donadora y receptora, dando lugar a la fusión de las membranas. Simultáneamente, o antes del proceso de fusión de membranas, la proteína acopladora (salmón) conduce el relaxosoma hacia el canal de secreción. **(3)** El substrato nucleo-proteico es transferido a TrwD/VirB11 (verde). La relaxasa es desplegada y translocada hacia el canal covalentemente unida al ADN. **(4)** TrwK/VirB4 (amarilla) es desplazada de la base del canal de secreción por la proteína acopladora, la cual asiste a la translocación del ADN en dirección 5'-3'. Tomado de [52].

7.2. Objetivos.

El objetivo de este trabajo es ampliar nuestro conocimiento sobre los sistemas de secreción tipo IV (T4SS) y sobre las bases moleculares del proceso conjugativo. Desde el punto de vista aplicado, pretendemos caracterizar el mecanismo de inhibición del plásmido conjugativo R388 por los inhibidores de la conjugación (COINs). Estos resultados podrían abrir una nueva vía para el diseño racional de nuevas y potentes drogas para luchar contra la diseminación de genes de resistencia a antibióticos.

Por ello, nuestros principales objetivos son:

1. Identificar la diana específica y caracterizar el mecanismo molecular de inhibición llevado a cabo por los inhibidores de la conjugación (COINs) en nuestro sistema modelo, el plásmido conjugativo R388.

2. Adquirir un mayor conocimiento sobre el papel biológico y el mecanismo de acción de la *traffic* ATPasa conjugativa TrwD.

3. Analizar *in vivo* mediante microscopía de fluorescencia de célula viva el proceso conjugativo y la localización de los diferentes componentes del T4SS.

7.3. Resultados y discusión.

7.3.1. Identificación de la diana molecular para inhibir la conjugación bacteriana mediante COINs.

Ensayos de cribado farmacológico de alto rendimiento (HTS, de sus siglas en inglés *high-throughput screening*), han permitido identificar a los ácidos grasos insaturados (uFAs, de sus siglas en inglés *unsaturated fatty acids*) como inhibidores específicos de la conjugación bacteriana (COINs), sin alterar el metabolismo ni al crecimiento bacteriano [322]. Sin embargo, al principio de este proyecto no se conocía el mecanismo exacto de inhibición mediada por estos compuestos. Durante esta tesis hemos identificado su diana molecular en nuestro modelo, el plásmido conjugativo R388. La diana es TrwD, una ATPasa del sistema de secreción tipo IV (T4SS). TrwD es la única ATPasa del sistema de secreción que se ve afectada de forma significativa por la presencia de uFAs, mientras que la proteína acopladora TrwB, la relaxasa TrwC y TrwK no son inhibidas de manera significativa (*Figure* 4.1).

Al contrario que los ácidos grasos insaturados, los ácidos grasos saturados no son capaces de inhibir la conjugación bacteriana [322]. Para determinar si existe una correlación entre los resultados obtenidos *in vivo* y el análisis *in vitro*, testamos el efecto de diferentes tipos de ácidos grasos sobre la hidrólisis de ATP llevada a cabo por TrwD. TrwD (2 µM) en presencia de ácidos grasos (50 µM) fue inhibida más del 90% por los ácidos grasos insaturados oleico ($C_{18:1\ (9)}$) y

linoleico ($C_{18:2\ (9,12)}$), mientras que con los saturados láurico ($C_{12:0}$) y palmítico ($C_{16:0}$) no se observó inhibición (*Figure* 4.2). Estos resultados sugieren la presencia de insaturaciones como característica esencial para el mecanismo de inhibición, y muestran una perfecta correlación con los resultados obtenidos *in vivo* [322].

Una nueva clase de ácidos grasos sintéticos denominados 2-alquinoicos y caracterizados por la presencia de un triple enlace entre los carbonos C-2 y C-3, han sido también identificados como inhibidores específicos de la conjugación (COINs) [329]. Hemos analizado la actividad ATPasa de TrwD (2 μM) en presencia de estos compuestos, obteniendo similares resultados. De nuevo hemos encontrado una correlación entre los resultados *in vitro* e *in vivo*. Los tres compuestos capaces de inhibir TrwD de forma estadísticamente significativa fueron los ácidos 2-hexadecinoico (2-HDA), 2-octadecinoico (2-ODA) y 2,6-hexadecadiinoico (2,6-HDA). Sin embargo, los derivados alcohol (OH) o tetrahidropiranil-éter (THP) de éstos compuestos no fueron capaces de inhibir ni la actividad ATPasa de TrwD ni la conjugación bacteriana *in vivo* (*Figure* 4.4). Por tanto, estos resultados establecen el grupo carboxílico como elemento esencial para la capacidad de inhibición de los COINs.

En resumen, nuestros resultados han determinado que exactamente los mismos compuestos capaces de inhibir la conjugación *in vivo*, son capaces de inhibir la actividad ATPasa de TrwD, y viceversa, aquellos sin efecto *in vivo* tampoco inhiben a TrwD *in vitro*. Por tanto, estos resultados apoyan la hipótesis de que TrwD es la diana molecular específica para ambos tipos de ácidos grasos, alquenoicos y alquinoicos.

7.3.2. Identificación de un inhibidor de la conjugación bacteriana (COIN) con nuevas características estructurales.

El grupo carboxílico de los COINs es esencial para el efecto inhibitorio, ya que derivados alcohol o tetrahidropiranil-éter de esos ácidos grasos no fueron capaces de inhibir a TrwD *in vitro* ni la conjugación de R388 *in vivo* [416]. Además, el efecto inhibitorio fue observado solamente en presencia de ácidos grasos insaturados, como los ácidos oleico y linoleico, pero no en presencia de ácidos grasos saturados, como los ácidos láurico o palmítico. Por lo tanto, nos planteamos determinar si la presencia de insaturaciones es otra característica esencial de los COINs o, por el contrario, ejercen su inhibición por la conformación que adquieren debido a las constricciones geométricas en su cadena alifática.

Para ello analizamos *in vitro* la actividad ATPasa de TrwD (2 μM) en presencia del ácido 2-Bromopalmítico (2-BP). Éste es un derivado del ácido palmítico que ha sido caracterizado como inhibidor de muchas enzimas asociadas a membranas [382–384]. Nuestros resultados mostraron que 2-BP (50 μM) inhibe la actividad de TrwD en el mismo rango de valores que otros COINs. En presencia de 2-BP la actividad de TrwD fue de 23,4 ± 4,3 %, mientras que en presencia de 2-HDA y ácido palmítico fue de 26,7 ± 7,3 % y 10,0 ± 2,4 %, respectivamente (*Figure* 4.5).

También analizamos el efecto de 2-BP (500 µM) en la conjugación bacteriana del plásmido R388. Calculamos la frecuencia de conjugación siguiendo un protocolo previamente descrito [329] basado en la emisión de fluorescencia por las células transconjugantes. La frecuencia de conjugación disminuyó a niveles similares en presencia de 2-BP, 2-HDA y ácido linoleico, respectivamente (*Figure* 4.6). Por tanto, podemos definir 2-BP como un nuevo COIN. La identificación de 2-BP como un inhibidor efectivo de la conjugación (COIN), nos permite concluir que los COINs no ejercen su efecto inhibitorio por la presencia de instauraciones en su cadena alifática.

7.3.3. Unión de COINs a TrwD: caracterización del mecanismo de inhibición.

Con el objetivo de determinar el mecanismo de inhibición de TrwD por COINs, decidimos realizar una caracterización de las cinéticas de inhibición. En primer lugar, la actividad ATPasa de TrwD (2 µM) fue medida a concentraciones crecientes de ácidos grasos. Como era de esperar, los ácidos grasos saturados no produjeron inhibición. Sin embargo, para todos los COINs las cinéticas de inhibición fueron similares. Los datos no se ajustaron a una cinética de inhibición de Michaelis-Menten, sino a una ecuación de Hill sigmoidea para inhibición, lo que sugiere la existencia de cooperatividad. Calculamos la $K_{i[app]}$ para cada compuesto; 21 µM para el ácido linoleico y 2-BP, respectivamente, y 30 µM para 2-HDA y 2-ODA, respectivamente (*Figure* 4.7 y 4.8).

Seguidamente se precedió a estudiar el efecto de los ácidos grasos en la unión de nucleótidos a TrwD. Para ello se midió la hidrólisis de ATP en estado estacionario a concentraciones crecientes de ATP en ausencia y presencia de ácidos grasos. La concentración de ácido graso utilizada fue la correspondiente a la constante de inhibición aparente ($K_{i[app]}$) calculada previamente. Los datos se ajustaron a una ecuación de Hill. Tal y como era de esperar, la V_{max} en presencia de COINs se redujo a la mitad. Pero la $K_{0,5}^{ATP}$ no se vio significantemente afectada, siendo 44 µM en ausencia de ácidos grasos, 66 µM en presencia de 2-HDA y 44 µM en presencia de ácido linoleico (*Figure* 4.9). Estos resultados sugieren que los COINs no modifican la afinidad por ATP. Por tanto, estamos ante un mecanismo de inhibición no competitivo.

Para realizar una mayor caracterización de la cinética de inhibición, también se estudió la actividad de TrwD a concentraciones crecientes de ADP en presencia y ausencia de inhibidor. Las cinéticas de inhibición por ADP se ajustaron usando una versión de la función de inhibición competitiva. Las constantes de disociación obtenidas indican que los COINs no afectan a la afinidad de TrwD por ADP, ya que en presencia de 2-HDA la K_d^{ADP} fue 51 µM y en su ausencia la K_d^{ADP} fue 44 µM (*Figure* 4.10). En conjunto, estos resultados, junto con los indicados en el párrafo anterior, muestran que la inhibición no es resultado de modificar las afinidades por los nucleótidos ATP (sustrato) o ADP (producto). Por tanto, los inhibidores están ejerciendo su acción sobre una región de la proteína diferente al sitio de unión a nucleótidos. Es muy probable que la unión del inhibidor a esa otra región resulte en cambios conformacionales de la proteína que dan lugar a la inhibición de su actividad ATPasa.

Para comprobar si realmente se producen cambios conformaciones en TrwD, analizamos la susceptibilidad de TrwD a la digestión parcial con papaína en presencia de diferentes ácidos grasos. La papaína es una proteasa inespecífica útil para delimitar los dominios estructurales en proteínas, ya que presenta baja actividad frente a estructuras secundarias o terciarias estables [362]. La incubación de TrwD a concentraciones crecientes de 2-HDA (de 1:10 a 1:100, TrwD:2-HDA ratios molares) resultó en una mayor susceptibilidad a la digestión por papaína. En cambio, similares experimentos realizados en presencia del ácido palmítico no produjeron ningún efecto en la susceptibilidad de TrwD a la digestión por papaína, ni siquiera a la concentración más elevada ensayada (1:100, TrwD:ácido palmítico ratio molar) (*Figure* 4.11). Estos resultados sugieren que la unión del inhibidor induce cambios conformaciones en TrwD dando lugar a una conformación abierta de la proteína, que resulta en la exposición de dominios a la papaína.

Con el objetivo de explorar posibles sitios de unión para los COINs en TrwD, realizamos un estudio de docking o acoplamiento molecular. Se trata de una simulación por ordenador para predecir la mejor unión entre dos moléculas desde un punto de vista estructural y energético. Para ello, un modelo estructural de TrwD fue construido mediante hilvanado molecular usando como modelo VirB11 de *Brucella suis* [228], tal y como se describió previamente [235]. TrwD consiste en un dominio N-terminal (NTD), que interacciona con la membrana interna bacteriana, y un dominio catalítico C-terminal (CTD), conectados ambos por un linker largo y flexible. Los ácidos grasos usados como ligandos fueron obtenidos del repertorio Pubchem (http://pubchem.ncbi.nlm.nih.gov/) y preparados para el docking como se describe en la sección de materiales y métodos. Las predicciones de docking obtenidas usando el motor de muestreo de espaciado diédrico EADock [371] del servidor web SwissDock (http://www.swissdock.ch/), mostraron una región comprendida entre el dominio NTD (residuos 37-54) y la región del linker (residuos 118-125) de TrwD como el sitio con la mayor probabilidad para la unión de COINs (*Figure* 4.12). Cuando se usó la estructura hexamérica de TrwD como diana, todas las posiciones de unión de los ligandos se agruparon en este mismo bolsillo localizado en la interfase entre el NTD y el linker (*Figure* 4.13). Curiosamente, las predicciones de docking con el ácido palmítico sugerían que el sitio de unión para este ácido graso saturado está en la misma región que la encontrada para los COINs: ácido linoleico, 2-HDA y ácido 2-Bromopalmítico.

Aunque todos los compuestos se unan al mismo sitio en TrwD, el bolsillo comprendido entre el NTD y el linker, la conformación del grupo carboxílico no es exactamente la misma en todos los compuestos. En el caso del 2,6-HDA el grupo carboxílico se sitúa a una mayor distancia de los residuos básicos de la región del linker, lo que podría explicar su menor efecto inhibitorio respecto a 2-HDA, 2-ODA y ácido linoleico. Por su parte, los derivados como el tetrahidropiranil-éter (2-HDPTHP) no pueden establecer interacciones electrostáticas con la región del linker debido a la ausencia del grupo carboxílico, lo que explicaría su incapacidad para inhibir a TrwD (*Figure* 4.14).

Si comparamos los resultados obtenidos mediante el docking con el ácido palmítico y su derivado 2-BP, observamos que los dos ácidos grasos se unen a ese mismo bolsillo localizado en la interfase entre NTD y el linker, al igual que el resto de COINs. La cadena alifática de estos dos

ácidos grasos adopta una orientación muy similar. Sin embargo, el grupo carboxílico del derivado 2-BP está enterrado dentro del bolsillo formado por el NTD y el linker de la proteína, estando el átomo de bromo estabilizado por grupos electrostáticos localizados en la región (residuos 115-118 del linker). En cambio, el grupo carboxílico del ácido palmítico presenta una orientación con 120 grados de diferencia, estableciendo un contacto más cercano con la lisina 52, situada fuera de la región del linker. Esto podría explicar por qué 2-BP es capaz de inhibir a TrwD mientras que el ácido palmítico no altera la actividad ATPasa de TrwD (*Figure* 4.15).

7.3.4. Incorporación de los COINs a la membrana plasmática.

Estudios previos han mostrado como la actividad ATPasa de TrwD es estimulada por fosfolípidos [221]. *In vitro,* TrwD interacciona con fosfolípidos en vesículas lipídicas, ocasionando la agregación, liberación de contenidos encapsulados y mezcla de lípidos [226]. Sin embargo, aunque es ampliamente reconocido que TrwD interacciona con el lado citoplasmático de la membrana interna bacteriana, las bases moleculares subyacentes a esta interacción aún no se conocen con precisión [387].

En la literatura, encontramos proteínas que se asocian a la membrana a través de enlaces no covalentes con ácidos grasos saturados, como el ácido palmítico [388]. Un ejemplo son los receptores Toll-like (TLRs) [389,390], los cuales son inhibidos por ácidos grasos poliinsaturados [391], como TrwD. Por otra lado, una amplia variedad de proteínas se asocian covalentemente a la membrana a través del ácido palmítico, por un proceso conocido como S-palmitoilación [392,393]. En estas proteínas palmitoiladas el ácido graso se une a un residuo de cisteína a través de un enlace tioéster. Es un proceso reversible que permite la unión transitoria con la membrana, jugando un papel crucial en muchos procesos biológicos [392–394].

El sitio con la mayor probabilidad para la unión los de ácidos grasos a TrwD según los resultados obtenidos mediante acoplamiento molecular se localiza en la interfase entre el dominio N-terminal y el linker de TrwD. Puesto que NTD es el dominio implicado en la unión de TrwD a la membrana [219], TrwD podría interactuar con la membrana a través de los ácidos grasos. Los COINs descritos en este trabajo ocuparían un sitio de unión en TrwD que de otra manera estaría ocupado por fosfolípidos de membrana.

Para determinar si los COINs son incorporados a las membranas bacterianas, se crecieron células *E. coli* en presencia y ausencia de 2-HDA. Tras 18 horas de incubación, las células se recogieron y la composición de ácidos grasos libres y ácidos grasos esterificados formando parte de fosfolípidos se analizó mediante cromatografía de gases-espectrometría de masas (GC-MS). Los resultados mostraron que los ácidos grasos esterificados de la fracción de fosfolípidos eran mayoritariamente saturados en las bacterias no tratadas, siendo el ácido palmítico el más abundante (44%). Estos datos fueron muy similares a los obtenidos en la fracción de ácidos grasos libres. Sin embargo, en las bacterias tratadas 2-HDA es el mayor componente de la fracción total de fosfolípidos (44%). Este hecho ilustra una significativa alteración en la utilización de ácidos

grasos endógenos para la biosíntesis de fosfolípidos e indica que 2-HDA puede ser activado e incorporado a la membrana bacteriana, lo que se acompaña por una significativa disminución de 2 veces en la proporción de ácido palmítico en la membrana. Aunque 2-HDA también está presente en la fracción de ácidos grasos libres, en esta fracción la proporción relativa de ácidos grasos no es alterada por el tratamiento (*Figure* 4.16).

Por tanto, tomando en consideración todos los resultados recapitulados hasta el momento, es razonable pensar que TrwD podría unirse a la membrana interna a través de la interacción con ácidos grasos de fosfolípidos, como el ácido palmítico. El reemplazamiento tan significativo del ácido palmítico por 2-HDA en células tratadas podría estar perturbando la interacción de TrwD con la membrana, resultando en un efecto inhibitorio.

7.3.5. Unión de ácidos grasos saturados a TrwD: caracterización del posible mecanismo de unión a membrana.

A pesar de que los COINs son capaces de inhibir la actividad ATPasa de TrwD mientras que los ácidos grasos saturados, como el ácido palmítico, no tienen ningún efecto en la hidrólisis de ATP, las predicciones de docking sugieren que todos ellos se unen a la misma región de TrwD. En un intento para probar esta posible interacción entre TrwD y el ácido palmítico, se realizó un ensayo de marcaje radioactivo. Proteína TrwD purificada fue incubada con ácido palmítico marcado radioactivamente con ^{14}C a diferentes ratios molares y la posible interacción proteína-ligando fue analizada en geles nativos en condiciones no desnaturalizantes. La señal radioactiva de TrwD estaba directamente correlacionada con el incremento de la relación molar proteína:ácido palmítico (desde 1:0,25 hasta 1:1; TrwD:ácido palmítico ratios molares). Como control, se analizó una proteína conjugativa citoplasmática, TrwA. No se observó señal radioactiva para esta proteína control, ni siquiera a la mayor concentración de ácido graso ensayada. Los resultados confirman por tanto una unión específica de TrwD al ácido palmítico (*Figure* 4.17). El mismo experimento se realizó con palmitoil-CoA, marcado también radioactivamente con ^{14}C, obteniendo los mismos resultados (*Figure* 4.18).

En un intento por determinar si los inhibidores y el ácido palmítico compiten por el mismo sitio de unión en TrwD, tal y como predice el docking molecular, realizamos una caracterización adicional del mecanismo de inhibición. La hidrólisis de ATP por TrwD (2 µM) fue medida a concentraciones crecientes de ácido graso. Como ya vimos, el ácido palmítico no inhibe, mientras que 2-BP inhibe a TrwD. Ajustando la cinética con una ecuación sigmoidea de Hill obtenemos que la $K_{i[app]}$ es 21 µM para 2-BP. En cambio, si TrwD ha sido preincubada con 500µM de ácido palmítico, al realizar el barrido con 2-BP la $K_{i[app]}$ se incrementa hasta 65 µM (*Figure* 4.19). Este mismo experimento fue realizado *in vivo*, calculando la frecuencia de conjugación de R388 en presencia del ácido graso. Cuando las células están en presencia de ácido palmítico (500 µM) se necesita una cantidad significativamente mayor de 2-BP para obtener la misma inhibición de la

conjugación (*Figure* 4.20). Esta exacta correlación entre los resultados *in vivo* e *in vitro* confirma que ambos ácidos grasos (2-BP y ácido palmítico) compiten por el mismo sitio de unión en TrwD.

El ácido 2-Bromopalmítico ha sido descrito como inhibidor de muchas enzimas asociadas a la membrana que unen ácido palmítico [382,393]. Se trata de un inhibidor irreversible que bloquea la incorporación del ácido palmítico en las proteína, pero el mecanismo exacto de la inhibición mediada por 2-BP no se conoce [396–398,392,394]. Por ello decidimos realizar una mayor caracterización de la interacción de TrwD con el ácido palmítico y 2-BP. Para ello, realizamos un estudio mutacional de la ATPasa TrwD. 2-BP es un inhibidor irreversible de la palmitoilación, una modificación postranslacional por la cual un ácido graso saturado es unido a una cisteína de la proteína [392,394]. Predicciones *in silico* con el servidor web CSS-Palm 4.0 [399] identificaron un residuo de cisteína (C44) de TrwD como un sitio potencial de palmitoilación. Por tanto, decidimos realizar una mutación puntual y cambiar esa cisteína por asparagina (mutante C44N). Si comparamos la secuencia de TrwD con sus homólogos [236], hay una región en el linker A con residuos básicos que en los homólogos resistentes a la acción de COINs son ácidos (HP0525 de *H. pylori* y TraG de pKM101). Por ello, decidimos modificar esta región; histidina 119 (H119) y valina 123 (V123) fueron reemplazadas por ácido aspártico (mutante H229D-V123D). Como TrwD además presenta el linker más largo en comparación con el resto de homólogos de VirB11 [236], decidimos realizar una mutación para acortar el linker de TrwD, eliminando los residuos entre la alanina 138 (A148) y la arginina 162 (R162) (mutante TrwDΔ15link) (*Figure* 4.21). Al realizar un análisis para determinar si estas mutaciones afectan al plegamiento y la estabilidad de TrwD, observamos que los mutantes C44N y H119D-V123D muestran el mismo comportamiento que la proteína TrwD nativa. Sin embargo, al acortar la longitud del linker en TrwDΔ15link se produce una proteína insoluble que forma cuerpos de inclusión y precipita a bajas velocidades de centrifugación (5.000 g) (*Figure* 4.22).

La capacidad de los mutantes de TrwD para reemplazar la función de la proteína TrwD nativa fue analizada por complementación funcional mediante ensayos de conjugación bacteriana. Sin un gen *trwD* funcional, no se produce la conjugación del plásmido pSU4039 (mutante del plásmido conjugativo R388 con un transposón insertado en *trwD*). La conjugación se restaura cuando pSU4039 es complementada con un plásmido que contiene un gen *trwD* funcional. Sólo el mutante C44N fue capaz de restaurar la conjugación. Sin embargo, la presencia de 2-BP (500 µM) inhibió a TrwD C44N, por lo que 2-BP no se está uniendo a la cisteína 44 de TrwD. La ausencia de transcomplementación de pSU4039 con TrwD H229D-V123D y TrwDΔ15link define que las regiones modificadas en estos mutantes son básicas para la funcionalidad de TrwD, pero no permiten determinar si son el sitio de unión de 2-BP a TrwD (*Table* 4.1).

Para determinar la naturaleza de la interacción entre palmítico y TrwD, se analizó la sensibilidad a la desnaturalización inducida por electroforesis en SDS. No se detectó señal radioactiva tras la incubación de TrwD con ácido palmítico marcado radioactivamente con ^{14}C ni con palmitoil-CoA, lo que sugiere que la unión es no covalente y por tanto no hay un enlace tioéster implicado en tal asociación del ácido palmítico con TrwD. Adicionalmente, TrwD fue analizado por espectrometría de masas en ausencia y presencia de 2-BP (500 µM). La incubación de TrwD con 2-BP en una relación molar de 1:10 (TrwD:2-BP) no resultó en una mayor masa

molecular de la proteína. Los resultados obtenidos fueron de 39.980,5±6,5 y 39.997,5±3,5 Da en ausencia y presencia de 2-BP, respectivamente (*Figure* 4.23). Por tanto, podemos concluir que ambos compuestos (ácido palmítico y 2-BP) interaccionan de forma no covalente con TrwD.

7.3.6. Mecanismo modelo para la inhibición de la actividad ATPasa de TrwD por COINs.

Los resultados obtenidos durante el transcurso de esta tesis nos han llevado a proponer un posible mecanismo de inhibición de la actividad de hidrólisis de ATP por TrwD en presencia de COINs.

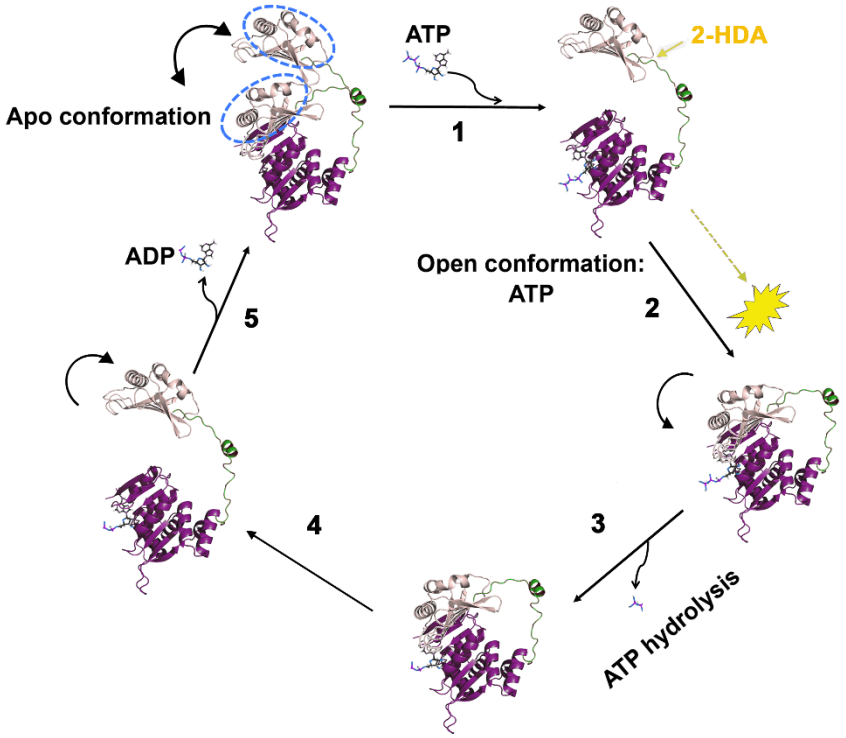

Figura 7.2. Mecanismo modelo de la inhibición de la actividad ATPasa de TrwD por COINs. Mecanismo propuesto para el ciclo catalítico de la hidrólisis de ATP (adaptado de [235]). Según este mecanismo, compartido por otros miembros de la superfamilia de ATPasas de secreción [233], en la conformación *apo*, TrwD puede alternar entre una conformación abierta y una cerrada, con el NTD pivotando sobre el CTD gracias al movimiento del linker flexible (paso 1), pero sólo en la conformación abierta es capaz de unir ATP. Tras la unión del ATP, el NTD se cierra sobre el CTD (paso 2) y así puede tener lugar la hidrólisis de ATP (paso 3). Tras la hidrólisis, el NTD se abre (paso 4), permitiendo la liberación del ADP y el ciclo puede reanudarse de nuevo (paso 5). Los resultados obtenidos en este trabajo nos hacen pensar que es muy probable que TrwD se inhiba porque es alterada la interacción entre el NTD y el CTD. La unión del ácido graso impediría el pivotamiento, y por tanto la progresión del ciclo catalítico, lo que resultaría en la inhibición de la hidrólisis de ATP. Tomada de [416].

7.3.7. Análisis de la interacción molecular entre TrwD y TrwC.

El substrato a ser transportado durante el proceso conjugativo es un complejo nucleo-proteico, ya que la proteína piloto TrwC es secretada a la célula receptora covalentemente unida al ADN [338,400]. El gran tamaño de TrwC (108 KDa), unido al reducido diámetro del canal de secreción (10-32 Å) [134,143], hace necesario un desplegamiento previo de la proteína TrwC para ser transportada [238]. TrwD presenta importantes similitudes estructurales con chaperonas de diferentes sistemas de secreción [401,402]. Por tanto, una de las hipótesis de trabajo de nuestro grupo es que TrwD, haciendo uso de la energía resultante de la hidrólisis de ATP, podría ser responsable del desplegamiento y/o de mantener desplegada TrwC para su translocación a través del canal de secreción.

Una interacción débil entre proteínas es muy difícil de observar mediante cromatografía de filtración, ya que el complejo podría no ser muy estable. Por ello, decidimos realizar un análisis del posible complejo TrwD:TrwC mediante electroforesis en condiciones nativas no desnaturalizantes (Native-PAGE). La interpretación de los geles nativos es compleja, pues los cambios en la movilidad relativa pueden reflejar cambios en la carga, masa o en ambas, pero las proteínas también podrían tener un punto isoeléctrico (pI) por encima del valor de pH del buffer, en cuyo caso no migrarían o lo harían en dirección opuesta (hacia fuera del gel). Los pI de TrwD y TrwC son 5,97 y 9,26, respectivamente. Tal diferencia no nos permitió encontrar una condición de electroforesis nativa para observar ambas proteínas en el mismo gel. El mejor resultado se obtuvo con geles de poliacrilamida al 4,5% en buffer electroforético de Tris-Glicina, pH 8,3. En estos geles sólo observamos a la proteína TrwD. Sin embargo, cuando TrwD es pre-incubada con TrwC, la intensidad de la banda de TrwD desaparece a concentraciones crecientes de TrwC (*Figure* 4.24). Este resultado fue observado tanto con TrwC nativa como con TrwC previamente desnaturalizada mediante choque térmico. Aunque no podemos descartar la posibilidad de que TrwD esté formando agregados, un control negativo consistente en TrwD incubada en presencia del buffer de TrwC (sin proteína TrwC), no mostró ninguna variación en la intensidad de la banda. Este resultado sugiere la formación de un complejo TrwD:TrwC que no es capaz de entrar en el gel bajo las condiciones ensayadas.

Adicionalmente, realizamos una electroforesis azul nativa en geles de poliacrilamida (BN-PAGE). Esta técnica permite la separación con gran resolución de complejos multiproteicos en una conformación nativa. Las muestras son teñidas con un colorante cargado (Coomassie Blue G-250) que les da una movilidad electroforética diferente sin desnaturalizar a las proteínas. Las muestras proteicas serán separadas según su tamaño y forma. Se emplearon geles en gradiente de acrilamida (4-13%) a un pH 7,0. En estas condiciones experimentales, TrwD migra en el gel, mientras que TrwC es detectada en los pocillos. La gran ventaja de este análisis es la aparición de una nueva banda tras la incubación de TrwD:TrwC, la cual podría corresponder a un complejo formado entre ambas proteínas. Tras esta primera dimensión con BN-PAGE, realizamos una segunda dimensión mediante electroforesis desnaturalizante con SDS (SDS-PAGE). Las bandas detectadas en BN-PAGE fueron cortadas, deshidratadas, empapadas en tampón desnaturalizante

con SDS y analizadas mediante SDS-PAGE. La interacción entre ambas proteínas fue evidente debido a que la nueva banda obtenida en la primera dimensión (BN-PAGE) tras incubar TrwD:TrwC fue disociada en TrwD y TrwC durante esta segunda dimensión (*Figure* 4.26).

Por consiguiente, hemos identificado la formación de un complejo entre TrwD y TrwC. Sin embargo, este complejo fue detectado sólo en condiciones nativas no desnaturalizantes. Otros experimentos realizados en condiciones desnaturalizantes o en cromatografía de filtración en gel dieron resultados negativos. Por tanto, TrwD y TrwC parecen presentar una interacción muy débil. Este hecho dificulta enormemente su estudio y podría explicar por qué no había sido descrita hasta ahora una interacción entre estas dos proteínas. No obstante, los resultados obtenidos en esta línea de trabajo son todavía muy preliminares y se requieren adicionales aproximaciones para caracterizar en detalle esta interacción molecular TrwD:TrwC.

7.3.8. Localización y dinámica *in vivo* de TrwD y otros componentes del T4SS.

Como parte de ese trabajo, también decidimos analizar la localización *in vivo* de TrwD y otros motores moleculares que podrían interaccionar con esta proteína. Debido a la amplia variedad de proteínas fluorescentes (FPs) con diversas características [403], los ensayos basados en fluorescencia constituyen una interesante opción para la visualización directa de la distribución de proteína y la conjugación a tiempo real entre células individuales. Nuestro objetivo inicial fue estudiar la localización y movilidad de dos motores moleculares: TrwD (*traffic* ATPasa) y TrwB (proteína acopladora). Ambas se fusionaron con proteínas fluorescentes y se estudiaron mediante microscopía de fluorescencia en presencia y ausencia del resto de componentes del sistema de secreción T4SS. Los resultados mostraron diferencias en la localización de las proteínas en función de la presencia o ausencia del resto de componentes del T4SS. TrwD fue localizada homogéneamente por toda la célula, pero en presencia del resto de componentes del T4SS estaba localizada en focos discretos en la membrana bacteriana (*Figure* 4.27). La proteína acopladora TrwB tiene un dominio transmembrana y, según lo esperado, fue observada siempre en la membrana. Sin embargo, cuando el resto de los componentes del T4SS estaban presentes, TrwB formaba focos más discretos y brillantes (*Figure* 4.28). Nuestros resultados preliminares sugieren que estos focos discretos en la membrana cercanos a los polos bacterianos podrían estar indicando las regiones donde los canales de secreción del T4SS son ensamblados. No obstante, se requieren estudios adicionales para confirmar esta hipótesis. Además, es importante señalar que estos experimentos se han llevado a cabo expresando estas proteínas en vectores de elevado número de copias y, por lo tanto, puede haber un exceso de proteína que distorsione la interpretación de estos resultados.

Actualmente estamos trabajando en la expresión de diferentes proteínas de fusión fluorescentes en el propio plásmido R388 presente en células donadoras, con el fin de observar y analizar cualquier cambio en su localización. Hemos puesto a punto procedimientos para diferenciar bacterias donadoras, receptoras y transconjugantes en una población compleja, así como para la directa visualización del plásmido tras ser transferido a la célula receptora. Mediante

microscopía de célula viva, esperamos dar respuesta a alguna de las cuestiones planteadas en este trabajo y entender mejor el proceso conjugativo bacteriano.

7.4. Conclusiones.

1. TrwD, una ATPasa esencial del sistema de secreción tipo IV en el plásmido conjugativo R388, es la diana molecular específica de inhibidores de la conjugación (COINs) derivados de ácidos grasos.
2. Los mismos compuestos capaces de inhibir la conjugación bacteriana fueron capaces también de inhibir la actividad ATPasa de TrwD, y viceversa, aquellos incapaces de inhibir la conjugación tampoco inhibieron la actividad de TrwD. Por lo tanto, podemos afirmar que existe una directa correlación entre los datos obtenidos *in vivo* e *in vitro*.
3. Hemos identificado el ácido 2-Bromopalmítico (2-BP), un análogo del ácido palmítico sin insaturaciones en su cadena alifática, como un inhibidor de la actividad ATPasa de TrwD y de la conjugación bacteriana.
4. El grupo carboxílico de los COINs es esencial para su efectividad. Sin embargo, la inhibición no depende de la presencia de dobles o triples enlaces en los ácidos grasos sino, indirectamente, de la conformación que estos ácidos grasos pueden adquirir en su unión a TrwD.
5. Este tipo de COINs actúan como inhibidores no competitivos, al no afectar la afinidad de TrwD por ATP o ADP. Por tanto, los COINs se unen a una región de TrwD diferente del sitio de unión a nucleótidos.
6. La unión de COINs induce cambios conformacionales en TrwD dando lugar a una conformación abierta de la proteína, que resulta en la exposición de dominios a proteasas inespecíficas como la papaína.
7. Ensayos de docking o acoplamiento molecular identificaron un bolsillo comprendido en la interfase entre el dominio N-terminal (NTD) y la región del linker de TrwD como un sitio de alta probabilidad para la unión de ácidos grasos. Es probable que la unión de COINs en esta región resulte en la restricción de un movimiento crucial del NTD sobre el CTD, lo que se traduce en una reducción de la actividad ATPasa de TrwD.
8. Cuando las bacterias crecen en presencia de 2-HDA, incorporan este ácido graso exógeno en sus membranas. Esta incorporación va acompaña por una significativa disminución del ácido palmítico presente en la fracción de fosfolípidos. Por tanto, es muy probable que el efecto inhibitorio de los COINs sea resultado de afectar la unión de TrwD a la membrana.
9. TrwD se une al ácido palmítico. El ácido palmítico compite con 2-BP por el mismo sitio de unión en TrwD. Ambos compuestos (ácido palmítico y 2-BP) se unen de forma no covalente a TrwD.
10. TrwD y la relaxasa TrwC forman un complejo que puede ser identificado por electroforesis en condiciones no desnaturalizantes. TrwD y TrwC parecen presentar una interacción muy débil.

Chapter 8
BIBLIOGRAPHY

Margaret Hamilton

1. Jain R, Rivera MC, Lake JA (1999) Horizontal gene transfer among genomes: the complexity hypothesis. *Proc Natl Acad Sci USA* **96**: 3801–3806.
2. Gogarten JP, Townsend JP (2005) Horizontal gene transfer, genome innovation and evolution. *Nat Rev Microbiol* **3**: 679–687.
3. Frost LS, Leplae R, Summers AO, Toussaint A (2005) Mobile genetic elements: the agents of open source evolution. *Nat Rev Microbiol* **3**: 722–732.
4. Potera C (2013) Germ warfare? Strategies for reducing the spread of antibiotic resistance. *Environ Health Perspect* **121**: A255.
5. Thomas CM, Nielsen KM (2005) Mechanisms of, and barriers to, horizontal gene transfer between bacteria. *Nat Rev Microbiol* **3**: 711–721.
6. Davison J (1999) Genetic exchange between bacteria in the environment. *Plasmid* **42**: 73–91.
7. Furuya EY, Lowy FD (2006) Antimicrobial-resistant bacteria in the community setting. *Nat Rev Microbiol* **4**: 36–45.
8. Halary S, Leigh JW, Cheaib B, Lopez P, Bapteste E (2010) Network analyses structure genetic diversity in independent genetic worlds. *Proc Natl Acad Sci USA* **107**: 127–132.
9. Norman A, Hansen LH, Sørensen SJ (2009) Conjugative plasmids: vessels of the communal gene pool. *Philos Trans R Soc Lond, B, Biol Sci* **364**: 2275–2289.
10. Arber W (2014) Horizontal Gene Transfer among Bacteria and Its Role in Biological Evolution. *Life* **4**: 217–224.
11. Amábile-Cuevas CF, Chicurel ME (1992) Bacterial plasmids and gene flux. *Cell* **70**: 189–199.
12. Smillie C, Garcillán-Barcia MP, Francia MV, Rocha EPC, Cruz F de la (2010) Mobility of Plasmids. *Microbiol Mol Biol Rev* **74**: 434–452.
13. Ziebuhr W, Ohlsen K, Karch H, Korhonen T, Hacker J (1999) Evolution of bacterial pathogenesis. *Cell Mol Life Sci* **56**: 719–728.
14. Silver S, Phung LT (1996) Bacterial heavy metal resistance: new surprises. *Annu Rev Microbiol* **50**: 753–789.
15. Mazel D, Davies J (1999) Antibiotic resistance in microbes. *Cell Mol Life Sci* **56**: 742–754.
16. Clewell DB, Gawron-Burke C (1986) Conjugative transposons and the dissemination of antibiotic resistance in streptococci. *Annu Rev Microbiol* **40**: 635–659.
17. Waters VL (1999) Conjugative transfer in the dissemination of beta-lactam and aminoglycoside resistance. *Front Biosci* **4**: D433-456.
18. Guiney DG (1984) Promiscuous Transfer of Drug Resistance in Gram-Negative Bacteria. *J Infect Dis* **149**: 320–329.
19. Ryan FJ, Lederberg J (1946) Reverse-Mutation and Adaptation in Leucineless Neurospora. *Proc Natl Acad Sci USA* **32**: 163–173.
20. Lederberg J, Tatum EL (1946) Gene recombination in Escherichia coli. *Nature* **158**: 558.
21. Tatum EL, Lederberg J (1947) Gene Recombination in the Bacterium Escherichia coli. *J Bacteriol* **53**: 673–684.
22. Davis BD (1950) Nonfiltrability of the agents of genetic recombination in Escherichia coli. *J Bacteriol* **60**: 507–508.
23. Watson JD, Hayes W (1953) Genetic Exchange in Escherichia Coli K(12): Evidence for Three Linkage Groups. *Proc Natl Acad Sci USA* **39**: 416–426.
24. Datta N, Hedges RW (1971) Compatibility groups among fi - R factors. *Nature* **234**: 222–223.
25. Brinton CC (1971) The properties of sex pili, the viral nature of 'conjugal' genetic transfer systems, and some possible approaches to the control of bacterial drug resistance. *CRC Crit Rev Microbiol* **1**: 105–160.
26. Cruz F de la, Lanka E (1998) Function of the Ti-Plasmid Vir Proteins: T-Complex Formation and Transfer to the Plant Cell. In, *The Rhizobiaceae* pp 281–301. Springer, Dordrecht.

27. Heredity, The Horizontal Gene Pool — Bacterial Plasmids and Gene Spread, Last updated February 1, 2001, Accessed on February 1, 2001.
28. Cho N-H, Kim H-R, Lee J-H, Kim S-Y, Kim J, Cha S, Kim S-Y, Darby AC, Fuxelius H-H, Yin J, et al. (2007) The Orientia tsutsugamushi genome reveals massive proliferation of conjugative type IV secretion system and host-cell interaction genes. *Proc Natl Acad Sci USA* **104**: 7981–7986.
29. Heinemann JA, Sprague GF (1989) Bacterial conjugative plasmids mobilize DNA transfer between bacteria and yeast. *Nature* **340**: 205–209.
30. Buchanan-Wollaston V, Passiatore JE, Cannon F (1987) The mob and oriT mobilization functions of a bacterial plasmid promote its transfer to plants. *Nature* **328**: 172–175.
31. Ward JE, Akiyoshi DE, Regier D, Datta A, Gordon MP, Nester EW (1988) Characterization of the virB operon from an Agrobacterium tumefaciens Ti plasmid. *J Biol Chem* **263**: 5804–5814.
32. Waters VL (2001) Conjugation between bacterial and mammalian cells. *Nat Genet* **29**: 375–376.
33. Zupan J, Ward D, Zambryski P (2002) Inter-kingdom DNA transfer decoded. *Nat Biotechnol* **20**: 129–131.
34. Grohmann E, Muth G, Espinosa M (2003) Conjugative plasmid transfer in gram-positive bacteria. *Microbiol Mol Biol Rev* **67**: 277–301, table of contents.
35. Couturier M, Bex F, Bergquist PL, Maas WK (1988) Identification and classification of bacterial plasmids. *Microbiol Rev* **52**: 375–395.
36. Francia MV, Varsaki A, Garcillán-Barcia MP, Latorre A, Drainas C, de la Cruz F (2004) A classification scheme for mobilization regions of bacterial plasmids. *FEMS Microbiol Rev* **28**: 79–100.
37. Green ER, Mecsas J (2016) Bacterial Secretion Systems – An overview. *Microbiol Spectr* **4**:.
38. Chagnot C, Zorgani MA, Astruc T, Desvaux M (2013) Proteinaceous determinants of surface colonization in bacteria: bacterial adhesion and biofilm formation from a protein secretion perspective. *Front Microbiol* **4**:.
39. Bleves S, Viarre V, Salacha R, Michel GPF, Filloux A, Voulhoux R (2010) Protein secretion systems in Pseudomonas aeruginosa: A wealth of pathogenic weapons. *Int J Med Microbiol* **300**: 534–543.
40. Michel GPF, Aguzzi A, Ball G, Soscia C, Bleves S, Voulhoux R (2011) Role of fimV in type II secretion system-dependent protein secretion of Pseudomonas aeruginosa on solid medium. *Microbiology (Reading, Engl)* **157**: 1945–1954.
41. Fisher AC, DeLisa MP (2004) A little help from my friends: quality control of presecretory proteins in bacteria. *J Bacteriol* **186**: 7467–7473.
42. Bendtsen JD, Kiemer L, Fausbøll A, Brunak S (2005) Non-classical protein secretion in bacteria. *BMC Microbiol* **5**: 58.
43. Bocian-Ostrzycka KM, Grzeszczuk MJ, Banaś AM, Jagusztyn-Krynicka EK (2017) Bacterial thiol oxidoreductases — from basic research to new antibacterial strategies. *Appl Microbiol Biotechnol* **101**: 3977–3989.
44. Tseng T-T, Tyler BM, Setubal JC (2009) Protein secretion systems in bacterial-host associations, and their description in the Gene Ontology. *BMC Microbiol* **9 Suppl 1**: S2.
45. Thomas CM (2003) *Horizontal Gene Pool: Bacterial Plasmids and Gene Spread*. CRC Press.
46. Llosa M, de la Cruz F (2005) Bacterial conjugation: a potential tool for genomic engineering. *Res Microbiol* **156**: 1–6.
47. Cascales E, Christie PJ (2003) The versatile bacterial type IV secretion systems. *Nat Rev Microbiol* **1**: 137–149.
48. Christie PJ (2004) Type IV secretion: the Agrobacterium VirB/D4 and related conjugation systems. *Biochim Biophys Acta* **1694**: 219–234.

49. Draper O, César CE, Machón C, de la Cruz F, Llosa M (2005) Site-specific recombinase and integrase activities of a conjugative relaxase in recipient cells. *Proc Natl Acad Sci USA* **102**: 16385–16390.
50. Llosa M, Gomis-Rüth FX, Coll M, de la Cruz Fd F (2002) Bacterial conjugation: a two-step mechanism for DNA transport. *Mol Microbiol* **45**: 1–8.
51. Waters VL, Guiney DG (1993) Processes at the nick region link conjugation, T-DNA transfer and rolling circle replication. *Mol Microbiol* **9**: 1123–1130.
52. Cabezón E, Ripoll-Rozada J, Peña A, de la Cruz F, Arechaga I (2015) Towards an integrated model of bacterial conjugation. *FEMS Microbiol Rev* **39**: 81–95.
53. Datta N, Hedges RW (1972) Trimethoprim resistance conferred by W plasmids in Enterobacteriaceae. *J Gen Microbiol* **72**: 349–355.
54. Ward JM, Grinsted J (1982) Physical and genetic analysis of the Inc-W group plasmids R388, Sa, and R7K. *Plasmid* **7**: 239–250.
55. Bradley DE, Cohen DR (1976) Basic characterization of W-pili. *J Gen Microbiol* **97**: 91–103.
56. Loper JE, Kado CI (1979) Host range conferred by the virulence-specifying plasmid of Agrobacterium tumefaciens. *J Bacteriol* **139**: 591–596.
57. Bradley DE (1980) Morphological and serological relationships of conjugative pili. *Plasmid* **4**: 155–169.
58. Olsen RH, Siak JS, Gray RH (1974) Characteristics of PRD1, a plasmid-dependent broad host range DNA bacteriophage. *J Virol* **14**: 689–699.
59. Fernández-López R, Garcillán-Barcia MP, Revilla C, Lázaro M, Vielva L, de la Cruz F (2006) Dynamics of the IncW genetic backbone imply general trends in conjugative plasmid evolution. *FEMS Microbiol Rev* **30**: 942–966.
60. Bolland S, Llosa M, Avila P, de la Cruz F (1990) General organization of the conjugal transfer genes of the IncW plasmid R388 and interactions between R388 and IncN and IncP plasmids. *J Bacteriol* **172**: 5795–5802.
61. Llosa M, Bolland S, de la Cruz F (1994) Genetic organization of the conjugal DNA processing region of the IncW plasmid R388. *J Mol Biol* **235**: 448–464.
62. Ilangovan A, Connery S, Waksman G (2015) Structural biology of the Gram-negative bacterial conjugation systems. *Trends in Microbiology* **23**: 301–310.
63. Moncalián G, Grandoso G, Llosa M, de la Cruz F (1997) OriT-processing and regulatory roles of TrwA protein in ploasmid R388 conjugation11Edited by J. Karn. *Journal of Molecular Biology* **270**: 188–200.
64. Rice PA, Yang S, Mizuuchi K, Nash HA (1996) Crystal structure of an IHF-DNA complex: a protein-induced DNA U-turn. *Cell* **87**: 1295–1306.
65. Moncalián G, Valle M, Valpuesta JM, de la Cruz F (1999) IHF protein inhibits cleavage but not assembly of plasmid R388 relaxosomes. *Mol Microbiol* **31**: 1643–1652.
66. César CE, Machón C, de la Cruz F, Llosa M (2006) A new domain of conjugative relaxase TrwC responsible for efficient oriT-specific recombination on minimal target sequences. *Mol Microbiol* **62**: 984–996.
67. Llosa M, Bolland S, de la Cruz F (1991) Structural and functional analysis of the origin of conjugal transfer of the broad-host-range IncW plasmid R388 and comparison with the related IncN plasmid R46. *Mol Gen Genet* **226**: 473–483.
68. Guasch A, Lucas M, Moncalián G, Cabezas M, Pérez-Luque R, Gomis-Rüth FX, de la Cruz F, Coll M (2003) Recognition and processing of the origin of transfer DNA by conjugative relaxase TrwC. *Nat Struct Biol* **10**: 1002–1010.
69. Llosa M, Grandoso G, de la Cruz F (1995) Nicking activity of TrwC directed against the origin of transfer of the IncW plasmid R388. *J Mol Biol* **246**: 54–62.

70. Craig NL, Nash HA (1984) E. coli integration host factor binds to specific sites in DNA. *Cell* **39**: 707–716.
71. Lucas M, González-Pérez B, Cabezas M, Moncalian G, Rivas G, de la Cruz F (2010) Relaxase DNA binding and cleavage are two distinguishable steps in conjugative DNA processing that involve different sequence elements of the nic site. *J Biol Chem* **285**: 8918–8926.
72. Moncalián G, de la Cruz F (2004) DNA binding properties of protein TrwA, a possible structural variant of the Arc repressor superfamily. *Biochim Biophys Acta* **1701**: 15–23.
73. Breg JN, van Opheusden JH, Burgering MJ, Boelens R, Kaptein R (1990) Structure of Arc repressor in solution: evidence for a family of beta-sheet DNA-binding proteins. *Nature* **346**: 586–589.
74. Tato I, Matilla I, Arechaga I, Zunzunegui S, de la Cruz F, Cabezon E (2007) The ATPase activity of the DNA transporter TrwB is modulated by protein TrwA: implications for a common assembly mechanism of DNA translocating motors. *J Biol Chem* **282**: 25569–25576.
75. Bowie JU, Sauer RT (1990) TraY proteins of F and related episomes are members of the Arc and Mnt repressor family. *J Mol Biol* **211**: 5–6.
76. Nelson WC, Howard MT, Sherman JA, Matson SW (1995) The traY gene product and integration host factor stimulate Escherichia coli DNA helicase I-catalyzed nicking at the F plasmid oriT. *J Biol Chem* **270**: 28374–28380.
77. Silverman PM, Sholl A (1996) Effect of traY amber mutations on F-plasmid traY promoter activity in vivo. *J Bacteriol* **178**: 5787–5789.
78. Garcillán-Barcia MP, Francia MV, de la Cruz F (2009) The diversity of conjugative relaxases and its application in plasmid classification. *FEMS Microbiol Rev* **33**: 657–687.
79. Grandoso G, Llosa M, Zabala JC, de la Cruz F (1994) Purification and biochemical characterization of TrwC, the helicase involved in plasmid R388 conjugal DNA transfer. *Eur J Biochem* **226**: 403–412.
80. Llosa M, Grandoso G, Hernando MA, de la Cruz F (1996) Functional domains in protein TrwC of plasmid R388: dissected DNA strand transferase and DNA helicase activities reconstitute protein function. *J Mol Biol* **264**: 56–67.
81. Grandoso G, Avila P, Cayón A, Hernando MA, Llosa M, de la Cruz F (2000) Two active-site tyrosyl residues of protein TrwC act sequentially at the origin of transfer during plasmid R388 conjugation. *J Mol Biol* **295**: 1163–1172.
82. César CE, Llosa M (2007) TrwC-mediated site-specific recombination is controlled by host factors altering local DNA topology. *J Bacteriol* **189**: 9037–9043.
83. Garcillán-Barcia MP, Jurado P, González-Pérez B, Moncalián G, Fernández LA, de la Cruz F (2007) Conjugative transfer can be inhibited by blocking relaxase activity within recipient cells with intrabodies. *Mol Microbiol* **63**: 404–416.
84. Agúndez L, González-Prieto C, Machón C, Llosa M (2012) Site-specific integration of foreign DNA into minimal bacterial and human target sequences mediated by a conjugative relaxase. *PLoS ONE* **7**: e31047.
85. Agúndez L, Machón C, César CE, Rosa-Garrido M, Delgado MD, Llosa M (2011) Nuclear targeting of a bacterial integrase that mediates site-specific recombination between bacterial and human target sequences. *Appl Environ Microbiol* **77**: 201–210.
86. Wallden K, Rivera-Calzada A, Waksman G (2010) Type IV secretion systems: versatility and diversity in function. *Cell Microbiol* **12**: 1203–1212.
87. Christie PJ, Cascales E (2005) Structural and dynamic properties of bacterial type IV secretion systems (review). *Mol Membr Biol* **22**: 51–61.
88. de Paz HD, Sangari FJ, Bolland S, García-Lobo JM, Dehio C, de la Cruz F, Llosa M (2005) Functional interactions between type IV secretion systems involved in DNA transfer and virulence. *Microbiology (Reading, Engl)* **151**: 3505–3516.

89. Kado CI (1994) Promiscuous DNA transfer system of Agrobacterium tumefaciens: role of the virB operon in sex pilus assembly and synthesis. *Molecular Microbiology* **12**: 17–22.
90. de Paz HD, Larrea D, Zunzunegui S, Dehio C, de la Cruz F, Llosa M (2010) Functional dissection of the conjugative coupling protein TrwB. *J Bacteriol* **192**: 2655–2669.
91. Llosa M, Zunzunegui S, de la Cruz F (2003) Conjugative coupling proteins interact with cognate and heterologous VirB10-like proteins while exhibiting specificity for cognate relaxosomes. *Proc Natl Acad Sci USA* **100**: 10465–10470.
92. Christie PJ, Valero LG, Buchrieser C (2017) Biological Diversity and Evolution of Type IV Secretion Systems. *Curr Top Microbiol Immunol* **413**: 1–30.
93. Frank AC, Alsmark CM, Thollesson M, Andersson SGE (2005) Functional divergence and horizontal transfer of type IV secretion systems. *Mol Biol Evol* **22**: 1325–1336.
94. Goodner B, Hinkle G, Gattung S, Miller N, Blanchard M, Qurollo B, Goldman BS, Cao Y, Askenazi M, Halling C, et al. (2001) Genome sequence of the plant pathogen and biotechnology agent Agrobacterium tumefaciens C58. *Science* **294**: 2323–2328.
95. Chen L, Chen Y, Wood DW, Nester EW (2002) A new type IV secretion system promotes conjugal transfer in Agrobacterium tumefaciens. *J Bacteriol* **184**: 4838–4845.
96. Broothaerts W, Mitchell HJ, Weir B, Kaines S, Smith LMA, Yang W, Mayer JE, Roa-Rodríguez C, Jefferson RA (2005) Gene transfer to plants by diverse species of bacteria. *Nature* **433**: 629–633.
97. Schröder G, Dehio C (2005) Virulence-associated type IV secretion systems of Bartonella. *Trends Microbiol* **13**: 336–342.
98. Alvarez-Martinez CE, Christie PJ (2009) Biological diversity of prokaryotic type IV secretion systems. *Microbiol Mol Biol Rev* **73**: 775–808.
99. Christie PJ (2016) The Mosaic Type IV Secretion Systems. *EcoSal Plus* **7**:.
100. Kumar N, Shariq M, Kumar A, Kumari R, Subbarao N, Tyagi RK, Mukhopadhyay G (2017) Analyzing the role of CagV, a VirB8 homolog of the type IV secretion system of Helicobacter pylori. *FEBS Open Bio* **7**: 915–933.
101. Christie PJ (2017) Structural biology: Loading T4SS substrates. *Nat Microbiol* **2**: 17125.
102. Merino E, Flores-Encarnación M, Aguilar-Gutiérrez GR (2017) Functional interaction and structural characteristics of unique components of Helicobacter pylori T4SS. *FEBS J* **284**: 3540–3549.
103. Backert S, Meyer TF (2006) Type IV secretion systems and their effectors in bacterial pathogenesis. *Curr Opin Microbiol* **9**: 207–217.
104. Bundock P, den Dulk-Ras A, Beijersbergen A, Hooykaas PJ (1995) Trans-kingdom T-DNA transfer from Agrobacterium tumefaciens to Saccharomyces cerevisiae. *EMBO J* **14**: 3206–3214.
105. Zupan J, Muth TR, Draper O, Zambryski P (2000) The transfer of DNA from agrobacterium tumefaciens into plants: a feast of fundamental insights. *Plant J* **23**: 11–28.
106. Christie PJ, Atmakuri K, Krishnamoorthy V, Jakubowski S, Cascales E (2005) Biogenesis, architecture, and function of bacterial type IV secretion systems. *Annu Rev Microbiol* **59**: 451–485.
107. Vincent CD, Friedman JR, Jeong KC, Buford EC, Miller JL, Vogel JP (2006) Identification of the core transmembrane complex of the Legionella Dot/Icm type IV secretion system. *Mol Microbiol* **62**: 1278–1291.
108. Voth DE, Howe D, Beare PA, Vogel JP, Unsworth N, Samuel JE, Heinzen RA (2009) The Coxiella burnetii ankyrin repeat domain-containing protein family is heterogeneous, with C-terminal truncations that influence Dot/Icm-mediated secretion. *J Bacteriol* **191**: 4232–4242.
109. Komano T, Yoshida T, Narahara K, Furuya N (2000) The transfer region of IncI1 plasmid R64: similarities between R64 tra and legionella icm/dot genes. *Mol Microbiol* **35**: 1348–1359.
110. Grohmann E, Christie PJ, Waksman G, Backert S (2018) Type IV secretion in Gram-negative and Gram-positive bacteria. *Mol Microbiol* **107**: 455–471.

111. Low HH, Gubellini F, Rivera-Calzada A, Braun N, Connery S, Dujeancourt A, Lu F, Redzej A, Fronzes R, Orlova EV, et al. (2014) Structure of a type IV secretion system. *Nature* **508**: 550–553.
112. Karnholz A, Hoefler C, Odenbreit S, Fischer W, Hofreuter D, Haas R (2006) Functional and topological characterization of novel components of the comB DNA transformation competence system in Helicobacter pylori. *J Bacteriol* **188**: 882–893.
113. Beijersbergen A, Smith SJ, Hooykaas PJ (1994) Localization and topology of VirB proteins of Agrobacterium tumefaciens. *Plasmid* **32**: 212–218.
114. Grahn AM, Haase J, Bamford DH, Lanka E (2000) Components of the RP4 conjugative transfer apparatus form an envelope structure bridging inner and outer membranes of donor cells: implications for related macromolecule transport systems. *J Bacteriol* **182**: 1564–1574.
115. Lawley TD, Klimke WA, Gubbins MJ, Frost LS (2003) F factor conjugation is a true type IV secretion system. *FEMS Microbiol Lett* **224**: 1–15.
116. Batchelor RA, Pearson BM, Friis LM, Guerry P, Wells JM (2004) Nucleotide sequences and comparison of two large conjugative plasmids from different Campylobacter species. *Microbiology (Reading, Engl)* **150**: 3507–3517.
117. Cao TB, Saier MH (2001) Conjugal type IV macromolecular transfer systems of Gram-negative bacteria: organismal distribution, structural constraints and evolutionary conclusions. *Microbiology (Reading, Engl)* **147**: 3201–3214.
118. Judd PK, Kumar RB, Das A (2005) The type IV secretion apparatus protein VirB6 of Agrobacterium tumefaciens localizes to a cell pole. *Mol Microbiol* **55**: 115–124.
119. Jakubowski SJ, Krishnamoorthy V, Cascales E, Christie PJ (2004) Agrobacterium tumefaciens VirB6 domains direct the ordered export of a DNA substrate through a type IV secretion System. *J Mol Biol* **341**: 961–977.
120. Draskovic I, Dubnau D (2005) Biogenesis of a putative channel protein, ComEC, required for DNA uptake: membrane topology, oligomerization and formation of disulphide bonds. *Mol Microbiol* **55**: 881–896.
121. Berger BR, Christie PJ (1994) Genetic complementation analysis of the Agrobacterium tumefaciens virB operon: virB2 through virB11 are essential virulence genes. *J Bacteriol* **176**: 3646–3660.
122. Hapfelmeier S, Domke N, Zambryski PC, Baron C (2000) VirB6 is required for stabilization of VirB5 and VirB3 and formation of VirB7 homodimers in Agrobacterium tumefaciens. *J Bacteriol* **182**: 4505–4511.
123. Jakubowski SJ, Krishnamoorthy V, Christie PJ (2003) Agrobacterium tumefaciens VirB6 protein participates in formation of VirB7 and VirB9 complexes required for type IV secretion. *J Bacteriol* **185**: 2867–2878.
124. Judd PK, Mahli D, Das A (2005) Molecular characterization of the Agrobacterium tumefaciens DNA transfer protein VirB6. *Microbiology (Reading, Engl)* **151**: 3483–3492.
125. Baron C (2006) VirB8: a conserved type IV secretion system assembly factor and drug target. *Biochem Cell Biol* **84**: 890–899.
126. Das A, Xie YH (2000) The Agrobacterium T-DNA transport pore proteins VirB8, VirB9, and VirB10 interact with one another. *J Bacteriol* **182**: 758–763.
127. Kumar RB, Xie YH, Das A (2000) Subcellular localization of the Agrobacterium tumefaciens T-DNA transport pore proteins: VirB8 is essential for the assembly of the transport pore. *Mol Microbiol* **36**: 608–617.
128. Yuan Q, Carle A, Gao C, Sivanesan D, Aly KA, Höppner C, Krall L, Domke N, Baron C (2005) Identification of the VirB4-VirB8-VirB5-VirB2 pilus assembly sequence of type IV secretion systems. *J Biol Chem* **280**: 26349–26359.

129. Patey G, Qi Z, Bourg G, Baron C, O'Callaghan D (2006) Swapping of periplasmic domains between Brucella suis VirB8 and a pSB102 VirB8 homologue allows heterologous complementation. *Infect Immun* **74**: 4945–4949.
130. Sharifahmadian M, Nlend IU, Lecoq L, Omichinski JG, Baron C (2017) The type IV secretion system core component VirB8 interacts via the β1-strand with VirB10. *FEBS Lett* **591**: 2491–2500.
131. Cascales E, Christie PJ (2004) Definition of a bacterial type IV secretion pathway for a DNA substrate. *Science* **304**: 1170–1173.
132. Paschos A, Patey G, Sivanesan D, Gao C, Bayliss R, Waksman G, O'callaghan D, Baron C (2006) Dimerization and interactions of Brucella suis VirB8 with VirB4 and VirB10 are required for its biological activity. *Proc Natl Acad Sci USA* **103**: 7252–7257.
133. Terradot L, Bayliss R, Oomen C, Leonard GA, Baron C, Waksman G (2005) Structures of two core subunits of the bacterial type IV secretion system, VirB8 from Brucella suis and ComB10 from Helicobacter pylori. *Proc Natl Acad Sci USA* **102**: 4596–4601.
134. Fronzes R, Schäfer E, Wang L, Saibil HR, Orlova EV, Waksman G (2009) Structure of a type IV secretion system core complex. *Science* **323**: 266–268.
135. Baron C, Thorstenson YR, Zambryski PC (1997) The lipoprotein VirB7 interacts with VirB9 in the membranes of Agrobacterium tumefaciens. *J Bacteriol* **179**: 1211–1218.
136. Anderson LB, Hertzel AV, Das A (1996) Agrobacterium tumefaciens VirB7 and VirB9 form a disulfide-linked protein complex. *Proc Natl Acad Sci USA* **93**: 8889–8894.
137. Das A, Anderson LB, Xie YH (1997) Delineation of the interaction domains of Agrobacterium tumefaciens VirB7 and VirB9 by use of the yeast two-hybrid assay. *J Bacteriol* **179**: 3404–3409.
138. Jakubowski SJ, Cascales E, Krishnamoorthy V, Christie PJ (2005) Agrobacterium tumefaciens VirB9, an outer-membrane-associated component of a type IV secretion system, regulates substrate selection and T-pilus biogenesis. *J Bacteriol* **187**: 3486–3495.
139. Stahl LE, Jacobs A, Binns AN (1998) The conjugal intermediate of plasmid RSF1010 inhibits Agrobacterium tumefaciens virulence and VirB-dependent export of VirE2. *J Bacteriol* **180**: 3933–3939.
140. Cascales E, Christie PJ (2004) Agrobacterium VirB10, an ATP energy sensor required for type IV secretion. *Proc Natl Acad Sci USA* **101**: 17228–17233.
141. Ward DV, Draper O, Zupan JR, Zambryski PC (2002) Peptide linkage mapping of the Agrobacterium tumefaciens vir-encoded type IV secretion system reveals protein subassemblies. *Proc Natl Acad Sci USA* **99**: 11493–11500.
142. Jakubowski SJ, Kerr JE, Garza I, Krishnamoorthy V, Bayliss R, Waksman G, Christie PJ (2009) Agrobacterium VirB10 domain requirements for type IV secretion and T pilus biogenesis. *Mol Microbiol* **71**: 779–794.
143. Chandran V, Fronzes R, Duquerroy S, Cronin N, Navaza J, Waksman G (2009) Structure of the outer membrane complex of a type IV secretion system. *Nature* **462**: 1011–1015.
144. Koraimann G (2003) Lytic transglycosylases in macromolecular transport systems of Gram-negative bacteria. *Cell Mol Life Sci* **60**: 2371–2388.
145. Mushegian AR, Fullner KJ, Koonin EV, Nester EW (1996) A family of lysozyme-like virulence factors in bacterial pathogens of plants and animals. *Proc Natl Acad Sci USA* **93**: 7321–7326.
146. Bayer M, Iberer R, Bischof K, Rassi E, Stabentheiner E, Zellnig G, Koraimann G (2001) Functional and mutational analysis of p19, a DNA transfer protein with muramidase activity. *J Bacteriol* **183**: 3176–3183.
147. Baron C, Llosa M, Zhou S, Zambryski PC (1997) VirB1, a component of the T-complex transfer machinery of Agrobacterium tumefaciens, is processed to a C-terminal secreted product, VirB1. *J Bacteriol* **179**: 1203–1210.

148. den Hartigh AB, Sun Y-H, Sondervan D, Heuvelmans N, Reinders MO, Ficht TA, Tsolis RM (2004) Differential requirements for VirB1 and VirB2 during Brucella abortus infection. *Infect Immun* **72**: 5143–5149.
149. Höppner C, Liu Z, Domke N, Binns AN, Baron C (2004) VirB1 orthologs from Brucella suis and pKM101 complement defects of the lytic transglycosylase required for efficient type IV secretion from Agrobacterium tumefaciens. *J Bacteriol* **186**: 1415–1422.
150. Zahrl D, Wagner M, Bischof K, Bayer M, Zavecz B, Beranek A, Ruckenstuhl C, Zarfel GE, Koraimann G (2005) Peptidoglycan degradation by specialized lytic transglycosylases associated with type III and type IV secretion systems. *Microbiology (Reading, Engl)* **151**: 3455–3467.
151. Lai EM, Kado CI (1998) Processed VirB2 is the major subunit of the promiscuous pilus of Agrobacterium tumefaciens. *J Bacteriol* **180**: 2711–2717.
152. Eisenbrandt R, Kalkum M, Lai EM, Lurz R, Kado CI, Lanka E (1999) Conjugative pili of IncP plasmids, and the Ti plasmid T pilus are composed of cyclic subunits. *J Biol Chem* **274**: 22548–22555.
153. Haase J, Lurz R, Grahn AM, Bamford DH, Lanka E (1995) Bacterial conjugation mediated by plasmid RP4: RSF1010 mobilization, donor-specific phage propagation, and pilus production require the same Tra2 core components of a proposed DNA transport complex. *J Bacteriol* **177**: 4779–4791.
154. Kalkum M, Eisenbrandt R, Lanka E (2004) Protein circlets as sex pilus subunits. *Curr Protein Pept Sci* **5**: 417–424.
155. Maher D, Sherburne R, Taylor DE (1993) H-pilus assembly kinetics determined by electron microscopy. *J Bacteriol* **175**: 2175–2183.
156. Costa TRD, Ilangovan A, Ukleja M, Redzej A, Santini JM, Smith TK, Egelman EH, Waksman G (2016) Structure of the Bacterial Sex F Pilus Reveals an Assembly of a Stoichiometric Protein-Phospholipid Complex. *Cell* **166**: 1436-1444.e10.
157. Hospenthal MK, Costa TRD, Waksman G (2017) A comprehensive guide to pilus biogenesis in Gram-negative bacteria. *Nat Rev Microbiol* **15**: 365–379.
158. Hwang H-H, Gelvin SB (2004) Plant proteins that interact with VirB2, the Agrobacterium tumefaciens pilin protein, mediate plant transformation. *Plant Cell* **16**: 3148–3167.
159. Llosa M, Roy C, Dehio C (2009) Bacterial type IV secretion systems in human disease. *Mol Microbiol* **73**: 141–151.
160. Schmidt-Eisenlohr H, Domke N, Angerer C, Wanner G, Zambryski PC, Baron C (1999) Vir proteins stabilize VirB5 and mediate its association with the T pilus of Agrobacterium tumefaciens. *J Bacteriol* **181**: 7485–7492.
161. Schmidt-Eisenlohr H, Domke N, Baron C (1999) TraC of IncN plasmid pKM101 associates with membranes and extracellular high-molecular-weight structures in Escherichia coli. *J Bacteriol* **181**: 5563–5571.
162. Aly KA, Baron C (2007) The VirB5 protein localizes to the T-pilus tips in Agrobacterium tumefaciens. *Microbiology (Reading, Engl)* **153**: 3766–3775.
163. Yeo H-J, Yuan Q, Beck MR, Baron C, Waksman G (2003) Structural and functional characterization of the VirB5 protein from the type IV secretion system encoded by the conjugative plasmid pKM101. *Proc Natl Acad Sci USA* **100**: 15947–15952.
164. Dehio C (2004) Molecular and cellular basis of bartonella pathogenesis. *Annu Rev Microbiol* **58**: 365–390.
165. Padmalayam I, Karem K, Baumstark B, Massung R (2000) The gene encoding the 17-kDa antigen of Bartonella henselae is located within a cluster of genes homologous to the virB virulence operon. *DNA Cell Biol* **19**: 377–382.
166. Moré MI, Pohlman RF, Winans SC (1996) Genes encoding the pKM101 conjugal mating pore are negatively regulated by the plasmid-encoded KorA and KorB proteins. *J Bacteriol* **178**: 4392–4399.

167. Backert S, Selbach M (2008) Role of type IV secretion in Helicobacter pylori pathogenesis. *Cell Microbiol* **10**: 1573–1581.
168. Cabezón E, Sastre JI, de la Cruz F (1997) Genetic evidence of a coupling role for the TraG protein family in bacterial conjugation. *Mol Gen Genet* **254**: 400–406.
169. Scheiffele P, Pansegrau W, Lanka E (1995) Initiation of Agrobacterium tumefaciens T-DNA processing. Purified proteins VirD1 and VirD2 catalyze site- and strand-specific cleavage of superhelical T-border DNA in vitro. *J Biol Chem* **270**: 1269–1276.
170. Tinland B, Schoumacher F, Gloeckler V, Bravo-Angel AM, Hohn B (1995) The Agrobacterium tumefaciens virulence D2 protein is responsible for precise integration of T-DNA into the plant genome. *EMBO J* **14**: 3585–3595.
171. Lai EM, Kado CI (2000) The T-pilus of Agrobacterium tumefaciens. *Trends Microbiol* **8**: 361–369.
172. Lai EM, Chesnokova O, Banta LM, Kado CI (2000) Genetic and environmental factors affecting T-pilin export and T-pilus biogenesis in relation to flagellation of Agrobacterium tumefaciens. *J Bacteriol* **182**: 3705–3716.
173. Tato I, Zunzunegui S, de la Cruz F, Cabezon E (2005) TrwB, the coupling protein involved in DNA transport during bacterial conjugation, is a DNA-dependent ATPase. *Proc Natl Acad Sci USA* **102**: 8156–8161.
174. Cabezón E, Lanka E, de la Cruz F (1994) Requirements for mobilization of plasmids RSF1010 and ColE1 by the IncW plasmid R388: trwB and RP4 traG are interchangeable. *J Bacteriol* **176**: 4455–4458.
175. Gomis-Rüth FX, Moncalián G, Pérez-Luque R, González A, Cabezón E, de la Cruz F, Coll M (2001) The bacterial conjugation protein TrwB resembles ring helicases and F1-ATPase. *Nature* **409**: 637–641.
176. Gomis-Rüth FX, Moncalían G, de la Cruz F, Coll M (2002) Conjugative plasmid protein TrwB, an integral membrane type IV secretion system coupling protein. Detailed structural features and mapping of the active site cleft. *J Biol Chem* **277**: 7556–7566.
177. Hormaeche I, Iloro I, Arrondo JLR, Goñi FM, de la Cruz F, Alkorta I (2004) Role of the transmembrane domain in the stability of TrwB, an integral protein involved in bacterial conjugation. *J Biol Chem* **279**: 10955–10961.
178. Vecino AJ, de la Arada I, Segura RL, Goñi FM, de la Cruz F, Arrondo JLR, Alkorta I (2011) Membrane insertion stabilizes the structure of TrwB, the R388 conjugative plasmid coupling protein. *Biochim Biophys Acta* **1808**: 1032–1039.
179. Hormaeche I, Alkorta I, Moro F, Valpuesta JM, Goni FM, De La Cruz F (2002) Purification and properties of TrwB, a hexameric, ATP-binding integral membrane protein essential for R388 plasmid conjugation. *J Biol Chem* **277**: 46456–46462.
180. Vecino AJ, Segura RL, Ugarte-Uribe B, Aguila S, Hormaeche I, de la Cruz F, Goñi FM, Alkorta I (2010) Reconstitution in liposome bilayers enhances nucleotide binding affinity and ATP-specificity of TrwB conjugative coupling protein. *Biochim Biophys Acta* **1798**: 2160–2169.
181. Hormaeche I, Segura RL, Vecino AJ, Goñi FM, de la Cruz F, Alkorta I (2006) The transmembrane domain provides nucleotide binding specificity to the bacterial conjugation protein TrwB. *FEBS Lett* **580**: 3075–3082.
182. Moncalián G, Cabezón E, Alkorta I, Valle M, Moro F, Valpuesta JM, Goñi FM, de La Cruz F (1999) Characterization of ATP and DNA binding activities of TrwB, the coupling protein essential in plasmid R388 conjugation. *J Biol Chem* **274**: 36117–36124.
183. Larrea D, de Paz HD, Matilla I, Guzmán-Herrador DL, Lasso G, de la Cruz F, Cabezón E, Llosa M (2017) Substrate translocation involves specific lysine residues of the central channel of the conjugative coupling protein TrwB. *Mol Genet Genomics* **292**: 1037–1049.

184. Beranek A, Zettl M, Lorenzoni K, Schauer A, Manhart M, Koraimann G (2004) Thirty-eight C-terminal amino acids of the coupling protein TraD of the F-like conjugative resistance plasmid R1 are required and sufficient to confer binding to the substrate selector protein TraM. *J Bacteriol* **186**: 6999–7006.
185. Sastre JI, Cabezón E, de la Cruz F (1998) The carboxyl terminus of protein TraD adds specificity and efficiency to F-plasmid conjugative transfer. *J Bacteriol* **180**: 6039–6042.
186. Haft RJF, Gachelet EG, Nguyen T, Toussaint L, Chivian D, Traxler B (2007) In vivo oligomerization of the F conjugative coupling protein TraD. *J Bacteriol* **189**: 6626–6634.
187. Chen Y, Zhang X, Manias D, Yeo H-J, Dunny GM, Christie PJ (2008) Enterococcus faecalis PcfC, a spatially localized substrate receptor for type IV secretion of the pCF10 transfer intermediate. *J Bacteriol* **190**: 3632–3645.
188. Gunton JE, Gilmour MW, Alonso G, Taylor DE (2005) Subcellular localization and functional domains of the coupling protein, TraG, from IncHI1 plasmid R27. *Microbiology (Reading, Engl)* **151**: 3549–3561.
189. Atmakuri K, Ding Z, Christie PJ (2003) VirE2, a type IV secretion substrate, interacts with the VirD4 transfer protein at cell poles of Agrobacterium tumefaciens. *Mol Microbiol* **49**: 1699–1713.
190. Kumar RB, Das A (2002) Polar location and functional domains of the Agrobacterium tumefaciens DNA transfer protein VirD4. *Mol Microbiol* **43**: 1523–1532.
191. Schröder G, Lanka E (2003) TraG-like proteins of type IV secretion systems: functional dissection of the multiple activities of TraG (RP4) and TrwB (R388). *J Bacteriol* **185**: 4371–4381.
192. Gomis-Rüth FX, Coll M (2001) Structure of TrwB, a gatekeeper in bacterial conjugation. *Int J Biochem Cell Biol* **33**: 839–843.
193. Sharp MD, Pogliano K (2002) MinCD-dependent regulation of the polarity of SpoIIIE assembly and DNA transfer. *EMBO J* **21**: 6267–6274.
194. Bath J, Wu LJ, Errington J, Wang JC (2000) Role of Bacillus subtilis SpoIIIE in DNA transport across the mother cell-prespore division septum. *Science* **290**: 995–997.
195. Errington J, Bath J, Wu LJ (2001) DNA transport in bacteria. *Nat Rev Mol Cell Biol* **2**: 538–545.
196. Recchia GD, Aroyo M, Wolf D, Blakely G, Sherratt DJ (1999) FtsK-dependent and -independent pathways of Xer site-specific recombination. *EMBO J* **18**: 5724–5734.
197. Ye J, Osborne AR, Groll M, Rapoport TA (2004) RecA-like motor ATPases—lessons from structures. *Biochimica et Biophysica Acta (BBA) - Bioenergetics* **1659**: 1–18.
198. Cabezon E, de la Cruz F (2006) TrwB: an F(1)-ATPase-like molecular motor involved in DNA transport during bacterial conjugation. *Res Microbiol* **157**: 299–305.
199. Boyer PD (1993) The binding change mechanism for ATP synthase--some probabilities and possibilities. *Biochim Biophys Acta* **1140**: 215–250.
200. Matilla I, Alfonso C, Rivas G, Bolt EL, de la Cruz F, Cabezon E (2010) The conjugative DNA translocase TrwB is a structure-specific DNA-binding protein. *J Biol Chem* **285**: 17537–17544.
201. Middleton R, Sjölander K, Krishnamurthy N, Foley J, Zambryski P (2005) Predicted hexameric structure of the Agrobacterium VirB4 C terminus suggests VirB4 acts as a docking site during type IV secretion. *Proc Natl Acad Sci USA* **102**: 1685–1690.
202. Rabel C, Grahn AM, Lurz R, Lanka E (2003) The VirB4 family of proposed traffic nucleoside triphosphatases: common motifs in plasmid RP4 TrbE are essential for conjugation and phage adsorption. *J Bacteriol* **185**: 1045–1058.
203. Dang TA, Christie PJ (1997) The VirB4 ATPase of Agrobacterium tumefaciens is a cytoplasmic membrane protein exposed at the periplasmic surface. *J Bacteriol* **179**: 453–462.
204. Gilmour MW, Lawley TD, Rooker MM, Newnham PJ, Taylor DE (2001) Cellular location and temperature-dependent assembly of IncHI1 plasmid R27-encoded TrhC-associated conjugative transfer protein complexes. *Mol Microbiol* **42**: 705–715.

205. Schandel KA, Muller MM, Webster RE (1992) Localization of TraC, a protein involved in assembly of the F conjugative pilus. *J Bacteriol* **174**: 3800–3806.
206. Arechaga I, Peña A, Zunzunegui S, del Carmen Fernández-Alonso M, Rivas G, de la Cruz F (2008) ATPase activity and oligomeric state of TrwK, the VirB4 homologue of the plasmid R388 type IV secretion system. *J Bacteriol* **190**: 5472–5479.
207. Berger BR, Christie PJ (1993) The Agrobacterium tumefaciens virB4 gene product is an essential virulence protein requiring an intact nucleoside triphosphate-binding domain. *J Bacteriol* **175**: 1723–1734.
208. Peña A, Ripoll-Rozada J, Zunzunegui S, Cabezón E, de la Cruz F, Arechaga I (2011) Autoinhibitory regulation of TrwK, an essential VirB4 ATPase in type IV secretion systems. *J Biol Chem* **286**: 17376–17382.
209. Peña A, Matilla I, Martín-Benito J, Valpuesta JM, Carrascosa JL, de la Cruz F, Cabezón E, Arechaga I (2012) The hexameric structure of a conjugative VirB4 protein ATPase provides new insights for a functional and phylogenetic relationship with DNA translocases. *J Biol Chem* **287**: 39925–39932.
210. Durand E, Waksman G, Receveur-Brechot V (2011) Structural insights into the membrane-extracted dimeric form of the ATPase TraB from the Escherichia coli pKM101 conjugation system. *BMC Struct Biol* **11**: 4.
211. Walldén K, Williams R, Yan J, Lian PW, Wang L, Thalassinos K, Orlova EV, Waksman G (2012) Structure of the VirB4 ATPase, alone and bound to the core complex of a type IV secretion system. *Proc Natl Acad Sci USA* **109**: 11348–11353.
212. Cabezon E, Lanza VF, Arechaga I (2012) Membrane-associated nanomotors for macromolecular transport. *Curr Opin Biotechnol* **23**: 537–544.
213. Kerr JE, Christie PJ (2010) Evidence for VirB4-mediated dislocation of membrane-integrated VirB2 pilin during biogenesis of the Agrobacterium VirB/VirD4 type IV secretion system. *J Bacteriol* **192**: 4923–4934.
214. Atmakuri K, Cascales E, Christie PJ (2004) Energetic components VirD4, VirB11 and VirB4 mediate early DNA transfer reactions required for bacterial type IV secretion. *Mol Microbiol* **54**: 1199–1211.
215. Draper O, Middleton R, Doucleff M, Zambryski PC (2006) Topology of the VirB4 C Terminus in the Agrobacterium tumefaciens VirB/D4 Type IV Secretion System. *J Biol Chem* **281**: 37628–37635.
216. Li F, Alvarez-Martinez C, Chen Y, Choi K-J, Yeo H-J, Christie PJ (2012) Enterococcus faecalis PrgJ, a VirB4-like ATPase, mediates pCF10 conjugative transfer through substrate binding. *J Bacteriol* **194**: 4041–4051.
217. Sagulenko E, Sagulenko V, Chen J, Christie PJ (2001) Role of Agrobacterium VirB11 ATPase in T-pilus assembly and substrate selection. *J Bacteriol* **183**: 5813–5825.
218. Zhong Q, Shao S, Cui L, Mu R, Ju X, Dong S (2007) Type IV secretion system in Helicobacter pylori: a new insight into pathogenicity. *Chin Med J* **120**: 2138–2142.
219. Yeo HJ, Savvides SN, Herr AB, Lanka E, Waksman G (2000) Crystal structure of the hexameric traffic ATPase of the Helicobacter pylori type IV secretion system. *Mol Cell* **6**: 1461–1472.
220. Krause S, Bárcena M, Pansegrau W, Lurz R, Carazo JM, Lanka E (2000) Sequence-related protein export NTPases encoded by the conjugative transfer region of RP4 and by the cag pathogenicity island of Helicobacter pylori share similar hexameric ring structures. *Proc Natl Acad Sci U S A* **97**: 3067–3072.
221. Rivas S, Bolland S, Cabezón E, Goñi FM, de la Cruz F (1997) TrwD, a protein encoded by the IncW plasmid R388, displays an ATP hydrolase activity essential for bacterial conjugation. *J Biol Chem* **272**: 25583–25590.
222. Stephens KM, Roush C, Nester E (1995) Agrobacterium tumefaciens VirB11 protein requires a consensus nucleotide-binding site for function in virulence. *J Bacteriol* **177**: 27–36.

223. Krause S, Pansegrau W, Lurz R, de la Cruz F, Lanka E (2000) Enzymology of type IV macromolecule secretion systems: the conjugative transfer regions of plasmids RP4 and R388 and the cag pathogenicity island of Helicobacter pylori encode structurally and functionally related nucleoside triphosphate hydrolases. *J Bacteriol* **182**: 2761–2770.
224. Sakai D, Horiuchi T, Komano T (2001) Atpase activity and multimer formation of Pilq protein are required for thin pilus biogenesis in plasmid R64. *J Biol Chem* **276**: 17968–17975.
225. Rashkova S, Spudich GM, Christie PJ (1997) Characterization of membrane and protein interaction determinants of the Agrobacterium tumefaciens VirB11 ATPase. *J Bacteriol* **179**: 583–591.
226. Machón C, Rivas S, Albert A, Goñi FM, de la Cruz F (2002) TrwD, the hexameric traffic ATPase encoded by plasmid R388, induces membrane destabilization and hemifusion of lipid vesicles. *J Bacteriol* **184**: 1661–1668.
227. Rashkova S, Zhou XR, Chen J, Christie PJ (2000) Self-assembly of the Agrobacterium tumefaciens VirB11 traffic ATPase. *J Bacteriol* **182**: 4137–4145.
228. Hare S, Bayliss R, Baron C, Waksman G (2006) A large domain swap in the VirB11 ATPase of Brucella suis leaves the hexameric assembly intact. *J Mol Biol* **360**: 56–66.
229. Savvides SN, Yeo H-J, Beck MR, Blaesing F, Lurz R, Lanka E, Buhrdorf R, Fischer W, Haas R, Waksman G (2003) VirB11 ATPases are dynamic hexameric assemblies: new insights into bacterial type IV secretion. *EMBO J* **22**: 1969–1980.
230. Planet PJ, Kachlany SC, DeSalle R, Figurski DH (2001) Phylogeny of genes for secretion NTPases: identification of the widespread tadA subfamily and development of a diagnostic key for gene classification. *Proc Natl Acad Sci USA* **98**: 2503–2508.
231. Aukema KG, Kron EM, Herdendorf TJ, Forest KT (2005) Functional dissection of a conserved motif within the pilus retraction protein PilT. *J Bacteriol* **187**: 611–618.
232. Savvides SN (2007) Secretion superfamily ATPases swing big. *Structure* **15**: 255–257.
233. Yamagata A, Tainer JA (2007) Hexameric structures of the archaeal secretion ATPase GspE and implications for a universal secretion mechanism. *EMBO J* **26**: 878–890.
234. Misic AM, Satyshur KA, Forest KT (2010) P. aeruginosa PilT structures with and without nucleotide reveal a dynamic type IV pilus retraction motor. *J Mol Biol* **400**: 1011–1021.
235. Ripoll-Rozada J, Peña A, Rivas S, Moro F, de la Cruz F, Cabezón E, Arechaga I (2012) Regulation of the type IV secretion ATPase TrwD by magnesium: implications for catalytic mechanism of the secretion ATPase superfamily. *J Biol Chem* **287**: 17408–17414.
236. Ripoll-Rozada J, Zunzunegui S, Cruz F de la, Arechaga I, Cabezón E (2013) Functional Interactions of VirB11 Traffic ATPases with VirB4 and VirD4 Molecular Motors in Type IV Secretion Systems. *J Bacteriol* **195**: 4195–4201.
237. Yeo H-J, Waksman G (2004) Unveiling molecular scaffolds of the type IV secretion system. *J Bacteriol* **186**: 1919–1926.
238. Trokter M, Waksman G (2018) Translocation through the conjugative Type 4 secretion system requires unfolding of its protein substrate. *J Bacteriol*.
239. Peña A, Arechaga I (2013) Molecular Motors in Bacterial Secretion. *J Mol Microbiol Biotechnol* **23**: 357–369.
240. Syvanen M, Kado CI (2001) *Horizontal Gene Transfer*. Academic Press.
241. de la Cruz F, Davies J (2000) Horizontal gene transfer and the origin of species: lessons from bacteria. *Trends Microbiol* **8**: 128–133.
242. Keese P (2008) Risks from GMOs due to horizontal gene transfer. *Environ Biosafety Res* **7**: 123–149.
243. Fleming A (2001) On the antibacterial action of cultures of a penicillium, with special reference to their use in the isolation of B. influenzae. 1929. *Bull World Health Organ* **79**: 780–790.

244. Davies J, Davies D (2010) Origins and evolution of antibiotic resistance. *Microbiol Mol Biol Rev* **74**: 417–433.
245. D'Costa VM, McGrann KM, Hughes DW, Wright GD (2006) Sampling the antibiotic resistome. *Science* **311**: 374–377.
246. Liu B, Pop M (2009) ARDB--Antibiotic Resistance Genes Database. *Nucleic Acids Res* **37**: D443-447.
247. Clatworthy AE, Pierson E, Hung DT (2007) Targeting virulence: a new paradigm for antimicrobial therapy. *Nat Chem Biol* **3**: 541–548.
248. Coates A, Hu Y, Bax R, Page C (2002) The future challenges facing the development of new antimicrobial drugs. *Nat Rev Drug Discov* **1**: 895–910.
249. Amyes SG, Emmerson AM, Smith JT (1978) R-factor mediated trimethoprim resistance: result of two three-month clinical surveys. *J Clin Pathol* **31**: 850–854.
250. Livermore DM (1992) Interplay of impermeability and chromosomal beta-lactamase activity in imipenem-resistant Pseudomonas aeruginosa. *Antimicrob Agents Chemother* **36**: 2046–2048.
251. Williams JB (1996) Drug efflux as a mechanism of resistance. *Br J Biomed Sci* **53**: 290–293.
252. Sykes RB, Matthew M (1976) The beta-lactamases of gram-negative bacteria and their role in resistance to beta-lactam antibiotics. *J Antimicrob Chemother* **2**: 115–157.
253. Abraham EP, Chain E (1940) An Enzyme from Bacteria able to Destroy Penicillin. *Nature* **146**: 837.
254. Cooper MA, Shlaes D (2011) Fix the antibiotics pipeline. *Nature* **472**: 32.
255. O'Neill J (2014) Antimicrobial resistance: tackling a crisis for the health and wealth of nations. *Rev Antimicrob Resist*.
256. Lomovskaya O, Zgurskaya HI, Totrov M, Watkins WJ (2007) Waltzing transporters and 'the dance macabre' between humans and bacteria. *Nat Rev Drug Discov* **6**: 56–65.
257. Reading C, Cole M (1977) Clavulanic acid: a beta-lactamase-inhiting beta-lactam from Streptomyces clavuligerus. *Antimicrob Agents Chemother* **11**: 852–857.
258. Thomson CJ, Amyes SG (1992) TRC-1: emergence of a clavulanic acid-resistant TEM beta-lactamase in a clinical strain. *FEMS Microbiol Lett* **70**: 113–117.
259. Heras B, Scanlon MJ, Martin JL (2015) Targeting virulence not viability in the search for future antibacterials. *Br J Clin Pharmacol* **79**: 208–215.
260. Shoop WL, Xiong Y, Wiltsie J, Woods A, Guo J, Pivnichny JV, Felcetto T, Michael BF, Bansal A, Cummings RT, et al. (2005) Anthrax lethal factor inhibition. *Proc Natl Acad Sci USA* **102**: 7958–7963.
261. Pan Q, Zhang X-L, Wu H-Y, He P-W, Wang F, Zhang M-S, Hu J-M, Xia B, Wu J (2005) Aptamers that preferentially bind type IVB pili and inhibit human monocytic-cell invasion by Salmonella enterica serovar typhi. *Antimicrob Agents Chemother* **49**: 4052–4060.
262. Pinkner JS, Remaut H, Buelens F, Miller E, Aberg V, Pemberton N, Hedenström M, Larsson A, Seed P, Waksman G, et al. (2006) Rationally designed small compounds inhibit pilus biogenesis in uropathogenic bacteria. *Proc Natl Acad Sci USA* **103**: 17897–17902.
263. Hung DT, Shakhnovich EA, Pierson E, Mekalanos JJ (2005) Small-molecule inhibitor of Vibrio cholerae virulence and intestinal colonization. *Science* **310**: 670–674.
264. Tang K, Zhang X-H (2014) Quorum quenching agents: resources for antivirulence therapy. *Mar Drugs* **12**: 3245–3282.
265. Williams JJ, Hergenrother PJ (2008) Exposing plasmids as the Achilles' heel of drug-resistant bacteria. *Curr Opin Chem Biol* **12**: 389–399.
266. Baquero F, Coque TM, de la Cruz F (2011) Ecology and evolution as targets: the need for novel eco-evo drugs and strategies to fight antibiotic resistance. *Antimicrob Agents Chemother* **55**: 3649–3660.

267. Guilhelmelli F, Vilela N, Albuquerque P, Derengowski L da S, Silva-Pereira I, Kyaw CM (2013) Antibiotic development challenges: the various mechanisms of action of antimicrobial peptides and of bacterial resistance. *Front Microbiol* **4**: 353.
268. Cavera VL, Arthur TD, Kashtanov D, Chikindas ML (2015) Bacteriocins and their position in the next wave of conventional antibiotics. *Int J Antimicrob Agents* **46**: 494–501.
269. Foley TL, Simeonov A (2012) Targeting iron assimilation to develop new antibacterials. *Expert Opin Drug Discov* **7**: 831–847.
270. Jain A, Duvvuri LS, Farah S, Beyth N, Domb AJ, Khan W (2014) Antimicrobial polymers. *Adv Healthc Mater* **3**: 1969–1985.
271. Hermoso JA, García JL, García P (2007) Taking aim on bacterial pathogens: from phage therapy to enzybiotics. *Curr Opin Microbiol* **10**: 461–472.
272. Woodford N, Wareham DW, UK Antibacterial Antisense Study Group (2009) Tackling antibiotic resistance: a dose of common antisense? *J Antimicrob Chemother* **63**: 225–229.
273. Beyth N, Houri-Haddad Y, Domb A, Khan W, Hazan R (2015) Alternative antimicrobial approach: nano-antimicrobial materials. *Evid Based Complement Alternat Med* **2015**: 246012.
274. Yin R, Dai T, Avci P, Jorge AES, de Melo WCMA, Vecchio D, Huang Y-Y, Gupta A, Hamblin MR (2013) Light based anti-infectives: ultraviolet C irradiation, photodynamic therapy, blue light, and beyond. *Curr Opin Pharmacol* **13**: 731–762.
275. Scully IL, Swanson K, Green L, Jansen KU, Anderson AS (2015) Anti-infective vaccination in the 21st century-new horizons for personal and public health. *Curr Opin Microbiol* **27**: 96–102.
276. Amara AA, Shibl A (2015) Role of Probiotics in health improvement, infection control and disease treatment and management. *Saudi Pharm J* **23**: 107–114.
277. Nobrega FL, Costa AR, Kluskens LD, Azeredo J (2015) Revisiting phage therapy: new applications for old resources. *Trends Microbiol* **23**: 185–191.
278. Frost LS, Koraimann G (2010) Regulation of bacterial conjugation: balancing opportunity with adversity. *Future Microbiol* **5**: 1057–1071.
279. Fernandez-Lopez R, Del Campo I, Revilla C, Cuevas A, de la Cruz F (2014) Negative feedback and transcriptional overshooting in a regulatory network for horizontal gene transfer. *PLoS Genet* **10**: e1004171.
280. Roberts RJ, Vincze T, Posfai J, Macelis D (2015) REBASE--a database for DNA restriction and modification: enzymes, genes and genomes. *Nucleic Acids Res* **43**: D298-299.
281. Oliveira PH, Touchon M, Rocha EPC (2014) The interplay of restriction-modification systems with mobile genetic elements and their prokaryotic hosts. *Nucleic Acids Res* **42**: 10618–10631.
282. Bertani G, Weigle JJ (1953) Host controlled variation in bacterial viruses. *J Bacteriol* **65**: 113–121.
283. Vasu K, Nagaraja V (2013) Diverse functions of restriction-modification systems in addition to cellular defense. *Microbiol Mol Biol Rev* **77**: 53–72.
284. Bickle TA (2004) Restricting restriction. *Mol Microbiol* **51**: 3–5.
285. Grissa I, Vergnaud G, Pourcel C (2007) The CRISPRdb database and tools to display CRISPRs and to generate dictionaries of spacers and repeats. *BMC Bioinformatics* **8**: 172.
286. Marraffini LA (2015) CRISPR-Cas immunity in prokaryotes. *Nature* **526**: 55–61.
287. Marraffini LA, Sontheimer EJ (2008) CRISPR interference limits horizontal gene transfer in staphylococci by targeting DNA. *Science* **322**: 1843–1845.
288. Samson JE, Magadan AH, Moineau S (2015) The CRISPR-Cas Immune System and Genetic Transfers: Reaching an Equilibrium. *Microbiol Spectr* **3**: PLAS-0034-2014.
289. Pennisi E (2013) The CRISPR craze. *Science* **341**: 833–836.
290. Chatterjee A, Cook LCC, Shu C-C, Chen Y, Manias DA, Ramkrishna D, Dunny GM, Hu W-S (2013) Antagonistic self-sensing and mate-sensing signaling controls antibiotic-resistance transfer. *Proc Natl Acad Sci USA* **110**: 7086–7090.

291. Koraimann G, Wagner MA (2014) Social behavior and decision making in bacterial conjugation. *Front Cell Infect Microbiol* **4**: 54.
292. Lederberg J, Cavalli LL, Lederberg EM (1952) Sex Compatibility in Escherichia Coli. *Genetics* **37**: 720–730.
293. Watanabe T (1963) Infective heredity of multiple drug resistance in bacteria. *Bacteriol Rev* **27**: 87–115.
294. Novick RP (1969) Extrachromosomal inheritance in bacteria. *Bacteriol Rev* **33**: 210–263.
295. Achtman M, Kennedy N, Skurray R (1977) Cell--cell interactions in conjugating Escherichia coli: role of traT protein in surface exclusion. *Proc Natl Acad Sci USA* **74**: 5104–5108.
296. Achtman M, Manning PA, Edelbluth C, Herrlich P (1979) Export without proteolytic processing of inner and outer membrane proteins encoded by F sex factor tra cistrons in Escherichia coli minicells. *Proc Natl Acad Sci USA* **76**: 4837–4841.
297. Watanabe T, Fukasawa T (1962) Episome-mediated transfer of drug resistance in Enterobacteriaceae IV. Interactions between resistance transfer factor and F-factor in Escherichia coli K-12. *J Bacteriol* **83**: 727–735.
298. Koraimann G, Teferle K, Markolin G, Woger W, Högenauer G (1996) The FinOP repressor system of plasmid R1: analysis of the antisense RNA control of traJ expression and conjugative DNA transfer. *Mol Microbiol* **21**: 811–821.
299. Gasson MJ, Willetts NS (1975) Five control systems preventing transfer of Escherichia coli K-12 sex factor F. *J Bacteriol* **122**: 518–525.
300. Gasson MJ, Willetts NS (1977) Further characterization of the F fertility inhibition systems of 'unusual' Fin+ plasmids. *J Bacteriol* **131**: 413–420.
301. Getino M, de la Cruz F (2018) Natural and Artificial Strategies To Control the Conjugative Transmission of Plasmids. *Microbiol Spectr* **6**:.
302. Nash RP, McNamara DE, Ballentine WK, Matson SW, Redinbo MR (2012) Investigating the impact of bisphosphonates and structurally related compounds on bacteria containing conjugative plasmids. *Biochem Biophys Res Commun* **424**: 697–703.
303. Michel-Briand Y, Laporte JM (1985) Inhibition of conjugal transfer of R plasmids by nitrofurans. *J Gen Microbiol* **131**: 2281–2284.
304. Hahn FE, Ciak J (1976) Elimination of resistance determinants from R-factor R1 by intercalative compounds. *Antimicrob Agents Chemother* **9**: 77–80.
305. Molnár J, Fischer J, Nakamura MJ (1992) Mechanism of chlorpromazine binding by gram-positive and gram-negative bacteria. *Antonie Van Leeuwenhoek* **62**: 309–314.
306. Lujan SA, Guogas LM, Ragonese H, Matson SW, Redinbo MR (2007) Disrupting antibiotic resistance propagation by inhibiting the conjugative DNA relaxase. *Proc Natl Acad Sci USA* **104**: 12282–12287.
307. Bidlack JE, Silverman PM (2004) An active type IV secretion system encoded by the F plasmid sensitizes Escherichia coli to bile salts. *J Bacteriol* **186**: 5202–5209.
308. Daugelavicius R, Bamford JK, Grahn AM, Lanka E, Bamford DH (1997) The IncP plasmid-encoded cell envelope-associated DNA transfer complex increases cell permeability. *J Bacteriol* **179**: 5195–5202.
309. Weisser J, Wiedemann B (1987) Inhibition of R-plasmid transfer in Escherichia coli by 4-quinolones. *Antimicrob Agents Chemother* **31**: 531–534.
310. Debbia EA, Massaro S, Campora U, Schito GC (1994) Inhibition of F'lac transfer by various antibacterial drugs in Escherichia coli. *New Microbiol* **17**: 65–68.
311. Smith MA, Coinçon M, Paschos A, Jolicoeur B, Lavallée P, Sygusch J, Baron C (2012) Identification of the binding site of Brucella VirB8 interaction inhibitors. *Chem Biol* **19**: 1041–1048.

312. Paschos A, den Hartigh A, Smith MA, Atluri VL, Sivanesan D, Tsolis RM, Baron C (2011) An in vivo high-throughput screening approach targeting the type IV secretion system component VirB8 identified inhibitors of Brucella abortus 2308 proliferation. *Infect Immun* **79**: 1033–1043.
313. Keyser P, Elofsson M, Rosell S, Wolf-Watz H (2008) Virulence blockers as alternatives to antibiotics: type III secretion inhibitors against Gram-negative bacteria. *J Intern Med* **264**: 17–29.
314. Casu B, Smart J, Hancock MA, Smith M, Sygusch J, Baron C (2016) Structural Analysis and Inhibition of TraE from the pKM101 Type IV Secretion System. *J Biol Chem* **291**: 23817–23829.
315. Anthony KG, Sherburne C, Sherburne R, Frost LS (1994) The role of the pilus in recipient cell recognition during bacterial conjugation mediated by F-like plasmids. *Mol Microbiol* **13**: 939–953.
316. Lin A, Jimenez J, Derr J, Vera P, Manapat ML, Esvelt KM, Villanueva L, Liu DR, Chen IA (2011) Inhibition of bacterial conjugation by phage M13 and its protein g3p: quantitative analysis and model. *PLoS ONE* **6**: e19991.
317. Wan Z, Goddard NL (2012) Competition between conjugation and M13 phage infection in Escherichia coli in the absence of selection pressure: a kinetic study. *G3 (Bethesda)* **2**: 1137–1144.
318. Ghigo JM (2001) Natural conjugative plasmids induce bacterial biofilm development. *Nature* **412**: 442–445.
319. May T, Tsuruta K, Okabe S (2011) Exposure of conjugative plasmid carrying Escherichia coli biofilms to male-specific bacteriophages. *ISME J* **5**: 771–775.
320. Harden V, Meynell E (1972) Inhibition of gene transfer by antiserum and identification of serotypes of sex pili. *J Bacteriol* **109**: 1067–1074.
321. Shaffer CL, Good JAD, Kumar S, Krishnan KS, Gaddy JA, Loh JT, Chappell J, Almqvist F, Cover TL, Hadjifrangiskou M (2016) Peptidomimetic Small Molecules Disrupt Type IV Secretion System Activity in Diverse Bacterial Pathogens. *MBio* **7**: e00221-00216.
322. Fernandez-Lopez R, Machón C, Longshaw CM, Martin S, Molin S, Zechner EL, Espinosa M, Lanka E, de la Cruz F (2005) Unsaturated fatty acids are inhibitors of bacterial conjugation. *Microbiology (Reading, Engl)* **151**: 3517–3526.
323. Spengler G, Molnár A, Schelz Z, Amaral L, Sharples D, Molnár J (2006) The mechanism of plasmid curing in bacteria. *Curr Drug Targets* **7**: 823–841.
324. Viljanen P, Boratynski J (1991) The susceptibility of conjugative resistance transfer in gram-negative bacteria to physicochemical and biochemical agents. *FEMS Microbiol Rev* **8**: 43–54.
325. Nakamura S, Inoue S, Shimizu M, Iyobe S, Mitsuhashi S (1976) Inhibition of conjugal transfer of R plasmids by pipemidic acid and related compounds. *Antimicrob Agents Chemother* **10**: 779–785.
326. Gussoni M, Greco F, Pegna M, Bianchi G, Zetta L (1994) Solid state and microscopy NMR study of the chemical constituents of Afzelia cuanzensis seeds. *Magn Reson Imaging* **12**: 477–486.
327. Di Vaio C, Nocerino S, Paduano A, Sacchi R (2013) Influence of some environmental factors on drupe maturation and olive oil composition. *J Sci Food Agric* **93**: 1134–1139.
328. Niki E, Yoshida Y, Saito Y, Noguchi N (2005) Lipid peroxidation: mechanisms, inhibition, and biological effects. *Biochem Biophys Res Commun* **338**: 668–676.
329. Getino M, Sanabria-Ríos DJ, Fernández-López R, Campos-Gómez J, Sánchez-López JM, Fernández A, Carballeira NM, de la Cruz F (2015) Synthetic Fatty Acids Prevent Plasmid-Mediated Horizontal Gene Transfer. *MBio* **6**:.
330. Gershon H, Shanks L (1978) Antifungal properties of 2-alkynoic acids and their methyl esters. *Can J Microbiol* **24**: 593–597.
331. Carballeira NM, Sanabria D, Cruz C, Parang K, Wan B, Franzblau S (2006) 2,6-hexadecadiynoic acid and 2,6-nonadecadiynoic acid: novel synthesized acetylenic fatty acids as potent antifungal agents. *Lipids* **41**: 507–511.

332. Carballeira NM, Cartagena M, Sanabria D, Tasdemir D, Prada CF, Reguera RM, Balaña-Fouce R (2012) 2-Alkynoic fatty acids inhibit topoisomerase IB from Leishmania donovani. *Bioorg Med Chem Lett* **22**: 6185–6189.
333. Tasdemir D, Sanabria D, Lauinger IL, Tarun A, Herman R, Perozzo R, Zloh M, Kappe SH, Brun R, Carballeira NM (2010) 2-Hexadecynoic acid inhibits plasmodial FAS-II enzymes and arrests erythrocytic and liver stage Plasmodium infections. *Bioorg Med Chem* **18**: 7475–7485.
334. Konthikamee W, Gilbertson JR, Langkamp H, Gershon H (1982) Effect of 2-alkynoic acids on in vitro growth of bacterial and mammalian cells. *Antimicrob Agents Chemother* **22**: 805–809.
335. Morbidoni HR, Vilchèze C, Kremer L, Bittman R, Sacchettini JC, Jacobs WR (2006) Dual inhibition of mycobacterial fatty acid biosynthesis and degradation by 2-alkynoic acids. *Chem Biol* **13**: 297–307.
336. Sanabria-Ríos DJ, Rivera-Torres Y, Maldonado-Domínguez G, Domínguez I, Ríos C, Díaz D, Rodríguez JW, Altieri-Rivera JS, Ríos-Olivares E, Cintrón G, et al. (2014) Antibacterial activity of 2-alkynoic fatty acids against multidrug-resistant bacteria. *Chem Phys Lipids* **178**: 84–91.
337. Getino M, Fernández-López R, Palencia-Gándara C, Campos-Gómez J, Sánchez-López JM, Martínez M, Fernández A, de la Cruz F (2016) Tanzawaic Acids, a Chemically Novel Set of Bacterial Conjugation Inhibitors. *PLoS One* **11**:.
338. Cabezón E, de la Cruz F, Arechaga I (2017) Conjugation Inhibitors and Their Potential Use to Prevent Dissemination of Antibiotic Resistance Genes in Bacteria. *Front Microbiol* **8**: 2329.
339. Grant SG, Jessee J, Bloom FR, Hanahan D (1990) Differential plasmid rescue from transgenic mouse DNAs into Escherichia coli methylation-restriction mutants. *Proc Natl Acad Sci USA* **87**: 4645–4649.
340. Sandler SJ, Clark AJ (1990) Factors affecting expression of the recF gene of Escherichia coli K-12. *Gene* **86**: 35–43.
341. Miroux B, Walker JE (1996) Over-production of proteins in Escherichia coli: mutant hosts that allow synthesis of some membrane proteins and globular proteins at high levels. *J Mol Biol* **260**: 289–298.
342. Studier FW, Moffatt BA (1986) Use of bacteriophage T7 RNA polymerase to direct selective high-level expression of cloned genes. *J Mol Biol* **189**: 113–130.
343. Blattner FR, Plunkett G, Bloch CA, Perna NT, Burland V, Riley M, Collado-Vides J, Glasner JD, Rode CK, Mayhew GF, et al. (1997) The complete genome sequence of Escherichia coli K-12. *Science* **277**: 1453–1462.
344. Bosak T, Losick RM, Pearson A (2008) A polycyclic terpenoid that alleviates oxidative stress. *Proc Natl Acad Sci USA* **105**: 6725–6729.
345. de la Cruz F, Grinsted J (1982) Genetic and molecular characterization of Tn21, a multiple resistance transposon from R100.1. *J Bacteriol* **151**: 222–228.
346. Rosenberg AH, Lade BN, Chui DS, Lin SW, Dunn JJ, Studier FW (1987) Vectors for selective expression of cloned DNAs by T7 RNA polymerase. *Gene* **56**: 125–135.
347. Ripoll-Rozada J, Peña A, Rivas S, Moro F, Cruz F de la, Cabezón E, Arechaga I (2012) Regulation of the Type IV Secretion ATPase TrwD by Magnesium IMPLICATIONS FOR CATALYTIC MECHANISM OF THE SECRETION ATPase SUPERFAMILY. *J Biol Chem* **287**: 17408–17414.
348. Avila P, de la Cruz F (1988) Physical and genetic map of the IncW plasmid R388. *Plasmid* **20**: 155–157.
349. Getino M, Sanabria-Ríos DJ, Fernández-López R, Campos-Gómez J, Sánchez-López JM, Fernández A, Carballeira NM, de la Cruz F (2015) Synthetic Fatty Acids Prevent Plasmid-Mediated Horizontal Gene Transfer. *MBio* **6**: e01032-01015.
350. Ripoll-Rozada J, García-Cazorla Y, Getino M, Machón C, Sanabria-Ríos D, de la Cruz F, Cabezón E, Arechaga I (2016) Type IV traffic ATPase TrwD as molecular target to inhibit bacterial conjugation. *Mol Microbiol* **100**: 912–921.

351. Sambrook J, Fritsch EF, Maniatis T (1989) Molecular cloning: a laboratory manual. *Molecular cloning: a laboratory manual*.
352. Hanahan D (1983) Studies on transformation of Escherichia coli with plasmids. *J Mol Biol* **166**: 557–580.
353. Dower WJ, Miller JF, Ragsdale CW (1988) High efficiency transformation of E. coli by high voltage electroporation. *Nucleic Acids Res* **16**: 6127–6145.
354. Bradford MM (1976) A rapid and sensitive method for the quantitation of microgram quantities of protein utilizing the principle of protein-dye binding. *Anal Biochem* **72**: 248–254.
355. Laemmli UK (1970) Cleavage of structural proteins during the assembly of the head of bacteriophage T4. *Nature* **227**: 680–685.
356. Meyer TS, Lamberts BL (1965) Use of coomassie brilliant blue R250 for the electrophoresis of microgram quantities of parotid saliva proteins on acrylamide-gel strips. *Biochim Biophys Acta* **107**: 144–145.
357. Schägger H (2006) Tricine-SDS-PAGE. *Nat Protoc* **1**: 16–22.
358. Schägger H, von Jagow G (1991) Blue native electrophoresis for isolation of membrane protein complexes in enzymatically active form. *Anal Biochem* **199**: 223–231.
359. Fiala GJ, Schamel WWA, Blumenthal B (2011) Blue native polyacrylamide gel electrophoresis (BN-PAGE) for analysis of multiprotein complexes from cellular lysates. *J Vis Exp*.
360. Arndt C, Koristka S, Bartsch H, Bachmann M (2012) Native Polyacrylamide Gels. In, *Protein Electrophoresis* pp 49–53. Humana Press, Totowa, NJ.
361. Kreuzer KN, Jongeneel CV (1983) Escherichia coli phage T4 topoisomerase. *Meth Enzymol* **100**: 144–160.
362. Karzai AW, McMacken R (1996) A Bipartite Signaling Mechanism Involved in DnaJ-mediated Activation of the Escherichia coli DnaK Protein. *J Biol Chem* **271**: 11236–11246.
363. Limpikirati P, Liu T, Vachet RW (2018) Covalent labeling-mass spectrometry with non-specific reagents for studying protein structure and interactions. *Methods*.
364. Cameron SJ, Takáts Z (2018) Mass Spectrometry Approaches to Metabolic Profiling of Microbial Communities within the Human Gastrointestinal Tract. *Methods*.
365. Notredame C, Higgins DG, Heringa J (2000) T-Coffee: A novel method for fast and accurate multiple sequence alignment. *J Mol Biol* **302**: 205–217.
366. Waterhouse AM, Procter JB, Martin DMA, Clamp M, Barton GJ (2009) Jalview Version 2--a multiple sequence alignment editor and analysis workbench. *Bioinformatics* **25**: 1189–1191.
367. Buchan DWA, Ward SM, Lobley AE, Nugent TCO, Bryson K, Jones DT (2010) Protein annotation and modelling servers at University College London. *Nucleic Acids Res* **38**: W563-568.
368. Kelley LA, Sternberg MJE (2009) Protein structure prediction on the Web: a case study using the Phyre server. *Nat Protoc* **4**: 363–371.
369. Pettersen EF, Goddard TD, Huang CC, Couch GS, Greenblatt DM, Meng EC, Ferrin TE (2004) UCSF Chimera--a visualization system for exploratory research and analysis. *J Comput Chem* **25**: 1605–1612.
370. Dunbrack RL (2002) Rotamer libraries in the 21st century. *Curr Opin Struct Biol* **12**: 431–440.
371. Grosdidier A, Zoete V, Michielin O (2011) SwissDock, a protein-small molecule docking web service based on EADock DSS. *Nucleic Acids Res* **39**: W270-277.
372. DeLano WL (2008) The PyMOL Molecuar Graphics System. *DeLano Scientific LLC; Palo Alto, CA*.
373. Dolinsky TJ, Czodrowski P, Li H, Nielsen JE, Jensen JH, Klebe G, Baker NA (2007) PDB2PQR: expanding and upgrading automated preparation of biomolecular structures for molecular simulations. *Nucleic Acids Res* **35**: W522-525.
374. Baker NA, Sept D, Joseph S, Holst MJ, McCammon JA (2001) Electrostatics of nanosystems: application to microtubules and the ribosome. *Proc Natl Acad Sci USA* **98**: 10037–10041.

375. Young JW, Locke JCW, Altinok A, Rosenfeld N, Bacarian T, Swain PS, Mjolsness E, Elowitz MB (2011) Measuring single-cell gene expression dynamics in bacteria using fluorescence time-lapse microscopy. *Nat Protoc* **7**: 80–88.
376. Bottomley AL, Turnbull L, Whitchurch CB, Harry EJ (2017) Immobilization Techniques of Bacteria for Live Super-resolution Imaging Using Structured Illumination Microscopy. *Methods Mol Biol* **1535**: 197–209.
377. Mizushina Y, Yoshida S, Matsukage A, Sakaguchi K (1997) The inhibitory action of fatty acids on DNA polymerase β. *Biochimica et Biophysica Acta (BBA) - General Subjects* **1336**: 509–521.
378. Swarts HG, Schuurmans Stekhoven FM, De Pont JJ (1990) Binding of unsaturated fatty acids to Na+, K(+)-ATPase leading to inhibition and inactivation. *Biochim Biophys Acta* **1024**: 32–40.
379. Mukhopadhyay S, Ramminger SJ, McLaughlin M, Gambling L, Olver RE, Kemp PJ (1997) Direct modulation of G-proteins by polyunsaturated fatty acids: a novel eicosanoid-independent regulatory mechanism in the developing lung. *Biochem J* **326 (Pt 3)**: 725–730.
380. Núñez B, De La Cruz F (2001) Two atypical mobilization proteins are involved in plasmid CloDF13 relaxation. *Mol Microbiol* **39**: 1088–1099.
381. Fernández-González E, de Paz HD, Alperi A, Agúndez L, Faustmann M, Sangari FJ, Dehio C, Llosa M (2011) Transfer of R388 derivatives by a pathogenesis-associated type IV secretion system into both bacteria and human cells. *J Bacteriol* **193**: 6257–6265.
382. Coleman RA, Rao P, Fogelsong RJ, Bardes ES (1992) 2-Bromopalmitoyl-CoA and 2-bromopalmitate: promiscuous inhibitors of membrane-bound enzymes. *Biochim Biophys Acta* **1125**: 203–209.
383. Webb Y, Hermida-Matsumoto L, Resh MD (2000) Inhibition of protein palmitoylation, raft localization, and T cell signaling by 2-bromopalmitate and polyunsaturated fatty acids. *J Biol Chem* **275**: 261–270.
384. Resh MD (2006) Use of analogs and inhibitors to study the functional significance of protein palmitoylation. *Methods* **40**: 191–197.
385. Davda D, El Azzouny MA, Tom CTMB, Hernandez JL, Majmudar JD, Kennedy RT, Martin BR (2013) Profiling targets of the irreversible palmitoylation inhibitor 2-bromopalmitate. *ACS Chem Biol* **8**: 1912–1917.
386. Oakes ND, Furler SM (2002) Evaluation of free fatty acid metabolism in vivo. *Ann N Y Acad Sci* **967**: 158–175.
387. Goñi FM (2002) Non-permanent proteins in membranes: when proteins come as visitors (Review). *Mol Membr Biol* **19**: 237–245.
388. Glatz JF, van Nieuwenhoven FA, Luiken JJ, Schaap FG, van der Vusse GJ (1997) Role of membrane-associated and cytoplasmic fatty acid-binding proteins in cellular fatty acid metabolism. *Prostaglandins Leukot Essent Fatty Acids* **57**: 373–378.
389. Kang HY, Park TJ, Jin SH (2009) Imiquimod, a Toll-like receptor 7 agonist, inhibits melanogenesis and proliferation of human melanocytes. *J Invest Dermatol* **129**: 243–246.
390. Nicholas DA, Zhang K, Hung C, Glasgow S, Aruni AW, Unternaehrer J, Payne KJ, Langridge WHR, De Leon M (2017) Palmitic acid is a toll-like receptor 4 ligand that induces human dendritic cell secretion of IL-1β. *PLoS ONE* **12**: e0176793.
391. Hwang DH, Kim J-A, Lee JY (2016) Mechanisms for the activation of Toll-like receptor 2/4 by saturated fatty acids and inhibition by docosahexaenoic acid. *Eur J Pharmacol* **785**: 24–35.
392. Seno K, Hayashi F (2017) Palmitoylation is a prerequisite for dimerization-dependent raftophilicity of rhodopsin. *J Biol Chem* **292**: 15321–15328.
393. Jiang H, Zhang X, Chen X, Aramsangtienchai P, Tong Z, Lin H (2018) Protein Lipidation: Occurrence, Mechanisms, Biological Functions, and Enabling Technologies. *Chem Rev*.
394. Blanc M, Blaskovic S, van der Goot FG (2013) Palmitoylation, pathogens and their host. *Biochem Soc Trans* **41**: 84–88.

395. Agudo-Ibáñez L, Herrero A, Barbacid M, Crespo P (2015) H-ras distribution and signaling in plasma membrane microdomains are regulated by acylation and deacylation events. *Mol Cell Biol* **35**: 1898–1914.
396. Pedro MP, Vilcaes AA, Tomatis VM, Oliveira RG, Gomez GA, Daniotti JL (2013) 2-Bromopalmitate reduces protein deacylation by inhibition of acyl-protein thioesterase enzymatic activities. *PLoS ONE* **8**: e75232.
397. DeJesus G, Bizzozero OA (2002) Effect of 2-fluoropalmitate, cerulenin and tunicamycin on the palmitoylation and intracellular translocation of myelin proteolipid protein. *Neurochem Res* **27**: 1669–1675.
398. Oakes ND, Kjellstedt A, Forsberg G-B, Clementz T, Camejo G, Furler SM, Kraegen EW, Ölwegård-Halvarsson M, Jenkins AB, Ljung B (1999) Development and initial evaluation of a novel method for assessing tissue-specific plasma free fatty acid utilization in vivo using (R)-2-bromopalmitate tracer. *J Lipid Res* **40**: 1155–1169.
399. Zhou F, Xue Y, Yao X, Xu Y (2006) A general user interface for prediction servers of proteins' post-translational modification sites. *Nature Protocols* **1**: 1318–1321.
400. de la Cruz F, Frost LS, Meyer RJ, Zechner EL (2010) Conjugative DNA metabolism in Gram-negative bacteria. *FEMS Microbiol Rev* **34**: 18–40.
401. Lee S, Sowa ME, Watanabe Y, Sigler PB, Chiu W, Yoshida M, Tsai FTF (2003) The structure of ClpB: a molecular chaperone that rescues proteins from an aggregated state. *Cell* **115**: 229–240.
402. Doyle SM, Wickner S (2009) Hsp104 and ClpB: protein disaggregating machines. *Trends Biochem Sci* **34**: 40–48.
403. Rodriguez EA, Campbell RE, Lin JY, Lin MZ, Miyawaki A, Palmer AE, Shu X, Zhang J, Tsien RY (2017) The Growing and Glowing Toolbox of Fluorescent and Photoactive Proteins. *Trends Biochem Sci* **42**: 111–129.
404. Babic A, Lindner AB, Vulic M, Stewart EJ, Radman M (2008) Direct visualization of horizontal gene transfer. *Science* **319**: 1533–1536.
405. Slater S, Wold S, Lu M, Boye E, Skarstad K, Kleckner N (1995) E. coli SeqA protein binds oriC in two different methyl-modulated reactions appropriate to its roles in DNA replication initiation and origin sequestration. *Cell* **82**: 927–936.
406. Lu M, Campbell JL, Boye E, Kleckner N (1994) SeqA: a negative modulator of replication initiation in E. coli. *Cell* **77**: 413–426.
407. Brendler T, Abeles A, Austin S (1995) A protein that binds to the P1 origin core and the oriC 13mer region in a methylation-specific fashion is the product of the host seqA gene. *EMBO J* **14**: 4083–4089.
408. WHO, WHO | Antimicrobial resistance: global report on surveillance 2014.
409. Carattoli A (2009) Resistance plasmid families in Enterobacteriaceae. *Antimicrob Agents Chemother* **53**: 2227–2238.
410. Mayr LM, Bojanic D (2009) Novel trends in high-throughput screening. *Curr Opin Pharmacol* **9**: 580–588.
411. Mishra KP, Ganju L, Sairam M, Banerjee PK, Sawhney RC (2008) A review of high throughput technology for the screening of natural products. *Biomed Pharmacother* **62**: 94–98.
412. Lounnas V, Ritschel T, Kelder J, McGuire R, Bywater RP, Foloppe N (2013) Current progress in Structure-Based Rational Drug Design marks a new mindset in drug discovery. *Comput Struct Biotechnol J* **5**: e201302011.
413. Scapin G (2006) Structural biology and drug discovery. *Curr Pharm Des* **12**: 2087–2097.
414. Yung BY, Kornberg A (1988) Membrane attachment activates dnaA protein, the initiation protein of chromosome replication in Escherichia coli. *Proc Natl Acad Sci USA* **85**: 7202–7205.

415. Aranovich A, Gdalevsky GY, Cohen-Luria R, Fishov I, Parola AH (2006) Membrane-catalyzed nucleotide exchange on DnaA. Effect of surface molecular crowding. *J Biol Chem* **281**: 12526–12534.
416. Ripoll-Rozada J, García-Cazorla Y, Getino M, Machón C, Sanabria-Ríos D, de la Cruz F, Cabezón E, Arechaga I (2016) Type IV traffic ATPase TrwD as molecular target to inhibit bacterial conjugation. *Mol Microbiol* **100**: 912–921.
417. Peña A, Arechaga I (2013) Molecular motors in bacterial secretion. *J Mol Microbiol Biotechnol* **23**: 357–369.
418. Cronan JE (1974) Regulation of the Fatty Acid Composition of the Membrane Phospholipids of Escherichia coli. *Proc Natl Acad Sci U S A* **71**: 3758–3762.
419. Furse S, Scott DJ (2016) Three-Dimensional Distribution of Phospholipids in Gram Negative Bacteria. *Biochemistry* **55**: 4742–4747.
420. Yao J, Rock CO (2017) Exogenous fatty acid metabolism in bacteria. *Biochimie* **141**: 30–39.
421. Quevillon-Cheruel S, Leulliot N, Muniz CA, Vincent M, Gallay J, Argentini M, Cornu D, Boccard F, Lemaître B, van Tilbeurgh H (2009) Evf, a virulence factor produced by the Drosophila pathogen Erwinia carotovora, is an S-palmitoylated protein with a new fold that binds to lipid vesicles. *J Biol Chem* **284**: 3552–3562.
422. Jennings BC, Nadolski MJ, Ling Y, Baker MB, Harrison ML, Deschenes RJ, Linder ME (2009) 2-Bromopalmitate and 2-(2-hydroxy-5-nitro-benzylidene)-benzo[b]thiophen-3-one inhibit DHHC-mediated palmitoylation in vitro. *J Lipid Res* **50**: 233–242.
423. Osipovitch M, Lambrecht M, Baker C, Madha S, Mills JL, Craig PA, Bernstein HJ (2015) Automated protein motif generation in the structure-based protein function prediction tool ProMOL. *J Struct Funct Genomics* **16**: 101–111.
424. Das A, Das A (2014) Delineation of polar localization domains of Agrobacterium tumefaciens type IV secretion apparatus proteins VirB4 and VirB11. *Microbiologyopen* **3**: 793–802.
425. Judd PK, Kumar RB, Das A (2005) Spatial location and requirements for the assembly of the Agrobacterium tumefaciens type IV secretion apparatus. *Proc Natl Acad Sci USA* **102**: 11498–11503.
426. Giske CG, Monnet DL, Cars O, Carmeli Y (2008) Clinical and Economic Impact of Common Multidrug-Resistant Gram-Negative Bacilli. *Antimicrob Agents Chemother* **52**: 813–821.
427. Boucher HW, Talbot GH, Bradley JS, Edwards JE, Gilbert D, Rice LB, Scheld M, Spellberg B, Bartlett J (2009) Bad bugs, no drugs: no ESKAPE! An update from the Infectious Diseases Society of America. *Clin Infect Dis* **48**: 1–12.
428. Hooper DC, Wolfson JS, Tung C, Souza KS, Swartz MN (1989) Effects of inhibition of the B subunit of DNA gyrase on conjugation in Escherichia coli. *J Bacteriol* **171**: 2235–2237.
429. Leite JRSA, Silva LP, Rodrigues MIS, Prates MV, Brand GD, Lacava BM, Azevedo RB, Bocca AL, Albuquerque S, Bloch C (2005) Phylloseptins: a novel class of anti-bacterial and anti-protozoan peptides from the Phyllomedusa genus. *Peptides* **26**: 565–573.
430. Conter A, Sturny R, Gutierrez C, Cam K (2002) The RcsCB His-Asp phosphorelay system is essential to overcome chlorpromazine-induced stress in Escherichia coli. *J Bacteriol* **184**: 2850–2853.

Chapter 9
PUBLICATIONS

Marie Curie

Molecular Microbiology (2016) 100(5), 912–921 ■
doi:10.1111/mmi.13359
First published online 22 March 2016

Type IV traffic ATPase TrwD as molecular target to inhibit bacterial conjugation

Jorge Ripoll-Rozada,[1†‡] Yolanda García-Cazorla,[1†] María Getino,[1] Cristina Machón,[1§] David Sanabria-Ríos,[2] Fernando de la Cruz,[1] Elena Cabezón[1*] and Ignacio Arechaga[1*]
[1]*Departamento de Biología Molecular and Instituto de Biomedicina y Biotecnología de Cantabria (IBBTEC), Universidad de Cantabria-CSIC, Santander, Spain.*
[2]*Inter American University of Puerto Rico-Metropolitan Campus, Faculty of Science and Technology, San Juan, Puerto Rico.*

Summary

Bacterial conjugation is the main mechanism responsible for the dissemination of antibiotic resistance genes. Hence, the search for specific conjugation inhibitors is paramount in the fight against the spread of these genes. In this pursuit, unsaturated fatty acids have been found to specifically inhibit bacterial conjugation. Despite the growing interest on these compounds, their mode of action and their specific target remain unknown. Here, we identified TrwD, a Type IV secretion traffic ATPase, as the molecular target for fatty acid-mediated inhibition of conjugation. Moreover, 2-alkynoic fatty acids, which are also potent inhibitors of bacterial conjugation, are also powerful inhibitors of the ATPase activity of TrwD. Characterization of the kinetic parameters of ATPase inhibition has led us to identify the catalytic mechanism by which fatty acids exert their activity. These results open a new avenue for the rational design of inhibitors of bacterial conjugation in the fight against the dissemination of antibiotic resistance genes.

Accepted 19 February, 2016. *For correspondence. E-mail cabezone@unican.es, arechagai@unican.es; Tel. (+34) 942202033; Fax (+34) 942201945. †JRR and YGC contributed equally to this work. ‡Present addresses: Instituto de Biologia Molecular e Celular, Porto, Portugal. §Institut de Biología Molecular de Barcelona (IBMB-CSIC), Spain.

Introduction

Antibiotic resistance has become one of the most challenging problems in health care (WHO-report, 2014), as morbidity and mortality rates upon infection by multiresistant pathogens have sharply increased over the last decades (Boucher *et al.*, 2009; Giske *et al.*, 2009; Hawkey and Jones, 2009; Rice, 2009). One of the main mechanisms whereby bacteria become resistant to antibiotics is the acquisition of antibiotic resistance genes by bacterial conjugation (Mazel and Davies, 1999; Waters, 1999; de la Cruz and Davies, 2000). Therefore, the search for specific *co*njugation *in*hibitors (COINs) is crucial for the control of the dissemination of antibiotic resistance genes. Most compounds reported to inhibit conjugation turned out to be unspecific growth inhibitors (Michel-Briand and Laporte, 1985; Hooper *et al.*, 1989; Conter *et al.*, 2002; Leite *et al.*, 2005; Lujan *et al.*, 2007). Bacterial conjugation has also been reported to be inhibited by the M13 phage coat protein g3p (Lin *et al.*, 2011). However, the most promising results have been obtained with unsaturated fatty acids (uFAs), which specifically inhibit plasmid conjugation without inhibiting *Escherichia coli* growth (Fernández-Lopez *et al.*, 2005; Getino *et al.*, 2015).

Bacterial conjugation is powered by a set of ATPases that energize every single step in the conjugative process: plasmid relaxation and DNA unwinding, DNA transfer, pilus biogenesis and protein transport (for a recent review see Cabezón *et al.*, 2015). These processes are catalyzed by TrwC, TrwB, TrwK and TrwD, which are the VirD2, VirD4, VirB4 and VirB11 homologues in the conjugative plasmid R388 respectively. TrwC is a protein that cleaves the DNA at the origin of transfer and presents relaxase and DNA helicase activities (reviewed in Garcillán-Barcia *et al.*, 2009; de la Cruz *et al.*, 2010). TrwB is a DNA-dependent ATPase that mediates the transfer of DNA to the secretion system (Tato *et al.*, 2005). TrwK is an ATPase (Arechaga *et al.*, 2008) that mediates the dislocation of the pilin molecules from the inner membrane during pilus biogenesis (Kerr and Christie, 2010). The fourth ATPase, TrwD, participates in pilus biogenesis (Kerr and Christie, 2010) and in DNA translocation (Atmakuri *et al.*, 2004), acting as a molecular switch between pilus

biogenesis and substrate transport (Ripoll-Rozada *et al.*, 2013).

Here, we have analyzed the effect of the uFAs on the ATPase activity of all conjugative ATPases. We found that only TrwD, the VirB11 homologue, is inhibited by the same uFAs that inhibit bacterial conjugation *in vivo*. These uFAs did not affect significantly any other ATPase of the T4SS or the DNA mobilization machinery. TrwD (VirB11) belongs to a large family of hexameric AAA^+ traffic ATPases, which includes proteins involved in Type II secretion and in Type IV pilus and flagellar biogenesis (Planet *et al.*, 2001). All members of this superfamily are characterized by the presence of an N-terminal domain (NTD), required for membrane association and a catalytic domain (CTD) connected by a linker region of variable length (Planet *et al.*, 2001; Hare *et al.*, 2006; Peña and Arechaga, 2013). Pivoting of the NTD relative to the CTD over the flexible linker has been proposed to be an essential step in ATP catalysis (Savvides *et al.*, 2003; Yamagata and Tainer, 2007; Ripoll-Rozada *et al.*, 2012). In this work, we have characterized the mechanism of inhibition of TrwD by uFAs. These compounds act as non-competitive inhibitors, with no effect on the affinity of the protein for ATP or ADP substrates. Blind docking of uFAs on the structural model of TrwD led to the identification of a region, comprising the NTD and the linker region of the protein, as the putative uFAs binding site. This result suggests a mechanism of inhibition that prevents the movement of the NTD over the CTD. In consequence, VirB11 traffic ATPases become promising targets for the development of specific COINs based on uFA derivatives. This novel antimicrobial approach opens up new perspectives in the fight against the spread of antibiotic resistance genes.

Results

TrwD is the molecular target of linoleic acid inhibition

Unsaturated fatty acids (uFAs) are inhibitors of bacterial conjugation (Fernández-Lopez *et al.*, 2005). It has been suggested that uFAs might target the conjugation machinery by affecting any of the ATPases associated with the Type IV secretion system (T4SS) of donor cells. In order to determine the specific target of uFAs in our model system, the conjugative plasmid R388, the activity of the four ATPases involved in the conjugative process (TrwB, TrwC, TrwD and TrwK) was analyzed *in vitro* in the presence of 50 μM linoleic acid. At this concentration, 95% reduction of the ATPase activity of TrwD was observed (Fig. 1), whereas no significant effect on the activity of any of the other three ATPases was detected. These results suggest that TrwD is a specific target of uFAs.

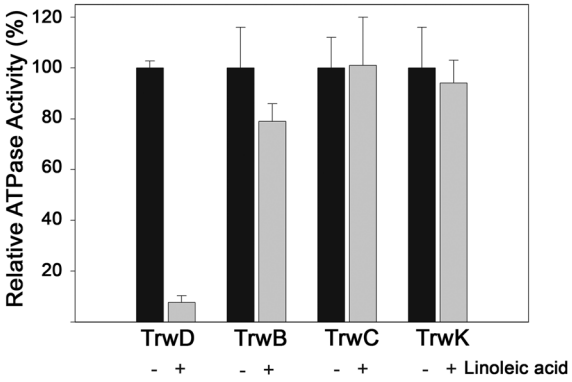

Fig. 1. Effect of linoleic acid on the ATPase activity of conjugative ATPases. ATPase activity by each of the four ATPases that power conjugation (TrwC, TrwB, TrwK and TrwD) (2 μM) was measured in the absence or presence of linoleic acid (50 μM). As ATPase rates are different for each ATPase, hydrolysis activity is expressed as relative ATPase activity (error bars: SD).

Unsaturation of fatty acids is essential for TrwD ATPase inhibition

In contrast to uFAs, saturated fatty acids are not able to inhibit bacterial conjugation (Fernández-Lopez *et al.*, 2005). In order to determine whether there was a correlation between the *in vivo* experiments and the *in vitro* analysis, we tested the effect of different types of fatty acids in TrwD ATPase activity. Oleic ($C_{18:1(9)}$) and linoleic ($C_{18:2\ (9,12)}$) acids (cis-unsaturated C_{18} fatty acids, with one and two double bonds respectively), previously identified as effective inhibitors of bacterial conjugation *in vivo* assays (Fernández-Lopez *et al.*, 2005), were selected as uFAs. Lauric acid ($C_{12:0}$) and Palmitic acid ($C_{16:0}$), which are unable to inhibit significantly R388-mediated conjugation (Fernández-Lopez *et al.*, 2005), were chosen as representative examples of saturated fatty acids. Stearic acid ($C_{18:0}$) is not soluble in our experimental conditions and, therefore, it was not possible to test its effect. TrwD ATPase activity was measured in the presence of each fatty acid (50 μM). At this concentration, oleic and linoleic acids were able to inhibit more than 90% of TrwD ATPase activity whereas in the presence of saturated fatty acids no inhibition was observed (Fig. 2). These results strongly support that the presence of a double bond at C-9 is important for the TrwD ATPase inhibitory activity by uFAs.

2-Alkynoic fatty acids are synthetic inhibitors of TrwD ATPase activity

Synthetic fatty acids, such as the 2-alkynoic fatty acids (2-aFAs), a class of acetylenic fatty acids with one triple bond between the C-2 and C-3 carbons of the alkyl chain, have been found to be effective in inhibiting bacterial conjugation (Getino *et al.*, 2015). In particular, the

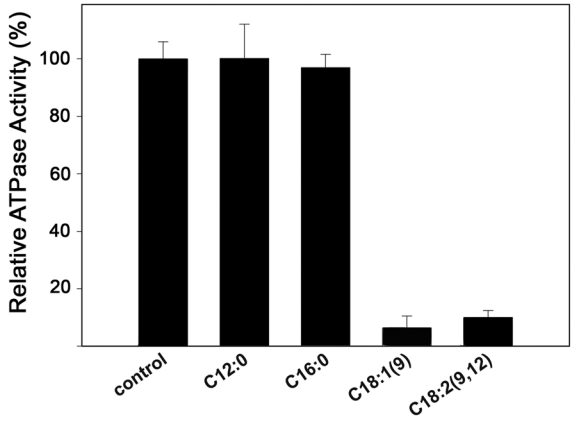

Fig. 2. Effect of saturated and unsaturated fatty acids on TrwD ATPase activity. The ATPase activity of TrwD (2 μM) was measured in the presence of 50 μM lauric ($C_{12:0}$), palmitic ($C_{16:0}$), oleic ($C_{18:1(9)}$) and linoleic ($C_{18:2(9,12)}$) acids (error bars: SD).

three compounds found to be more effective in inhibiting bacterial conjugation were 2-hexadecynoic acid (2-HDA), 2-octadecynoic acid (2-ODA) and 2,6-hexadecadiynoic acid (2,6-HDA). Interestingly, alcohol (OH) or tetrahydropyranyl-ether (THP) derivatives of these compounds were unable to inhibit bacterial conjugation, suggesting an essential role of the carboxylic group in the mechanism of inhibition (Fig. 3A). Therefore, we decided to test whether TrwD was the molecular target of 2-aFAs, as in the case of the linoleic acid. Analysis of TrwD ATPase activity in the presence of 2-aFAs (50 μM) corroborated the results observed *in vivo*, as the same compounds that inhibited bacterial conjugation were also able to inhibit TrwD ATPase activity, whereas those with no effect *in vivo*, such as alcohol or tetrahydropyranyl-ether derivatives, did not have any effect on the *in vitro* TrwD activity (Supporting Information Fig S3). Moreover, the lack of inhibitory effect of these derivatives was still present even at concentrations as high as 500 μM (Fig. 3B). These results strongly reinforce the hypothesis that TrwD is the specific target of both, alkenoic and alkynoic fatty acids.

Inhibition of ATP hydrolysis by fatty acids is non-competitive

With the aim of better understanding the mechanism of inhibition of TrwD ATP hydrolysis by fatty acids, a characterization of the inhibition kinetics was carried out. First, ATPase activity rates of TrwD (2 μM) at increasing concentrations of linoleic acid, 2-HDA 2,6-HDA or 2-ODA were determined (Fig. 4). Analysis of the kinetics of inhibition of TrwD ATPase activity by the four compounds showed a similar inhibition pattern. In all cases, data did not fit to a Michaelis-Menten inhibition kinetic

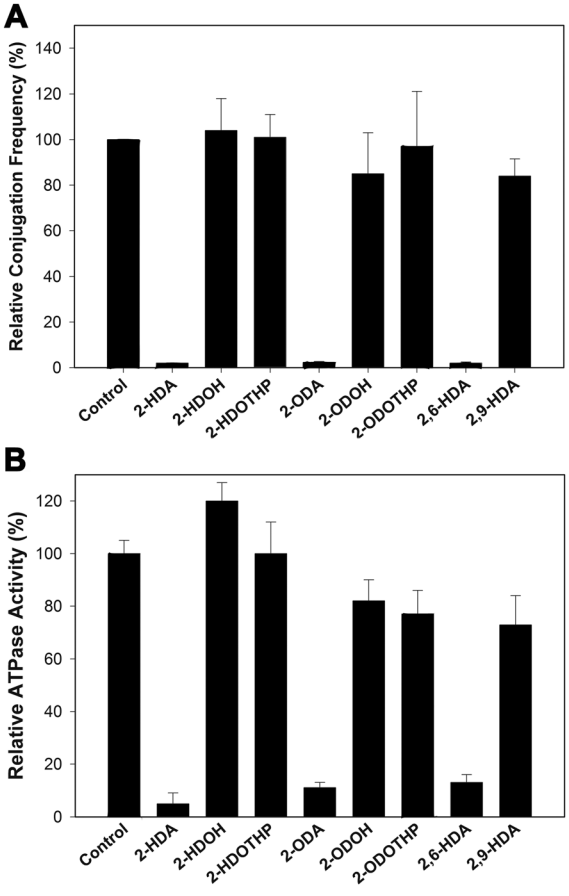

Fig. 3. Effect of 2-alkynoic fatty acids and derivatives on TrwD ATPase activity and bacterial conjugation.
A. Bacterial conjugation was monitored in the presence of 2-alkynoic fatty acid derivatives (500 μM).
B. ATPase activity by TrwD (2 μM) was tested in the presence of 500 μM of 2-octa (2-ODA) and 2-hexa-decynoic acids (2-HDA, 2,6-HDA and 2,9-HDA), and alcohol (-OH) or tetrahydropyranyl-ether (THP) derivatives (error bars: SD).

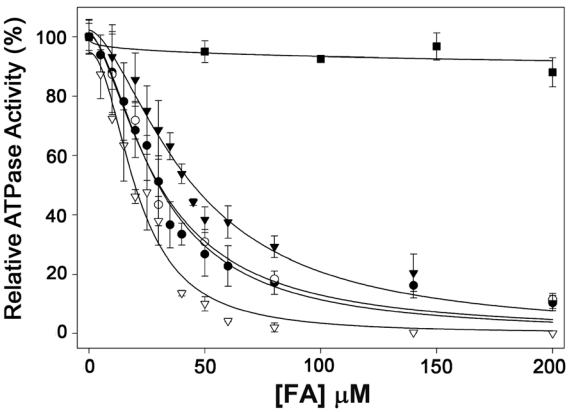

Fig. 4. Determination of the kinetic parameters of inhibition by fatty acids. ATP hydrolysis by TrwD (2 μM) was measured at increasing concentrations of linoleic acid (*white triangles*), 2-HDA (*black circles*), 2-ODA (*white circles*), 2,6-HDA (*black triangles*) and palmitic acid (*black squares*). Data were fitted to a Hill inhibition equation (error bars: SD).

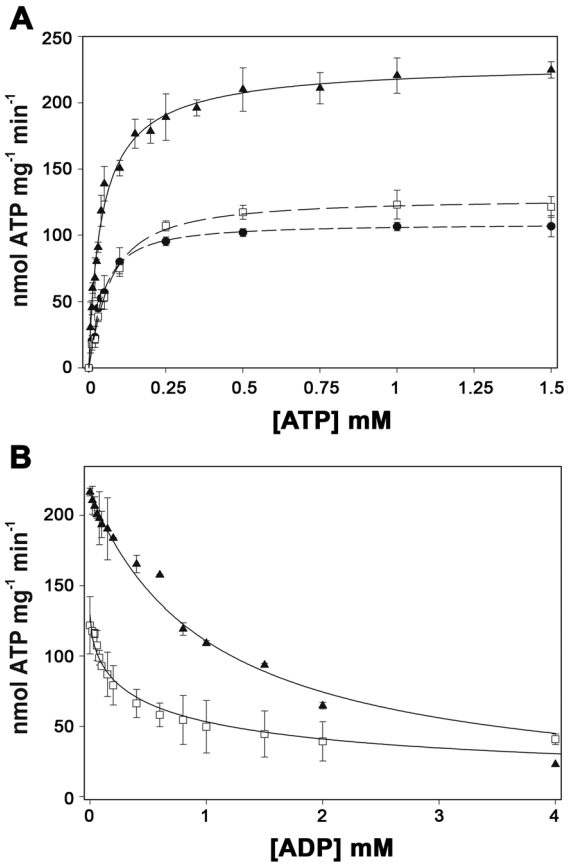

Fig. 5. Effect of fatty acids on nucleotide binding.
A. ATP hydrolysis by TrwD (2 μM) was measured in the presence of 21 μM of linoleic acid (*black circles*) and 30 μM of 2-HDA (*white squares*), and in the absence of fatty acids (*black triangles*). Data were fitted to a Hill equation. The $K_{0.5}^{ATP}$ was 66 μM in the presence of 2-HDA and 44 μM in the presence of linoleic acid and in the absence of added fatty acids.
B. ATP hydrolysis by TrwD (2 μM) was measured at increasing concentrations of ADP in the presence of 30 μM of 2-HDA (white squares) and in its absence (black triangles). Data were fitted as previously described (Ripoll-Rozada *et al.*, 2012). The K_d^{ADP} in the presence of 2-HDA and in the control were 51 μM and 45 μM respectively (error bars: SD).

curve, but to a sigmoidal Hill equation for inhibition, which suggested a cooperative effect in the inhibition kinetics. The apparent inhibition constants ($K_{i[app]}$) of linoleic acid, 2-HDA, 2-ODA and 2,6-HDA were 20.9 ± 1.6 μM, 29.7 ± 2.1 μM, 29.8 ± 4.1 μM and 43.8 ± 2.8 μM respectively.

Further characterization of the mechanism of inhibition at steady-state was conducted in the presence of linoleic acid and 2-HDA. ATP turnover was measured at increasing concentrations of ATP in the presence or absence of fatty acids (Fig. 5A). The concentration of fatty acid was 21 μM linoleic acid or 30 μM 2-HDA, which correspond to their respective $K_{i[app]}$. In both cases, the mechanism of inhibition was non-competitive, as V_{max} was reduced without affecting the $K_{0.5}^{[ATP]}$. This result indicated that ATP binding was not affected by fatty acids.

In order to determine whether the inhibition by uFAs was caused by the stabilization of the enzyme in an ADP inhibited state, we analyzed the effect of ADP on TrwD ATPase activity in the presence and absence of 2-HDA (Fig. 5B). Interestingly, 2-HDA did not affect significantly the affinity of the enzyme for the ADP. In the presence of 2-HDA, the calculated K_d^{ADP} was 51.7 ± 9.8 μM, and its absence this K_d^{ADP} was 45.1 ± 4.1 μM. Altogether, these results show that the inhibitory effect of uFAs was not exerted by modifying the affinities of the enzyme for ATP or for the product, ADP.

Molecular docking of fatty acids into TrwD structure

Kinetic analysis of TrwD inhibition indicated that uFAs were binding to the protein in a site different from the nucleotide binding site, exerting the inhibition without affecting significantly ATP and ADP affinities. In order to explore putative binding sites for uFAs in TrwD, computer assisted analysis was performed. TrwD structural model was built by molecular threading using *Brucella suis* VirB11 (Hare *et al.*, 2006) as a template, as previously described (Supporting Information Fig. S4) (Ripoll-Rozada *et al.*, 2012). Fatty acid ligands were retrieved from Pubchem repository (https://pubchem.ncbi.nlm.nih.gov/) and prepared for docking as described in Methods. Blind docking predictions using the EADock dihedral spacing sampling engine (Grosdidier *et al.*, 2011) of the Swiss-dock server (http://www.swissdock.ch/) showed a region comprised by the NTD (residues 37–54) and the linker region (residues 118–125) of TrwD as the site with the highest probability for 2-HDA and linoleic acid binding (Fig. 6). All binding poses clustered at the same site when the structure of the hexameric form of TrwD was used as a target (Supporting Information Fig. S5). The binding mode with the best energy and Full-Fitness is shown in Fig. 6. Similar results were obtained upon docking of 2-ODA and 2,6-HDA (Supporting Information Fig. S7). Interestingly, tetrahydropyrane derivatives, such as 2-HDOTHP, although were able to fit in the same region, were adopting a different conformation due to the pyranyl ring (Supporting Information Fig. S7).

Docking predictions with palmitic acid suggest that the binding site for this fatty acid is in the same region than the one found for linoleic acid and 2-HDA. However, uFAs and aFAs fill much better the binding pocket.

Partial proteolysis of TrwD in the presence of fatty acids

Blind docking search of 2-HDA and linoleic acid binding sites identified the pocket comprised by the N-terminal domain (NTD) and the linker region of TrwD as the most

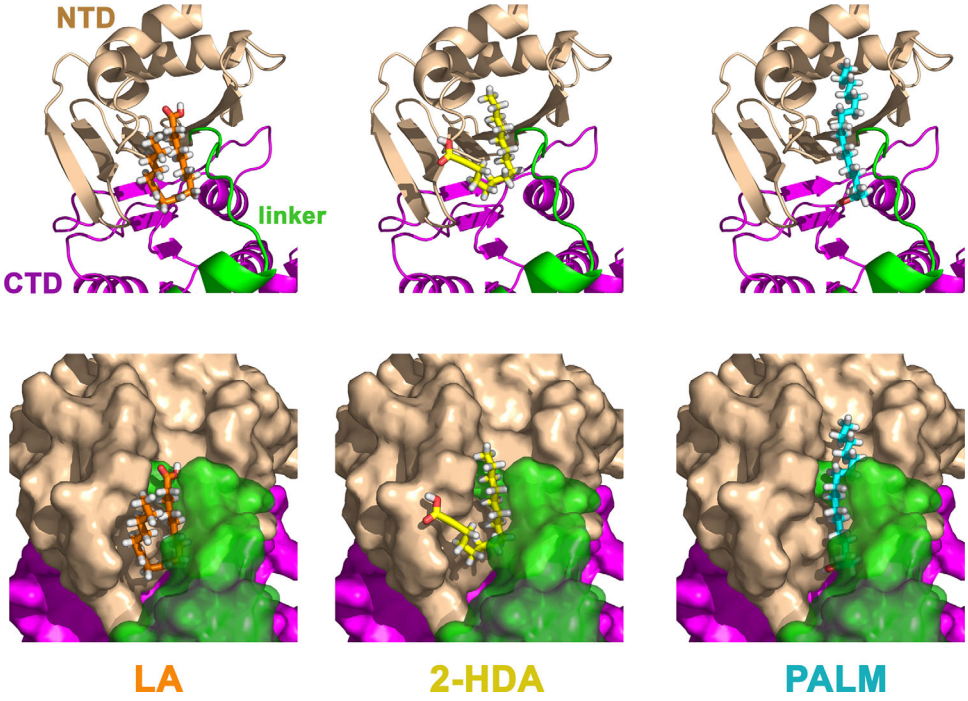

Fig. 6. Blind docking of fatty acids into the molecular model of TrwD. Blind docking predictions between a molecular model of TrwD (Ripoll-Rozada *et al.*, 2012) and fatty acid ligands (linoleic acid (LA), 2-hexadecanoic acid (2-HDA) and palmitic acid (PALM)), were performed using the EADock dihedral spacing sampling engine of the Swissdock server (Grosdidier *et al.*, 2011). Most of the binding poses clustered at a pocket localized at the interface between the N-terminal domain (NTD, *wheat*) and the linker region (*green*), which connects the NTD with the catalytic C-terminal domain (CTD, *purple*). The binding modes with the best energy and Full-Fitness are shown. Upper and bottom panels correspond to the same views in cartoon and surface representations respectively. For clarity, transparency was applied to the linker region (*green*) in the surface representations (*bottom panel*).

likely site for binding (previous section). This linker region is essential during ATP catalysis, since it facilitates the movement of the NTD over the CTD in the catalytic mechanism of TrwD/VirB11 proteins. Therefore, ATPase inhibition by uFAs and aFAs might be caused by protein conformational changes upon fatty acid binding to this region. To test this hypothesis, we analyzed the susceptibility of TrwD to partial digestion by papain in the presence of fatty acids. The unspecific protease papain is useful for delimiting structural domains in proteins, since it presents a low activity on stable secondary and tertiary structures (Karzai and McMacken, 1996). Thus, well-ordered structures would show low susceptibly to papain digestion. Incubation of TrwD with increasing concentrations of 2-HDA (1:10 to 1:100 TrwD: 2-HDA molar ratios) resulted in high susceptibility to papain degradation (Fig. 7). In contrast, similar experiments performed in the presence of palmitic acid (1:100 TrwD: pamitic acid) did not affect the susceptibility of TrwD to papain digestion. These results suggest that 2-HDA binding induces an open conformation of TrwD, resulting in the exposition of protein domains to papain. Such a conformational change was not induced by palmitic acid, which is in accordance with the fact that saturated fatty acids do not exert any inhibitory effect.

Discussion

The search of conjugation inhibitors (COINs) is essential in the fight against multiresistant bacteria. In this pursuit,

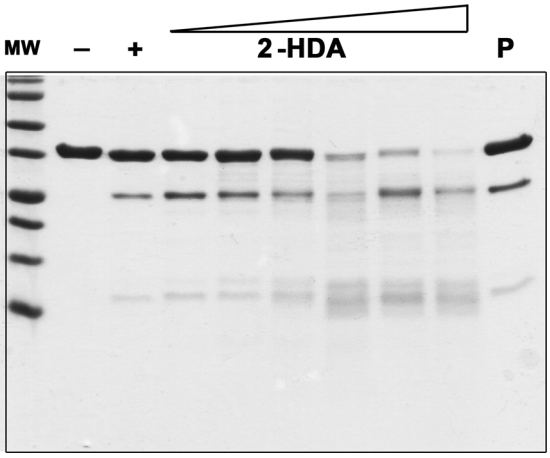

Fig. 7. Partial proteolysis of TrwD by papain. TrwD (*lane* –) was incubated with papain at a molar ratio of 1:80 (TrwD: papain) (*lane* +). Digestion performed in the presence of increasing concentrations of 2-HDA (1:10 to 1:100, TrwD: 2-HDA molar ratios) or palmitic acid (1:100, TrwD: palmitic acid molar ratio, *lane P*) revealed a different proteolysis pattern. Digestion was performed for 90 min at 25°C and proteolytic products were analysed by Tricine- SDS-PAGE (16.5% polyacrylamide gels).

high-throughput (HTS) methods have been developed to identify potential COINs. Although these methods have been widely used by pharmaceutical companies in hit identification (Wu and Doberstein, 2006; Mishra *et al*., 2008; Mayr and Bojanic, 2009), the finding of a molecular target for the structural-based design of new inhibitors could be a powerful tool in the development of new drugs, as it allows the investigation of the interactions between ligands and targets (Scapin, 2006; Lounnas *et al*., 2013). By using one of these HTS assays, uFAs have been identified as effective bacterial conjugation inhibitors (Fernández-Lopez *et al*., 2005). In that sense, the main goal of this work has been the identification and characterization of the molecular target for the inhibition by fatty acids. uFAs are known to affect the function of some proteins that have a transient association with the bacterial membrane, such as the AAA+ ATPase DnaA (Yung and Kornberg, 1988). The ATPase activity of this DNA replication initiator is regulated by acidic phospholipids. The presence of saturated or unsaturated fatty acids on these phospholipids regulates the ADP-ATP exchange in the protein (Aranovich *et al*., 2006). Based on this, we decided to investigate the effect of uFAs on the ATPases involved in bacterial conjugation. In our model system, the conjugative plasmid R388, four ATPases provide the energy for the conjugative process: the relaxase TrwC, the coupling protein TrwB, TrwK and the traffic ATPase TrwD (Cabezón *et al*., 2015). Analysis of ATP hydrolysis rates by each of the four proteins in the presence of linoleic acid showed that only TrwD was inhibited under the tested conditions. This inhibitory effect was observed only in the presence of uFAs, such as oleic and linoleic acids, but not in the presence of saturated fatty acids like lauric or palmitic acids. These results correlate with previous observations, in which uFAs but not saturated ones were able to inhibit bacterial conjugation (Fernández-Lopez *et al*., 2005).

One of the down sides of uFAs is that they are prone to auto-oxidation, which could affect their effectiveness as deliverable COINs. In order to circumvent this, a series of synthetic uFAs containing triple bonds, which belong to the family of 2-alkynoic fatty acids (2-aFAs), were used as alternatives. These compounds are also good conjugation inhibitors (Getino *et al*., 2015). This family of fatty acids has been found to display antibacterial activity against Gram positive bacteria, such as *Staphylococcus aureus* and *Bacillus cereus*, and Gram negative bacteria like *Klebsiella pneumoniae* and *Pseudomonas aeruginosa* (Sanabria-Rios *et al*., 2014; 2015) but they do not have any effect on *E. coli* growth (Konthikamee *et al*., 1982). In our experimental conditions, these compounds did not have any effect on bacterial growth either. Thus, the observed inhibition was specific to bacterial conjugation, which is a desirable property, since it might help to control the dissemination of resistance genes without affecting the growth of commensal bacteria.

The carboxylic acid group of the fatty acid is essential to exert the inhibitory effect, since alcohol or tetrahydropyranyl-ether derivatives of these fatty acids were unable to inhibit TrwD ATPase activity (Fig. 3B). These results are in agreement with *in vivo* experiments in which these derivatives were also unable to inhibit bacterial conjugation (Fig. 3A). These experiments showed that 2-aFAs analogues, like 2-octadecynoic acid (2-ODA) and 2,6-hexadecynoic acid, were also efficient conjugation inhibitors. Fatty acid composition is also important, as unsaturation placed in C-9 instead of C-6, abolished the inhibitory effect of the hexadecynoic acid, both *in vivo* and *in vitro* experiments. Therefore, there is a direct correlation between the *in vivo* and *in vitro* data, as the same compounds able to inhibit bacterial conjugation were also capable of inhibiting TrwD ATPase activity, and *vice versa*, those unable to inhibit conjugation also failed to inhibit TrwD activity.

Kinetic analysis of TrwD ATPase inhibition by linoleic acid and 2-HDA showed similar $K_{i[app]}$ parameters. In addition, ATP titration in the presence of either of the two compounds (at their respective MIC_{50}) revealed no significant variation of the $K_{0.5}^{ATP}$ when compared with the control, whereas the V_{max} value was reduced by half, suggesting a non-competitive inhibition. The affinity for ADP did not change significantly, either. Altogether, these results suggest the presence of a binding site for uFAs and aFAs in TrwD different from the nucleotide binding site.

VirB11 proteins belong to a large superfamily of secretion ATPases (Planet *et al*., 2001), characterized by the presence of two distinct domains, NTD and CTD, connected by a flexible linker. This linker region is of particular importance during ATP catalysis, as movement of the NTD over the CTD has been suggested to be essential for the catalytic mechanism of TrwD/VirB11 (Savvides *et al*., 2003, Ripoll-Rozada *et al*., 2012). This catalytic mechanism has been proposed not only for VirB11 proteins but it has been extended to all members of the secretion ATPase superfamily (Yamagata and Tainer, 2007). According to this mechanism (Fig. 8), in the apo-state the enzyme could adopt two conformations, with the NTD alternating between an open and closed state, but only the open state is able to bind ATP. Upon ATP binding, the NTD closes over the CTD and ATP is hydrolyzed. The release of the γ-phosphate after ATP hydrolysis induces a conformational change to an open state that favours ADP release, so the cycle can resume. In a previous study (Ripoll-Rozada *et al*., 2012), we demonstrated that physiological

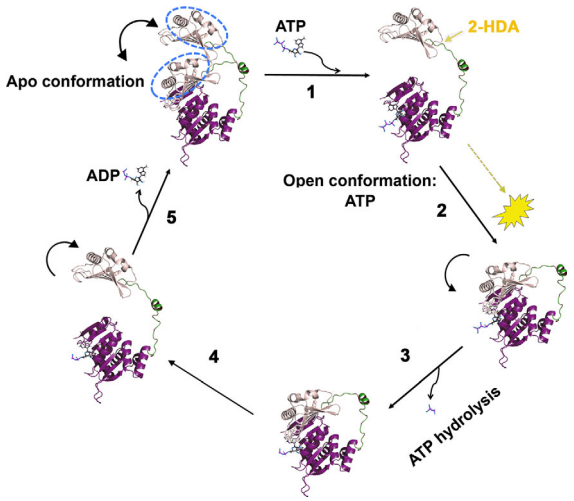

Fig. 8. Mechanistic model of TrwD ATPase inhibition by fatty acids. Proposed mechanism of the catalytic cycle of ATP hydrolysis (adapted from Ripoll-Rozada *et al.*, 2012). According to this mechanism, which is shared by other members of the secretion ATPase superfamily (Yamagata and Tainer, 2007), in an *apo*-conformation, the protein can alternate between an open and a closed state, with the NTD pivoting over the CTD about the linker (*step 1*), but only the open conformation is able to bind ATP. Upon ATP binding, the NTD closes over the CTD (*step 2*) so ATP hydrolysis can take place (*step 3*). After ATP hydrolysis, the NTD opens up (*step 4*) allowing ADP release, so the cycle can resume (*step 5*). Considering that the binding affinities for ATP and ADP are not significantly affected by linoleic acid or 2-HDA, it is likely that the inhibitory effect of these COINs is exerted by preventing the movement of the NTD over the linker, which, in turn, results in inhibition of ATP hydrolysis.

concentrations of Mg^{2+} stabilizes the ADP-state of the enzyme (the affinity for ADP in the presence of Mg^{2+} was 100 times higher than in its absence), which, in turn, prevented the catalytic cycle to resume, thus reducing ATP turnover. In contrast, the results with fatty acids indicate a different mode of inhibition, as the affinty for ADP is hardly affected.

As uFAs do not affect ATP or ADP significantly, they may act over another region of the protein. In fact, blind docking search of a putative binding site identified a pocket comprised by the N-terminal domain (NTD) and the linker region of TrwD with high probability to bind 2-HDA and linoleic acid (Fig. 6). It is likely, then, that binding of uFAs on this region results in the restriction of movement of the NTD over CTD, which, in turn, would result in a reduction of TrwD ATPase activity (Fig. 8). This binding pocket is not present in other VirB11 homologues, such as HP0525 from *Helicobacter pylori* or TraB from conjugative plasmid RP4 (Supporting Information Fig. S4). The absence of this structural domain in TraB could explain previous reports in which no effect of these fatty acids on RP4-mediated conjugation was observed (Fernández-Lopez *et al.*, 2005; Getino *et al.*, 2015).

Further evidence of the conformational changes induced by uFAs was obtained by partial digestion of TrwD with papain, an unspecific protease widely used in the study of conformational modifications of proteins (Karzai and McMacken, 1996). In the presence of 2-HDA, the susceptibility of the protein to the digestion with papain increases (Fig. 7), which reinforces the idea of 2-HDA inducing conformational rearrangements in TrwD structure. Moreover, such conformational changes are not observed in the presence of palmitic acid, even at a 1:100 TrwD: palmitic acid molar ratio, which might explain the inability of saturated acids to inhibit TrwD activity. Although the blind docking search of the palmitic acid revealed a binding site similar to that found for uFAs and 2-HDA, the mode of binding is different. Unsaturated fatty acids acquire a *cis*-conformation which helps them to fill the cavity in the binding site, whereas saturated fatty acids have a rigid straight conformation. The finding of the binding site for uFAs at the NTD is also in accordance with previous data, which suggest that VirB11 proteins interact with the cytoplasmic site of the membrane through the NTD (Yeo *et al.*, 2000). In addition, TrwD ATPase activity is stimulated by phospholipids (Rivas *et al.*, 1997), and the protein has been shown to interact with phospholipids in lipid vesicles (Machón *et al.*, 2002). Thus, it is very likely that uFAs and aFAs are occupying a binding site in TrwD, which is otherwise occupied by bacterial membrane phospholipids involved in the association of the protein to the membrane. In fact, *E. coli* cells treated with 2-HDA incorporate this fatty acid into the phospholipids (D.J. Sanabria-Rios *et al.*, unpubl. obs.). This result would make possible the *in vivo* interaction of 2-HDA with the membrane associated form of TrwD. Paradoxically, uFAs were also reported to inhibit conjugation of F-like plasmids (Getino *et al.*, 2015) although no VirB11 homologue has yet been identified in F plasmids, begging the question of which is the target of COIN inhibition in F-like plasmids. Given the fact that F-like plasmids are narrow host range (i.e. appear only in *Enterobacteriaceae*), it is tempting to speculate that the VirB11 function is carried out by a traffic ATPase provided by the host.

In summary, in this work we have identified the conjugative T4SS traffic ATPase TrwD as the target for the inhibition of bacterial conjugation by fatty acids. The finding of conjugative traffic ATPases as potential targets for inhibiting bacterial conjugation opens a new avenue for the development of rational design drugs based on the interactions between this protein and potential inhibitors, which may help in the fight against the emergence of antibiotic multiresistant bacteria. Future research should address the development of compounds with

increased affinities for the target capable to inhibit conjugation irreversibility.

Experimental procedures

Cloning, overexpression and purification of proteins

Cloning, overexpression and purification of TrwD, TrwC, TrwB and TrwK were carried out as described previously (Grandoso *et al*., 1994; Tato *et al*., 2005; Arechaga *et al*., 2008; Ripoll-Rozada *et al*., 2012). TrwC purification was modified as follows. After a P11 phosphocellulose column (Whatman), TrwC-enriched fractions were pooled and applied to a HiTrap SP-Sepharose (5 ml) column (Amersham, GE), followed by a Mono S HR 5/5 (1 ml) column (Amersham, GE). Protein was eluted from both columns in a linear gradient of NaCl. Finally, the protein was concentrated and loaded onto a 200 HR Superdex column (Amersham, GE). Fractions were pooled and stored as described previously (Grandoso *et al*., 1994).

Chemicals and inhibitory compounds

Commercial fatty acids were purchased from Sigma-Aldrich (St. Louis, MO, USA). The 2-alkynoic fatty acids (2-aFAs) and derivatives were synthesized as described in Carballeira *et al*., 2006; 2012. Alcohol, methyl ester and tetrahydropyranyl ether compounds derivatives were obtained as described in Sanabria-Rios *et al*. (2014).

ATP hydrolysis assays

Steady-state ATP hydrolysis activity was measured with the EnzCheck™ Kit (Invitrogen) in a UV-1800 spectrophotometer (Shimadzu). Inorganic phosphate (Pi) released after ATP hydrolysis was monitored as an increase of absorption at 360 nm for 10 min following manufacturer's instructions and components: 0.2 mM of 2-amino-6-mercapto-7-methylpurine riboside (MESG) and 1 U/ml of purine nucleoside phosphorylase (PNP). A specific buffer was used for each ATPase to register ATP hydrolysis at optimal conditions. TrwD and TrwC ATP hydrolysis rates were determined in buffer DC (50 mM Tris-HCl pH 8.5, 75 mM potassium acetate, 10 μM magnesium acetate and 10% glycerol (w/v)). ATP hydrolysis by TrwB and TrwK was measured in buffers B and K respectively. Buffer B; 50 mM Pipes-NaOH pH 6.2, 35 mM sodium chloride, 5 mM magnesium acetate and 5% glycerol (w/v). Buffer K; 50 mM Pipes-NaOH pH 6.45, 75 mM potassium acetate, 10 mM magnesium acetate, 5% glycerol (w/v), 1 mM sodium acetate, 1 mM DTT and 0.1 mM EDTA. Before starting the reaction by adding the corresponding ATPase, ATP and fatty acids diluted in DMSO were added to the concentrations indicated in the text.

Conjugation assays

Conjugation frequencies were estimated using the high-throughput conjugation method previously described (Getino *et al*., 2015). *E. coli* DH5α and BL21(DE3) strains were used as donor and recipient strains respectively. Cells were mixed in 1:1 ratio and spotted onto LB-agar plates with different compounds. Mating plates were incubated at 37°C for 6 h and bacteria were resuspended in M9 broth. OD_{600} and GFP emission from transconjugant cells were measured to quantify R388 transfer.

Papain proteolysis

Limited papain digestions were performed as described in Ripoll-Rozada *et al*. (2012) with some modifications. Papain digestion was performed at 25°C in 20 mM Tris (pH 8.5), 75 mM AcK, 10% (w/v) glycerol. Papain stocks were dissolved in the same buffer and activated by addition of 50 mM β-mercaptoethanol (37°C, 30 min) just before use. TrwD (18 μM) was incubated for 15 min at 25°C in the presence fatty acids (2-HDA or palmitic acid). Proteolysis was initiated by addition of papain from the activated stocks at 1:80 papain: TrwD molar ratios. The reaction was stopped after 90 min at 25°C by addition of 100 μM E-64 inhibitor (Sigma). Proteolysis products were analyzed by Tricine-SDS-PAGE (16.5% polyacrylamide gels) followed by staining with Coomassie Brilliant Blue.

Molecular modelling and ligand docking

An atomic model of TrwD was generated by molecular threading using as template the atomic coordinates of *B. suis* VirB11 (2gza.pdb) (Hare *et al*., 2006), as previously described (Ripoll-Rozada *et al*., 2012). The structural coordinates of 2-hexadecynoic acid (2-HDA) and linoleic acid were retrieved from PubChem database (https://pubchem.ncbi.nlm.nih.gov/). Molecules were prepared for docking using the DockPrep tool of UCSF Chimera software package (Pettersen *et al*., 2004). This involved the addition of hydrogens, the replacement of incomplete side chains with Dunbrack rotamer library (Dunbrack, 2002), the removal of solvent water molecules, and the inclusion of partial charges using AMBERff12SB force field. Files containing the atomic coordinates of the target protein and the fatty acids were submitted to the SwissDock server (http://www.swissdock.ch/), which uses an EADock dihedral spacing sampling (DSS) engine for docking drug-like ligands into macromolecules (Grosdidier *et al*., 2011). Docking runs were blind performed over the entire molecule, without defining any specific region of the protein in order to prevent bias. Results were examined with UCSF chimera and outer clusters were ranked according to Full-Fitness (FF) score of Swissdock. Binding poses with the best FF score and minimal energy were finally selected. Structural molecular representations were rendered with PyMOL (DeLano, 2008). Control runs were performed with the atomic coordinates of VirB11 from *B. suis* (2gza.pdb) (Hare *et al*., 2006) and HP0525 from *H. pylori* (1g6o.pdb) (Yeo *et al*., 2000) as target molecules. Electrostatic potential maps were calculated with the PDB2PQR application (Dolinsky *et al*., 2007), using PROPKA for pKa calculations, and the resulting APBS files (Baker *et al*., 2001) were rendered with Pymol.

Acknowledgements

This work was supported by the Spanish Ministerio de Economía y Competitividad (MINECO) grants BFU2011-22874 (to

E.C. and I.A.) and BFU2014-55534 (to F.D.L.C.) and EU VII Framework Program projects 282004/FP7-HEALTH-2011-2.3.1-2 and 612146/ICT-2013-10 (to F.D.L.C.). D.S.R. thanks the support of the National Center for Research Resources and the National Institute of General Medical Sciences of the National Institutes of Health through Grant Number 5P20GM103475-13 and the Inter American University of Puerto Rico. The authors declare that they do not have any conflict of interest.

References

Aranovich, A., Gdalevsky, G.Y., Cohen-Luria, R., Fishov, I., and Parola, A.H. (2006) Membrane-catalyzed nucleotide exchange on DnaA. Effect of surface molecular crowding. *J Biol Chem* **281**: 12526–12534.

Arechaga, I., Peña, A., Zunzunegui, S., del Carmen Fernandez-Alonso, M., Rivas, G., and de la Cruz, F. (2008) ATPase activity and oligomeric state of TrwK, the VirB4 homologue of the plasmid R388 type IV secretion system. *J Bacteriol* **190**: 5472–5479.

Atmakuri, K., Cascales, E., and Christie, P.J. (2004) Energetic components VirD4, VirB11 and VirB4 mediate early DNA transfer reactions required for bacterial type IV secretion. *Mol Microbiol* **54**: 1199–1211.

Baker, N.A., Sept, D., Joseph, S., Holst, M.J., and McCammon, J.A. (2001) Electrostatics of nanosystems: application to microtubules and the ribosome. *Proc Natl Acad Sci U S A* **98**: 10037–10041.

Boucher, H.W., Talbot, G.H., Bradley, J.S., Edwards, J.E., Gilbert, D., Rice, L.B., Scheld, M., Spellberg, B., and Bartlett, J. (2009) Bad bugs, no drugs: no ESKAPE! An update from the Infectious Diseases Society of America. *Clin Infect Dis* **48**: 1–12.

Cabezón, E., Ripoll-Rozada, J., Peña, A., de la Cruz, F., and Arechaga, I. (2015) Towards an integrated model of bacterial conjugation. *FEMS Microbiol Rev* **39**: 81–95.

Carballeira, N.M., Sanabria, D., Cruz, C., Parang, K., Wan, B., and Franzblau, S. (2006) 2,6-Hexadecadiynoic acid and 2,6-nonadecadiynoic acid: novel synthesized acetylenic fatty acids as potent antifungal agents. *Lipids* **41**: 507–511.

Carballeira, N.M., Cartagena, M., Sanabria, D., Tasdemir, D., Prada, C.F., Reguera, R.M., and Balana-Fouce, R. (2012) 2-Alkynoic fatty acids inhibit topoisomerase IB from Leishmania donovani. *Bioorg Med Chem Lett* **22**: 6185–6189.

Conter, A., Sturny, R., Gutierrez, C., and Cam, K. (2002) The RcsCB His-Asp phosphorelay system is essential to overcome chlorpromazine-induced stress in *Escherichia coli*. *J Bacteriol* **184**: 2850–2853.

de la Cruz, F., and Davies, J. (2000) Horizontal gene transfer and the origin of species: lessons from bacteria. *Trends Microbiol* **8**: 128–133.

de la Cruz, F., Frost, L.S., Meyer, R.J., and Zechner, E.L. (2010) Conjugative DNA metabolism in Gram-negative bacteria. *FEMS Microbiol Rev* **34**: 18–40.

DeLano, W.L. (2008) *The PyMOL Molecuar Graphics System*. Palo Alto, CA: DeLano Scientific LLC.

Dolinsky, T.J., Czodrowski, P., Li, H., Nielsen, J.E., Jensen, J.H., Klebe, G., and Baker, N.A. (2007) PDB2PQR: expanding and upgrading automated preparation of biomolecular structures for molecular simulations. *Nucleic Acids Res* **35**: W522–W525.

Dunbrack, R.L., Jr. (2002) Rotamer libraries in the 21st century. *Curr Opin Struct Biol* **12**: 431–440.

Fernández-Lopez, R., Machon, C., Longshaw, C.M., Martin, S., Molin, S., Zechner, E.L., *et al.* (2005) Unsaturated fatty acids are inhibitors of bacterial conjugation. *Microbiology* **151**: 3517–3526.

Garcillán-Barcia, M.P., Francia, M.V., and de la Cruz, F. (2009) The diversity of conjugative relaxases and its application in plasmid classification. *FEMS Microbiol Rev* **33**: 657–687.

Getino, M., Campos, J., Fernández-López, R., Fernández, A., Caballeira, N.M., Sanabria-Ríos, D.J., and de la Cruz, F. (2015) 2-alkynoic fatty acids as chemically stable conjugation inhibitors. *mBio* **6**: e01032–e01015.

Giske, C.G., Sundsfjord, A.S., Kahlmeter, G., Woodford, N., Nordmann, P., Paterson, D.L., *et al.* (2009) Redefining extended-spectrum beta-lactamases: balancing science and clinical need. *J Antimicrob Chemother* **63**: 1–4.

Grandoso, G., Llosa, M., Zabala, J.C., and de la Cruz, F. (1994) Purification and biochemical characterization of TrwC, the helicase involved in plasmid R388 conjugal DNA transfer. *Eur J Biochem* **226**: 403–412.

Grosdidier, A., Zoete, V., and Michielin, O. (2011) SwissDock, a protein-small molecule docking web service based on EADock DSS. *Nucleic Acids Res* **39**: W270–W277.

Hare, S., Bayliss, R., Baron, C., and Waksman, G. (2006) A large domain swap in the VirB11 ATPase of *Brucella suis* leaves the hexameric assembly intact. *J Mol Biol* **360**: 56–66.

Hawkey, P.M., and Jones, A.M. (2009) The changing epidemiology of resistance. *J Antimicrob Chemother* **64**: i3–i10.

Hooper, D.C., Wolfson, J.S., Tung, C., Souza, K.S., and Swartz, M.N. (1989) Effects of inhibition of the B subunit of DNA gyrase on conjugation in *Escherichia coli*. *J Bacteriol* **171**: 2235–2237.

Karzai, A.W., and McMacken, R. (1996) A bipartite signaling mechanism involved in DnaJ-mediated activation of the *Escherichia coli* DnaK protein. *J Biol Chem* **271**: 11236–11246.

Kerr, J.E., and Christie, P.J. (2010) Evidence for VirB4-mediated dislocation of membrane-integrated VirB2 pilin during biogenesis of the *Agrobacterium* VirB/VirD4 type IV secretion system. *J Bacteriol* **192**: 4923–4934.

Konthikamee, W., Gilbertson, J.R., Langkamp, H., and Gershon, H. (1982) Effect of 2-alkynoic acids on in vitro growth of bacterial and mammalian cells. *Antimicrob Agents Chemother* **22**: 805–809.

Leite, J.R., Silva, L.P., Rodrigues, M.I., Prates, M.V., Brand, G.D., Lacava, B.M., *et al.* (2005) Phylloseptins: a novel class of anti-bacterial and anti-protozoan peptides from the *Phyllomedusa* genus. *Peptides* **26**: 565–573.

Lin, A., Jimenez, J., Derr, J., Vera, P., Manapat, M.L., Esvelt, K.M., *et al.* (2011) Inhibition of bacterial conjugation by phage M13 and its protein g3p: quantitative analysis and model. *PLoS One* **6**: e19991.

Lounnas, V., Ritschel, T., Kelder, J., McGuire, R., Bywater, R.P., and Foloppe, N. (2013) Current progress in Structure-Based Rational Drug Design marks a new mindset in drug discovery. *Comput Struct Biotechnol J* **5**: e201302011.

Lujan, S.A., Guogas, L.M., Ragonese, H., Matson, S.W., and Redinbo, M.R. (2007) Disrupting antibiotic resistance propagation by inhibiting the conjugative DNA relaxase. *Proc Natl Acad Sci U S A* **104**: 12282–12287.

Machón, C., Rivas, S., Albert, A., Goñi, F.M., and de la Cruz, F. (2002) TrwD, the hexameric traffic ATPase encoded by plasmid R388, induces membrane destabilization and hemifusion of lipid vesicles. *J Bacteriol* **184**: 1661–1668.

Mayr, L.M., and Bojanic, D. (2009) Novel trends in high-throughput screening. *Curr Opin Pharmacol* **9**: 580–588.

Mazel, D., and Davies, J. (1999) Antibiotic resistance in microbes. *Cell Mol Life Sci* **56**: 742–754.

Michel-Briand, Y., and Laporte, J.M. (1985) Inhibition of conjugal transfer of R plasmids by nitrofurans. *J Gen Microbiol* **131**: 2281–2284.

Mishra, K.P., Ganju, L., Sairam, M., Banerjee, P.K., and Sawhney, R.C. (2008) A review of high throughput technology for the screening of natural products. *Biomed Pharmacother* **62**: 94–98.

Peña, A., and Arechaga, I. (2013) Molecular motors in bacterial secretion. *J Mol Microbiol Biotechnol* **23**: 357–369.

Pettersen, E.F., Goddard, T.D., Huang, C.C., Couch, G.S., Greenblatt, D.M., Meng, E.C., and Ferrin, T.E. (2004) UCSF Chimera – a visualization system for exploratory research and analysis. *J Comput Chem* **25**: 1605–1612.

Planet, P.J., Kachlany, S.C., DeSalle, R., and Figurski, D.H. (2001) Phylogeny of genes for secretion NTPases: identification of the widespread tadA subfamily and development of a diagnostic key for gene classification. *Proc Natl Acad Sci U S A* **98**: 2503–2508.

Rice, L.B. (2009) The clinical consequences of antimicrobial resistance. *Curr Opin Microbiol* **12**: 476–481.

Ripoll-Rozada, J., Peña, A., Rivas, S., Moro, F., de la Cruz, F., Cabezón, E., and Arechaga, I. (2012) Regulation of the type IV secretion ATPase TrwD by magnesium: implications for catalytic mechanism of the secretion ATPase superfamily. *J Biol Chem* **287**: 17408–17414.

Ripoll-Rozada, J., Zunzunegui, S., de la Cruz, F., Arechaga, I., and Cabezón, E. (2013) Functional interactions of VirB11 traffic ATPases with VirB4 and VirD4 molecular motors in type IV secretion systems. *J Bacteriol* **195**: 4195–4201.

Rivas, S., Bolland, S., Cabezón, E., Goñi, F.M., and de la Cruz, F. (1997) TrwD, a protein encoded by the IncW plasmid R388, displays an ATP hydrolase activity essential for bacterial conjugation. *J Biol Chem* **272**: 25583–25590.

Sanabria-Rios, D.J., Rivera-Torres, Y., Maldonado-Dominguez, G., Dominguez, I., Rios, C., Diaz, D., *et al.* (2014) Antibacterial activity of 2-alkynoic fatty acids against multidrug-resistant bacteria. *Chem Phys Lipids* **178**: 84–91.

Sanabria-Rios, D.J., Rivera-Torres, Y., Rosario, J., Gutierrez, R., Torres-Garcia, Y., Montano, N., *et al.* (2015) Chemical conjugation of 2-hexadecynoic acid to C5-curcumin enhances its antibacterial activity against multi-drug resistant bacteria. *Bioorg Med Chem Lett* **25**: 5067–5071.

Savvides, S.N., Yeo, H.J., Beck, M.R., Blaesing, F., Lurz, R., Lanka, E., *et al.* (2003) VirB11 ATPases are dynamic hexameric assemblies: new insights into bacterial type IV secretion. *EMBO J* **22**: 1969–1980.

Scapin, G. (2006) Structural biology and drug discovery. *Curr Pharm Des* **12**: 2087–2097.

Tato, I., Zunzunegui, S., de la Cruz, F., and Cabezón, E. (2005) TrwB, the coupling protein involved in DNA transport during bacterial conjugation, is a DNA-dependent ATPase. *Proc Natl Acad Sci U S A* **102**: 8156–8161.

Waters, V.L. (1999) Conjugative transfer in the dissemination of beta-lactam and aminoglycoside resistance. *Front Biosci* **4**: D433–D456.

WHO-report (2014) Antimicrobial Resistance. Global report on surveillance. World Health Organization. Geneva, Switzerland. URL http://www.who.int/drugresistance/documents/surveillancereport/en/

Wu, G., and Doberstein, S.K. (2006) HTS technologies in biopharmaceutical discovery. *Drug Discov Today* **11**: 718–724.

Yamagata, A., and Tainer, J.A. (2007) Hexameric structures of the archaeal secretion ATPase GspE and implications for a universal secretion mechanism. *EMBO J* **26**: 878–890.

Yeo, H.J., Savvides, S.N., Herr, A.B., Lanka, E., and Waksman, G. (2000) Crystal structure of the hexameric traffic ATPase of the *Helicobacter pylori* type IV secretion system. *Mol Cell* **6**: 1461–1472.

Yung, B.Y., and Kornberg, A. (1988) Membrane attachment activates dnaA protein, the initiation protein of chromosome replication in *Escherichia coli*. *Proc Natl Acad Sci U S A* **85**: 7202–7205.

Supporting information

Additional supporting information may be found in the online version of this article at the publisher's web-site.

SUPPLEMENTARY INFORMATION

Type IV traffic ATPase TrwD as molecular target to inhibit bacterial conjugation

Jorge Ripoll-Rozada,[1†#] Yolanda García-Cazorla,[1#] María Getino,[1] Cristina Machón,[1±] David Sanabria-Ríos,[2] Fernando de la Cruz,[1] Elena Cabezón,[1*] Ignacio Arechaga[a*]

[1]Departamento de Biología Molecular and Instituto de Biomedicina y Biotecnología de Cantabria (IBBTEC), Universidad de Cantabria- CSIC, Santander, Spain. [2]Inter American Univerisity of Puerto Rico-Metropolitan Campus, Faculty of Science and Technology, San Juan, Puerto Rico. [†]Present address: Instituto de Biologia Molecular e Celular, Porto, Portugal. [±]Present address: Institut de Biología Molecular de Barcelona (IBMB-CSIC), Spain.

[*]Address correspondence to: Elena Cabezón (cabezone@unican.es) & Ignacio Arechaga (arechagai@unican.es)

Figures included as Supplementary Information:

-Fig. S1: Chemical formula of saturated and unsaturated fatty acids used in this study.

-Fig. S2: Chemical formula of 2-alkynoic fatty acids and derivatives used in this study.

-Fig. S3: Effect of 2-alkynoic fatty acids and derivatives on TrwD ATPase activity. This figure complements Fig.3B, but using 50 μM concentration of fatty acid instead of 500 μM.

-Fig. S4: Structure of VirB11 proteins. Models of VirB11 from *Brucella suis*, TrwD from conjugative plasmid R388, HP0525 from *Helicobacter pylori* and TraB from RP4 plasmid are shown.

-Fig.S5: Side and top views of TrwD hexamer and 2-HDA docking. This figure complements Fig.6. It shows all 2-HDA binding poses on the hexameric form of trwD.

-Fig.S6: Docking of 2-HDA into the TrwD model. This figure complements Fig.6. It highlights the putative location of 2-HDA carboxylate group.

-Fig. S7. Docking of 2-alkynoic fatty acids and derivatives into TrwD. This figure complements Fig.6. It shows the binding of 2-HDA, 2,6-HDA and 2-ODA, as example of effective inhibitors, and 2-HDOTHP as example of a compound with no effect.

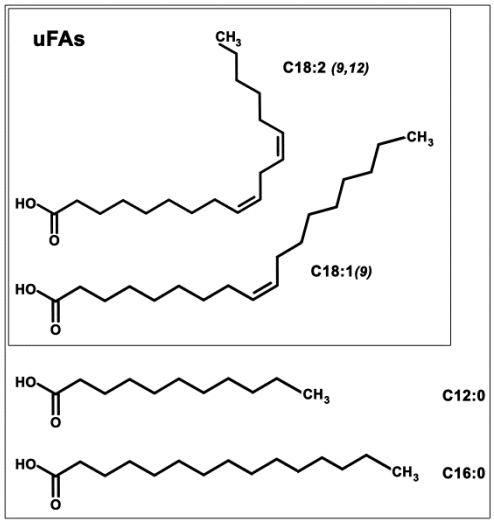

Fig. S1. **Saturated and unsaturated fatty acids used in this study**. TrwD ATPase activity was monitored in the presence of lauric (C12:0), palmitic (C16:0), oleic (C18:1*(9)*) or linoleic (C18:2*(9,12)* acids, as representatives of saturated and unsaturated fatty acids, respectively.

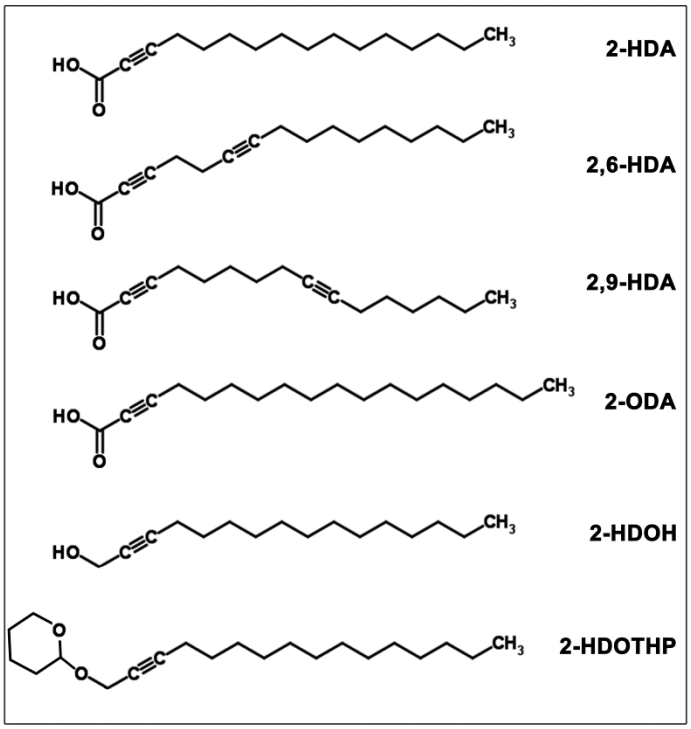

Fig.S2. **2-alkynoic fatty acids and derivatives used in this study**. TrwD ATPase activity was monitored in the presence of 2-hexadecynoic acid (2-HDA), 2-octadecynoic acid (2-ODA), 2,6-hexadecadiynoic acid (2,6-HDA), 2,9-hexadecadiynoic acid (2,9-HDA) and their corresponding alcohol (OH) or tetrahydropyranyl-ether (THP) derivatives. For simplicity, only the 2-HDA derivatives, 2-HDOH and 2-HDOTHP derivatives are shown.

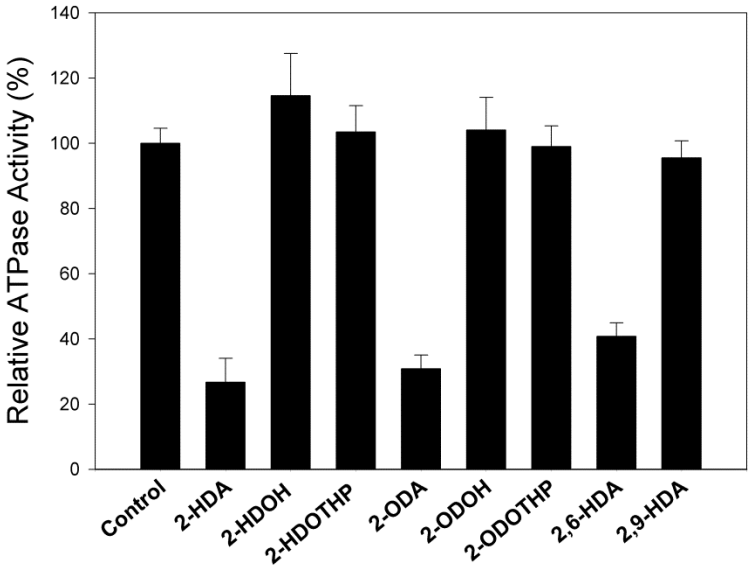

Fig. S3.- **Effect of 2-alkynoic fatty acids and derivatives on TrwD ATPase activity.** ATPase activity by TrwD (2 μM) was tested in the presence of 50 μM of 2-octa (2-ODA) and 2-hexa-decynoic acids (2-HDA, 2,6-HDA and 2,9-HDA), and alcohol (-OH) or tetrahydropyranyl-ether (THP) derivatives. (error bars: SD).

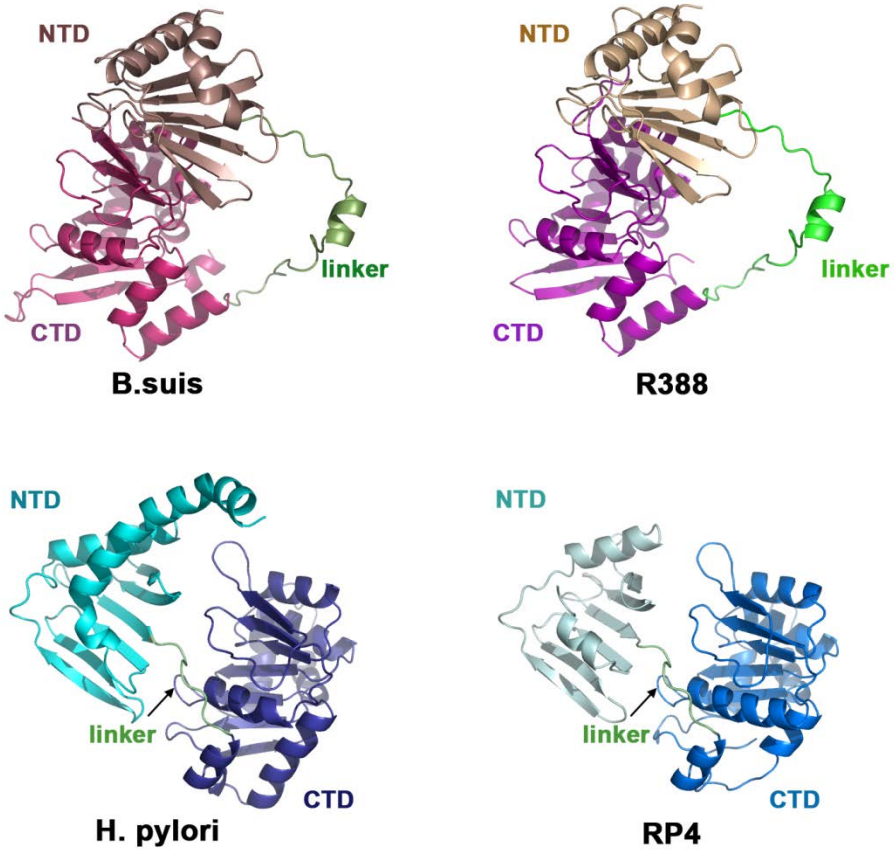

Fig. S4.- **Structure of VirB11 proteins**. VirB11 proteins are members of the superfamily of traffic AAA+ ATPases. The atomic structures of VirB11 from *Brucella suis* (2gza.pdb) and HP0525, its homolog in *Helicobacter pylori* (1g6O.pdb) are known. Models of TrwD of plasmid R388 and TraB of plasmid RP4, obtained by molecular threading using *B. suis* and *H. pylori* structures as templates, respectively, have been previously described (Ripoll-Rozada et al., 2012, Ripoll-Rozada et al, 2013). The general architecture of these proteins consists of an N-terminal domain (NTD), suggested to interact with the membrane, and a catalytic C-terminal domain (CTD) connected by a linker region. The size of the linker is very short in *H. pylori* and RP4 homologs, in comparison to the linker of *B. suis* and R388 counterparts. As a consequence, the NTD-CTD inter-domain interactions are different in both types of structures.

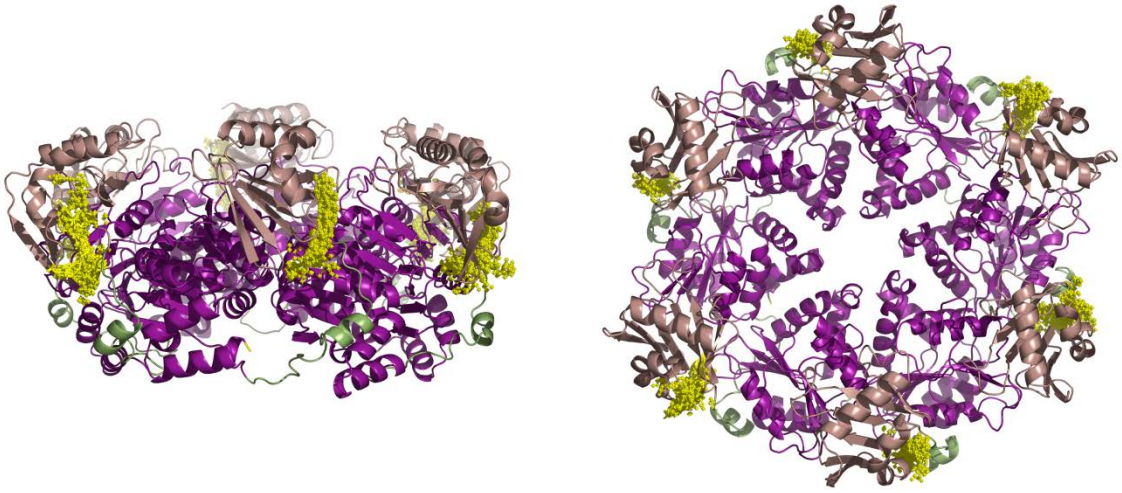

Fig.S5.- **Side and top views of TrwD hexamer and 2-HDA docking**. Blind docking of 2-HDA (*yellow*) into hexameric TrwD using SwissDock (http://www.swissdock.ch), an EADock dihedral spacing sampling engine (Grosdidier *et al.*, 2011). All the hits retrieved from Swissdock (256 compounds) were grouped in 6 clusters. Each of these clusters was mapping exactly the same region within each monomer, in a pocket comprised between the N-terminal domain (*salmon*) and the linker region of the protein (*green*).

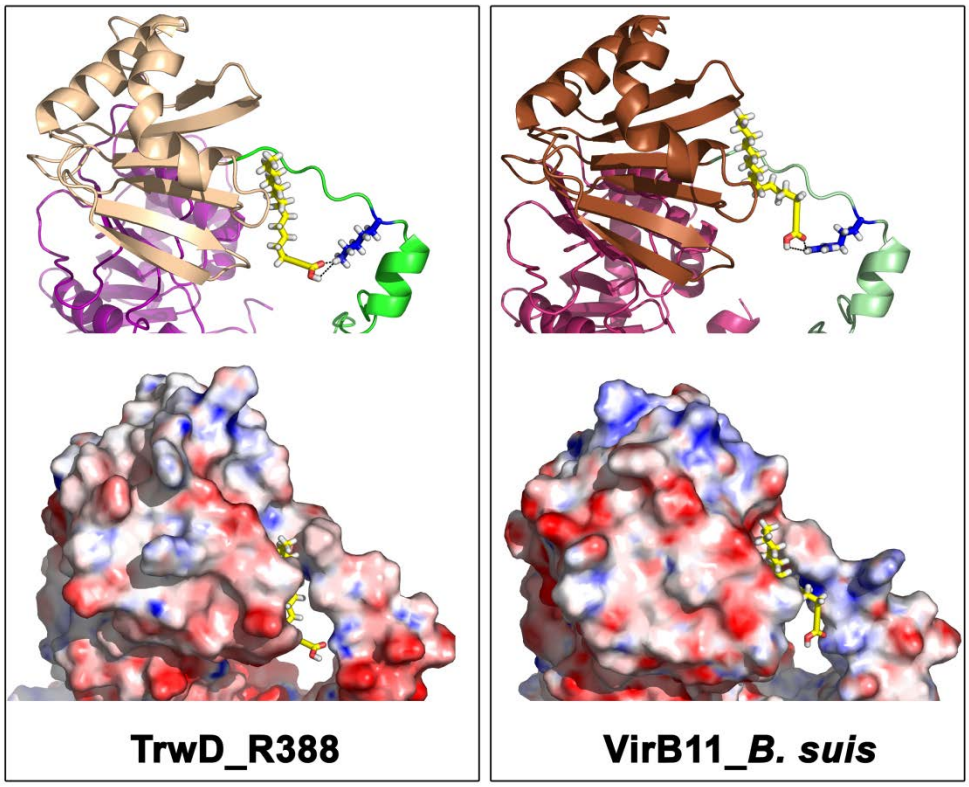

Fig.S6. **2-HDA binding pocket**. Best binding poses after blind docking of 2-HDA (*yellow*) into monomeric TrwD from plasmid R388 (*left panel*) and VirB11 from *Brucella suis* (*right panel*). Putative interactions between the carboxylate group of 2-HDA and a basic residue in the linker region of TrwD (K124) and VirB11 (R127) are shown. Cartoon and surface representations of the binding pockets are depicted at the top and the bottom sides of both panels, respectively. Electrostatic maps were calculated with the PDB2PQR application (Dolinsky *et al.*, 2007) and the resulting APBS files (Baker *et al.*, 2001) were rendered with Pymol (DeLano, 2008).

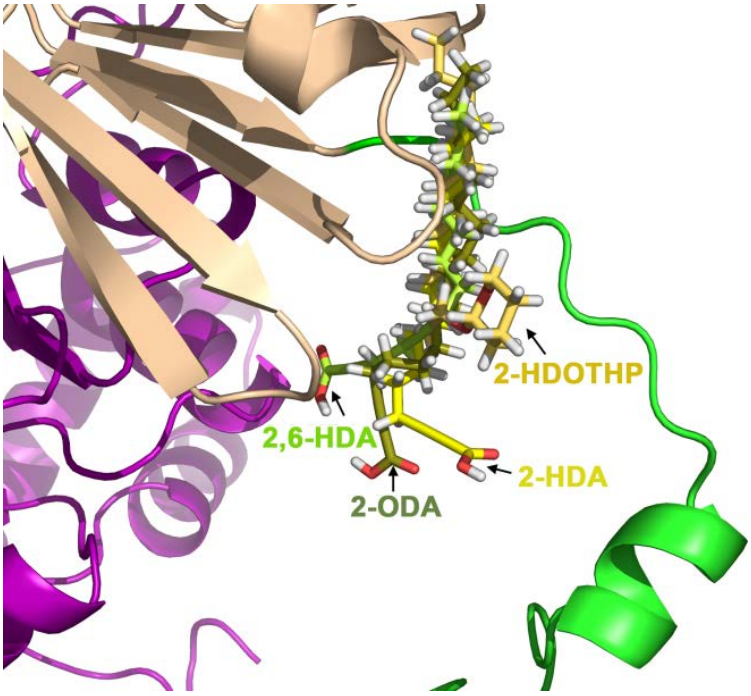

Fig. S7. **Docking of 2-alkynoic fatty acids and derivatives into TrwD.** Blind docking of 2-HDA, 2,6-HDA, 2-ODA and 2-HDOTHP into TrwD. Although all compounds bind to the same site the conformation of the carboxylate group is not exactly the same. In the case of 2,6-HDA the carboxylate group is at a larger distance from the basic residue at the linker region, which could explain its lower inhibitory effect. The tetrahydropyrane ester derivative (2-HDOTHP) cannot make electrostatic interactions with the linker region as it lacks the carboxylate group.

***Artículo publicado*:**

García-Cazorla Y, Getino M, Sanabria-Ríos D, Carballeira N.M, de la Cruz F, Arechaga I, Cabezón E. ***"Conjugation inhibitors compete with palmitic acid for binding to the conjugative traffic ATPase TrwD, providing a mechanism to inhibit bacterial conjugation"*** Journal of Biological Chemistry, (2018, September 10). pii: jbc.RA118.004716. doi: 10.1074/jbc.RA118.004716.

Palmitic acid binding to conjugative traffic ATPases provides a drug-target interaction to inhibit bacterial conjugation

(Manuscript in preparation)

Yolanda García-Cazorla [a], María Getino [a,*], David J. Sanabria-Ríos [b], Néstor M. Carballeira [b], Fernando de la Cruz [a], Ignacio Arechaga [a,#] and Elena Cabezón [a,#]

[a]*Departamento de Biología Molecular and Instituto de Biomedicina y Biotecnología de Cantabria (IBBTEC), Universidad de Cantabria- CSIC, Santander, Spain.* [b]*Inter American Univerisity of Puerto Rico-Metropolitan Campus, Faculty of Science and Technology, San Juan, Puerto Rico*

Running Title: Drug-target interactions to inhibit bacterial conjugation

[#]*Address correspondence to:* Elena Cabezón (cabezone@unican.es) & Ignacio Arechaga (arechagai@unican.es)

[*] *Present address: Faculty of Health and Medical Sciences. University of Surrey. Guildford, UK*

ABSTRACT

Conjugation inhibitors (COINs) are promising compounds in the fight against the spread of antibiotic resistance genes. Unsaturated fatty acids (uFAs) and alkynoic fatty acid derivatives, such as 2-HDA, were previously described as effective COINs. The traffic ATPase TrwD, a VirB11-homolog in plasmid R388, was the molecular target of these compounds. In this work, we demonstrate that COINs are liberally incorporated to bacterial membranes, replacing palmitic acid as the major component of the membrane. We also show that TrwD binds palmitic acid, thus facilitating its interaction with the membrane. Data suggest that COINs bind TrwD at a site that is otherwise occupied by palmitic acid. Accordingly, docking predictions with palmitic acid indicate that it shares the same binding site than uFAs and 2-HDA, albeit it differs in the contacts involved in the interaction. We have also identified 2-Bromopalmitate acid, a palmitate analog, as a new inhibitor of TrwD ATPase activity and bacterial conjugation. Moreover, we demonstrate that 2-bromopalmitate and palmitic acid compete for the same binding site in TrwD. Altogether, these new findings open a new avenue in the search of effective synthetic inhibitors of bacterial conjugation, which may be pivotal in the forthcoming war against multi-resistant bacteria.

IMPORTANCE

Antibiotic resistance is becoming a major threat for human health. Bacterial conjugation is one of the main mechanisms whereby bacteria spread antibiotic resistance genes. Therefore, COnjugation INhibitors (COINs) are of great interest to fight this threat. Some fatty acid derivatives were recently described as effective COINs, inhibiting the ATPase activity of an essential conjugative protein localized in the bacterial membrane. In this work, we show that this protein binds palmitic acid, which is the main component in membrane phospholipids. We also show that COINs are incorporated into the bacterial membrane, displacing the palmitic acid. Both, COINs and palmitate, bind to the same pocket in the target protein, albeit with important differences in the contacts involved. These differences might explain why COINs inhibit the catalytic mechanism of the enzyme. Following this line of research, we identified 2-bromopalmitate as a new inhibitor, opening a new avenue in the search of more effective inhibitors by structure-based drug design methods.

INTRODUCTION

Bacterial conjugation is one of the main mechanisms whereby bacteria become resistant to antibiotics (1). Therefore, there is a major interest in the search for conjugation inhibitors (COINs). In conjugation, DNA is transferred between two bacterial cells through a type IV secretion system (T4SS), a multi-subunit complex encoded by the conjugative plasmid. Canonical T4SS consists of 11 proteins, named VirB1 to VirB11, after *Agrobaterium tumefaciens* T4SS (2, 3). T4SS architecture is well preserved in most conjugative bacteria, consisting of four distinct sections: the pilus, the core channel complex, the inner membrane platform and the ATPases that provide the energy for substrate transport and pilus biogenesis (4). COINs have been proposed to target essential components of the T4SS (5). Promising results have been obtained with unsaturated fatty acids (uFAs), which specifically inhibit plasmid conjugation without inhibiting *Escherichia coli* growth (6, 7). The traffic ATPase TrwD, the VirB11 homolog in plasmid R388, was shown to be the target for this inhibition by uFAs (8). TrwD contributes to pilus biogenesis and DNA translocation (9), thus working as a molecular switch between pilus synthesis and substrate transport (10). TrwD was specifically inhibited *in vitro* by the same uFAs and alkynoic fatty acid derivatives (2-aFAs) that inhibited bacterial conjugation *in vivo*, such as linoleic acid or 2-hexadecynoic acid (2-HDA), respectively. These compounds acted as non-competitive inhibitors, with no effect on the affinity of the protein for ATP or ADP substrates (8). In contrast, saturated fatty acids, such as palmitic acid, showed no inhibitory effect in conjugation experiments and in ATPase assays.

TrwD belongs to the secretion ATPase superfamily, which also includes members of Type II secretion, Type IV pilus and flagellar biogenesis machineries (11). All members of this superfamily are hexameric ATPases, in which each monomer is formed by two domains at the N- and C- termini (NTD and CTD, respectively), connected by a flexible linker of variable length (11, 12). ATPase catalysis is driven by swapping the NTD over the CTD, due to the flexibility of the linker (13, 14). Blind docking predictions suggested a putative binding site for uFAs and 2-aFAs located at the end of the NTD and beginning of the linker region that connects it to the CTD, where the nucleotide binding site is located (8). These predictions are compatible with a model in which the mode of action of the inhibitors consisted in

preventing the swapping movements between the N- and C- terminal domains that are required in the catalytic cycle of the protein. VirB11 ATPases interact with the cytoplasmic site of the membrane through its N-terminal domain (15, 16). Therefore, it is likely that the inhibitory effect of uFAs and 2-aFAs occurs by affecting the membrane binding capability of TrwD. In this work, we demonstrate that 2-alkynoic fatty acids, such as 2-HDA, incorporate to bacterial membranes, replacing the palmitic acid as the major component of the membrane. We also show that TrwD binds palmitic acid, which suggests that uFAs and 2-AFAs act as inhibitors by binding TrwD at a site that is otherwise occupied by palmitic acid. Accordingly, docking predictions with palmitic acid indicate that it shares the same binding site than linoleic acid and 2-HDA.

Interestingly, we also discovered that 2-Bromopalmitate acid (2-BP), a proven compound to block palmitate incorporation onto a variety of membrane-associated eukaryotic proteins (17), is an inhibitor of TrwD ATPase activity and bacterial conjugation. Moreover, we demonstrate that 2-bromopalmitate and palmitic acid compete for the same binding site in TrwD, as shown by the increase in the value of the apparent inhibition constant in the presence of the saturated fatty acid. Recently, tanzawaic acids also appeared as a novel group of bacterial conjugation inhibitors (18). All these compounds share similar chemical characteristics: a carboxylic group, a long unsaturated aliphatic chain and the presence of double or triple bonds. The finding of 2-BP as an effective inhibitor allows us to conclude that inhibition does not occur by the presence of double or triple bonds in these compounds but, indirectly, by the conformation these fatty acids acquire upon TrwD binding. These new findings open a new avenue in the search of new and more effective synthetic inhibitors by structure-based drug design methods.

RESULTS

2-Alkynoic fatty acids incorporate to bacterial membranes, where they exert an inhibitory effect on conjugation

Unsaturated fatty acids (uFAs) and 2-alkynoic fatty acids specifically inhibit plasmid conjugation without inhibiting *E. coli* growth (6, 7). Recently, we identified TrwD, the VirB11 homolog in plasmid R388, as their molecular target (8). As VirB11 traffic ATPases transiently interact with the cytoplasmic site of the membrane, 2-alkynoic fatty acids, such as 2-HDA, must be incorporated into the bacterial membrane to exert an inhibitory conjugation effect.

In an attempt to find out if fatty acid derivatives that act as inhibitors (COINs) do incorporate into membranes, *E. coli* cells were grown in the presence and absence of the inhibitor 2-HDA. After 18 h incubation, the composition in esterified fatty acids (FAMEs) from membrane phospholipids and free fatty acids was checked by Gas Chromatography-Mass Spectrometry (GC-MS). Results revealed that the phospholipid fatty acids present in untreated bacteria are primarily saturated, being palmitic acid (16:0) the most abundant (almost 50% of the total membrane phospholipids contained palmitic acid) (Figure 1). When cells were grown in the presence of 2-HDA (50 µg/ml), bacteria incorporated this exogenous fatty acid to their membranes. Moreover, the major component of the total phospholipids in treated bacteria was 2-HDA (44% w/w). The incorporation of 2-HDA to the bacterial membrane was accompanied by a 2-fold decrease of palmitic acid in the phospholipid fraction. In contrast, the percentage of palmitic acid in the free fatty acid fraction was not altered when cells were treated with 2-HDA (Figure 1). As result of this experiment, we conclude that incorporation of 2-HDA into the bacterial membrane alters the utilization of endogenous fatty acids in the biosynthesis of phospholipids, with a significant amount of palmitic acid being replaced by 2-HDA in the membrane.

TrwD binds palmitic acid

The surprising effect observed in the previous experiment suggested that such a replacement might in turn affect the association of TrwD to the membrane. In contrast to uFAs or 2-HDA, saturated fatty acids neither inhibit bacterial conjugation (6), nor TrwD ATPase activity *in vitro* (8). Nonetheless, docking predictions with palmitic acid suggested that its binding site was the same as that for uFAs and 2-HDA, albeit adopting a different conformation due to the lack of double or triple bonds (8).

The molecular bases that underlie TrwD binding to the membrane are unknown. Therefore, we investigated a possible lipid-protein association via palmitic acid, by studying the binding of TrwD to ^{14}C-labeled palmitic acid. Purified TrwD protein was incubated with palmitic acid at different ratios, and samples were analyzed by polyacrylamide gel electrophoresis under non-denaturing conditions (Figure 2A). Radiolabeling of TrwD with palmitic acid was directly related to increasing palmitate/protein ratios. As control, TrwA protein (a conjugative protein that does not bind to the membrane) was incubated with palmitic acid at the highest palmitic acid/protein ratio. No radioactivity signal was observed for this control protein. Similar experiments, carried out with ^{14}C-labeled palmitoyl-CoA, gave identical results. In this latter case, it was possible to observe the unbound labeled palmitoyl-CoA running at the front of the gel (Figure 2B).

TrwD contains five cysteine residues in its sequence, with one of them placed at the N-terminal domain (Cys44). S-palmitoylation enhances the surface hydrophobicity and membrane affinity of proteins, playing an important role in modulating protein trafficking. Although this a post-translational modification observed in eukaryotic proteins, we wanted to check if TrwD was covalently bound to palmitic acid. The association of labeled palmitate with TrwD was sensitive to denaturation induced by SDS gel electrophoresis (data not shown), which suggests that the binding is non-covalent and there is not a thioester bond involved in such association.

2-Bromopalmitate acid inhibits TrwD ATPase activity

2-bromopalmitate (2-BP) is a palmitate analog that acts as inhibitor of many membrane-associated enzymes (17). It is an irreversible inhibitor that blocks palmitate incorporation onto proteins. The exact mechanism responsible for 2-BP mediated inhibition is not known. It is thought to inhibit protein acyl transferases (19), but recent reports showed that 2-BP is a nonselective probe, with many other different targets (20).

Thus, we analyzed the ATPase activity of TrwD in the presence of increasing concentrations of 2-BP (Figure 3). Analysis of the kinetics showed an inhibition pattern similar to 2-HDA or unsaturated fatty acids. In all cases, data did not fit to a Michaelis-Menten inhibition kinetic curve, but to a sigmoidal Hill equation, which suggested a cooperative effect in the inhibition kinetics. The apparent inhibition constant (Ki(app)) of 2-Bromohexadecanoic acid was 21,5±1,5 μM, similar to that obtained for 2-HDA [Ki(app) = 29,7±2,1 μM] (Figure 2).

Previously discovered conjugation inhibitors (COINs), such as uFAs (oleic and linoleic acids), chemically synthesized 2-HDA and derivatives (7) or tanzawaic acids (18), shared similar chemical characteristics: a carboxylic group, a long unsaturated aliphatic chain and the presence of double or triple bonds. The finding of 2-BP as an effective inhibitor was at first surprising. Nevertheless, the results shown above allow us to conclude that inhibition does not occur by the presence of double or triple bonds in these compounds but, indirectly, by the conformation these fatty acids acquire when bound to TrwD. Docking predictions with 2-BP indicate that the binding site for the palmitate analog is also in the same region than that found for linoleic acid, 2-HDA and palmitic acid (Figure 4). In this case, the presence of a halogen group (2-bromo) within the saturated fatty acid would result in a similar inhibitory effect, modifying the mode of binding.

2-bromopalmitate and palmitic acid compete for the same binding site in TrwD

In an attempt to determine if 2-Bromopalmitate and palmitic acid compete for the same binding site, we conducted a further characterization of the mechanism of inhibition. ATP turnover was measured at increasing concentrations of 2-Bromopalmitate in the presence of palmitic acid (500 μM) (Figure 5). Under these experimental conditions, the apparent inhibition constant (Ki(app)) of 2-Bromopalmitate increased 3-fold (from 21.47±1.5 μM to 65,42±1.4 μM) (Figure 3), suggesting that palmitic acid and 2-BP compete for the same binding site in TrwD.

2-Bromopalmitate inhibits R388 conjugation

In a previous work (8), we observed that 2-alkynoic fatty acids that inhibited bacterial conjugation, such as 2-hexadecynoic acid (2-HDA), 2-octadecynoic acid (2-ODA) or 2,6-hexadecadiynoicacid (2,6-HDA) also inhibited TrwD ATPase activity *in vitro*. In contrast, those with no effect *in vivo*, such as alcohol or tetrahydropyranyl-ether derivatives, did not affect the *in vitro* TrwD ATPase activity either. Therefore, once we discovered that 2-BP was an effective inhibitor of TrwD ATPase activity, we checked if this compound was also an inhibitor of bacterial conjugation. R388 conjugation frequencies at increased concentrations of 2-bromopalmitate are shown in Fig. 6.

Bacterial conjugation was monitored by a HTC assay based on fluorescence emission by transconjugant cells. Control assays were carried out to discard any effect on bacterial growth, plasmid stability or lux expression. Addition of 2-BP (0.3 mM) resulted in the inhibition of R388 conjugation (Figure 6), as confirmed by plate-conjugation assay. 2-BP inhibited R388 conjugation to levels similar to those obtained with 2-HDA (to about 2 % of w.t. levels). Moreover, when palmitic acid (500 μM) was added to the LB media, a higher concentration of 2-BP was required to reach a similar inhibitory effect. This result perfectly correlates with that obtained *in vitro*, on TrwD ATPase activity, and confirms 2-BP as an effective COIN.

DISCUSSION

VirB11 proteins belong to a large family of hexameric AAA+ traffic ATPases, which includes proteins involved in Type II secretion and in Type IV pilus and flagellar biogenesis (11). VirB11 from *Agrobacterium tumefaciens* localized at the cell pole, as shown by epifluorescence microscopy of a GFP-VirB11 fusion protein (21). The protein required neither ATP nor other VirB proteins for its polar localization (22). In contrast, in the presence of a complete T4SS machinery, VirB11 localized all over the bacterial cell perimeter (23). Accordingly, in vitro experiments had previously shown that TrwD, the VirB11 homolog in plasmid R388, interacts with phospholipids in lipid vesicles, causing lipid vesicle aggregation and intervesicular lipid mixing, supporting the hypothesis that TrwD also behaves as a membrane protein (16). Therefore, although it is proven that the protein localizes to the bacterial inner membrane, the molecular bases underlying this interaction with membrane lipids were unknown.

Recently, we identified TrwD as the molecular target for fatty acid-mediated inhibition of conjugation (8), showing that unsaturated fatty acids (uFAs) and 2-alkynoic fatty acids (aFAs) that inhibited bacterial conjugation, such as 2-HDA, 2-ODA or 2,6-HDA, also inhibited TrwD ATPase activity. In contrast, saturated fatty acids such as palmitic acid, neither showed an inhibitory effect in conjugation experiments nor in ATPase assays. In an attempt to explain how these compounds can act as inhibitors of bacterial conjugation, we investigated the putative interaction of uFAs and aFAs with the bacterial membrane. Indeed, our results revealed that the phospholipid fatty acids present in untreated bacteria are mainly saturated, being palmitic acid the most abundant. However, when cells were grown in the presence of 2-HDA, this compound was incorporated to the membrane and became the major component of the total phospholipid fraction (Figure 1). More importantly, a significant amount of palmitic acid was replaced by 2-HDA in the membrane. Therefore, it was reasonable to think that this replacement of palmitic acid by fatty acids with double or triple bonds might be responsible of such an inhibitory effect. Thus, we wondered whether TrwD interaction with the membrane was occurring via palmitic acid under normal growth conditions. Supporting this idea, a blind docking search of the palmitic acid in TrwD structure revealed the same binding site as for uFAs and 2-HDA, albeit it differs in the contacts

involved in the interaction (8). In order to confirm the putative binding of saturated fatty acids, purified TrwD was incubated with ^{14}C-labeled palmitic acid and the resulting complex was analyzed in native gels (Figure 2). Radiolabeling of TrwD with palmitic acid was directly related to increasing palmitate/protein ratios.

A wide variety of proteins associate to the membrane by a covalent attachment to palmitic acid (24). In these palmitoylated proteins, the fatty acid is bound to a cysteine residue through a thioester linkage. This is a reversible process that allows a transient binding to the membrane, which is crucial in many biological processes. This lipid modification is common in eukaryotic cells (24) but is poorly documented in prokaryotes. To our knowledge, there is only one example of *S*-palmitoylation for a bacterial protein (25). TrwD presents five cysteine residues. One of them is placed at the NTD, so palmitoylation might be a possible mechanism of interaction of TrwD with the membrane. Therefore, we checked if the association of radio-labeled palmitate with TrwD was resistant to denaturation induced by SDS gel electrophoresis. No signal of radiolabeled protein was observed in these gels. Samples of purified protein incubated with palmitic acid were also analyzed by mass spectrometry, but no difference in molecular mass was observed when the sample was compared to a control in the absence of the fatty acid. Therefore, our data indicate that the binding to palmitic acid is non-covalent, excluding the possibility that the association of palmitate with TrwD is due to protein palmitoylation. In the literature, there are also several examples of proteins that associate to the membrane via a non-covalent binding to saturated fatty acids, such as Toll-like receptors (TLRs) (26). In this case, the polyunsaturated fatty acid binds to a lipid binding pocket in the protein receptor. Intriguingly, TLRs are also inhibited by polyunsaturated fatty acids (27), as in the case of TrwD.

In order to study the binding of palmitic acid to TrwD we also explored the binding capacity of an analogue compound, 2-bromopalmitate (2-BP). This fatty acid was found to act as inhibitor of many membrane-associated enzymes that bind palmitic acid (17). Therefore, we checked if this palmitate analog also inhibited TrwD activity. We analyzed the ATPase activity of the protein in the presence of increasing concentrations of 2-BP (Figure 3). The inhibition pattern was similar to that obtained with 2-HDA or uFAs, with an apparent

inhibition constant similar to that obtained for 2-HDA. In a previous work, we found that the same fatty acid derivatives that were effective inhibitors of bacterial conjugation were also capable of inhibiting TrwD ATPase activity, and *vice versa*, those unable to inhibit conjugation also failed to inhibit TrwD activity, with a perfect correlation between the *in vivo* and *in vitro* data (8). In the same way, in this work we demonstrate that 2-BP inhibited R388 conjugation, as in the case of 2-HDA (Figure 6). Moreover, when palmitic acid was added to the LB media, a higher concentration of 2-BP was required to reach a similar inhibitory effect. This effect is probably due to the incorporation of 2-BP to the bacterial membrane and the consequent replacement of palmitic acid by 2-BP, an effect that has already been observed for 2-HDA (Figure 1). Therefore, these inhibitors seem to act by displacing the more abundant saturated acid in the membrane.

In an attempt to determine if 2-BP and palmitic acid compete for the same binding site in TrwD, ATP turnover was measured at increasing concentrations of 2-BP in the presence of palmitic acid (Figure 5). The apparent inhibition constant (Ki(app)) of 2-BP raised from 21.47±1.5 μM to 65.42±1.4 μM (Figure 3), which suggests that both fatty acids (palmitic acid and 2-BP) compete for the same binding site in TrwD. Although it is generally accepted that 2-BP blocks S-palmitoylation by inhibiting protein acyl transferases (19), recent work has shown that 2-BP has many other targets, leading the authors to suggest that the compound might exert the inhibition by direct competition with palmitic acid (20). The results obtained with TrwD in this work are in agreement with this hypothesis and might be extensive to proteins that associate to the inner membrane via interaction with palmitic acid.

In summary, in this work we describe 2-BP, a palmitate analog, as a new inhibitor of bacterial conjugation. Similarly to previously described inhibitors, which are also fatty acid derivatives, 2-BP acts on the traffic ATPase TrwD as its molecular target. The results presented here demonstrate that inhibitors such as 2-HDA, incorporate into the bacterial membrane and replace a significant fraction of palmitic acid. Although it was known that VirB11 proteins localize in the bacterial inner membrane, the molecular bases of this interaction had not been identified. We have proven that TrwD interacts with palmitic acid, which suggests TrwD interacts with the membrane by binding this fatty acid. This work

shows that COINs act by competing with palmitic acid for the same binding site in TrwD. Although all COINs bind to the same pocket in TrwD, there are differences in their mode of binding that might explain the different behavior of palmitic acid and the fatty acid derivatives that act as inhibitors, such as 2-BP (Figure 4). In the latter case, the bromide ion induces a different conformation in the carboxylic group, which is forced to move 120 degrees apart, creating closer contacts with residues 115-118 (residues RKHS of the flexible linker). This linker plays an essential role in ATP catalysis, allowing the movement of the N-terminal domain (NTD) over the C-terminal domain (CTD) (13, 14). In contrast, binding predictions for palmitic acid locate its carboxylic group in the opposite direction, with closer contacts with residue lysine 52, out of the linker region. These differences might explain why the presence of the bromide ion or double and triple bonds in the fatty acid derivatives that act as inhibitors affect the catalytic mechanism of TrwD.

It is worth noting that uFAs and 2-aFAs are effective inhibitors of IncW plasmids such as R388, but other plasmid groups, such as IncN and IncP, are not affected by them (6, 7). Interestingly, a blind docking search of putative binding sites for uFAs and aFAs in the atomic model of TrbB, the VirB11 homolog in IncP RP4 plasmid, revealed no binding sites for these COINs. The closest homolog of TrbB is HP0525, the VirB11 of *H. pylori* (10). This protein has a very short loop and the monomer interactions in the hexameric oligomer differ substantially from those homologs with long linkers, such as TrwD. Therefore, it was not surprising to find that there is no COIN binding site in TrbB. Yet, TraG, the homolog in the IncN pKM101 plasmid (which is similar to the VirB11 members of the *Brucella* branch), is not inhibited by uFAs. Close inspection of this structure revealed substantial differences between TraG and TrwD. A suggestive difference in the binding site is a substitution of a basic residue (K52) in TrwD by an acidic one (D35) in TraG, which might alter the global charge balance of the binding pocket and, therefore, explain the lack of inhibition of TraG by uFAs and other derivatives. These new findings will allow us to optimize the chemical structure of these compounds by structure-based drug design methods, in order to design new and more effective derivatives that act as COINs.

MATERIALS & METHODS

Proteins and fatty acids. Cloning, overexpression and purification of TrwD and TrwA proteins was carried out as described previously (28, 29). Palmitic and 2-Bromopalmitic acids were purchased from Sigma-Aldrich. Palmitic acid derivatives, such as [^{14}C(U)] and Palmitoyl Coenzyme A, [Palmitoyl-1-^{14}C] were purchased from PerkinElmer. 2-HDA was synthesized as previously described (30).

Gas Chromatography-Mass Spectrometry (GC-MS). *E. coli* ATCC 25922 (American Type Culture Collection, Manassas, VA) was grown in Luria-Bertani Broth (LB, Lennox, Fisher Scientific, Fair Lawn, NJ) medium in the presence and absence of 2-HDA (50µg/mL) at 37˚C for 18 h. Then, cells were collected, extracted by using 15 mL of chloroform:methanol (2:1, v/v), shaken (Labnet, Edison, NJ) for 30 min at 200 rpm, and sonicated into Ultrasonic Cleaner (Fisher Brand FB11201, Germany) at 37 kHz (100% power, 390 W) for 15 min at room temperature. Phospholipids and free fatty acids were separated from total lipids by using silica gel column chromatography. Free fatty acids were eluted by adding 15 mL of acetone, while phospholipids were eluted by adding 15 mL of hexane. Solvents from both acetone and hexane fractions were removed by rotoevaporation (Büchi, Rotavapor R-114, Switzerland) and the resulting lipid content was treated with 3 mL of methanol and catalytic amounts of 12M HCl and subsequently refluxed for 3h. Once the transesterification reaction was completed, methanol was removed by rotoevaporation and fatty acid methyl esters (FAMEs) were analyzed by using GC-MS (Hewlett Packard Series II MS ChemsStation coupled to an Hewlett Packard 5972 Series Mass Selective Detector equipped with a 30 m x 0.25 mm special performance capillary column HP-5MS of polymethyl siloxane crosslinked with 5% phenyl methylpolysiloxane). The selected temperature method was: 120°C initial temperature, 5°C/min temperature rate, and 260°C final temperature. The split ratio was set at 10:1 for all analyses. All fatty acids were identified based on their molecular ion, base peak, fragmentation pattern and retention time and then expressed as a percentage of relative abundance (%) of total FAs.

Radio-labeling Assays. Purified proteins were incubated with ^{14}C-labeled fatty acids for 10 min at room temperature. Then, samples were analyzed by native polyacrylamide gel electrophoresis (Native-PAGE), following the protocol previously described (31). 4,5% polyacrylamide gels were run at pH 8.5 for 140min in an ice bath, with a constant amperage (30 mA). Then, gels were dried, exposed overnight and reveled using a Fluoro Image Analyzer FLA-5100 (FujiFilm) to detect radiolabeled protein on electrophoretic bands.

ATP hydrolysis Assays. Steady-state ATP hydrolysis activity *in vitro* was measured with the EnzCheck™ Kit (Invitrogen) in a UV-1800 spectrophotometer (Shimadzu), as described previously (28). Inorganic phosphate (Pi) released after ATP hydrolysis was monitored as an increase of absorption at 360 nm for 10 min following manufacturer's instructions and components: 0.2 mM 2-amino-6-mercapto-7-methylpurine riboside (MESG) and 1 unit/ml of purine nucleoside phosphorylase (PNP). Fatty acids diluted in DMSO were added to the reaction buffer, consisting of 50 mM Tris-HCl pH 8.5, 75 mM potassium acetate, 10 μM magnesium acetate, 1 mM ATP and 10% glycerol (w/v). Reactions were started by the addition of the ATPase TrwD (2 μM).

Conjugation Assays. Conjugation frequencies (CF) were obtained with the fluorescence-based assay previously described (7). Strain DH5α carrying the conjugative plasmid pJC01, which expresses GFP under the control of T7 promoter p10, was used as a donor. A streptomycin-resistant derivative of *E. coli* BL21 (DE3), expressing T7 RNA polymerase from the inserted phage, was used as recipient strain. Both strains at stationary phase were concentrated 4-fold and mixed at a 1:1 ratio. Mixture samples (10 μl) were spotted onto 96-well microtiter plates (Bioster a.s.) with the help of a Biomek 3000 liquid-handling robot (Beckman Coulter). Cells were grown in 150μl LB, 1% agar, 1mM IPTG and different concentrations of fatty acids. After incubation at 37ºC for 6 h to allow conjugation, cells were resuspended in Phosphate-Buffered Saline (PBS) and transferred to a new plate. The optical density at 600 nm (OD600) and GFP emission were measured in a Victor3 multi-label counter (PerkinElmer). Conjugation frequencies (CF) were calculated as the ratio of absolute fluorescence emitted by transconjugant cells and the total number of cells (OD600). Relative CF in the presence of a compound was determined as a fraction of the CF observed in controls performed in the absence of the inhibitor. To reproduce the conditions, equivalent volumes of solvent (DMSO) were added to control samples.

Molecular modelling and ligand docking. An atomic model of TrwD was generated by molecular threading using as template the atomic coordinates of *B. suis* VirB11 (2gza.pdb) (14), as previously described (28). The structural coordinates of palmitic acid, 2-HDA and 2-Bromopalmitic acid were retrieved from PubChem database (https://pubchem.ncbi.nlm.nih.gov/) and prepared for docking as previously described (8). Files containing the atomic coordinates of the TrwD model and the fatty acids were submitted to the SwissDock server (http://www.swissdock.ch/) to run blind docking. Results were examined with UCSF Chimera. Binding poses with the best Full-Fitness (FF) score and minimal energy were finally selected.

FUNDING INFORMATION

This work was supported by the Spanish Ministerio de Economia y Competitividad (MINECO) grants BFU2016-78521-R (to E.C. and I.A.) and BFU2014-55534 (to F.D.L.C.) and by the Grant P20GM103475-16 from the National Center for Research Resources and the National Institute of General Medical Sciences of the National Institutes of Health (to D.S.R.). The authors declare that they do not have any conflict of interest.

REFERENCES

1. Mazel D, Davies J. 1999. Antibiotic resistance in microbes. Cell Mol Life Sci 56:742-54.
2. Christie PJ, Atmakuri K, Krishnamoorthy V, Jakubowski S, Cascales E. 2005. Biogenesis, architecture, and function of bacterial type IV secretion systems. Annu Rev Microbiol 59:451-85.
3. Christie PJ, Whitaker N, Gonzalez-Rivera C. 2014. Mechanism and structure of the bacterial type IV secretion systems. Biochim Biophys Acta 1843:1578-91.
4. Cabezón E, Ripoll-Rozada J, Peña A, de la Cruz F, Arechaga I. 2015. Towards an integrated model of bacterial conjugation. FEMS Microbiol Rev 39:81-95.
5. Cabezon E, de la Cruz F, Arechaga I. 2017. Conjugation Inhibitors and Their Potential Use to Prevent Dissemination of Antibiotic Resistance Genes in Bacteria. Front Microbiol 8:2329.
6. Fernandez-Lopez R, Machon C, Longshaw CM, Martin S, Molin S, Zechner EL, Espinosa M, Lanka E, de la Cruz F. 2005. Unsaturated fatty acids are inhibitors of bacterial conjugation. Microbiology 151:3517-26.
7. Getino M, Sanabria-Rios DJ, Fernandez-Lopez R, Campos-Gomez J, Sanchez-Lopez JM, Fernandez A, Carballeira NM, de la Cruz F. 2015. Synthetic Fatty Acids Prevent Plasmid-Mediated Horizontal Gene Transfer. MBio 6:e01032-15.
8. Ripoll-Rozada J, Garcia-Cazorla Y, Getino M, Machon C, Sanabria-Rios D, de la Cruz F, Cabezon E, Arechaga I. 2016. Type IV traffic ATPase TrwD as molecular target to inhibit bacterial conjugation. Mol Microbiol 100:912-21.
9. Atmakuri K, Cascales E, Christie PJ. 2004. Energetic components VirD4, VirB11 and VirB4 mediate early DNA transfer reactions required for bacterial type IV secretion. Mol Microbiol 54:1199-211.
10. Ripoll-Rozada J, Zunzunegui S, de la Cruz F, Arechaga I, Cabezon E. 2013. Functional interactions of VirB11 traffic ATPases with VirB4 and VirD4 molecular motors in type IV secretion systems. J Bacteriol 195:4195-201.

11. Planet PJ, Kachlany SC, DeSalle R, Figurski DH. 2001. Phylogeny of genes for secretion NTPases: identification of the widespread tadA subfamily and development of a diagnostic key for gene classification. Proc Natl Acad Sci U S A 98:2503-8.
12. Pena A, Arechaga I. 2013. Molecular motors in bacterial secretion. J Mol Microbiol Biotechnol 23:357-69.
13. Savvides SN, Yeo HJ, Beck MR, Blaesing F, Lurz R, Lanka E, Buhrdorf R, Fischer W, Haas R, Waksman G. 2003. VirB11 ATPases are dynamic hexameric assemblies: new insights into bacterial type IV secretion. EMBO J 22:1969-80.
14. Hare S, Bayliss R, Baron C, Waksman G. 2006. A large domain swap in the VirB11 ATPase of Brucella suis leaves the hexameric assembly intact. J Mol Biol 360:56-66.
15. Yeo HJ, Savvides SN, Herr AB, Lanka E, Waksman G. 2000. Crystal structure of the hexameric traffic ATPase of the Helicobacter pylori type IV secretion system. Mol Cell 6:1461-72.
16. Machon C, Rivas S, Albert A, Goni FM, de la Cruz F. 2002. TrwD, the hexameric traffic ATPase encoded by plasmid R388, induces membrane destabilization and hemifusion of lipid vesicles. J Bacteriol 184:1661-8.
17. Coleman RA, Rao P, Fogelsong RJ, Bardes ES. 1992. 2-Bromopalmitoyl-CoA and 2-bromopalmitate: promiscuous inhibitors of membrane-bound enzymes. Biochim Biophys Acta 1125:203-9.
18. Getino M, Fernandez-Lopez R, Palencia-Gandara C, Campos-Gomez J, Sanchez-Lopez JM, Martinez M, Fernandez A, de la Cruz F. 2016. Tanzawaic Acids, a Chemically Novel Set of Bacterial Conjugation Inhibitors. PLoS One 11:e0148098.
19. Jennings BC, Nadolski MJ, Ling Y, Baker MB, Harrison ML, Deschenes RJ, Linder ME. 2009. 2-Bromopalmitate and 2-(2-hydroxy-5-nitro-benzylidene)-benzo[b]thiophen-3-one inhibit DHHC-mediated palmitoylation in vitro. J Lipid Res 50:233-42.
20. Davda D, El Azzouny MA, Tom CT, Hernandez JL, Majmudar JD, Kennedy RT, Martin BR. 2013. Profiling targets of the irreversible palmitoylation inhibitor 2-bromopalmitate. ACS Chem Biol 8:1912-7.

21. Das A, Das A. 2014. Delineation of polar localization domains of Agrobacterium tumefaciens type IV secretion apparatus proteins VirB4 and VirB11. Microbiologyopen 3:793-802.
22. Judd PK, Kumar RB, Das A. 2005. Spatial location and requirements for the assembly of the Agrobacterium tumefaciens type IV secretion apparatus. Proc Natl Acad Sci U S A 102:11498-503.
23. Aguilar J, Cameron TA, Zupan J, Zambryski P. 2011. Membrane and core periplasmic Agrobacterium tumefaciens virulence Type IV secretion system components localize to multiple sites around the bacterial perimeter during lateral attachment to plant cells. MBio 2:e00218-11.
24. Linder ME, Deschenes RJ. 2007. Palmitoylation: policing protein stability and traffic. Nat Rev Mol Cell Biol 8:74-84.
25. Quevillon-Cheruel S, Leulliot N, Muniz CA, Vincent M, Gallay J, Argentini M, Cornu D, Boccard F, Lemaitre B, van Tilbeurgh H. 2009. Evf, a virulence factor produced by the Drosophila pathogen Erwinia carotovora, is an S-palmitoylated protein with a new fold that binds to lipid vesicles. J Biol Chem 284:3552-62.
26. Jin MS, Lee JO. 2008. Structures of the toll-like receptor family and its ligand complexes. Immunity 29:182-91.
27. Hwang DH, Kim JA, Lee JY. 2016. Mechanisms for the activation of Toll-like receptor 2/4 by saturated fatty acids and inhibition by docosahexaenoic acid. Eur J Pharmacol 785:24-35.
28. Ripoll-Rozada J, Pena A, Rivas S, Moro F, de la Cruz F, Cabezon E, Arechaga I. 2012. Regulation of the type IV secretion ATPase TrwD by magnesium: implications for catalytic mechanism of the secretion ATPase superfamily. J Biol Chem 287:17408-14.
29. Moncalian G, Grandoso G, Llosa M, de la Cruz F. 1997. oriT-processing and regulatory roles of TrwA protein in plasmid R388 conjugation. J Mol Biol 270:188-200.
30. Carballeira NM, Sanabria D, Cruz C, Parang K, Wan B, Franzblau S. 2006. 2,6-hexadecadiynoic acid and 2,6-nonadecadiynoic acid: novel synthesized acetylenic fatty acids as potent antifungal agents. Lipids 41:507-11.

31. Arndt C, Koristka S, Bartsch H, Bachmann M. 2012. Native polyacrylamide gels. Methods Mol Biol 869:49-53.
32. Grosdidier A, Zoete V, Michielin O. 2011. SwissDock, a protein-small molecule docking web service based on EADock DSS. Nucleic Acids Res 39:W270-7.

FIGURE LEGENDS

***Figure 1*. Composition of phospholipid fatty acids and free fatty acids in *E. coli* after the exposure to 2-HDA**. *E. coli* cells were grown at 37°C for 18 h in Luria Broth (LB) containing 50 µg/mL 2-HDA. Fatty acids were eluted, converted to methyl-esters and analyzed by Gas Chromatography – Mass Spectrometry (GC-MS), as described in M&M. Values were obtained from three separated experiments. Fatty acid nomenclature indicates the number of carbons followed by the number of double bonds. 2-HDA refers to 2-hexadecynoic acid.

***Figure 2*. TrwD binding to ^{14}C-labeled palmitic acid and palmitoyl CoA. (**A). TrwD (80 µM) was incubated at increasing ^{14}C-labeled palmitic acid ratios (1:0.25, 1:0.5, 1:0.75 and 1:1 protein: palmitic acid molar ratios, respectively). Lane C1 corresponds to TrwD (80 µM) in the absence of fatty acids. Lane C2 is also a control experiment in which an alien protein, TrwA (80 µM), was incubated with ^{14}C-palmitic acid. (B) TrwD (80 µM) was incubated at increasing ^{14}C-labeled palmitoyl CoA ratios (1:0.5, 1:0.75 and 1:1 protein: palmitoyl CoA molar ratios, respectively). Lane C1 corresponds to ^{14}C-palmitoyl CoA (80 µM) in the absence of any protein. Lane C2, as in panel A, corresponds to TrwA (80 µM) incubated with ^{14}C-palmitoyl CoA (80 µM). Lane C1 and C2 radioactivity signals at the front of the gel correspond to free ^{14}C-labeled palmitoyl CoA. In both cases, protein-fatty acid complexes were analyzed by Native- PAGE and radiolabeled images were obtained after overnight exposure, as described in M&M. (C) TrwD (80 µM; Lane D1) and TrwA (80 µM; Lane D2) were analyzed by Coomassie Brilliant Blue-stained Native-PAGE, as described in M&M.

***Figure 3*. Determination of the kinetic parameters of inhibition by 2-bromopalmitate**. ATP hydrolysis by TrwD (2 µM) was measured at increasing concentrations of 2-bromopalmitate (white circles) and compared with the values obtained at increasing concentrations of 2-HDA (black circles). Data were fitted to a Hill inhibition equation (error bars: SD).

Figure 4. **Blind docking of fatty acids into the molecular model of TrwD**. Blind docking predictions between a molecular model of monomeric TrwD and fatty acid ligands (palmitic and 2-bromopalmitic acid) were performed using the EADock dihedral spacing sampling engine of the Swiss-dock server (32). Both fatty acids fit into a pocket located at the interface between the N-terminal domain (NTD, *pink*) and the linker region (*light orange*), which connects the NTD with the catalytic C-terminal domain (CTD, *brown*). Upper left and right panels correspond to the same view in cartoon and surface representation, respectively. The carbon chains of both fatty acids have a similar orientation (colors blue and yellow for the palmitic and 2-bromopalmitic acids, respectively). However, the carboxylic group of the 2-bromo derivative is buried inside a pocket formed by the NTD and the linker domain of the protein, being the bromide atom (*dark green*) stabilized by electrostatic groups located in the region (residues 115-118 of the flexible linker). On the contrary, the carboxylic group of the palmitic acid (red) is 120 degrees apart, making closer contacts with lysine 52, out of the linker region. The bottom panel shows a zoom of the binding pocket, with relevant residues on TrwD that might be interacting with 2-BP and palmitic acid.

Figure 5. **2-bromopalmitate and palmitic acid compete for the same TrwD binding site**. TrwD ATPase rates (2 µM) were measured as described in M&M, at increasing concentrations of palmitic acid (*dark cicles*), 2-bromopalmitate (*white circles*) and mixtures of both fatty acids consisting of a fixed concentration of palmitic acid (500 µM) and increasing concentrations of 2-bromopalmitate (*dark triangles*). In the latter case, protein sample was first incubated with palmitic acid for 5 min, and then 2-bromopalmitate was added at the indicated concentrations. Data were fitted to a sigmoidal Hill equation for inhibition (error bars: SD).

Figure 6. **R388 Conjugation frequency (CF) in the presence of increasing concentrations of 2-bromopalmitate**. Bacterial conjugation experiments were performed as described in M&M. Values represent the mean CF ± SD of at least four independent experiments, measured by fluorescence-based HTC assay and relative to positive control in the absence of any inhibitor (100%). Panel B (inset figure) shows the R388 conjugation frequency in vivo measured in the presence of 2-Bromopalmitic acid (50µM) (*black cicles*)

and a mixture of both palmitic (500 µM) and 2-Bromopalmitic acids (50µM) (*grey squares*). Horizontal and vertical bars represent the mean ± SD of each group of data. Statistical significance analyzed by Student's t-test (**$p < 0.05$).

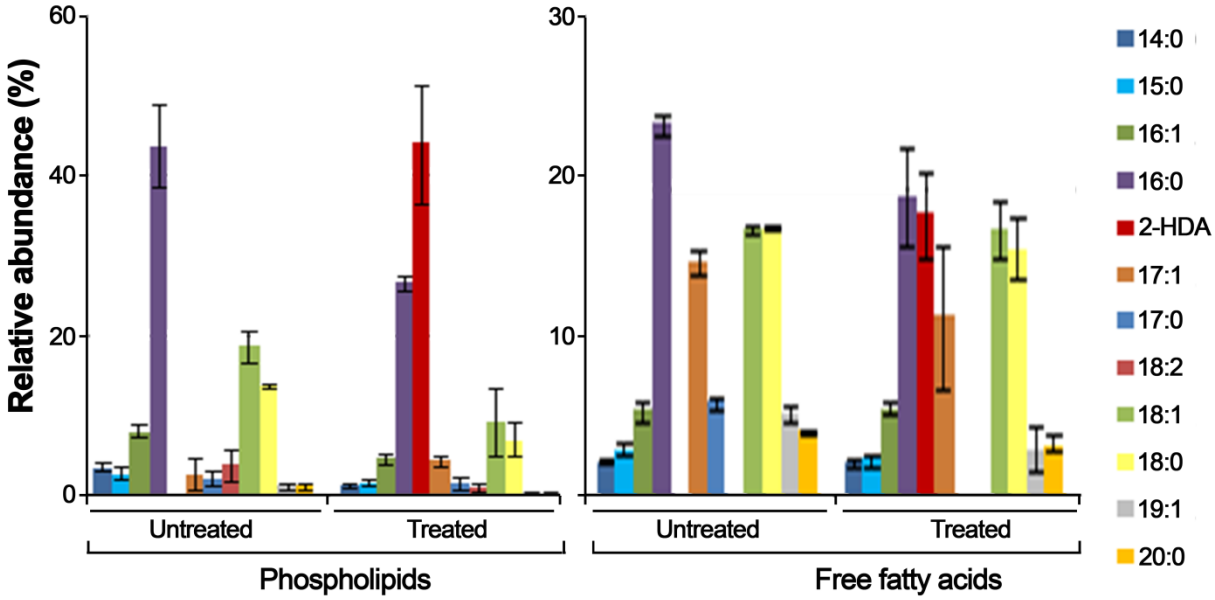
Relative abundance (%)
60
40
20
0
30
20
10
Untreated
Treated
Untreated
Treated
Phospholipids
Free fatty acids
14:0
15:0
16:1
16:0
2-HDA
17:1
17:0
18:2
18:1
18:0
19:1
20:0

FIGURE 1

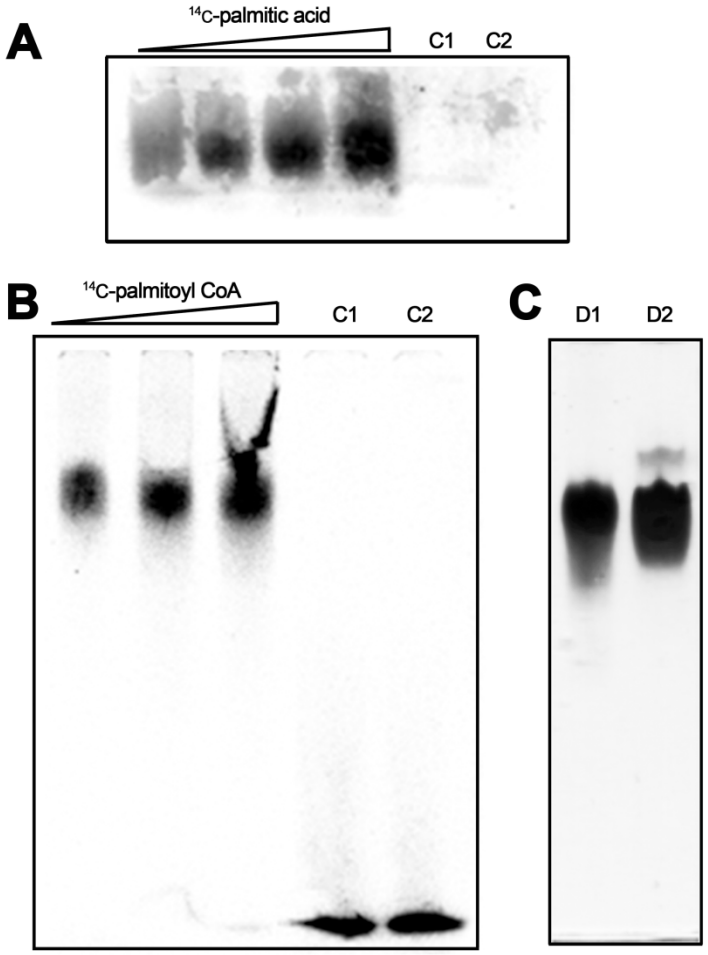

FIGURE 2

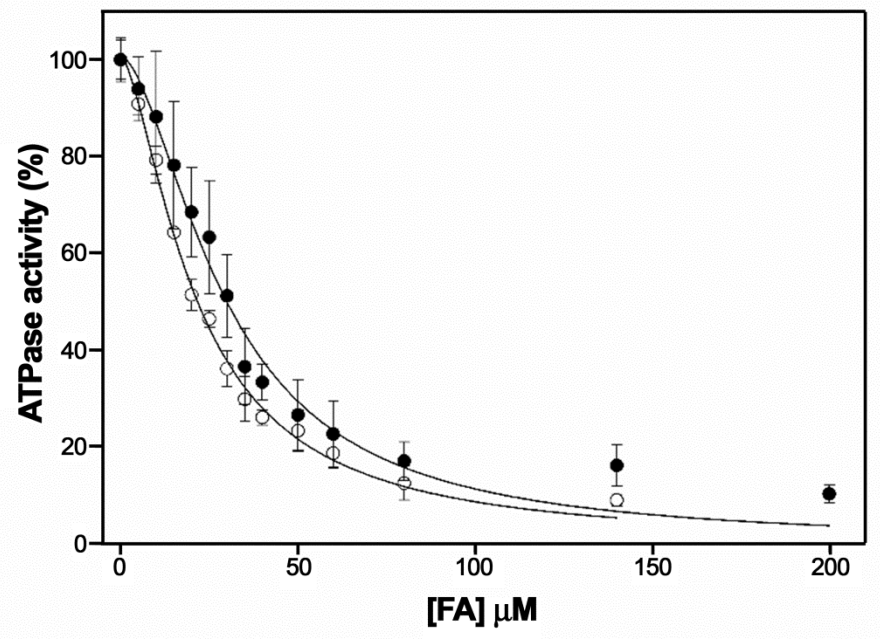

FIGURE 3

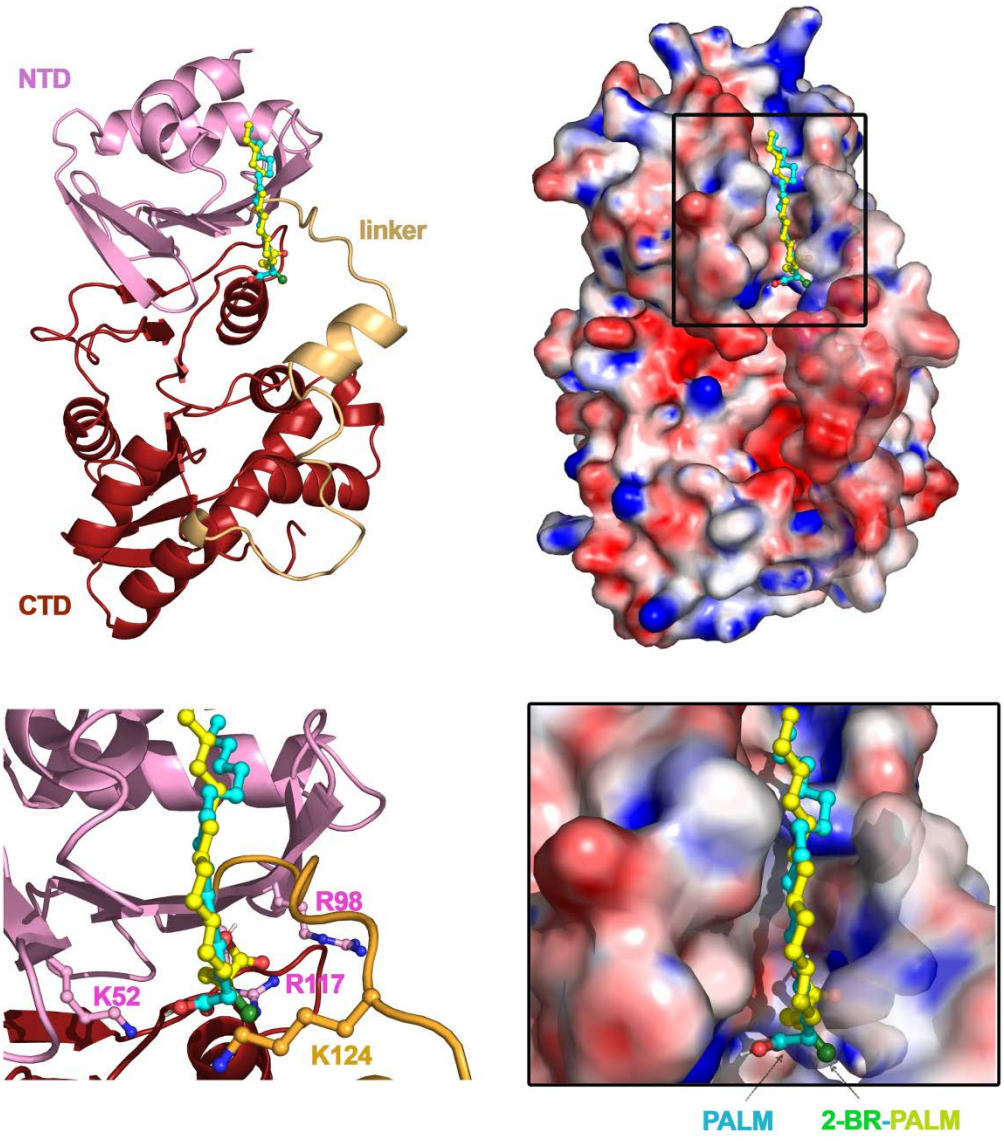

FIGURE 4

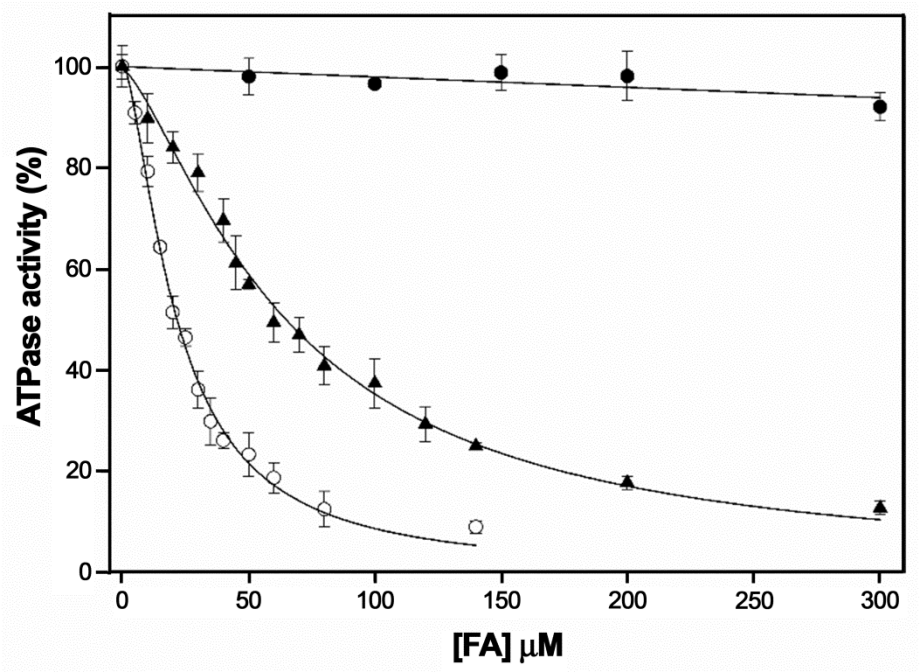

FIGURE 5

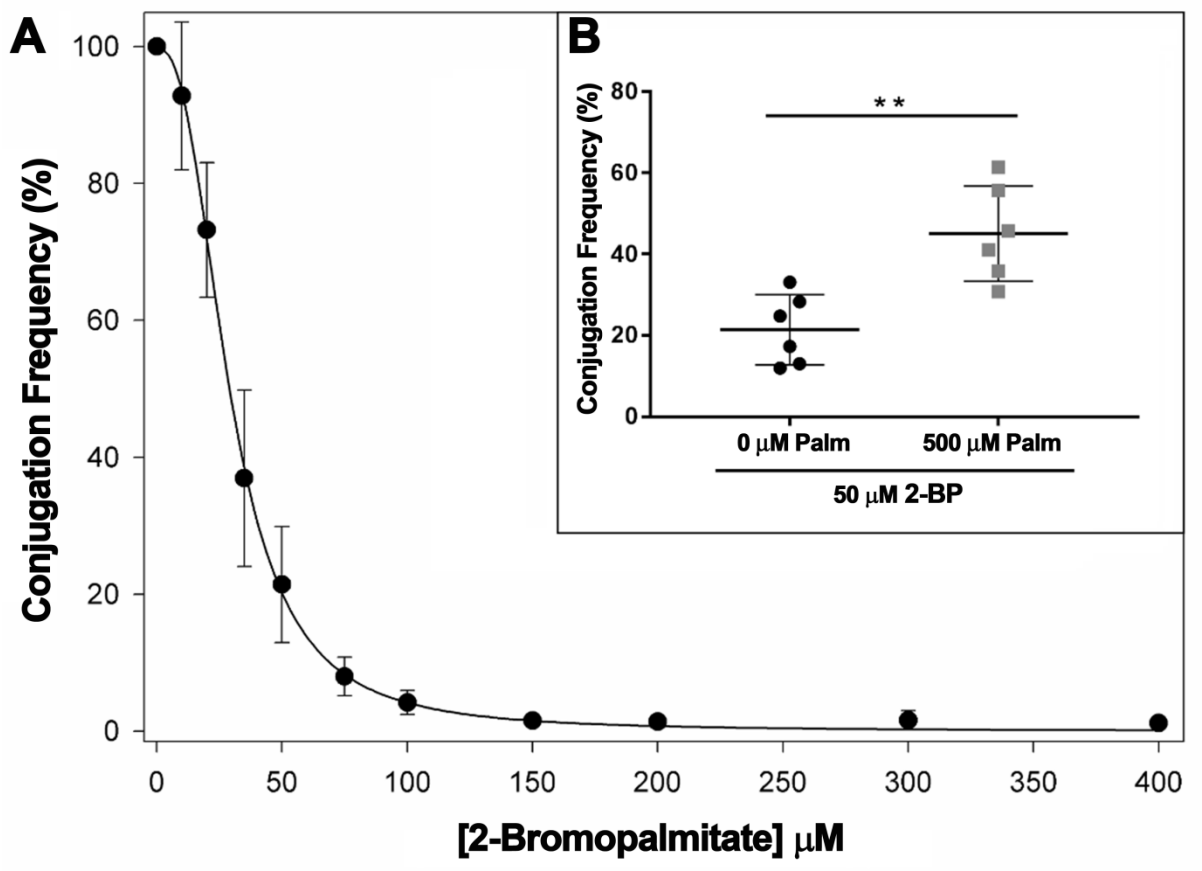
A
Conjugation Frequency (%)
100
80
60
40
20
0
0
50
100
150
200
250
300
350
400
[2-Bromopalmitate] μM
B
Conjugation Frequency (%)
80
60
40
20
0
* *
0 μM Palm
500 μM Palm
50 μM 2-BP

FIGURE 6